UNIVERSITEIT GENT

FACULTEIT GENEESKUNDE EN GEZONDHEIDSWETENSCHAPPEN

Surface mineralization of fibrous polyester scaffolds for bone tissue engineering purposes

Nathalie Luickx

Thesis submitted in fulfillment of the requirements for the degree of "Doctor in Biomedical Sciences"

Promotor: Prof. Dr. Ria Cornelissen

2016

Cover picture: Scanning electron microscope (SEM) image of electrospun poly(D,L-lactide) (PDLLA)

Thesis submitted as fulfillment of the requirements to obtain the degree of “Doctor in Biomedical Sciences”.

Promotor Prof. Dr. Ria Cornelissen
Ghent University, Department of Basic Medical Sciences

Members of the examination committee:

Prof. Dr. Johan Vande Walle (Chairman)
Ghent University, Department of Pediatrics and medical genetics

Dr. Stéphane Hocquet
Belgian Ceramic Research Centre (BCRC), Mons

Prof. Dr. Rino Morent
Ghent University, Department of Applied physics

Prof. Dr. Gwen Sys
Ghent University, Department of Physical medicine and orthopaedic surgery

Dr. Giuseppe Cama
Ghent University, Polymer Chemistry and Biomaterials Group (PBM)

Dr. Els De Canck
Ghent University, Department of Inorganic and physical chemistry

Dr. Hilde Browaeys
Ghent University, Department of Otorhinolaryngology

Begin

At the beginning and

Go on till you

Come to the end: then

Stop

-Alice's adventures in Wonderland, Lewis Carroll-

Dankwoord

Zo, 150 jaar na het verschijnen van Alice in Wonderland van Lewis Carroll, verschijnt het doctoraat van Nathalie Luickx. Dat kan geen toeval zijn. De weg naar een doctoraat lijkt dan ook veel mee te hebben van het avontuur van Alice. Hoewel de meeste mensen denken dat Alice in Wonderland een vermakelijk kinderboek is, maakt Alice niet altijd zo'n leuke dingen mee. Ze komt van de ene verwarrende situatie in de andere, maakt kennis met allerlei wezens die haar te pas en te onpas vertellen hoe dom ze is, en ze weent te helft van de tijd.

Nu, zo erg was het niet, maar het was toch een ferme sprong in het konijnenhol!

Bij deze wil ik dan ook graag enkele mensen bedanken die mij bijgestaan hebben in de zes jaar in Wonderland.

De eerste die ik tegen het lijf liep en die me mee op sleeptouw nam was Prof. Verbeeck. Bedankt om mij de kans te geven om de wondere wereld van de biomaterialen te ontdekken, voor de ondersteuning tijdens het onderzoek en het schrijven van artikels. Op het einde van mijn doctoraat werd het promotorschap overgenomen door Prof. Cornelissen. En hoewel dit geen evidentie was heb ik toch heel veel steun aan u gehad, waarvoor dank. Ook Prof. Van Hengel, bedankt voor uw luisterend oor en aanstekend enthousiasme.

Lieve collega's, Chris, Natasja, Tamara en Marleen, bedankt om altijd voor mij klaar te staan met raad, daad, praat en zo veel meer! Ik ben blij dat jullie in mijn team zaten! Natasja, je was altijd zeer nauw betrokken bij het denk-, experimenteer- en schrijfwerk. Dit doctoraat is ook een pluim op jouw hoed! Tamara, ik zal het missen om niet meer op een stoeldraai van je vandaan te zitten, maar je bent er ook bijna, we zijn er geraakt!

Verder heb ik nog met een aantal mensen samengewerkt die ook een bedankje verdienen. Leen en Johanna, heel erg bedankt voor het uitvoeren van de celexperimenten, en Heidi voor de ondersteuning en interpretatie van de data. Karen De Clerck van de Textielkunde wil ik bedanken voor het ter beschikking stellen van het labo. Het was ook altijd goed samenwerken met de reeds afgestudeerde doctoraatstudenten van deze groep, Lien en Iline. Kim Ragaert van de vakgroep toegepaste materiaalwetenschappen, hartelijk bedankt voor de goede, vlotte en constructieve samenwerking. En bedankt dat ik Nicolas af en toe mocht lenen. Nicolas bedankt voor de vele staaltjes die je voor ons gemaakt hebt, ik wens je verder ook alle succes toe met je eigen onderzoek. Olivier, bedankt voor de vele SEM foto's en de leuke babbels tijdens het nemen ervan.

'Mijn' thesisstudenten, Jonas, Willem, Felke, bedankt voor de liters SBF die jullie gemaakt hebben en alle calcium fosfaatbehandeling die jullie voor mij uitgevoerd hebben.

Tom, Koen, Pieter, ik keek er werkelijk elke dag naar uit om met jullie te gaan lunchen! De lunches zullen gemist worden, maar ik weet zeker dat wij elkaar hierna niet uit het oog zullen verliezen. Ook de rest van de Gentbende, met naam en toenaam, Brecht, Lies, Lieselotte, Lucie, Jacy, Pieter, Tine, Thomas, jullie zijn werkelijk het mooiste wat ik aan Biomedische Wetenschappen overgehouden heb.

De beste vriendinnen ooit, Hanne en Lauren, bedankt voor de dagelijkse whatsapp'jes, het plezier in de leuke momenten en de steun in de minder leuke.

Papa, mama, lieve familie en schoonfamilie, ik denk dat jullie nog altijd geen idee hebben wat ik de afgelopen zes jaar gedaan heb, desalniettemin, bedankt voor de leuke familiemomenten en bedankt om in mij te blijven geloven. Bomma en perain, zonder jullie stond ik hier niet. Er bestaan geen woorden om jullie genoeg te bedanken.

En dan, de persoon die mij doorheen Wonderland bijgestaan heeft, die mijn hand vastnam en mij verder op weg trok toen ik weg wou vluchten, mijn liefde en mijn beste vriend, Simon, bedankt voor ALLES. Ik draag dan ook graag de helft van dit boekje aan jou op. De andere helft is voor mijn nieuwe liefde, onze lieve kleine Ares. Jullie schreven mee aan het doctoraatshoofdstuk, en nu is het tijd voor een nieuw hoofdstuk, één met ons drie!

"Would you tell me please, which way I ought to go from here?"
"That depends a good deal on where you want to get to," said the Cat.
"I don't much care where-" said Alice
"Then it doesn't matter which way you go," said the Cat
"-so long as I get SOMEWHERE," Alice added as an explanation.
"Oh, you're sure to do that," said the Cat, "if you walk long enough."
-Alice's adventures in Wonderland, Lewis Carroll-

Summary

Despite the remarkable ability of bone to remodel and spontaneously regenerate, the body is incapable of self-healing in case of a critical sized bone defect caused by severe trauma or after a bone tumor resection. In such a case a surgical intervention is needed. Concerns regarding autogeneic and allogeneic bone tissue transplantation necessitate the search for synthetic bone tissue engineering alternatives. Such a bone substitute or scaffold has to be biocompatible, bioactive and biodegradable so that the implant material can integrate with the surrounding bone matrix, promote bone formation and finally be replaced by newly generated bone tissue. Additionally, in order to allow cell in-growth, vascularization and efficient transport of nutrients, oxygen, growth factors and metabolites, the scaffold should be porous with a high degree of interconnectivity.

In this thesis, two biodegradable polyesters, poly(ε-caprolactone) (PCL) and poly(D,L-lactide) (PDLLA), were processed by means of electrospinning and 3D plotting. As such, four potential bone tissue engineering scaffolds were fabricated: electrospun PCL, electrospun PDLLA, 3D plotted PCL and a multiscale PCL scaffold fabricated by combining electrospinning and 3D plotting.

In order to enhance the bioactivity of these scaffolds, a surface coating with an apatite was applied. The apatite structure is chemically comparable to the mineral phase found in natural bone and acts as an excellent cell support to maintain desirable cell-substrate interactions. Moreover, as bone apatite has carbonate content of 3 – 13 weight percent (wt%), and several studies showed that the cell adhesion, proliferation and metabolic activity of bone cells was increased on apatites with a high carbonate content, the incorporation of carbonate in the apatite lattice of the coating was of interest.

In the first part of the thesis, the electrospun PCL and PDLLA scaffolds were coated with a thin and homogenous primer layer of calcium deficient hydroxyapatite (CDHAp). Coating was achieved in two steps: activation and nucleation. During the first step, reactive groups were created on the fiber surface. These served as nucleation points for apatite deposition during the second step in which the samples were alternately dipped in calcium and phosphate rich solutions. A cell study was conducted to determine whether the CDHAp coating enhanced cell viability. CDHAp coated electrospun PCL and PDLLA demonstrated to be a good substrates for cell attachment and growth of MC3T3-E1 cells.

In the second part of the thesis, coating of the 3D PCL scaffold with hydroxyapatite with various carbonate contents was achieved. Analysis of the cell viability and adhesion of MC3T3-E1 cells showed that a hydroxyapatite coating with a carbonate content of at least 10 wt% carbonate improved the osteogenic cell response when compared to uncoated 3D plotted PCL scaffolds and scaffolds coated with a hydroxyapatite with a lower carbonate content.

In the final part of the thesis the previously optimized protocols for the coating of electrospun and 3D plotted PCL were combined for the coating of the innovative multiscale scaffold with hydroxyapatite with a low and medium carbonate content. Seeding of MC3T3-E1 cells on these coated

scaffolds showed that the cells reached confluence after 1 day of culture and formed a monolayer after 7 days of culture. Moreover, the cells were able to infiltrate and colonize the interior of the scaffold.

Samenvatting

Bot is een dynamisch en actief weefsel, waardoor het in staat is om kleine defecten en breuken spontaan te herstellen. Grotere botdefecten, bijvoorbeeld ten gevolge van de resectie van een bottumor, kunnen echter niet spontaan genezen. Bij dergelijke botdefecten is chirurgische interventie nodig. Problemen geassocieerd met het gebruik van autogeen en allogeen bot, zoals schaarste van botdonors en afstoting, hebben geleid tot het onderzoek naar synthetische botsubstituten. Dergelijk synthetisch materiaal moet biocompatibel, bioactief en biodegradeerbaar zijn, zodat integratie met het omliggend weefsel mogelijk is, botvorming bevorderd wordt en het materiaal geleidelijk vervangen wordt door nieuw botweefsel. Om de ingroei van cellen, bloedvaten en transport van voedingstoffen, zuurstof en metabolieten mogelijk te maken is het bovendien noodzakelijk dat de structuur poreus is met een hoge graad van interconnectiviteit van de poriën.

In deze thesis werden twee biodegradeerbare polyesters, poly(ε-caprolacton) (PCL) en poly(D,L-lactide) (PDLLA) verwerkt via twee fabricatietechnieken, elektrospinnen en 3D plotting. Op die manier werden vier poreuze constructen gefabriceerd die mogelijks gebruikt kunnen worden bij botweefselgeneratie toepassingen: 1) elektrogesponnen PCL, 2) elektrogesponnen PDLLA, 3) 3D geplot PCL en 4) een construct bestaande uit een combinatie van elektrogesponnen en 3D geplot PCL.

Het voordeel van PCL en PDLLA is hun biocompatibiliteit en biodegradeerbaarheid. Door hun hydrofobe karakter is de bioactiviteit van deze polyesters echter beperkt. Ter verhoging van de bioactiviteit kunnen de stalen gecoat worden met een calcium fosfaatlaag, bij voorkeur apatiet met een hoog carbonaatgehalte. Dergelijke apatietstructuur is chemisch vergelijkbaar met de minerale fase van bot.

In het eerste deel van deze thesis werden elektrogesponnen PCL en PDLLA gecoat met een dunne en homogene calcium deficiënte hydroxyapatietlaag (CDHAp) in twee stappen. De eerste stap bestond uit de activatie van de polyesters, waarbij reactieve groepen gecreëerd werden op het vezeloppervlak. In de tweede stap dienden deze reactieve groepen als aanhechtingsplaatsen voor calcium fosfaatkristallen tijdens een alternerende onderdompeling van de stalen in calcium- en fosfaatrijke oplossingen. Een celstudie met MC3T3-E1 pre-osteoblasten toonde aan dat de celviabiliteit verhoogd was op de gecoate stalen in vergelijking met de onbehandelde elektrogesponnen PCL en PDLLA stalen.

In het tweede deel van de thesis werden 3D geplotte PCL structuren gecoat met hydroxyapatiet met variërende carbonaatconcentraties door incubatie in mineralisatieoplossingen met ion concentraties gebaseerd op deze van humaan bloedplasma. Analyse van de celviabiliteit en adhesie van MC3T3-E1 cellen toonde aan dat een hydroxyapatietlaag met een carbonaatinhoud van minstens 10 gewichtspercent (gew%) carbonaat resulteerde in een verbetering van de celrespons in

vergelijking met onbehandelde 3D geplotte PCL en stalen gecoat met hydroxyapatiet met een lagere carbonaatconcentratie.

Tenslotte werden de coatingprocedures die geoptimaliseerd werden voor het elektrogesponnen en 3D geplotte PCL toegepast op de meest innovatie PCL structuur bestaande uit een combinatie van electrogesponnen nanovezels en 3D geplotte microvezels. Zo werd deze 'hybride' structuur gecoat met een laagje carbonaat bevattend hydroxyapatiet. Incubatie van MC3T3-E1 cellen op deze gecoate stalen toonde aan dat de cellen reeds na 1 dag in een confluente laag aanwezig waren en dat de cellen na 7 dagen een 'monolayer' vormden op de stalen. Histologische coupes van de stalen toonden bovendien aan dat de cellen in staat waren om de structuren binnen te dringen en te koloniseren. Bijgevolg zijn dergelijke structuren bestaande uit nano- en microvezels, gecoat met een laagje carbonaat bevattend hydroxyapatiet goede kandidaten voor botregeneratie toepassingen.

Table of content

List of abbreviations

3D	three-dimensional
3DP	3D printing
ACP	amorphous calcium phosphate
ADSCs	adipose derived stem cells
bFGF	basic fibroblast growth factor
BMPs	bone morphogenetic proteins
BTE	bone tissue engineering
CAD	computer aided design
CDHAp	calcium deficient hydroxyapatite
CP	calcium phosphate
CT	computer tomography
DCPD	dicalcium phosphate dihydrate
ECM	extracellular matrix
EtOH	ethanol
FD	filament diameter
FDA	Food and Drug Administration
FDM	fused deposition modeling
HAp	hydroxyapatite
HBP	human blood plasma
MRI	magnetic resonance imaging
MSCs	mesenchymal stem cells
NCPs	non-collagenous proteins
OCP	octacalcium phosphate
PCL	poly(ε-caprolactone)
PDLLA	poly(D,L-lactic acid)
PDLA	poly(D-lactic acid)
PEEK	polyetheretherketone
PEG	polyethylene glycol
PGA	poly(glycolic acid)
PLA	poly(lactic acid)
PLGA	poly(lactic-co-glycolic acid)
PLLA	poly(L-lactid acid)
PMMA	poly(methyl methacrylate)
PP	polypropylene
rhBMP-2	recombinant morphogenetic protein-2
RP	rapid prototyping
SBF	simulated body fluid
SD	strand distance
SEM	scanning electron microscopy
SES	screw extrusion system
SFF	solid freeform fabrication
SLA	stereolithography
SLS	selective laser synthering
TIPS	thermally induced phase separation
TRIS	trishydroxymethylaminomethane
UHMWPE	ultra-high molecular weight polyethylene
VEGF	vascular endothelial growth factor
wt%	weight percent
XRD	X-ray diffraction

Chapter 1: Introduction

1 Bone

A total of 213 bones make up the adult human skeleton, ranging from long bones in the limbs, short bones in the wrists and ankles and flat bones in the sternum and skull, to irregular bones such as the pelvis and vertebrae. The skeleton serves as structural support for the body, permits movement by providing levers for the muscles, protects vital internal organs and structures, provides maintenance of mineral homeostasis and acid-base balance, serves as a reservoir of growth factors and cytokines and provides the environment for hematopoiesis within the marrow spaces.[1] Bone consists of several tissues, but the most prevalent type is osseous tissue or bone tissue. Bone tissue is arranged in either a compact pattern (compact or cortical bone) or a trabecular pattern (spongy or cancellous bone). The adult human skeleton is composed of 80% compact bone and 20% spongy bone.[2]

Compact bone is dense and solid with a porosity of only 5-10%. It is found as the external layer or cortex of the bones and has a smooth, dense and continuous structure (Figure 1A). This type of bone is built up by osteons or Haversian systems, which are composed of lamellae that are concentrically oriented around a central Haversian canal, which contains blood vessels for nutrient supply and nerve fibers (Figure 1B).[1-3]

Spongy bone has a high porosity (50-95%) and is found in the extremities of long bones and in the center of short, flat and irregular bones. As seen in figure 1A, the matrix structure is composed of a network of trabeculae, small bone rods and plates that form a three-dimensional (3D) interconnected porous network. Within this structure, nutrients are supplied from capillaries that surround the bone trabecula.[2,3]

The outer surface of compact bone is surrounded by the periosteum, a fibrous connective tissue layer, which contains blood vessels, nerves, fibroblasts and osteoprogenitor cells (Figure 1A). The endosteum is a thin membranous structure that covers the inner surfaces of bone. Although considerably thinner than the periosteum, the endosteum also contains fibroblasts and osteoprogenitor cells (Figure 1A).[1]

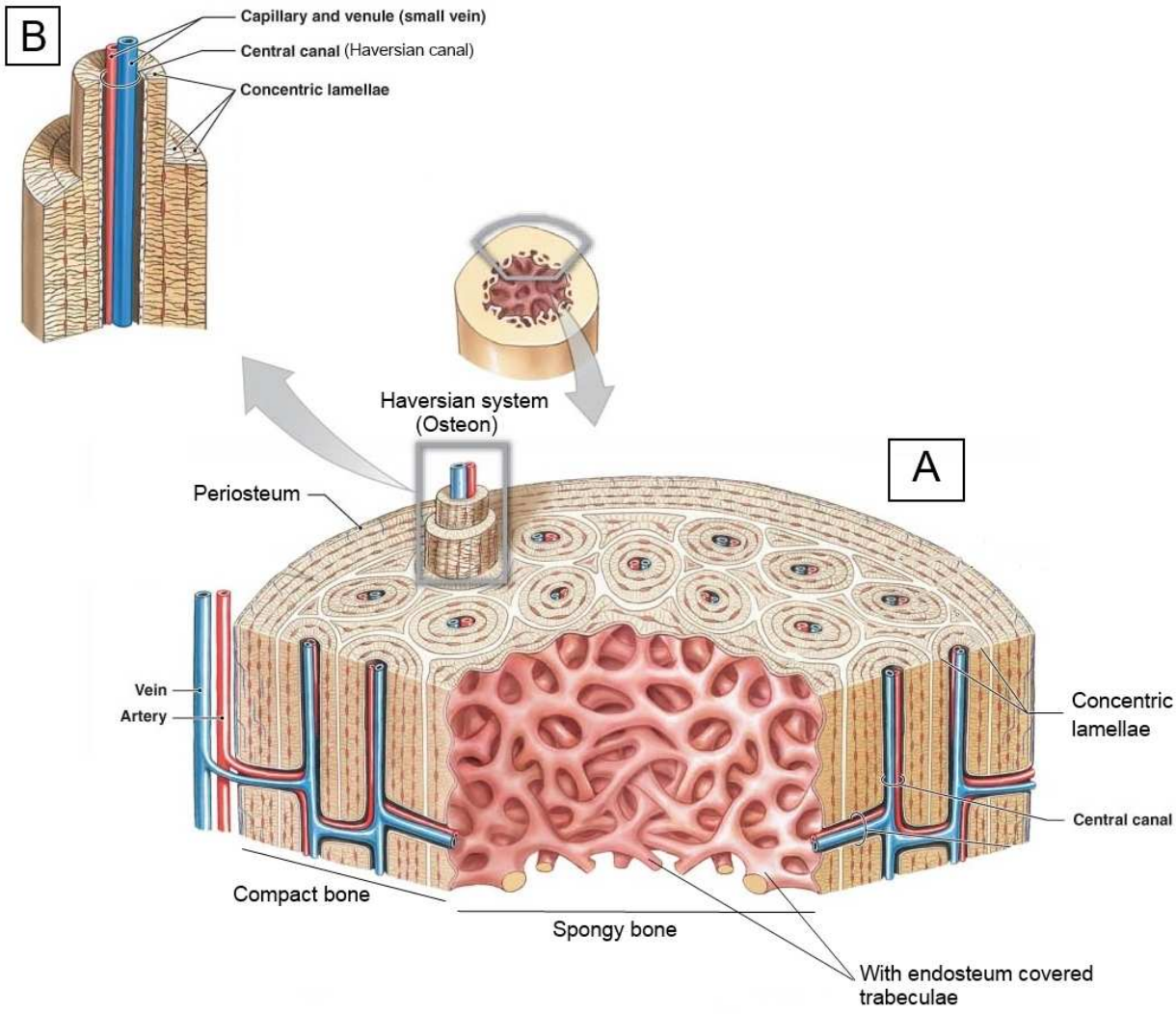

Figure 1: Structure of a typical long bone showing both compact (cortical) and spongy (cancellous) bone. © 2011 Pearson Education, Inc.

1.1 Bone extracellular matrix

Like other connective tissues, bone consists of cells embedded in an organic extracellular matrix (ECM). The latter is comprised of fibers and an amorphous gel-like ground substance, produced by the cells. A characteristic elementary unit of the bone ECM is the mineralized collagen fibril. These fibrils consist of an organic phase strengthened by an inorganic mineral phase of calcium phosphate crystals.

1.1.1 Collagen

Side-by-side cross-linking of collagen fibrils forms collagen fibers. According to the collagen fiber arrangement, two types of bone can be identified microscopically; woven bone and lamellar bone. The presence of the characteristic 67 nm repeat structure in the collagen fibers of both the ordered and disordered materials, indicates that type I collagen is the major component of both types.[4]

Woven bone is characterized by a disordered organization of collagen fibers and is mechanically weak. It is produced very quickly by osteoblasts and is a transient tissue type that is characteristically found in the fetus and in the callus produced during fracture repair. Woven bone contains blood vessels and a high portion of osteocytes.[4,5]

Lamellar bone is the most common structural type found in bones and is laid down much more slowly than woven bone. The collagen fibers and their associated mineral show a plywood-like arrangement and even though the final degree of mineralization of lamellar bone is less than that of woven bone, lamellar bone is mechanically much stronger. It is formed in the fetus during the third trimester and after fracture woven bone is gradually replaced by lamellar bone during the process of hard callus or bony formation (see section 1.3).[5]

1.1.2 Mineral phase

The inorganic mineral phase of mature bone is a calcium phosphate with an X-ray diffraction (XRD) pattern that closely resembles that of stoichiometric hydroxyapatite [HAp; $Ca_{10}(PO_4)_6(OH)_2$]. The apatite crystals are intimately associated with the organic matrix and account for 60 to 70 wt% of the bone's dry weight. The diffraction peaks in the pattern of bone mineral are much broader and less resolved compared to the ones found in HAp, which confirms the presence of nanometer sized plate-shaped crystals.[4] Chemical analysis has shown that bone mineral lacks hydroxyl groups but contains impurities such as F^-, Cl^-, Na^+, K^+, Fe^{2+}, Zn^{2+}, Sr^{2+}, Mg^{2+}, CO_3^{2-} and HPO_4^{2-}.[2,6-8] As the impurities are incorporated in the apatite lattice by a substitution of the lattice ions, the properties of the apatite mineral change, especially the crystal size, solubility, strength and brittleness. Consequently, the solubility of the apatite mineral in the body can be fine-tuned by the controlled incorporation of impurities in the apatite lattice. As a result, the concentration of impurities depends on the location of the apatite in the skeleton.[6,7] For example, bone mineral contains approximately 7wt% carbonate which makes this apatite amenable to dissolution. In contrast, the carbonate content in the less soluble apatite of enamel approximates 3.5wt%.

1.1.3 Non-collagenous proteins and water

Proteoglycans and other non-collagenous proteins (NCPs) such as osteocalcin, osteonectin, osteopontin and bone sialoproteins are present as ground substance. These proteins account for approximately 5% of the total protein content of bone and are thought to play a crucial role in bone formation and modulation of cell adhesion, migration, proliferation and differentiation. However, little is known about the location and function of the NCPs.[2,4] Proteoglycans have a high water-absorbing capacity, however the water content of bone is lower than in other connective tissues.

The complex composite structure gives bone its requisite strength and high fracture toughness.[9] The inorganic component of bone makes the tissue hard and rigid, while the organic component provides flexibility and resilience.[3,10] Each bone constantly undergoes modeling during life to help it adapt to changing biomechanical forces, as well as remodeling to remove old and/or microdamaged bone.[1] The forces that a bone needs to withstand and hence its composition varies depending on its place in the body. In addition, the properties of bone differ with species, race, gender and age.[11,12] In general, the mechanical properties of both compact and spongy bone have been demonstrated to depend on density, porosity, architecture and the mineral and matrix components.[2] Table 1 shows some illustrative values of the compact bone properties of various bones in the human body.

Table 1: Average values for mechanical and physical properties of wet compact human bone.

Bone	Age	Breaking load	Ultimate tensile strength	Young's modulus	Density	Ref
		kg	MPa/m^2	GPa/m^2	g/cm^3	
Femur	20-39	-	124	17.6	-	11
	41	71.2	100.03	14.61	1.91	12
	71	57.2	66.69	13.34	1.85	12
Tibia	20-39	-	174	18.4	-	11
	41	83.0	103.95	18.53	1.96	12
	72	70.8	82.38	15.89	1.83	12
Fibula	33	64.9	98.07	18.83	1.91	12
	59	57.6	78.45	14.91	1.73	12
Humerus	20-39	-	125	17.5	-	11
Radius	20-39	-	152	18.9	-	11

1.2 Bone cells

The calcified matrix embeds bone cells which play a crucial role in modeling and remodeling of the bone, both tailored by mechanical, hormonal and physiological parameters. The first process modulates the bone size and shape while the remodeling process renews old or damaged bone to maintain bone strength and homeostasis of calcium and phosphate. In adults, bone modeling occurs less frequent when compared to remodeling.[1]

There are three types of fully differentiated bone cells: osteoblasts, osteocytes and osteoclasts (Figure 2). Apart from these cell types, osteoprogenitor cells are present in the periosteum, endosteum and bone-marrow. Osteoprogenitor cells can be defined as persistent migratory stem cells, which can proliferate and differentiate into osteoblasts.[3]

Osteoblasts are present at the bone surface, where they form a tight layer of cells (Figure 2). The primary function of osteoblasts is to actively synthesize and deposit the organic components of the bone matrix: the ground substance and the collagen fibers. The non-mineralized bone matrix secreted by osteoblasts is called osteoid. Extracellular matrix vesicles are also synthesized by the osteoblast. These serve as protected microenvironments in which calcium and phosphate concentrations can increase sufficiently to precipitate apatite crystals within the osteoid. Osteoblasts transform into osteocytes after becoming embedded in their own bone matrix (Figure 2). Osteocytes lie within lacunae within mineralized bone where they maintain the bone matrix and regulate mechanotransduction. Osteoblasts are also responsible for the regulation of osteoclast differentiation and activity. Osteoclasts are the only cells that are known to be capable of resorbing bone. Bone resorption depends on osteoclast secretion of hydrochloric acid, which dissolves the mineral component of the bone matrix, and proteolytic enzymes such as cathepsin K, which digest the proteinaceous matrix. The released calcium and phosphate ions enter the tissue fluid and the blood stream, whereas the collagen is taken up by the osteoclasts by phagocytosis.[1,3]

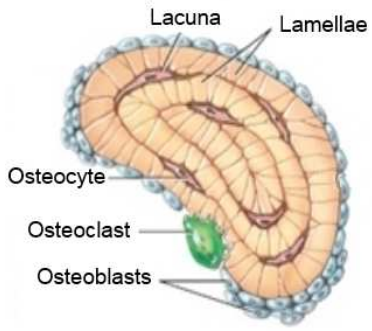

Figure 2: Bone trabeculae section showing the position of the bone cells. © 2011 John Wiley & Sons, Inc.

1.3 Bone healing

Bone is a dynamic and active tissue that is constantly being remodeled in response to mechanical stress and hormonal stimuli. The spongy bone in the skeleton is entirely replaced every 3 to 4 years, the compact bone every 10 years.[3] Due to this remarkable property, bone has a high regenerative capacity including the ability to repair fractures with complete restoration of form and function.

1.3.1 Spontaneous bone healing

Repair is divided into four subsequent biological processes, each characterized by a specific set of cellular and molecular events (Figure 3):

Stage 1: Inflammation and hematoma formation (Figure 3A)

When a bone fracture occurs the local soft tissue, including blood vessels and marrow, is damaged. The bleeding within the defect is contained by the surrounding tissue and forms a hematoma. Degranulating platelets, macrophages and other inflammatory cells

infiltrate the hematoma between the fractured fragments and remove degenerated cells and necrotic tissue and secrete cytokines and growth factors.[13]

Stage 2: Soft callus (fibrocartilage) formation (Figure 3B)

Within a few days blood vessels, osteoblasts and fibroblasts infiltrate the hematoma. The fibroblasts secrete collagen fibers that bridge the defect site. Some of the fibroblasts differentiate into chondrocytes that lay down cartilage. At this moment a semi-rigid *soft callus* is formed which provides some mechanical support to the fracture. As more fibers and cartilage are produced, the soft callus becomes a fibrocartilaginous callus.[3,13]

Stage 3: Hard callus (bony) formation (Figure 3C)

This stage represents the most active period of osteogenesis and starts within a week. It is characterized by high levels of osteoblast activity and the formation of mineralized woven bone directly in the peripheral callus. Trabeculae of new bone span the width of the callus, uniting the two fragments of the broken bone. The new woven bone or *hard callus* is typically irregular.[13]

Stage 4: Bone remodeling (Figure 3D)

The final stage of fracture repair takes many months and involves the remodeling of the woven bone in the hard callus into the original lamellar bone configuration. The process of neo-vascularization is maintained. The key cells involved in the resorption of mineralized bone are the osteoclasts. Once completed, osteoblasts are able to lay down new bone on the eroded surfaces. Eventually, the bone structure will be identical to the original bone morphology.[3,13]

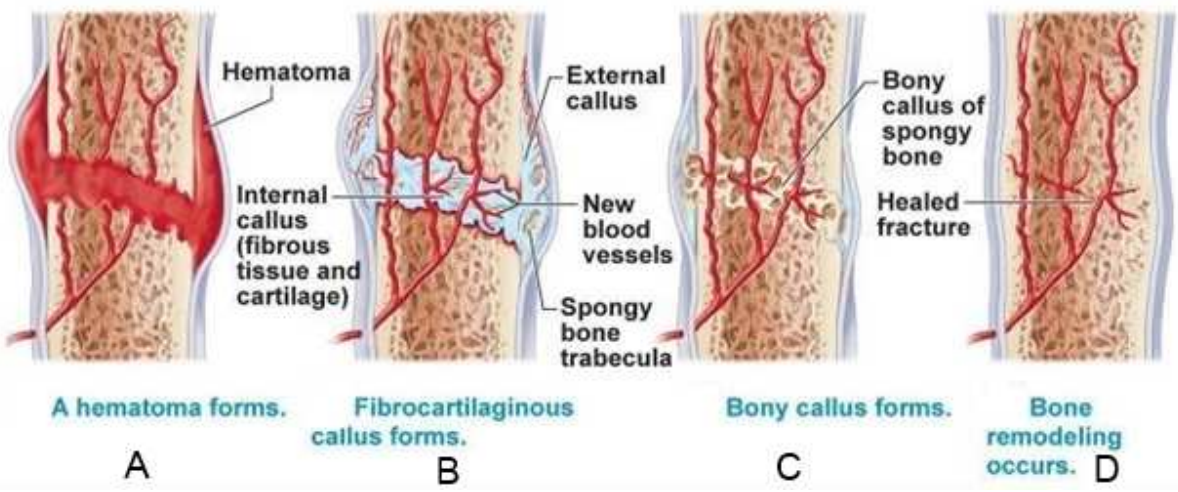

Figure 3: The four stages of bone healing. Copyright © 2010 Pearson Education, Inc. All rights reserved.

The fracture healing time will depend on its complexity, its place in the human body and the patient's age. In adults, a simple fracture the bone is healed in about 6 to 8 weeks.[3]

Despite the high regenerative capacity of bone tissue, the healing process can be compromised by an unfavorable wound environment and biomechanical instability. In addition, large osseous deficiencies arising from disease, trauma, congenital disorders or surgery will not heal spontaneously and can generate critical sized defects. These bone defects are defined as, "the smallest size intraosseous wound in a particular bone and species of animal that will not heal spontaneously during the lifetime of that animal".[14] The repair of such bone defects remains a major clinical challenge.[14-16]

1.3.2 Repair of critical sized bone defects

1.3.2.1 Bone grafts

Current procedures to repair critical sized bone defects are autologous or allogeneic bone grafts. These grafts provide structural and mechanical support.

a Autografts

In autografting, 'donor' bone is harvested from a non-load-bearing site in the patient (mostly iliac crest, but also femur, tibia, mandible and calvarium) and implanted in the defect. A bone autograft has osteogenic, osteoinductive and osteoconductive properties. Autografting is considered the *gold standard* of bone grafting because it contains the patient's bone cells, proteins, and calcified matrix. Although the graft does not provide mechanical stability, it is rapidly incorporated into the host tissue.[17,18] While clinical successes with autografts are notable, limited supply and donor site morbidity are a major concern.[18]

b Allografts

In allografting the bone is harvested from a donor from the same species. Bone is one of the two most commonly transplanted tissues, second only to blood.[19] As the allograft is obtained from a human donor the need for an additional surgery on the patient is avoided. Allograft bone has different properties depending on its preparation, but allograft bone has no osteogenic potential. An allograft mostly serves as an osteoconductive scaffold in which revascularization and new bone formation can occur. Nevertheless, there are risks of disease transmission and a high rate of non-union and fracture with an approximate prevalence of 15-30% in the case of large structural bone allografts.[18] In addition, the maintenance of bone banks is expensive and the problem with insufficient donor tissue availability remains.[15,16,20-25]

1.3.2.2 Biomaterials

The problems associated with auto- and allografts, have led to the exploration of biomaterials and their development as bone grafts substitutes or implants.[26] These biomaterials are synthetic preformed materials such as metals, ceramics and polymers.[27]

a Metals

Metals such as stainless steel and various alloys with cobalt, titanium and magnesium have played an important role as structural implants in reconstructive surgery, especially orthopedics and reconstructive maxillofacial surgery. These metallic materials provide the strength and toughness that are required in load-bearing parts of the body. Nevertheless, concerns include the systemic toxicity of released metal ions due to corrosion and fatigue failure of structural components caused by repeated loading. In addition, metals generally are not able to form a strong bond with the surrounding tissues.[28,29]

b Bioactive ceramics

This category of ceramics includes calcium phosphates (hydroxyapatite (HAp) in particular), calcium carbonate, glass, and their composites. These materials contain ions commonly found in the physiological environment (such as K^+, Mg^{2+}, Na^+) and/or ions showing very limited toxicity to body tissues. Hence, these materials can be called biocompatible. In addition, they have the capability to interact with the biological environment to improve host response as well to form a direct bond with the surrounding tissue. However, due to their brittle nature and low strength the clinical use of ceramics alone is limited. [17,26,29]

c Synthetic polymers

For orthopedic and craniofacial applications, polymers currently used include acrylics, polyamides, polyurethanes, polyetheretherketone (PEEK), ultra-high molecular weight polyethylene (UHMWPE) and polypropylene (PP). These polymer materials are considered biocompatible and bioinert in the human body. The main advantage of these materials include the possibility to tailor their composition and structure according to the specific need. However, due to their hydrophobic nature, polymers generally show unfavorable protein adsorption which leads to poor cell attachment. The latter can be enhanced by the addition of a bioactive material to the polymer.[29]

2 Bone tissue engineering

Since current techniques for the reconstruction of bone defects have significant drawbacks, there is a strong need for alternative bone substitutes. Bone tissue engineering (BTE) holds promise in providing an improved clinical therapy for the functional and structural restoration of damaged or lost bone tissue.

In general, tissue engineering has been defined as “The interdisciplinary field of study that applies the principles of engineering and life sciences towards the development of biological substitutes that restore, maintain or improve function or a whole organ”.[30] Recent scientific progress in biomedical research has created exceptional advances in the development of engineered tissues. There are three main components, the so-called tissue engineering triad, in the field of tissue engineering. These include (1) a scaffold that provides structure and acts as substrate for tissue growth and development, (2) a source of cells to facilitate required tissue formation, and (3) growth factors to direct the growth and differentiation of cells within the scaffold (Figure 4).[16,31]

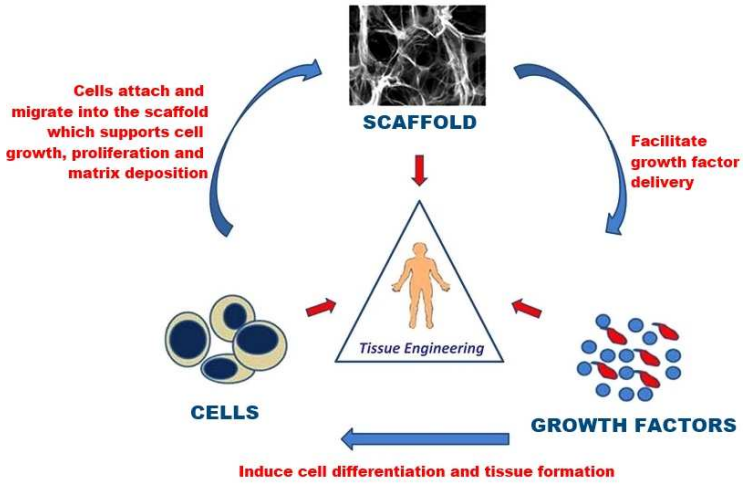

Figure 4: The tissue engineering triad.[16]

Even though ideally all three components should be incorporated, the generally applied BTE strategies can be divided in three categories: cell/scaffold-based strategies, scaffold-based strategies and growth-factor/scaffold-based strategies.[32,33]

2.1 BTE strategies

2.1.1 Cells/scaffold-based strategies

Bone regeneration is biologically driven by osteoprogenitor cells that are able to form new osteoblasts. In the cellular approach specific cells are harvested directly from the patient (autologous cells) or from a donor (allogenic cells) and expanded in culture. Next, the cells

are seeded *ex vivo* onto the scaffold. The cellularized scaffold is then cultured in a bioreactor that is capable of providing the multi-parametric signals needed for graft development and maturation. Finally the construct is implanted in the patient where it can integrate with the surrounding tissue.[16] For BTE purposes, bone marrow derived mesenchymal stem cells (MSCs) are popular due to their multipotency.[34] Adipose tissue has also been shown to contain a population of multipotent cells, the adipose tissue-derived stem cells (ADSCs).[35]

The isolation and expansion of autologous stem cells was once considered to be the future of BTE. However, as somewhat contradictory results exist regarding the (pre)clinical successes of cell-based tissue engineering constructs, no products have yet reached the clinic.[36] Additional challenges associated with production costs, storage, culture times, the transport of cell-cultured scaffolds and the practical handling for the surgeon as well as limited demonstrations of efficiency have led to a re-focusing on the acellular scaffold-based approach.

2.1.2 Scaffold-based strategies

In this approach the tissue formation is due to cells which are already present in the body. The advantage of the latter is the reduced amount of operations needed, resulting in a shorter recovery time for the patient. Even though the amount of cells that migrate in the acellular scaffold is few, the osteogenic response can be enhanced by adding growth factors to the scaffold.[16,37] Such scaffold could offer a more economical and practical alternative.

2.1.3 Growth factors/scaffold-based strategies

Growth factors, such as vascular endothelial growth factor (VEGF), basic fibroblastic growth factor (bFGF) and bone morphogenetic proteins (BMPs), can be incorporated onto the scaffold by simple soaking, encapsulation or covalent immobilization. The addition of growth factors to the scaffold is a relatively easy and widely studied approach. Because growth factor delivery is either driven by passive diffusion or coupled to the rate of material degradation, growth factor release may be altered only to some extent by the amount of growth factor added or by varying the degradation rate of the material. The release profile for this method is, therefore, often not in tune with the actual healing process and cellular demands. In general, the incorporation of growth factors into the scaffold is not an efficient method. Adding the high cost associated with the human recombinant growth factors makes the growth factor-loaded scaffold approach less attractive.[38,39]

2.2 Basic requirements of a BTE scaffold

As the structure of bone depends on the type of bone and its location in the body, the properties of the scaffold are of the utmost importance if the construct needs to mimic the organization, functionality and structure of the bone as closely as possible. For instance, fractures in load-bearing long bones require scaffolds with high mechanical stability. This factor is less crucial for non-load-bearing applications such as the reconstruction of craniofacial defects. For the reconstruction of these defects the scaffold should preferentially be shapeable in order to be fitted into the defect.

An ideal scaffold should fulfill the following requirements:

a Biocompatibility

First, biocompatibility of the substrate material is imperative; the material and any degradation by-products must not elicit any inflammatory response nor demonstrate immunogenicity or cytotoxicity so that fibrous capsule formation and/or cell death is avoided.

b Biodegradability and/or bioresorbability

The scaffold should degrade and/or resorb at a controlled rate.[20] In an ideal case, the *in vivo* degradation and/or resorption rate of the scaffold is comparable with the rate of new bone formation. In this way, the scaffold can be replaced by new bone without affecting the mechanical stability. Importantly, biodegradation and/or resorption of the scaffold eliminates the need for a second surgery to remove the implant.[37]

c Osteoinductiviy and osteoconductivity

An osteoinductive material has the ability to induce bone formation by attracting pluripotent progenitor cells from the surrounding tissue and stimulating them to differentiate into chondrocytes and osteoblasts. An osteoconductive scaffold supports bone growth and encourages the ingrowth of capillaries and cells from the surrounding host tissue.[20,21]

Due to the osteoinductive and osteoconductive properties, the implant forms a direct and strong bond with the bone tissue and is considered bioactive.[40]

d Porosity

The goal of the scaffold is to provide a 3D environment for cell adhesion, proliferation and differentiation. A porous structure with interconnected pores promotes tissue ingrowth into the interior of the scaffold and the exchange of nutrients and metabolites between its interior and exterior.[41-43] *In vitro*, lower porosity stimulates osteogenesis, whereas, *in vivo* higher porosity and pore size result in greater bone ingrowth.[44] Certain cell types thrive at different pore sizes. For example, it was found that osteoblasts and chondrocytes grow better

within a pore size of 380-405 µm, whereas fibroblasts prefer a pore size of 186-200 µm.[45] Moreover, a pore size of at least 100 µm is known to be compulsory to allow cell penetration and proper vascularization of the ingrown tissue and it was recommended that the pore size should be greater than 300 µm for increasing the formation of new bone.[42,46] As the average size of a human osteon is 223 µm, it was also suggested that the optimal pore size range is 200-400 µm.[20] Overall, as osteogenesis progression is affected by pore size, large pores (>300 µm) that are well vascularized are expected to induce direct osteogenesis.[46]

e Mechanical stability

The mechanical strength of the scaffold needs to be similar to that of the surrounding tissue. The scaffold should offer adequate mechanical integrity to provide stable fixation, as mechanical loading is expected in patients during bone regeneration.[20,24] In addition, the Young's modulus value for the scaffold should be similar to that of the surrounding tissue. Scaffolds that are stiffer than the surrounding and regenerating tissues can cause adverse physiological responses, such as tissue resorption and stress-shielding.[24,47]

f Sterilization

The material needs to be easily sterilizable to prevent infection without affecting the material properties.[20] Different sterilization techniques are available such as exposure to ethylene oxide vapour, heat sterilization, ethanol treatment and irradiation with γ-rays or UV light.[48,49] In recent years, various reports describing the noxious effects of ethylene oxide have been published. Due to the growing concern on the effects of this sterilizing agent, sterilization by radiation is now considered more appropriate for the sterilization of complex geometries.[49]

2.3 Scaffold fabrication techniques

Whether or not cells and/or growth factors are added to the BTE construct, the scaffold plays a crucial role in cell seeding, proliferation and new tissue formation in three dimensions. A scaffold with a 3D structure and high porosity with interconnected pores is imperative to allow cells to migrate into the scaffold. Currently, scaffold design is a complex science, in which several aspects are carefully addressed in order to produce successful constructs. Various fabrication techniques have been investigated in order to fabricate 3D scaffolds with high porosity and surface area.[22,41,50-52] These techniques can be classified in two categories: conventional and advanced processing techniques.

2.3.1 Conventional processing techniques

2.3.1.1 Freeze-drying

In this technique an emulsion is created by homogenization of two immiscible solutions, a polymer solution (dissolved in an organic solvent) and water. The emulsion is then rapidly cooled down to a certain temperature at which all materials are in a frozen state. Next, the solvent and water are removed by applying pressure lower than the equilibrium vapor pressure of the frozen substances. When all the water and solvent are completely sublimated, a scaffold with a porous microstructure remains.[50,53]

2.3.1.2 Thermally induced phase separation (TIPS)

In this approach, the polymer is first dissolved in a solvent at a high temperature. The polymer solution is then quenched and undergoes a liquid-liquid phase separation to form two phases; a polymer-rich phase and a polymer-poor phase. The polymer-rich phase solidifies and subsequent removal of the solvent-poor phase by sublimation leaves a porous polymer scaffold. In general, the micro-and macrostructure is controlled by varying the polymer type, polymer concentration, quenching temperature and solvents.[53-55]

2.3.1.3 Solvent-casting

Solvent casting, salt leaching or particulate leaching has shown promise for its ability to produce scaffolds at room temperature. In this technique, a scaffold is produced by mixing a polymer solution, dissolved in an organic solvent, with water-soluble salt particles of a specific diameter. The mixture is then cast into a mold of desired shape, after which the solvent evaporates leaving behind a polymer matrix embedded with salt particles. During subsequent processing the porogen is leached out by immersing the scaffolds in water to form a pore structure within the scaffold. The pore size can be varied by changing the size of the porogen particles. In order to have a uniform pore structure, the thickness of scaffolds made by this technique should be less than 4 mm, making it difficult to produce larger 3D scaffolds.[22] To overcome this, a centrifugal technology[56] and the addition of polyethylene glycol (PEG)[57] have been used to improve the pore uniformity of the scaffolds.

The conventional techniques enable the fabrication of scaffolds with interconnected porous structures but offer limited capacity to control pore size, pore geometry, pore interconnectivity and spatial distribution of the pores (Table 2).[46] As an alternative, advanced fabrication techniques have been evolving in tissue engineering, such as electrospinning and rapid prototyping.[53]

Table 2: Advantages and disadvantages of conventional polymer processing techniques.

Fabrication method	Advantages	Disadvantages
Freeze Drying[41,50,55]	High porosity (~ 90%) Controlled pore size	Closed pore structure Low reproducibility
Thermally induced phase separation (TIPS)[50,53-55]	High porosity (~ 95%) Highly interconnected porous structure Good mechanical properties	Small pore size (10-100µm) Small scale production Low reproducibility Use of organic solvents
Solvent casting/Particulate leaching[22,50]	Controlled porosity Controlled interconnectivity	Use of organic solvents Low reproducibility Limited scaffold size

2.3.2 Advanced processing techniques

2.3.2.1 Electrospinning

Although the process of electrospinning has been known for 80 years and the patent was issued to Formhals in 1934 (U.S. Patent, 1-975-504), polymeric nanofibers produced by electrospinning have only recently become a topic of great interest in BTE.[58-60] Polymer materials that have been investigated to form a 3D scaffold with the electrospinning technique are synthetic aliphatic polymers such as poly(hydroxyalkanoates)[61] and poly(α-hydroxyesters)[62]. Also natural polymers such as hyaluronic acid, collagen and gelatin have been investigated.[51,63]

An electrospinning system consists of four major components: the polymer solution, a high voltage source, a spinneret and a grounded collecting plate (Figure 5). A polymer solution is loaded into a syringe and forced through a needle connected with the high voltage source. When the voltage source is turned on, the charge is transferred into the polymer solution. Increasing the electric field strength causes the repulsive interactions between equal charges in the liquid and the attractive forces between the oppositely charged liquid and collector to begin to exert tensile forces on the liquid, elongating the pendant drop at the tip of the needle. As the electric field is increased further a point will be reached at which the electrostatic forces balance out the surface tension of the liquid leading to the development of the Taylor cone. If the applied voltage is increased beyond this point a fiber jet will be drawn from the apex of the cone. As the jet moves towards the collector plate, it is elongated by electrostatic interactions between charges on nearby segments of the same jet. Meanwhile, the solvent evaporates and finally the jet solidifies into a fiber which is collected onto the collector surface where it forms a mesh with an ordered or random network of fibers with a high surface to volume ratio.[58,59,64,65] The diameter of the fibers can vary between tens of nanometers to several micrometers and depends on the electrospinning parameters such as polymer solution (viscosity, conductivity, molecular weight of polymer, solvent),

processing parameters (applied voltage, distance between needle-tip and collector surface, flow rate) and environment parameters (humidity, temperature).[53] Once these parameters are optimized electrospinning is a simple and cheap technique to fabricate scaffolds with an interconnected pore system, a reproducible fiber morphology and nano – to microscale topographies similar to the natural ECM.

Fiber orientation, porosity and surface-to-volume ratio of electrospun scaffolds are shown to influence cell response.[58]

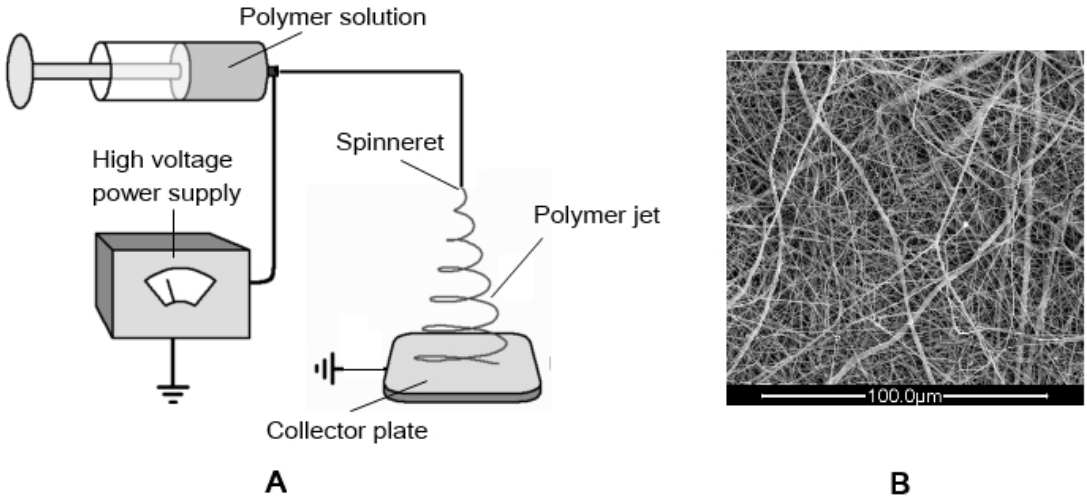

Figure 5: A) Schematic diagram of an electrospinning set-up and B) SEM image of electrospun nanofibers.

2.3.2.2 Rapid prototyping

A few rapid prototyping (RP) technologies, also called solid freeform fabrication (SFF) or additive manufacturing, have been developed to fabricate 3D scaffolds consisting of various polymers, ceramics and their composites.[66-69] The process of RP begins with the scanning of an object (or patient) using computed tomography (CT) or magnetic resonance imaging (MRI) scans. These data are used to generate a 3D model by Computer-Aided Design (CAD) software. The CAD file is typically converted to a stereolithography file format (STL), which is then numerically sliced into 2D cross-sections. These 2D elements are fabricated and stacked in such a manner that the 3D object is formed with the desired dimensions.[22,46]

With the RP technology both the geometry and material composition can be controlled in a reproducible manner. RP technologies enable the fabrication of well-defined and highly reproducible 3D tissue engineering scaffolds with controllable porosity, pore size, permeability and mechanical properties, with varying internal architectures.[22,46] Compared to

electrospinning, that produces fibers in the nanometer range, 3D scaffolds fabricated with RP techniques have filaments in the micrometer range and larger pore sizes.

Various methods for RP have been developed over the past 30 years starting with the invention of stereolithography (SLA) in 1986 (U.S. Patent 4575330 A). Several common RP processes, which have been used for the fabrication of BTE scaffolds have been reviewed in literature[22,46,70-74] and will be discussed briefly in the following sections. The advantages and disadvantages of the different RP techniques are summarized in Table 3.

a Stereolithography

In SLA the base material is a resin of photo reactive monomer liquids like acrylate and epoxies. A platform supporting the developing model is brought near the surface of a liquid vat, and a laser of UV source is used to solidify the first cross-sectional layer of the model. By lowering the platform and repeating the process layer by layer the complete 3D structure is formed.[22,46] A disadvantage of SLA is the limited choice of material, as the base material needs to be photocrosslinkable. Recently, photocrosslinkable PCL[75]- and PDLLA[76]-based resins were developed and applied in the fabrication of tissue engineering scaffolds. Furthermore HAp scaffolds with well-defined channel size can be fabricated with SLA. The bioceramic powder is then mixed with a photopolymer, which acts as a binder, prior to SLA processing.[77] However, to date the use of SLA in biomedical industry has mainly focused on building anatomical models for surgical planning.[46]

b Selective laser sintering

In selective laser sintering (SLS) parts are made by passing a laser beam (mostly CO_2 source) over a powder bed. The laser will raise the temperature of the powder, which will cause neighboring particles to fuse together both laterally and to the preceding layer below.[22,46] SLS showed great potential in producing complex porous ceramic[78] and titanium-based[79] scaffolds suitable for implantation in a bone defect. Williams *et al.* have fabricated porous polyester scaffolds with sufficient mechanical properties for BTE applications using SLS.[80]

c Three-dimensional printing

3D printing (3DP) uses ink-jet printing technology to precisely place a “binder” solution on a bed of powder thus gluing the powder together in a cross-sectional layer. A platform is lowered and more powder is deposited and processed in a layer by layer fashion.[22] As reviewed by Bose *et al*.[81], a large variety of ceramic, polymeric and composite materials can be processed using 3DP. In general, the binder selection and process parameter optimization are the keys to a successful scaffold fabrication.[81]

d Extrusion based systems

Among the available RP techniques, the extrusion based techniques are the most advanced scaffold fabrication techniques due their ability of using different materials and their feasibility of deposition on demand with high precision.[82]

In 1992 Crump developed the first commercially available extrusion based system known as fused deposition modeling (FDM) (U.S. Patent 5121329 A). In this system, a thin thermoplastic filament is melted by heating and the semi molten material is extruded through a small opening and deposited onto a platform while it is guided by a robotic device. At the end of the deposition of each layer, the platform is lowered so that the next layer can be deposited (Figure 6A). By changing the direction of each layer and the spacing between materials, scaffolds with highly uniform internal structures are obtained.[82,83] However, the commercial FDM system requires the material in the form of filaments with specific size and material properties to ensure regular material flow. This imposes a limitation on the processing window and the number of materials that can be used (Table 3).[67,68]

To widen the range of possible materials, a screw-extrusion system (SES) or 3D plotting can be used (Table 3). The 3D plotting system consists of a robotic arm and a heated barrel with an extrusion screw inside. The barrel can contain the polymer in its original form. A robotic arm enables movement of the barrel in x-y-z directions over a fixed platform. The heater melts the material, which is then extruded by pressure created by a turning screw feed (Figure 6B). Parameters that determine the quality of 3D plotted scaffolds include motor speed, dispensing speed, melt temperature, platform temperature, layer thickness and nozzle size.[46]

For both FDM and 3D plotting, different process parameters like melt flow behavior, pore size and porosity of extrusion based systems have been investigated for various scaffold materials such as polyesters[66,84,85], polyurethanes[82,86] and polyester/HAp composites[87].

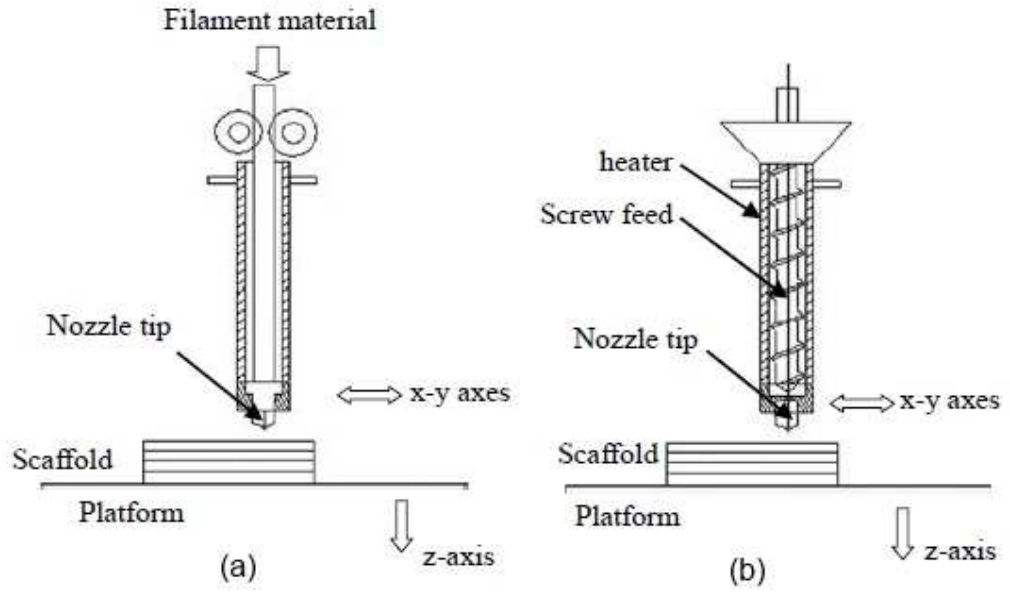

Figure 6: Graphical illustration of (a) the conventional fused deposition modeling (FDM) system and (b) the screw extrusion system or 3D plotting.[46]

The main difference between 3D plotting and FDM is that FDM uses a coiled filament as precursor material and 3D plotting uses the raw (granulate, powder or even regrind) polymer. This results in some distinct advantages for 3D plotting compared to FDM, which are:

(i) There is no need for the polymer to be supplied in a filament shape, something which requires a separate extrusion procedure prior to actual processing on the FDM device. Therefore:
   a. The thermo-mechanical load on the polymer, which is induced by this first extrusion is avoided;
   b. There is no dependency on the limited number of commercially available material types for the precursor filaments. Any thermoplastic polymer can be processed;

(ii) In 3D plotting, the size of the plotted filaments (and subsequently, the layer thickness) is not restricted by the dimensions of the precursor filament used.[88]

Furthermore, the major advantages of extrusion based systems compared to material solidification techniques (such as SLA and SLS) are that:

(i) Much smaller amounts of material are required for start-up: a large amount of base material is required for both the standard SLA and SLS, while a little more

than the material required for the scaffold itself is sufficient for FDM and 3D plotting.

(ii) The technique can be used for the processing of any thermoplastic material and is not restricted to photopolymers (SLA) or the limited spectrum of polymers which are available in the appropriate powder form for SLS.[88]

Table 3: Advantages and disadvantages of common rapid prototyping techniques.[22,46,74,81,88]

Fabrication method	Advantages	Disadvantages
Stereolithography (SLA)	High-resolution and accuracy	Only photocrosslinkable resins Only possible to use a single resin at a time Post-processing Expensive material and equipment
Selective laser sintering (SLS)	Good accuracy Low material cost	Only thermostable polymers Expensive equipment Small pore size (<50µm)
3D printing	Processing at room temperature	Small pore size (<50µm)
Fused deposition modeling (FDM)	High pore interconnectivity High reproducibility	Only thermostable polymers Materials may degrade during process
3D plotting	High pore interconnectivity High reproducibility Wider variety of materials	Materials may degrade during process

3 Materials for BTE scaffold fabrication

One of the major components of a tissue engineering construct is the material used to make the scaffold. There are numerous biomaterials that have been used for the fabrication of BTE scaffolds. The material selection depends on multiple factors including the intended application of the scaffold and the processing technique to fabricate the scaffold. Among all types of biomaterials, polymers offer great potential in design and processing of scaffolds as they can be processed by some interesting scaffold fabrication techniques, such as electrospinning and 3D plotting. In addition, the implementation of biocompatible and biodegradable polymers enables the fabrication of temporary porous construct that mimics the ECM in supporting cell proliferation and organization.[41,50]

3.1 Natural polymers

Natural polymers such as polysaccharides (e.g. starch, chitosan, hyaluronic acid) and proteins (e.g. collagen, gelatin, silk), are interesting candidates for tissue engineering since they are biocompatible, promote cell attachment and stimulate the normal cellular function.[42] However, concern exists about antigenicity, toxicity and the potential risk of disease transmission. In addition, natural polymers are expensive, have weak mechanical properties and special care must be taken to prevent denaturation when proteins are used.[9,21,63,89]

3.2 Synthetic polymers

Synthetic polymers have a longer shelf-life, are producible in large-scale and are easy to handle. The most extensively used synthetic biodegradable and resorbable polymers are the Food and Drug Administration (FDA) approved aliphatic polyesters poly(glycolic acid) or polyglycolide (PGA), poly(lactic acid) or polylactide (PLA), poly(ε-caprolactone) (PCL) (Figure 7; Table 4) and their copolymers, such as poly(lactic-co-glycolic acid) (PLGA).[41,42,63,90,91] These thermoplastic polymers are easy to manufacture into different shapes and the mechanical properties and degradation kinetics can be tailored.

3.2.1 PGA

The semicrystalline (45-55% crystallinity) thermoplastic PGA has a high melting temperature (>200°C) and a high tensile strength (12.5 GPa). *In vivo* the hydrolytic degradation of PGA produces glycolic acid monomers, which are converted enzymatically into glycine or pyruvate. Glycine can be used in protein synthesis, whereas pyruvate enters the Krebs cycle yielding energy, CO_2 and water.[92] Due to its low solubility in organic solvents, lack of sufficient mechanical integrity and very fast degradation (2-4 weeks), PGA is less suitable for the fabrication of BTE scaffolds.[89]

3.2.2 PLA

PLA is more hydrophobic than PGA due to the additional methyl group in its structure (Figure 7) and thus has a slower degradation rate. This makes PLA more suitable for both *in vitro* and *in vivo* applications where long-term mechanical integrity is required. Lactic acid, a normal human metabolic by-product, is the degradation product of PLA and it is also converted to water and CO_2 in the Krebs cycle.[92] PLA exists in three isomeric forms D, L and racemic (D, L) due to the chiral nature of its monomer. PDLA and PLLA, the two stereo-regular polymers are semicrystalline and have similar physical characteristics, provided that molecular weights are comparable. PDLLA is the racemic polymer obtained from a mixture of PDLA and PLLA in a 1/1 ratio and is amorphous. For the semi-crystalline polyesters, degradation takes place preferentially in the amorphous regions because these sections exhibit a higher rate of water uptake due to the less dense, less ordered structure than the crystalline regions. In comparison with the semi-crystalline polyesters, the amorphous PDLLA degrades faster which makes it potentially useful as drug delivery system or for tissue reconstruction.[93]

3.2.3 PCL

PCL is the most widely studied in the family of the aliphatic polyesters. PCL is a semicrystalline (crystallinity 45 – 67%) polymer with a low melting temperature (55 – 60°C) (Figure 7; Table 4). Since PCL is one of the most hydrophobic polymers, it degrades much

slower than PGA and PLA which makes PCL suitable for use in tissues that have a long regeneration process.[91,94,95] Based on a large number of tests, PCL is currently regarded as non-toxic and biocompatible on both short-term and long-term in different animal models.[95,96]

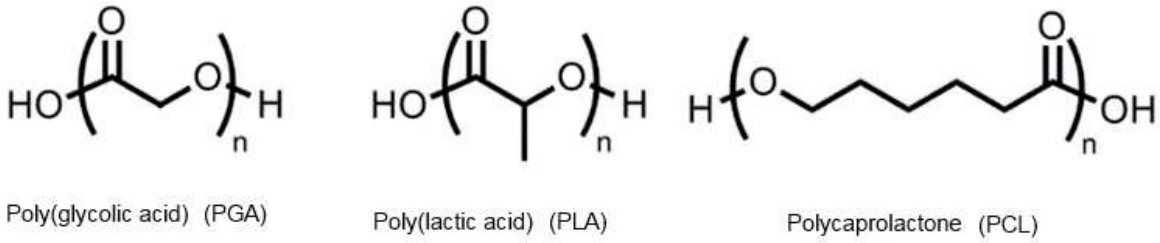

Figure 7: Structures of the biodegradable polymers

Table 4: Properties of most extensively used biodegradable polymers for BTE applications.[41,63,91,97]

Polymer	Melting temperature (T_m) (°C)	Glass transition temperature (T_g) (°C)	Lose strength (months)	Mass loss (months)*	Degradation product
PGA	225	36	1-2	6-12	glycolic acid → urine and respiration
PLLA	175	60-65	9-15	> 24	L-lactic acid → respiration and urine
PDLLA	Amorphous	55-60	1-2	12-16	D,L-lactic acid → respiration and urine
PCL	58	-72	9-12	> 24	caproic acid → urine and feces

3.2.4 Biodegradation of aliphatic polyesters

The aforementioned polyesters are hydrolytically degradable due to their hydrolytically unstable ester bonds in their backbone. In aqueous environments, their degradation mainly comprises chemical hydrolysis of the ester bonds in the polymer chain. In short, water penetrates the scaffold, preferentially attacking the chemical bonds in the amorphous phase. The long polymer chains are converted into shorter fragments of different lengths with both hydroxyl and carboxyl end groups (Figure 8). The latter are capable of catalyzing the hydrolysis of other ester bonds.

The degradation rate depends on the size of the scaffold, acidity of the environment, the amount of ester groups, copolymer ratio, crystallinity, molecular weight, porosity, incorporation of different biomaterials and site of implantation.[91]

For instance, in large compact scaffolds, the soluble degradation products close to the implant surface leach out towards the aqueous medium faster than the degradation

products located inside the bulk matrix. As a result, acids accumulate inside the matrix, accelerating the acid catalyzed degradation process in these areas (Figure 8).[24,41]

For porous scaffolds with interconnected pores, the degree of porosity and the pore size determine the degradation rate. Scaffolds with a higher porosity or a smaller pore size degrade slower than scaffolds with lower porosity or larger pore size. The effect is attributed to both a wall effect and a surface area effect because scaffolds with a lower porosity or larger pores possess thicker pore walls and smaller surface area, which depress the diffusion of acidic degradation by-products and thus results in a stronger acid-catalyzed hydrolysis.[24,98]

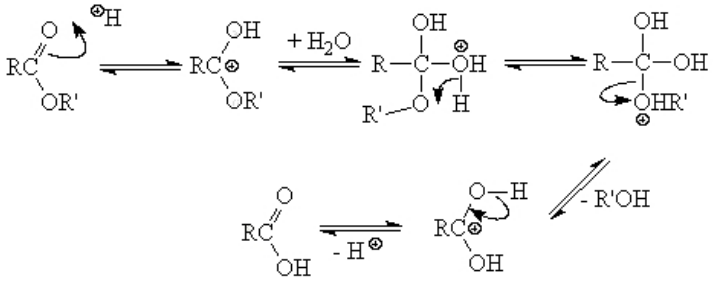

Figure 8: Acid catalyzed hydrolysis of a polyester.

3.2.5 Biomedical use of aliphatic polyesters

Both *in vitro* and *in vivo* studies have been carried out to evaluate the biocompatibility of PGA, PLA and PCL. Although many studies suggest that these polymers are sufficiently biocompatible[99,100], certain studies emphasize that the release of acidic degradation by-products, especially from PGA and PLA, can result in an inflammatory reaction around the implanted biomaterial.[63] Such response is attributed to a slow metabolism or a hampered blood flow, both resulting in a too slow elimination of the acid degradation by-products. The concomitant local pH drop can be detrimental for the surrounding tissue.[41,101]

Despite the occasional inflammation reactions, PGA, PLA, PCL and their copolymers are extensively investigated in the biomedical field. The major applications include resorbable sutures, drug delivery systems and orthopedic fixation devices.[89,102] These polyesters are also studied intensively as scaffold materials for (B)TE purposes.[42,91,96,103] However, it is widely observed that cell adhesion and subsequent bioactivity are generally low on hydrophobic materials such as PCL and, to some extent, PLA. This imposes a problem for the use of these biomaterials in tissue engineering applications. Modifications can be made to ensure that newly synthesized polymers become bioactive, for instance the addition of HAp.[9,104,105]

3.3 3D biodegradable polyester scaffolds for BTE

3.3.1 Electrospun scaffold

Electrospinning and the nanofibrous matrices thus fabricated have gained tremendous interest, mainly due to the structural similarity to the ECM, the processing availability to a wide range of biomaterials, as well as a simple set-up (Figure 5) and operation at low cost. In BTE, the electrospun nanofibers have also attracted considerable attention aimed at identifying suitable biomaterials and exploiting them into electrospinning.

In literature, numerous reviews are available on the electrospinning of biodegradable polyester scaffolds.[9,60,106-109] Table 5 represents a small selection of the most recent studies published on electrospun polyester scaffolds. It is clear that PCL, PLA, PGA and their co-polymers have been studied extensively. Earlier studies mainly focused on the optimization of the electrospinning process, in which various polymer solution properties (polymer concentration and solvent system) and processing parameters were investigated for polyesters such as PGA[62], PLGA[110], PLA[111-113] and PCL[108,114]. As can be seen in table 5, more recent studies investigate the BTE scaffold potential of electrospun scaffolds by means of *in vitro* cell viability, proliferation and differentiation studies. Several studies showed a higher osteoblastic cell attachment and enhanced osteogenic differentiation on electrospun matrices compared to solid films.[115-117] However, in most cases cell adhesion, proliferation and differentiation is still low on electrospun samples compared to a positive control (Table 5).[118-122] This could be explained by the hydrophobic nature of most polyesters and lack of functional groups. In addition, as the pore diameters of electrospun samples are very small (< 100 nm), cells are not able to infiltrate into the interior of the scaffold leading to the formation of a monolayer of cells on the scaffold surface rather than a 3D cellular construct (Table 5).[58,64,109,123,124]

Table 5: A small selection of literature on electrospun biodegradable polymer scaffolds for BTE purposes.

Polymer	Solvent	Fiber diameter	Application	Results	Ref
PCL	Acetone	2.34 µm	*In vitro* culture of MC3T3-E1 pre-osteoblasts	Hydrophobic surface and lack of functional groups: no good substrate for cell adhesion	118
PCL	Chloroform/DMF (70/30)	n.a.	*In vitro* culture of Saos-2 cells and MG63 cells	Cell attachment and proliferation low compared to positive control	119,120
PCL	MC/DMF (80/20)	418±164 nm	*In vitro* culture of Vero cells	Lack of cell infiltration due to the small pore diameters of the pores of nanofibrous scaffold (< 10 µm)	125
PLGA (85/15)	HFIP	1.4 µm	• *In vitro* culture of MC3T3-E1 pre-osteoblasts • *In vitro* differentiation of rat MSCs	• Low cell attachment, spreading and proliferation • Low osteogenic differentiation and calcium deposition	121
PLA (95DL/5L)	TFE	1.09 µm	*In vitro* culture of HDF cells	Low cell proliferation due to lack of surface functional groups	122
PDLLA	HFIP	850 nm	*In vitro* cell infiltration study of 3T3/NIH fibroblasts	Cells are unable to infiltrate the electrospun scaffolds due to small pore size (17 µm)	124

HFIP: 1,1,1,3,3,3-hexafluoro-2-propanol; MC: methylene chloride; DMF: dimethylformamide; TFE: 2,2,2-trifluoroethanol

3.3.2 3D plotted scaffolds

Among the available RP techniques, 3D plotting is the most advanced scaffold fabrication techniques due to its milder operation conditions, ability of using different biomaterials, possibility of manufacturing scaffolds in a cell-friendly environment, and feasibility of controlled drop-on demand high precision deposition.[82,84] Thus, 3D plotting appears to be a very appropriate method for producing BTE scaffolds.

3D plotted biodegradable scaffolds for BTE purposes, which are investigated in literature, are given in Table 6. Due to its superior thermostability in molten state (Table 4), PCL is the preferred and most studied thermoplastic polyester for 3D plotting.

Son *et al*.[125] and Lee *et al*.[126] compared the mechanical properties of conventional PCL scaffolds fabricated by a salt-leaching process and PCL scaffolds manufactured by the 3D plotting process and showed that the latter have superior mechanical properties.

In 3D plotting, the filament diameter (FD; Figure 9), which depends on the inner diameter of the mounted nozzle tip, and the strand distance (SD; Figure 9) are adjustable. By setting the SD, the scaffold porosity can be regulated. The pore geometry can be varied by changing the deposition angle between adjacent layers. The simplest scaffold has cube-cube shaped pores formed by orthogonal rasters in the 0°/90° lay-down pattern (Figure 10A). Upon introducing an angle shift between each layer, scaffolds with so-called honeycomb-like patterns are created. Figure 10B and 10C illustrate examples of a 60° and a 45° stacking sequence, respectively. The stacking sequence refers to the pattern angle shift between each layer.[88,127]

A number of *in vitro* studies showed that the large porous structure of 3D plotted scaffolds enables the migration of cells through the construct with cell adhesion and proliferation throughout the whole scaffold (Table 6).[85,126,128,129] These large pores (> 50 µm) could also facilitate diffusion of nutrients during *in vitro* culture. However, the study of Yilgor *et al*.[84] reported an important relation between the lay-down pattern of the filaments and the cell seeding efficiency and proliferation. The lowest cell seeding efficiency and proliferation was obtained on the 0/90° design. This could be attributed to the scaffold open channels and the relatively large pore sizes, which increases the likelihood of cells passing the scaffold. In addition, it is reported that cells attached to neighboring filaments are hardly able to interact with each other due to the large interfilament distance of hundreds of micrometers, causing limited bridging between cells.[68,130,131] Yilgor *et al*.[84] found that scaffolds with a 0/45° design resulted in significantly higher cell attachment and proliferation. This was explained by the fact that the PCL fibers act as obstacles to cell suspension flow and higher available fiber surface area for cells to attach to.

However, irrespective of the specific scaffold architecture, the pore size of 3D plotted scaffolds is relatively large as compared to the dimensions of a cell. This, in combination with the smooth nature of the filaments and the hydrophobic nature of PCL, tends to hinder initial cell attachment.[130,132] Therefore, a high number of cells is needed to obtain sufficient attached cells that produce enough ECM to successfully engineer a 3D tissue construct.

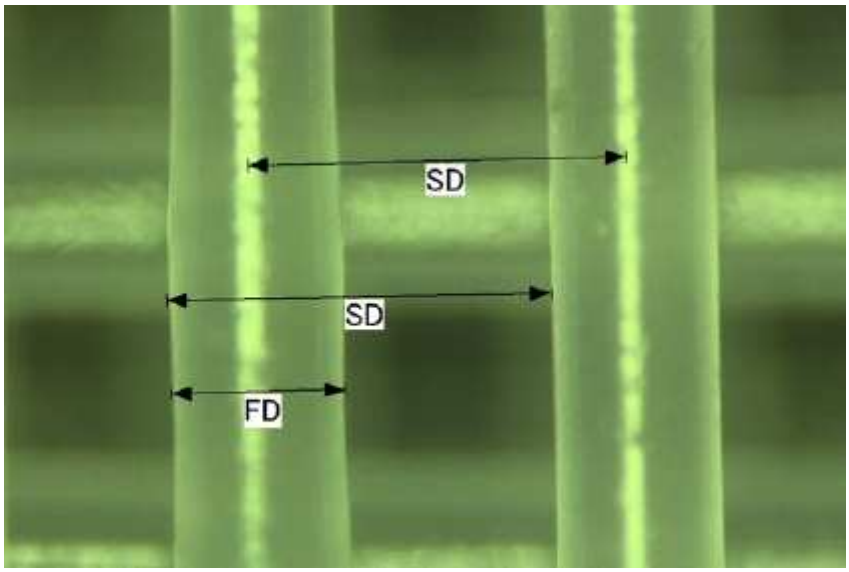

Figure 9: Illustration of the concepts filament diameter (FD) and strand distance (SD) in a 3D plotted scaffold.[66]

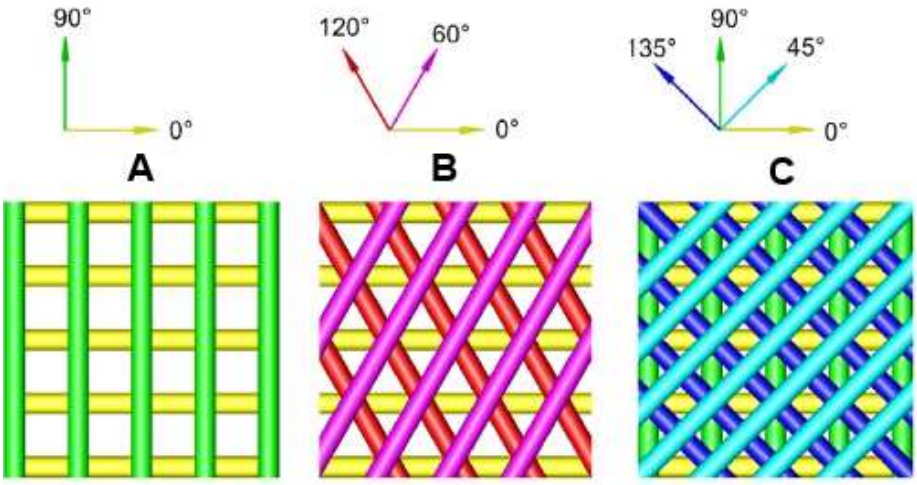

Figure 10: Some examples of lay-down patterns of 3D plotted scaffolds. A) 0°/90°, B) 0°/60°/120° and C) 0°/45°/90°/135° or 0°/45°/90°/-45°.[127]

Table 6: Literature on 3D plotted biodegradable polymer scaffolds for bone tissue engineering purposes.

Polymer	Lay-down pattern	Filament diameter	Strand distance	Application	Results	Ref
PCL	0/90°	200 µm 250 µm 330 µm	300 µm 500 µm 700 µm	• Mechanical testing • *In vitro* culture of porcine derived chondrocytes	• Compressive modulus of scaffolds with lowest strand distance is the highest. Compressive modulus of 3D plotted scaffolds is 20-50 times higher than that of salt-leached scaffolds. • Higher migration and attachment through the interconnected scaffold compared to salt-leached PCL scaffold	126
PCL	0/90° 0/45°	n.a.	n.a.	*In vitro* culture of rat MSCs	0/45° scaffolds show higher cell proliferation than 0/90° scaffolds	84
PCL	0/90°	200 µm	900 µm	*In vitro* culture of human MSCs	Cells only adhered to and grew on the strands of the scaffolds but did not fill the pores.	128
PCL	0/90°	300 µm	200 µm	*In vitro* culture of D11 mouse MSCs	Cells are located across the entire surface of the scaffold.	85
PCL	0/90°	300 µm	200 µm	*In vitro* culture of MC3T3-E1 pre-osteobalsts	Low initial cell adhesion, but complete colonization of the scaffold after 14 days of culture.	129

3.3.3 Multiscale scaffolds

In order to overcome the limitations of both electrospinning and 3D plotting, multiscale scaffolds fabricated by a combination of RP and electrospinning are very recently being investigated. A combination of nanofibers and microfibers is a promising approach to attempt to mimic the hierarchical tissue structure of bone. In these multiscale scaffolds, the microfibrous structure provides the porous 3D structural environment with a porous structure large enough for the migration of cells through the construct, while the nanofibers provide the favorable surface topography with nanoscale features for cell attachment and cell viability.[90,130,131,133-135] An overview of the recent literature on multiscale scaffold research is summarized in Table 7.

Pham *et al.*[136] were one of the first to develop a bimodal scaffold. These scaffolds were developed by a sequential electrospinning technique wherein the multiscale PCL layers were electrospun with different fiber diameters. The scaffolds consisted of a top layer of nanofibers and a bottom microfiber layer. The extent of nanofiber deposition was evaluated as a function of the duration of electrospinning. Electrospinning for longer periods resulted in an increased thickness of the nanofibrous top-layer. Hence, the thickness and coverage of the nanofibrous layer could be controlled by modulating the electrospinning time. An *in vitro* cell culture study with rat MSCs showed that cell attachment at different time intervals was similar, whereas cell spreading, proliferation and differentiation were affected by the presence of nanofibers. However, the presence of nanofibers was also found to hinder cell migration. This could be due to the nanofibrous layers which were formed in a sheet-like structure around the microfibrous structure and prevented the cells from infiltrating adequately into the scaffold.

In order to overcome the shielding effect of a nanofibrous outer layer, later studies fabricated multiscale scaffolds with randomly mixed nanofibers and microfibers[137,138], successive layers of nanofibers and microfibers[130] or more centrally positioned nanofibers[132,133,135]. These studies showed enhanced adhesion, proliferation and spreading of chondrocytes[130,134,135], MSCs[134] and pre-osteoblastic cells[131] on the multiscale polyester scaffolds compared to scaffolds built up by either nanofibers or microfibers alone. The interaction between the cells and the hybrid scaffold were improved as the cells were able to colonize the interfilament gap due to the presence of a nanofibrous layer between the microfibers. The multiscale scaffolds also showed a higher amount of cells distributed throughout the scaffold.

However, the initial problem with the hydrophobicity of the polyesters remains. In order to enhance the bioactivity of all polyester scaffolds, a surface modification, such as a calcium phosphate coating, can be applied.

Table 7: An overview of multiscale scaffold research in literature.

Material		Technique Fiber diameter		Scaffold Architecture	Application	Multiscale scaffold improvement compared to MF fiber	Ref
MF	NF	MF	NF				
PCL	PCL	ES 5 µm	ES 610±120 nm	Bilayered: Top NF, bottom MF	*In vitro* culture of rat MSCs	Cell attachment = Cell spreading ↑ Cell infiltration ↓	136
PCL	PCL	BP 260 µm	ES 700-3000 nm	Successive layers	*In vitro* culture of porcine chondrocytes	Initial cell attachment ↑ Cell spreading ↑	130
PCL	PCL	FDM 350 µm	ES 431±148 nm	NF layer in-between two MF layers	*In vitro* culture of bovine chondrocytes	Cell adhesion ↑ Cell proliferation ↑	135
PCL	PCL	ES 8-10 µm	ES 200-300 nm	random	• Focus on effect of plasma treatment • *In vitro* culture of hMSCs	• Plasma treatment: spreading, elongation and proliferation ↑ • Multiscale scaffold: cumulative effect on cell responsiveness	137
PCL	PLLA	BP 300µm	ES ± 1µm	10 NF mats in between 22 MF layers	• Cytotoxicity mouse cell line L929 • Mechanical strength	• No toxic effects from the fabrication process • Multiscale scaffold is less stiff	132
PCL	PLLA	FDM 300 µm	ES 450±150 nm	tubular NF scaffold armored in the outer wall with a MF coil	*In vitro* culture of human MSCs	Initial cell attachment ↑ Cell spreading ↑	133

Material		Technique Fiber diameter		Scaffold Architecture	Application	Multiscale scaffold improvement compared to MF fiber	Ref
MF	NF	MF	NF				
PCL	PLGA	BP 365±18µm	ES ± 1µm	NF on top of 3D MF scaffold	*In vitro* culture of MC3T3 pre-osteoblast	Cell viability ↑ Cell adhesion ↑ Cell infiltration ↑	131
PLGA	PLGA	Melt ES 28±3 µm	ES 530±240 nm	random	• *In vitro* culture of NHEK and NHEF • Tensile properties	• Cell adhesion ↑ Cell spreading ↑ Cell infiltration ↑ • Tensile strength ↑	138

MF: Microfibers; NF: Nanofibers; ES: Electrospinning; BP: Bioplotting; NHEK: Normal human epidermal keratinocytes; NHEF: Normal human epidermal fibroblasts

4 Bioactivation of polymer scaffolds

Although several biodegradable synthetic polymers have been used as tissue engineering scaffolding materials, a shortcoming of these biomaterials is their lack of biological recognition.[9] In recent years biomaterial research has focused on the improvement of implant design features in an attempt to accelerate bone healing after implantation. Considering the surface is the first part of the implant that interacts with the host, various types of modifications have been investigated in order to enhance biocompatibility and osteoconductivity of the implant. Cellular responses to an implanted biomaterial are highly complicated biological and chemical processes related to several surface properties. It has been reported that the cell-substrate interactions are influenced by both the surface chemistry and the surface structure of the biomaterial, such as topography, roughness and architecture. These surface aspects affect cells and tissues because they modify the adsorption of proteins from biological fluids. The adsorption of proteins onto an implant surface has been shown to be one of the key events to occur within a few minutes after implantation. Furthermore, it is with these adsorbed proteins that the cells will interact because cells are not able to interact directly with the biomaterial.[139]

4.1 Apatite coating

Coating of a synthetic implant with a thin layer of calcium phosphate has been proven to be an effective, easy and convenient approach making the scaffold more bioactive, biocompatible and osteoconductive.[139-142] In general, calcium phosphates, or more accurately calcium orthophosphates, are salts of the orthophospheric acid (H_3PO_4), and thus contain $H_2PO_4^-$, HPO_4^{2-} or PO_4^{3-}. The calcium phosphate salts constitute a wide group of compounds that are described below and summarized in Table 8 and 9. Calcium phosphates come in different amorphous and crystalline forms which have different physico-chemical properties.[143]

Especially apatite is an interesting calcium phosphate for use in BTE as bone tissue itself consists of up to 70% biological apatite. Stoichiometric apatite is a group of calcium phosphate mineral with general formula $Ca_{10}(PO_4)_6OH_2$ (Table 8). However, both the composition and the structure of the mineral are flexible as apatite has a strong tendency to incorporate numerous impurities. Such substitutions can change the crystallite size and often influence mineral properties such as solubility, hardness and brittleness. The variations that may occur must fulfill the overall charge balance in the mineral and provide a geometric fit of the substituting ions within the apatite lattice. For example, Ca^{2+} can be partially substituted by cations such as Na^+, K^+, Sr^{2+} and Mg^{2+}, and PO_4^{3-} can be substituted by anionic species such as CO_3^{2-} (B-type substitution) and HPO_4^{2-}. In addition, OH^- can also be replaced by

CO_3^{2-} (A-type substitution). The replacement of PO_4^{3-} by either CO_3^{2-} or HPO_4^{2-} causes the creation of a deficit in negative charge, which can be compensated by the loss of positive charge, as through removal of Ca^{2+} from the lattice. As a result HPO_4^{2-} containing apatites are calcium-deficient, with a Ca/P ratio smaller than 1.67 (Table 8). With regard to stoichiometry, the substitution by CO_3^{2-} creates lacuna in the crystals and affects the lattice parameters. The crystal size is decreased, and thereby the surface area is increased. In addition, Ca-CO_3^{2-} bonds are weaker than Ca-PO_4^{3-} bonds, which results in a higher solubility than carbonate-free apatites. [6,144,145]

Biological trials in which MC3T3-E1[146-150], SaOS-2[120] and MSCs[85] were seeded on apatite coated biomaterial revealed that these coatings enhance cellular adhesion, proliferation and differentiation to promote bone regeneration compared to the pure scaffolds. Apatite-based coatings typically increase the ALP activity and the osteocalcin and protein levels.[139,151] Moreover, Pieters *et al*.[152] showed that apatites with a high carbonate content (> 11 wt%) support high cell adhesion and proliferation. A decrease in charge density and crystallinity at the apatite surface, as well as the formation of more spheroidal crystals with increasing carbonate content might attribute to changes in composition and three-dimensional structure of the protein adsorption layer and hence the observed cell behavior.

Table 8: Possible stoichiometry for apatitic calcium phosphates [6,145]

Chemical formula	Name	Ca/P ratio
$Ca_{10}(PO_4)_6(OH)_2$	hydroxyapatite	1.67
$Ca_{10}(PO_4)_6(OH)_{2-2x}(CO_3)_x$	A-type carbonated apatite	1.67
$Ca_{10-x}[(PO_4)_{6-2x}(CO_3)_{2x}](OH)_2$	B-type carbonated apatite	≥ 1.67
$Ca_{10-x}[(PO_4)_{6-2x}(CO_3)_{2x}](OH)_{2-2y}(CO_3)_y$ with $0 \leq x \leq 1.1$ and $0 \leq y \leq 0.2$	AB-type carbonated apatite	≥ 1.67
$Ca_{10-x}[(PO_4)_{6-x}(HPO_4)_x](OH)_{2-x}$	Calcium deficient apatite	≤ 1.67

After implantation the implant surface is in direct contact with the surrounding physiological fluid, which contains numerous ions and proteins that guide the adhesion of particular cell types to the surface. One of the first events to occur upon contact of an apatite coating with body fluid, is its physiological dissolution or active resorption, which is believed to be at the origin of the bioactivity and osteoconductivity of apatite.[143,153] Schematically, the process of osteoconduction induced by a calcium phosphate coating such as apatite on a biomaterial after implantation into bone tissue is shown in figure 11. Active resorption is the result of the cellular activity of osteoclasts. These cells decrease the pH of their surroundings

to about 5.5 so that the dissolution rate of the apatite is decreased. Partial dissolution of apatite results in the release of Ca^{2+} and PO_4^{3-} ions. This dissolution is followed by the reprecipitation of a biological apatite layer with the adsorption of proteins. The increased concentrations of Ca^{2+} and PO_4^{3-} ions also stimulate chemotaxis. As a result cells like osteoprogenitor cells, osteoclasts and osteoblasts colonize the biomaterial.[139,143,144]

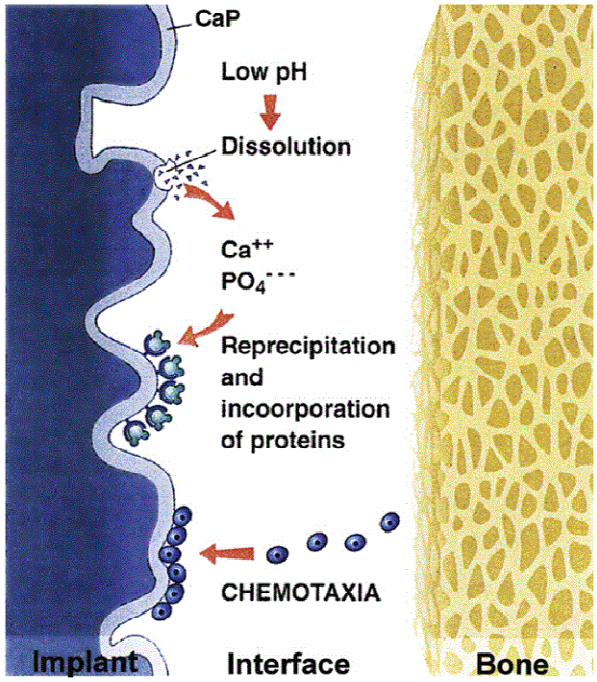

Figure 11: Schematic representation of osteoconduction induced by a calcium phosphate coating.[154]

The degree of crystallinity and the specific surface area of the apatite coating affect the physico-chemical dissolution *in vitro* and hence the cellular activity.[143,155,156] Several studies have shown that there is no new bone formation on highly crystalline calcium phosphates, but bone regeneration has been observed on poorly crystalline calcium phosphates. Hence the use of poorly crystalline apatites should increase the bioactivity, which in turn could lead to a faster establishment of a strong bond between the implant and surrounding tissue.[140]

Besides the positive effects on a cellular level, mineralization of a polyester scaffold has additional advantageous effects for tissue engineering. Multiple studies found that the addition of a mineral coating improves the mechanical strength of the scaffold.[106,157] In addition, the presence of a mineral phase can, due to the alkalinity of calcium phosphates, neutralize the acidic degradation by-products of the commonly used degradable

polyesters.[158,159] The latter is ascribed to the reaction of calcium ions and the carboxyl end-groups generated during degradation of the polymer, to form calcium carboxylate chain ends. This complexation results in an increased solubility of the calcium phosphate, causing an increase of the pH. As a result the acidic autocatalytic degradation of the polymer is slowed down, so that the risk of inflammation is reduced. [41]

4.1.1 Other calcium phosphates of biological interest

Octacalcium phosphate (OCP; $Ca_8(HPO_4)_2(PO_4)_4.5H_2O$; Table 9) is often found as an unstable transient intermediate during the precipitation of a thermodynamically more stable hydroxyapatite and biological apatite. Structurally OCP consists of alternating “apatite layers” (arrangements of calcium and phosphate groups similar to that of apatite) and “hydrated layers” (water molecules). The close relationship between hydroxyapatite and OCP has been used to explain the incorporation of impurities, particularly carbonate, magnesium and sodium ions.[160,161]

Dicalcium phosphate dihydrate or brushite (DCPD; $CaHPO_4.2H_2O$ (correct IUPAC name is calcium hydrogen phosphate dihydrate); Table 9) can be easily crystallized from aqueous solutions. It is one of the most soluble calcium phosphates and is the most stable at a pH of 5. DCPD has been proposed as an intermediate in both bone mineralization and dental erosion. In medicine, DCPD is used in calcium phosphate cements.[161]

Amorphous calcium phosphates (ACP; $Ca_xH_y(PO_4)_z.nH_2O$, n = 3 - 4.5; 15 - 20% H_20; Table 9) vary widely in composition due to the possible insertion of several secondary ions. Usually, ACP is the first phase to precipitate from a supersaturated solution prepared by rapid mixing of solutions containing calcium and phosphate ions. It is thought to be formed at the beginning of precipitation due to the lower surface energy than that of OCP and apatites. ACP is a transient phase during the formation of calcium phosphates in aqueous systems. Its lifetime was reported to be as a function of the presence of additive ions, pH, ionic strength and temperature. Also, the chemical composition of ACP strongly depends on the pH of the solution and the concentrations of the mixing solutions. As for all amorphous compounds, ACP is characterized by broad X-ray diffraction bumps, which makes it hard to analyze its crystal structure. In medicine, pure ACP is used in calcium phosphate cements and as a filling material in dentistry.

Table 9: non-apatitic calcium phosphate phases [145]

Name	Chemical formula	pH formation	Precursor for	Typical shape	Ca/P ratio
OCP	$Ca_8(HPO_4)_2(PO_4)_4.5H_2O$	5-6	hydroxyapatite	-	1.33
DCPD Brushite	$CaHPO_4.2H_2O$	4-5	hydroxyapatite	Large plates	1
ACP	$Ca_xH_y(PO_4)_z.nH_2O$	All	various crystalline phases	Beads	1.5

Recently, calcium phosphates have been found to induce bone formation when implanted in ectopic sites such as muscles of dogs[162,163], mice[164] and rabbits[165] which could indicate osteoinductivity of calcium phosphates. The exact mechanism behind osteoinduction is incompletely understood. Indications and hypotheses exist identifying surface features, including microporosity and grain size, as well as dissolution/reprecipitation events occurring on the surface, as properties responsible for the osteoinductive potential.[162,165,166]

4.2 Incubation in simulated body fluid

A well-known technique for the coating of polymer scaffolds with an apatite layer is based on the incubation in solutions supersaturated with respect to apatite, such as simulated body fluid (SBF).

4.2.1 SBF

SBF is a type of medium with ion concentrations approximating those of human blood plasma (HBP). Since the introduction of SBF by Kokubo *et al.* the biomimetic mineral formation has attracted extensive research interest as it is similar to biological mineralization in bone.[167-169] The original SBF used by Kokubo *et al*.[170] lacks SO_4^{2-} ions present in HBP (Table 10). The composition of the SBF was corrected by Kokubo *et al*.[171] and since then the corrected SBF (c-SBF) has been used as SBF by many researchers. However, as the corrected SBF was still richer in Cl^- ions and poorer in HCO_3^- ions than HBP, Oyane *et al.*[172] prepared a revised SBF (r-SBF) in which the concentration of Cl^--ions and HCO_3^--ions are equal to the concentrations in HBP. In this r-SBF however, calcite has a strong tendency to precipitate. Hence, a newly improved SBF (n-SBF) was proposed in which only the Cl^- ion concentration was decreased to that of HBP, leaving the HCO_3^- concentration equal to that of c-SBF.[167] Several tests on both the c-SBF and n-SBF concluded that c-SBF does not differ from n-SBF in stability and reproducibility. As a result, c-SBF is predominantly used in research. The detailed description for the preparation of this c-SBF or simply SBF with pH 7.4 at 36.5°C is described by Kokubo *et al*.[167]. Generally, in order to maintain the pH of the solution at the physiological pH of 7.4, SBF is buffered with a mixture of trishydroxymethylaminomethane (TRIS; $(CH_2OH)_3CNH_2$) and HCl. Under these physiological conditions of pH and temperature, SBF is supersaturated with respect to apatite.

Table 10: Ion concentrations of human blood plasma (HBP) and different SBFs described in literature.

	Ion concentration (mM)								Buffer
Ion solution	**Na^+**	**K^+**	**Mg^{2+}**	**Ca^{2+}**	**Cl^-**	**HCO_3^-**	**HPO_4^{2-}**	**SO_4^{2-}**	
HBP	142	5	1.5	2.5	103	27	1	0.5	
Original SBF	142	5	1.5	2.5	148.8	4.2	1	-	TRIS/HCl
Corrected SBF (c-SBF)	**142**	**5**	**1.5**	**2.5**	**147.8**	**4.2**	**1**	**0.5**	TRIS/HCl
Revised SBF (r-SBF)	142	5	1.5	2.5	103	27	1	0.5	TRIS/HCl
Newly improved SBF (n-SBF)	142	5	1.5	2.5	103	4.2	1	0.5	TRIS/HCl

Research involving SBF focuses on three main areas: the precipitation of bioactive calcium phosphate in SBF solutions [173,174], the coating of potential bone implants with a calcium phosphate coating [168,169] and the assessment of bioactivity of implants [167]. For the first two research areas the compositions of the SBFs vary and are often denoted by a multiplier such as 1.5xSBF[120], 5xSBF[175] and even 10xSBF[146,176,177], indicating the concentration of components relative to normal SBF. The specific composition and concentration of the SBF, but also the temperature, agitation and renovation used for mineral formation have been shown to influence the chemical composition and morphology of the resultant mineral phase.[178,179] For the utility of mineralization in SBF as a marker of *in vivo* bone bioactivity it was found that only mineralization in normal SBF correlated well to *in vivo* bioactivity.[167,178]

4.2.2 Coating

As SBF is supersaturated with respect to apatite under physiological conditions of pH and temperature, immersion of a substrate will result in the heterogeneous nucleation of apatite onto the surface, which grows overtime and covers the substrate homogenously. The ease of fabrication, the low cost and effectiveness, makes this method one of the most popular for creating a bioactive calcium phosphate coating.

There is a considerable amount of published work using the biomimetic route for the formation of calcium phosphate layers on the surface of different biomaterials. To enable the calcium phosphate formation on hydrophobic polymer scaffolds, it is necessary to form certain functional groups on the scaffold surface.[106] Surface charge influences the heterogeneous nucleation of calcium phosphate from SBF. It has been shown that negatively charged groups are favorable for the nucleation of calcium phosphates, whereas positively charged substrates do not induce the deposition of calcium phosphates under similar conditions.[180] Hence, the production of anionic surface groups onto the polymer backbone,

the so-called activation of the fiber surface, is a common approach to induce mineralization of polymer scaffolds.[178] In addition, the creation of functional groups on the surface will also increase the wettability of the substrate. In order to introduce these functional groups, a chemical activation can be used such as plasma treatment[177,181,182] and surface hydrolysis[119,157,183,184]. The mechanism of alkali surface hydrolysis is shown in figure 12. During this activation step, the ester bonds in the polyester backbone are broken with formation of reactive carboxyl – and hydroxylgroups. The mechanism of calcium phosphate deposition upon SBF immersion of the activated substrate is based on the interaction of the calcium ions present in the solution with the anionic functional groups on the polymer surface, followed by the binding of phosphate ions.

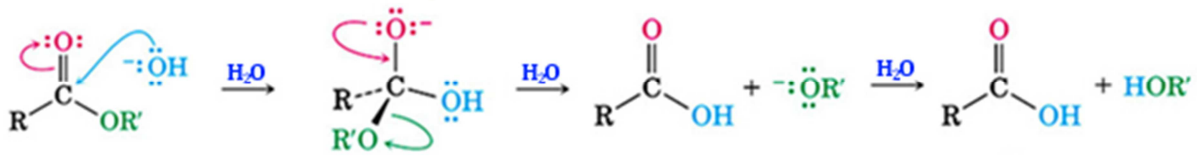

Figure 12: Hydrolysis of the ester bond in alkali medium with the formation of reactive hydroxyl – and carboxylgroups.

Additionally, the use of more concentrated SBF solutions accelerates the mineralization process, whereas the chemical composition and morphology of the deposited mineral phase can be adapted by varying the specific formulation of the SBF solution.[178,185] For instance,

(i) The pH of the solution is known to affect the apatite formation kinetics in the SBF solution, so that an apatite coating only forms when the SBF is within a critical pH range.[186,187] Chou *et al.* showed apatite crystals formed in SBF with pH 6.5 were smaller than the apatite crystals formed in SBF with pH 5.8.[188]

(ii) Qu *et al.*[187] studied the effect of the immersion temperature of the solution on biomimetic coating formation. At higher temperatures, a lower amount of carbonate/bicarbonate ions remained in the SBF solutions as the decomposition rate of bicarbonate is increased. It was reported that the decomposition of bicarbonate ions increases the pH of the solution ($HCO_3^- \rightarrow CO_2 + OH^-$).

(iii) The concentration of specific ions like CO_3^{2-} and Mg^{2+} ions, which are known to inhibit apatite crystal growth, have a great influence on the crystallinity and surface morphology of apatite coatings.[175,187]

4.3 Alternate soaking in calcium and phosphate- rich solutions

Immersing polymer scaffolds in alternating calcium and phosphate rich solutions is another method of creating a biomimetic calcium phosphate coating. [69,182,189,190] The schematic representation of the alternate dipping procedure is shown in figure 13. Just like with the incubation in SBF, the surface of the polymer has to be functionalized with anionic functional groups prior to the alternate soaking treatment. The coating mechanism is similar to that of coating in SBF solutions. It has been suggested that the alternate soaking procedure is more effective to induce a calcium phosphate coating, probably due to the introduction of larger amounts of calcium and phosphate ions in the highly concentrated solutions.[106] Nucleation is initiated as large amounts of calcium ions are introduced to the anionic functional groups present on the polymer surface, which allows for mineral growth.

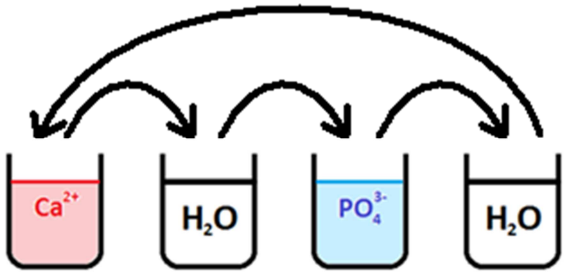

Figure 13: Schematic representation of the alternate dipping procedure.

For this method, the calcium solution typically consists of $CaCl_2$ [120,147,182,190] and the phosphate solution typically used is K_2HPO_4 [120,182] or Na_2HPO_4 [147,190].

Often, the alternate dipping procedure is applied prior to the incubation in SBF, as it was shown that the calcium phosphate nuclei deposited during the alternate dipping procedure enhance and accelerate calcium phosphate coating upon subsequent incubation in SBF.[119,147,183]

4.4 Biomimetic calcium phosphate coating on biodegradable polyester

4.4.1 Electrospun scaffolds

A selection of electrospun polymer scaffolds coated with a calcium phosphate layer by an alternate soaking treatment (nucleation) and/or incubation in a SBF solution (maturation) studied in literature are summarized in Table 11.

Introduction

Focusing on the fabrication of BTE scaffolds, the most commonly electrospun polymers are PCL[119,146,147,177,191-193] and PLA (both PDLLA[149,194] and PLLA[195]). In some cases, PLA is co-electrospun with the hydrophilic polymer gelatin in order to overcome the hydrophobic nature of the polyester.[196,197] However, due to the weak mechanical properties of gelatin, co-electrospun scaffolds show reduced mechanical properties compared to pure polyester scaffolds.[198]

Coating of the electrospun scaffolds is generally achieved in several consecutive steps. In most studies the first step is the activation of the fiber surface with plasma[177] or NaOH treatment[119,147,191-193,195]. Various NaOH concentration and incubation times are used. In the studies of Vaquette *et al*.[193], Zou *et al*.[194] and Cui *et al*.[199], the samples are first treated with ethanol. Since ethanol is a well-known wetting medium of polyesters, it can be applied to enhance the wettability of the scaffolds.[200,201]

After activation of the fiber surface, mineralization of the electrospun fibers is achieved either by alternate dipping in calcium – and phosphate rich solutions[197], by incubation in a SBF solution[177,193-195,199], or by a combination of both procedures[147,191,192]. There is a great variation in the applied concentrations, the duration of each treatment and the number of cycles of the alternate dipping procedure between different studies. Regardless of the conditions of the activation and nucleation step, the mineralization treatment results in the deposition of ACP[149,119,192,194,] or semi-crystalline HAp[147,191,197] with a low carbonate content of about 3 wt%. In the study of Yu *et al*.[147,191] rat MSCs and MC3T3 pre-osteoblast cells showed enhanced adhesion, spreading and growth on the surface-mineralized electrospun PCL scaffolds compared to untreated scaffolds.

When highly concentrated SBF solutions are used, such as 5xSBF[196] or 10xSBF[177,146,193], the calcium phosphate deposition is accelerated. However, a DCPD coating is deposited onto the fiber surface and bone cells showed a lower cell adhesion on DCPD compared to apatites.[156]

It is clear that there is a great variety in the mineralization parameters reported in literature, even for the same type of polyester. The mineralization parameters not only influence the composition and the morphology of the deposited calcium phosphate layer, but also the reproducibility of the procedure. Moreover, the scanning electron microscope (SEM) images of the electrospun samples show fibers with a broad diameter distribution, indicating the electrospinning process was not optimized.

As there is no general protocol for the calcium phosphate coating of electrospun polyester scaffolds, there is a strong need for the optimization of the procedure for every type of polyester.

Table 11: Selection of electrospun polyester scaffolds coated with a calcium phosphate layer investigated in the literature.

Material	Fiber diameter	Activation		Nucleation		Maturation		CP phase	Ref
		Medium	Conditions	Medium	Conditions	Medium	Conditions		
PCL	1.5 µm	Argon plasma	10 min	-	-	10xSBF	RT 2-6 h	DCPD	177
PCL	792±345 nm	2 N NaOH	12h	150 mM $CaCl_2$ 150 mM Na_2HPO_4	30 s 30 s } 6x	SBF	37°C Up to 21 d	HAp	147,191
PCL	250 nm - 2.5 µm	0.5 M NaOH	12h	100 mM $CaCl_2$ 100 mM $K_2HPO_4.3H_2O$	1 d 15 min	1.5xSBF	37°C Up to 7 d	ACP	192,119
PCL	±15 µm	Ethanol 2 M NaOH	10 min 5 min	-	-	10xSBF	37°C 1 h	DCPD/HAp	193
PDLLA	1.14±0.12 µm	Ethanol	Until soaked	-	-	SBF *	25°C 3 d	ACP	194,149
PLLA/ gelatin	± 1 µm	-	-	-	-	5xSBF	36.5°C	DCPD	196
PLLA/ gelatin	615 nm	-	-	500 mM $CaCl_2$ 300 mM Na_2HPO_4	30 s 30 min } 5x	-	-	HAp	197
PLLA	1070±300 nm	0.5 M NaOH	5, 10 or 30 min	-	-	SBF	37°C Up to 28 d	HAp	195

* SBF with double the concentrations of calcium and phosphate
RT: room temperature

4.4.2 Rapid prototyped scaffolds

Table 12 shows an overview of the literature on the calcium phosphate coating of polymer scaffolds produced by extrusion based rapid prototyping techniques. To date, the research on the calcium phosphate coating of 3D degradable polyester scaffolds is limited to PCL scaffolds. Due to its very good thermal stability, PCL is most suitable for use with melt processing techniques like 3D plotting and FDM. Dorj *et al.*[150] used robocasting for the fabrication of the PCL scaffold. Robocasting is also an extrusion based RP system, but it is less interesting as the material is dissolved in an organic solvent prior to extrusion. The use of toxic organic solvents requires thorough washing or solvent evaporation treatment before the use with cells.

In the study of Oliveira *et al.*[202], PCL was mixed with starch, a natural degradable polymer, prior to 3D plotting. The major common drawbacks of such blend scaffolds is the incompatibility between starch and PCL and the poor physical and mechanical properties of the blends with increased starch content.[203]

A review of the literature shows that the calcium phosphate coating of RP PCL scaffolds includes up to three consecutive steps, in analogy with the coating procedure of electrospun polyesters; activation, nucleation and maturation.

Activation of the filament surface is obtained by treatment with NaOH[150,157,183] in different concentrations and incubations times. The pre-wetting step with ethanol is only applied in the study of Oyane *et al*.[183] It should be noted that in this study, the high NaOH concentration in combination with the long incubation time could cause degradation of the biomaterial. However, no information is given on the effect of such intense activation treatment on the morphology of the PCL filaments.

Oyane *et al*.[183] and Dorj *et al*.[150] used an alternate dipping step for the nucleation of calcium phosphate particles on the filament surface. Choong *et al*.[157] and Oliveira *et al*.[202] introduced the use of sodium silicate as catalyst for the deposition of calcium phosphate. The mechanism for the growth of a calcium phosphate layer on a sodium silicate gel upon incubation in SBF was previously studied by Miyaji *et al*.[204]. In brief, a calcium phosphate layer is grown as a consequence of electrostatic interactions of negatively charged $Si\text{-}O^-$ units, formed by deprotonation of Si-OH groups, with the positively charged Ca^{2+} ions in the SBF solution. A positively charged calcium silicate layer is then formed which will interact with the negatively charged PO_4^{3-} ions in the SBF solution to form calcium phosphate.[202,204]

For the coating of 3D plotted PCL, Park *et al*.[85] simply immersed the scaffolds in a 2xSBF solution, and obtained a HAp coating after 7 days. This is in contrast with the results of Oyane *et al*.[183], who showed that the activation of the PCL surface was a prerequisite to obtain any coating upon subsequent immersion in a SBF solution.

Choong *et al*.[157] obtained a HAp coating on the scaffolds in a three-step procedure. An *in vitro* analysis showed more viable human MSCs with a higher proliferation rate within the coated scaffold than within the uncoated scaffolds. Similar results were obtained by Park *et al*.[85] with D1 mouse MSCs and by Dorj *et al*.[150] with MC3T3-E1 pre-osteoblastic cells.

Even though the coating of the PCL scaffolds is a successful approach for the improvement of the bioactivity of the scaffolds, the pores of RP scaffolds are still too large compared to the dimensions of cells, which tends to discourage initial cell attachment.

Table 12: Selection of polyester scaffolds fabricated by extrusion based rapid prototyping (RP) techniques, coated with a calcium phosphate layer investigated in the literature.

Material **RP Technique**	**Filament diameter**	**Activation**		**Nucleation**		**Maturation**		**CP phase**	**Ref**
		Medium	**Conditions**	**Medium**	**Conditions**	**Medium**	**Conditions**		
PCL **FDM**	n.a.	EtOH 5 M NaOH	30 min 48 h	200 mM $CaCl_2$ 200 mM $K_2HPO_4.3H_2O$	10 s 10 s } x3	SBF	36.5°C 24 h	HAp	183
PCL **FDM**	n.a.	5 M NaOH	8 h	Na_2SiO_3 gel	6 h	1.5xSBF	36.5°C 14 days	HAp	157
PCL **3D plotting**	300 µm	-	-	-	-	2xSBF	37°C 7 days	HAp	85
PCL **Robocasting**	245 µm	1 M NaOH	1h	150 mM $CaCl_2$ 150 mM Na_2HPO_4	x5	1.5xSBF	37°C 14 days	HAp	150
PCL/Starch 70/30 wt% **3D plotting**	500 µm	-	-	Na_2SiO_3 gel	1 h	SBF	14 days	HAp	202

References

1. Clarke B. Normal Bone Anatomy and Physiology. Clinical Journal of the American Society of Nephrology 2008;3:S131-S139.
2. Rho JY, Kuhn-Spearing L, Zioupos P. Mechanical properties and the hierarchical structure of bone. Medical Engineering & Physics 1998;20(2):92-102.
3. Elaine M, Patricia W, Jon M. Human Anatomy. Sansome, San Francisco: Pearson Benjamin Cummings; 2010.
4. Reznikov N, Shahar R, Weiner S. Bone hierarchical structure in three dimensions. Acta Biomaterialia 2014;10(9):3815-3826.
5. Currey JD. The many adaptations of bone. Journal of Biomechanics 2003;36(10):1487-1495.
6. Wopenka B, Pasteris JD. A mineralogical perspective on the apatite in bone. Materials Science & Engineering C-Biomimetic and Supramolecular Systems 2005;25(2):131-143.
7. Driessens F, Verbeeck R. Biominerals: CRC Press; 1990.
8. Boskey A. Bone mineral crystal size. Osteoporosis International 2003;14:S16-S20.
9. Holzwarth JM, Ma PX. Biomimetic nanofibrous scaffolds for bone tissue engineering. Biomaterials 2011;32(36):9622-9629.
10. Rogers K. Bone and muscle: structure, force and motion. New York: Britannica Educational Publishing; 2011.
11. Pal S. Design of artificial human joints and organs. New York: Springer; 2014. 419 p.
12. Evans FG. Mechanical properties and histology of cortical bone from younger and older men. Anatomical Record 1976;185(1):1-12.
13. Schindeler A, McDonald MM, Bokko P, Little DG. Bone remodeling during fracture repair: The cellular picture. Seminars in Cell & Developmental Biology 2008;19(5):459-466.
14. Reichert JC, Saifzadeh S, Wullschleger ME, Epari DR, Schutz MA, Duda GN, Schell H, van Griensven M, Redl H, Hutmacher DW. The challenge of establishing preclinical models for segmental bone defect research. Biomaterials 2009;30(12):2149-2163.
15. Shrivats AR, McDermott MC, Hollinger JO. Bone tissue engineering: state of the union. Drug Discovery Today 2014;19(6):781-786.
16. Murphy CM, O'Brien FJ, Little DG, Schindeler A. Cell-scaffold interactions in the bone tissue engineering triad. European Cells & Materials 2013;26:120-132.
17. Sen MK, Miclau T. Autologous iliac crest bone graft: Should it still be the gold standard for treating nonunions? Injury-International Journal of the Care of the Injured 2007;38:S75-S80.
18. Van Isacker T, Cornu O, Barbier O, Dufrane D, de Gheldere A, Delloye C. Bone autografting, allografting and banking. In: Bentley G, editor. European Surgical Orthopaedics and Traumatology. The EFORT Textbook.: Springer; 2014.
19. Singh H, Levi A. Bone grafts and bone substitute biology. Spine surgery basics: Springer; 2014.
20. Burg KJL, Porter S, Kellam JF. Biomaterial developments for bone tissue engineering. Biomaterials 2000;21(23):2347-2359.
21. Stevens MM. Biomaterials for bone tissue engineering. Materials Today 2008;11(5):18-25.
22. Stevens B, Yang YZ, MohandaS A, Stucker B, Nguyen KT. A review of materials, fabrication to enhance bone regeneration in methods, and strategies used engineered bone tissues. Journal of Biomedical Materials Research Part B-Applied Biomaterials 2008;85B(2):573-582.
23. Kanczler JM, Oreffo ROC. Osteogenesis and angiogenesis: The potential for engineering bone. European Cells & Materials 2008;15:100-114.

24. Wu SL, Liu XM, Yeung KWK, Liu CS, Yang XJ. Biomimetic porous scaffolds for bone tissue engineering. Materials Science & Engineering R-Reports 2014;80:1-36.
25. Parsons AJ, Ahmed I, Han N, Felfel R, Rudd CD. Mimicking Bone Structure and Function with Structural Composite Materials. Journal of Bionic Engineering 2010;7:S1-S10.
26. Tagil M. Bone substitutes, grafts and cement. In: Hove L, Lindau T, Holmer P, editors. Distal radius fractures: Springer; 2014.
27. Lichte P, Pape HC, Pufe T, Kobbe P, Fischer H. Scaffolds for bone healing: Concepts, materials and evidence. Injury-International Journal of the Care of the Injured 2011;42(6):569-573.
28. Chen QZ, Thouas GA. Metallic implant biomaterials. Materials Science & Engineering R-Reports 2015;87:1-57.
29. Mantripragada VP, Lecka-Czernik B, Ebraheim NA, Jayasuriya AC. An overview of recent advances in designing orthopedic and craniofacial implants. Journal of Biomedical Materials Research Part A 2013;101(11):3349-3364.
30. Langer R, Vacanti JP. Tissue Engineering. Science 1993;260(5110):920-926.
31. Honsawek S, Parkpian V. Tissue engineering for bone regeneration: stem cells and growth factors in biomaterial scaffolds. Asian Biomedicine 2007;1(3):229-238.
32. Mistry AS, Mikos AG. Tissue engineering strategies for bone regeneration. Regenerative Medicine Ii: Clinical and Preclinical Applications 2005;94:1-22.
33. Ikada Y. Challenges in tissue engineering. Journal of the Royal Society Interface 2006;3(10):589-601.
34. Nassif L, El Sabban M. Mesenchymal Stem Cells in Combination with Scaffolds for Bone Tissue Engineering. Materials 2011;4(10):1793-1804.
35. Zanetti AS, Sabliov C, Gimble JM, Hayes DJ. Human adipose-derived stem cells and three-dimensional scaffold constructs: A review of the biomaterials and models currently used for bone regeneration. Journal of Biomedical Materials Research Part B-Applied Biomaterials 2013;101B(1):187-199.
36. Moroni L, Nandakumar A, Barrere-de Groot F, van Blitterswijk CA, Habibovic P. Plug and play: combining materials and technologies to improve bone regenerative strategies. Journal of Tissue Engineering and Regenerative Medicine 2015;9(7):745-759.
37. Ko IK, Lee SJ, Atala A, Yoo JJ. In situ tissue regeneration through host stem cell recruitment. Experimental and Molecular Medicine 2013;45.
38. Amini AR, Laurencin CT, Nukavarapu SP. Bone tissue engineering: recent advances and challenges. Crit Rev Biomed Eng 2012;40(5):363-408.
39. Howard D, Buttery LD, Shakesheff KM, Roberts SJ. Tissue engineering: strategies, stem cells and scaffolds. Journal of Anatomy 2008;213(1):66-72.
40. LeGeros RZ. Properties of osteoconductive biomaterials: Calcium phosphates. Clinical Orthopaedics and Related Research 2002(395):81-98.
41. Hutmacher DW. Scaffolds in tissue engineering bone and cartilage. Biomaterials 2000;21(24):2529-2543.
42. Rezwan K, Chen QZ, Blaker JJ, Boccaccini AR. Biodegradable and bioactive porous polymer/inorganic composite scaffolds for bone tissue engineering. Biomaterials 2006;27(18):3413-3431.
43. Atala A, Lanza R. Methods of tissue engineering. USA; 2002.
44. Hutmacher DW, Cool S. Concepts of scaffold-based tissue engineering-the rationale to use solid free-form fabrication techniques. Journal of Cellular and Molecular Medicine 2007;11(4):654-669.
45. Oh SH, Park IK, Kim JM, Lee JH. In vitro and in vivo characteristics of PCL scaffolds with pore size gradient fabricated by a centrifugation method. Biomaterials 2007;28(9):1664-1671.
46. Arafat MT, Gibson I, Li X. State of the art and future direction of additive manufactured scaffolds-based bone tissue engineering. Rapid Prototyping Journal 2014;20(1):13-26.

47. Hollister SJ. Scaffold Design and Manufacturing: From Concept to Clinic. Advanced Materials 2009;21(32-33):3330-3342.
48. Rainer A, Centola M, Spadaccio C, Gherardi G, Genovese JA, Licoccia S, Trombetta M. Comparative study of different techniques for the sterilization of poly-L-lactide electrospun microfibers: effectiveness vs. material degradation. International Journal of Artificial Organs 2010;33(2):76-85.
49. Shearer H, Ellis MJ, Perera SP, Chaudhuri JB. Effects of common sterilization methods on the structure and properties of poly(D,L lactic-co-glycolic acid) scaffolds. Tissue Engineering 2006;12(10):2717-2727.
50. Liu XH, Ma PX. Polymeric scaffolds for bone tissue engineering. Annals of Biomedical Engineering 2004;32(3):477-486.
51. Dahlin RL, Kasper FK, Mikos AG. Polymeric Nanofibers in Tissue Engineering. Tissue Engineering Part B-Reviews 2011;17(5):349-364.
52. Ma PX. Biomimetic materials for tissue engineering. Advanced Drug Delivery Reviews 2008;60(2):184-198.
53. Pignatello R, editor. Advances in Biomaterials Science and Biomedical Applications. Rijeka, Croatia: InTech; 2013. 568 p.
54. Nam YS, Park TG. Porous biodegradable polymer scaffolds for tissue engineering prepared by thermally-induced phase separation. Abstracts of Papers of the American Chemical Society 1998;216:U270-U270.
55. Akbarzadeh R, Yousefi AM. Effects of processing parameters in thermally induced phase separation technique on porous architecture of scaffolds for bone tissue engineering. Journal of Biomedical Materials Research Part B-Applied Biomaterials 2014;102(6):1304-1315.
56. Yang Q, Chen L, Shen X, Tan Z. Preparation of polycaprolactone tissue engineering scaffolds by improved solvent casting/particulate leaching method. Journal of Macromolecular Science Part B-Physics 2006;45(6):1171-1181.
57. Thadavirul N, Pavasant P, Supaphol P. Development of polycaprolactone porous scaffolds by combining solvent casting, particulate leaching, and polymer leaching techniques for bone tissue engineering. Journal of Biomedical Materials Research Part A 2014;102(10):3379-3392.
58. Sill TJ, von Recum HA. Electro spinning: Applications in drug delivery and tissue engineering. Biomaterials 2008;29(13):1989-2006.
59. Lannutti J, Reneker D, Ma T, Tomasko D, Farson DF. Electrospinning for tissue engineering scaffolds. Materials Science & Engineering C-Biomimetic and Supramolecular Systems 2007;27(3):504-509.
60. Jang JH, Castano O, Kim HW. Electrospun materials as potential platforms for bone tissue engineering. Advanced Drug Delivery Reviews 2009;61(12):1065-1083.
61. Sombatmankhong K, Sanchavanakit N, Pavasant P, Supaphol P. Bone scaffolds from electrospun fiber mats of poly (3-hydroxybutyrate), poly(3-hydroxybutyrate-co-3-hydroxyvalerate) and their blend. Polymer 2007;48(5):1419-1427.
62. Li WJ, Cooper JA, Mauck RL, Tuan RS. Fabrication and characterization of six electrospun poly(alpha-hydroxy ester)-based fibrous scaffolds for tissue engineering applications. Acta Biomaterialia 2006;2(4):377-385.
63. Ozdil D, Aydin HM. Polymers for medical and tissue engineering applications. Journal of Chemical Technology and Biotechnology 2014;89(12):1793-1810.
64. Bhardwaj N, Kundu SC. Electrospinning: A fascinating fiber fabrication technique. Biotechnology Advances 2010;28(3):325-347.
65. Pham QP, Sharma U, Mikos AG. Electrospinning of polymeric nanofibers for tissue engineering applications: A review. Tissue Engineering 2006;12(5):1197-1211.
66. Ragaert K, Cardon L, Dekeyser A, Degrieck J. Machine design and processing considerations for the 3D plotting of thermoplastic scaffolds. Biofabrication 2010;2(1).
67. Zein I, Hutmacher DW, Tan KC, Teoh SH. Fused deposition modeling of novel scaffold architectures for tissue engineering applications. Biomaterials 2002;23(4):1169-1185.

68. Hutmacher DW, Schantz T, Zein I, Ng KW, Teoh SH, Tan KC. Mechanical properties and cell cultural response of polycaprolactone scaffolds designed and fabricated via fused deposition modeling. Journal of Biomedical Materials Research 2001;55(2):203-216.
69. Luickx N, Van den Vreken N, D'Oosterlinck W, Van der Schueren L, Declercq H, De Clerck K, Cornelissen M, Verbeeck R. Optimization of the activation and nucleation steps in the precipitation of a calcium phosphate primer layer on electrospun poly(ε-caprolactone). Journal of Biomedical Materials Research Part A 2015;103:511-524.
70. Peltola SM, Melchels FPW, Grijpma DW, Kellomaki M. A review of rapid prototyping techniques for tissue engineering purposes. Annals of Medicine 2008;40(4):268-280.
71. Yeong WY, Chua CK, Leong KF, Chandrasekaran M. Rapid prototyping in tissue engineering: challenges and potential. Trends in Biotechnology 2004;22(12):643-652.
72. Yang SF, Leong KF, Du ZH, Chua CK. The design of scaffolds for use in tissue engineering. Part II. Rapid prototyping techniques. Tissue Engineering 2002;8(1):1-11.
73. Ho CMB, Ng SH, Yoon YJ. A review on 3D printed bioimplants. International Journal of Precision Engineering and Manufacturing 2015;16(5):1035-1046.
74. Leong KF, Cheah CM, Chua CK. Solid freeform fabrication of three-dimensional scaffolds for engineering replacement tissues and organs. Biomaterials 2003;24(13):2363-2378.
75. Elomaa L, Teixeira S, Hakala R, Korhonen H, Grijpma DW, Seppala JV. Preparation of poly(epsilon-caprolactone)-based tissue engineering scaffolds by stereolithography. Acta Biomaterialia 2011;7(11):3850-3856.
76. Melchels FPW, Bertoldi K, Gabbrielli R, Velders AH, Feijen J, Grijpma DW. Mathematically defined tissue engineering scaffold architectures prepared by stereolithography. Biomaterials 2010;31(27):6909-6916.
77. Scalera F, Corcione CE, Montagna F, Sannino A, Maffezzoli A. Development and characterization of UV curable epoxy/hydroxyapatite suspensions for stereolithography applied to bone tissue engineering. Ceramics International 2014;40(10):15455-15462.
78. Shuai CJ, Gao CD, Nie Y, Hu HL, Zhou Y, Peng SP. Structure and properties of nano-hydroxypatite scaffolds for bone tissue engineering with a selective laser sintering system. Nanotechnology 2011;22(28):9.
79. Van Bael S, Kerckhofs G, Moesen M, Pyka G, Schrooten J, Kruth JP. Micro-CT-based improvement of geometrical and mechanical controllability of selective laser melted Ti6Al4V porous structures. Materials Science and Engineering a-Structural Materials Properties Microstructure and Processing 2011;528(24):7423-7431.
80. Williams JM, Adewunmi A, Schek RM, Flanagan CL, Krebsbach PH, Feinberg SE, Hollister SJ, Das S. Bone tissue engineering using polycaprolactone scaffolds fabricated via selective laser sintering. Biomaterials 2005;26(23):4817-4827.
81. Bose S, Vahabzadeh S, Bandyopadhyay A. Bone tissue engineering using 3D printing. Materials Today 2013;16(12):496-504.
82. Hoque ME, Chuan YL, Pashby I. Extrusion based rapid prototyping technique: An advanced platform for tissue engineering scaffold fabrication. Biopolymers 2012;97(2):83-93.
83. Turner BN, Strong R, Gold SA. A review of melt extrusion additive manufacturing processes: I. Process design and modeling. Rapid Prototyping Journal 2014;20(3):192-204.
84. Yilgor P, Sousa RA, Reis RL, Hasirci N, Hasirci V. 3D plotted PCL scaffolds for stem cell based bone tissue engineering. Macromolecular Symposia 2008;269:92-99.
85. Park SA, Lee JB, Kim YE, Kim JE, Lee JH, Shin JW, Kwon IK, Kim W. Fabrication of biomimetic PCL scaffold using rapid prototyping for bone tissue engineering. Macromolecular Research 2014;22(8):882-887.

86. Pfister A, Landers R, Laib A, Hubner U, Schmelzeisen R, Mulhaupt R. Biofunctional rapid prototyping for tissue-engineering applications: 3D bioplotting versus 3D printing. Journal of Polymer Science Part a-Polymer Chemistry 2004;42(3):624-638.
87. Park SA, Lee SH, Kim WD. Fabrication of porous polycaprolactone/hydroxyapatite (PCL/HA) blend scaffolds using a 3D plotting system for bone tissue engineering. Bioprocess and Biosystems Engineering 2011;34(4):505-513.
88. Ragaert K. Micro-extrusion of thermoplastics for 3D plotting of scaffolds for tissue engineering. Ghent: Ghent University; 2011.
89. Nair LS, Laurencin CT. Biodegradable polymers as biomaterials. Progress in Polymer Science 2007;32(8-9):762-798.
90. Srinivasan S, Jayakumar R, Chennazhi KP, Levorson EJ, Mikos AG, Nair SV. Multiscale Fibrous Scaffolds in Regenerative Medicine. In: Jayakumar R, Nair SV, editors. Biomedical Applications of Polymeric Nanofibers; 2012. p 1-20.
91. Gunatillake P, Adhikari R. Biodegradable synthetic polymers for tissue engineering. European Cells and Materials 2003;5:1-16.
92. Maurus PB, Kaeding CC. Bioabsorbable implant material review. Operative Techniques in Sports Medicine 2004;12(3):158-160.
93. Grizzi I, Garreau H, Li S, Vert M. Hydrolytic degradation of devices based on poly(DL-lactic acid) size-dependence. Biomaterials 1995;16(4):305-311.
94. Dong Y, Liao S, Ngiam M, Chan CK, Ramakrishna S. Degradation Behaviors of Electrospun Resorbable Polyester Nanofibers. Tissue Engineering Part B-Reviews 2009;15(3):333-351.
95. Lam CXF, Hutmacher DW, Schantz J-T, Woodruff MA, Teoh SH. Evaluation of polycaprolactone scaffold degradation for 6 months in vitro and in vivo. Journal of Biomedical Materials Research Part A 2009;90A(3):906-919.
96. Engelberg I, Kohn J. Physicochemical properties of degradable polymers used in medical applications - A comparative-study. Biomaterials 1991;12(3):292-304.
97. Sun HF, Mei L, Song CX, Cui XM, Wang PY. The in vivo degradation, absorption and excretion of PCL-based implant. Biomaterials 2006;27(9):1735-1740.
98. Wu LB, Ding JD. Effects of porosity and pore size on in vitro degradation of three-dimensional porous poly(D,L-lactide-co-glycolide) scaffolds for tissue engineering. Journal of Biomedical Materials Research Part A 2005;75A(4):767-777.
99. Vaquette C, Fawzi-Grancher S, Lavalle P, Frochot C, Viriot ML, Muller S, Wang X. In vitro biocompatibility of different polyester membranes. Bio-Medical Materials and Engineering 2006;16(4):S131-S136.
100. Idris SB, Danmark S, Finne-Wistrand A, Arvidson K, Albertsson AC, Bolstad AI, Mustafa K. Biocompatibility of Polyester Scaffolds with Fibroblasts and Osteoblast-like Cells for Bone Tissue Engineering. Journal of Bioactive and Compatible Polymers 2010;25(6):567-583.
101. Taylor MS, Daniels AU, Andriano KP, Heller J. Six bioabsorbable polymers: in vitro acute toxicity of accumulated degradation products. J Appl Biomater 1994;5(2):151-7.
102. Lichtens.Il. Polyglycolic acid (PGA) sutures. Journal of the American Medical Association 1970;214(4):760-&.
103. Robinson BP, Hollinger JO, Szachowicz EH, Brekke J. Calvarial bone repair with porous D,L-polylactide. Otolaryngology-Head and Neck Surgery 1995;112(6):707-713.
104. Ma PX, Zhang RY, Xiao GZ, Franceschi R. Engineering new bone tissue in vitro on highly porous poly(alpha-hydroxyl acids)/hydroxyapatite composite scaffolds. Journal of Biomedical Materials Research 2001;54(2):284-293.
105. Zhang RY, Ma PX. Poly(alpha-hydroxyl acids) hydroxyapatite porous composites for bone-tissue engineering. I. Preparation and morphology. Journal of Biomedical Materials Research 1999;44(4):446-455.
106. Katsanevakis E, Wen X, Zhang N. Creating Electrospun Nanofiber-Based Biomimetic Scaffolds for Bone Regeneration. Biomedical Applications of Polymeric Nanofibers 2012;246:63-100.

107. Cui W, Zhou Y, Chang J. Electrospun nanofibrous materials for tissue engineering and drug delivery. Science and Technology of Advanced Materials 2010;11(1).
108. Cipitria A, Skelton A, Dargaville TR, Dalton PD, Hutmacher DW. Design, fabrication and characterization of PCL electrospun scaffolds-a review. Journal of Materials Chemistry 2011;21(26):9419-9453.
109. Subbiah T, Bhat GS, Tock RW, Pararneswaran S, Ramkumar SS. Electrospinning of nanofibers. Journal of Applied Polymer Science 2005;96(2):557-569.
110. Katti DS, Robinson KW, Ko FK, Laurencin CT. Bioresorbable nanofiber-based systems for wound healing and drug delivery: Optimization of fabrication parameters. Journal of Biomedical Materials Research Part B-Applied Biomaterials 2004;70B(2):286-296.
111. Zong XH, Kim K, Fang DF, Ran SF, Hsiao BS, Chu B. Structure and process relationship of electrospun bioabsorbable nanofiber membranes. Polymer 2002;43(16):4403-4412.
112. Gu SY, Ren J. Process optimization and empirical modeling for electrospun poly(D,L-lactide) fibers using response surface methodology. Macromolecular Materials and Engineering 2005;290(11):1097-1105.
113. Cui W, Li X, Zhou S, Weng J. Investigation on process parameters of electrospinning system through orthogonal experimental design. Journal of Applied Polymer Science 2007;103(5):3105-3112.
114. Van der Schueren L, De Schoenmaker B, Kalaoglu OI, De Clerck K. An alternative solvent system for the steady state electrospinning of polycaprolactone. European Polymer Journal 2011;47(6):1256-1263.
115. Smith LA, Liu XH, Hu JA, Ma PX. The Enhancement of human embryonic stem cell osteogenic differentiation with nano-fibrous scaffolding. Biomaterials 2010;31(21):5526-5535.
116. Woo KM, Jun J-H, Chen VJ, Seo J, Baek J-H, Ryoo H-M, Kim G-S, Somerman MJ, Ma PX. Nano-fibrous scaffolding promotes osteoblast differentiation and biomineralization. Biomaterials 2007;28(2):335-343.
117. Woo KM, Chen VJ, Ma PX. Nano-fibrous scaffolding architecture selectively enhances protein adsorption contributing to cell attachment. Journal of Biomedical Materials Research Part A 2003;67A(2):531-537.
118. Ko YM, Choi DY, Jung SC, Kim BH. Characteristics of Plasma Treated Electrospun Polycaprolactone (PCL) Nanofiber Scaffold for Bone Tissue Engineering. Journal of Nanoscience and Nanotechnology 2015;15(1):192-195.
119. Araujo JV, Cunha-Reis C, Rada T, da Silva MA, Gomes ME, Yang Y, Ashammakhi N, Reis RL, El-Haj AJ, Neves NM. Dynamic Culture of Osteogenic Cells in Biomimetically Coated Poly(Caprolactone) Nanofibre Mesh Constructs. Tissue Engineering Part A 2010;16(2):557-563.
120. Araujo JV, Martins A, Leonor IB, Pinho ED, Reis RL, Neves NM. Surface controlled biomimetic coating of polycaprolactone nanofiber meshes to be used as bone extracellular matrix analogues. Journal of Biomaterials Science-Polymer Edition 2008;19(10):1261-1278.
121. Li DW, Sun HZ, Jiang LM, Zhang K, Liu WD, Zhu Y, Fangteng JZ, Shi C, Zhao L, Sun HC and others. Enhanced Biocompatibility of PLGA Nanofibers with Gelatin/Nano-Hydroxyapatite Bone Biomimetics Incorporation. Acs Applied Materials & Interfaces 2014;6(12):9402-9410.
122. Mateos-Timoneda MA, Castano O, Planell JA, Engel E. Effect of structure, topography and chemistry on fibroblast adhesion and morphology. Journal of Materials Science-Materials in Medicine 2014;25(7):1781-1787.
123. Ghasemi-Mobarakeh L, Morshed M, Karbalaie K, Fesharaki M, Nasr-Esfahani MH, Baharvand H. Electrospun poly (epsilon-caprolactone) nanofiber mat as extracellular matrix. Yakhteh 2008;10(3):179-184.
124. Leong MF, Rasheed MZ, Lim TC, Chian KS. In vitro cell infiltration and in vivo cell infiltration and vascularization in a fibrous, highly porous poly(D,L-lactide) scaffold

fabricated by cryogenic electrospinning technique. Journal of Biomedical Materials Research Part A 2009;91A(1):231-240.
125. Son J, Kim G, Park SA, Kim W. Fabrication of tailor-made 3D PCL scaffold using a bio-plotting process. Polymer-Korea 2008;32(2):163-168.
126. Lee J-H, Park S-A, Park K, Kim J-H, Kim K-S, Lee J, Kim W. Fabrication and characterization of 3D scaffold using 3D plotting system. Chinese Science Bulletin 2010;55(1):94-98.
127. Giannitelli SM, Accoto D, Trombetta M, Rainer A. Current trends in the design of scaffolds for computer-aided tissue engineering. Acta Biomaterialia 2014;10(2):580-594.
128. Seyednejad H, Gawlitta D, Dhert WJA, van Nostrum CF, Vermonden T, Hennink WE. Preparation and characterization of a three-dimensional printed scaffold based on a functionalized polyester for bone tissue engineering applications. Acta Biomaterialia 2011;7(5):1999-2006.
129. Jacobs T, Declercq H, De Geyter N, Cornelissen R, Dubruel P, Leys C, Morent R. Improved cell adhesion to flat and porous plasma-treated poly-epsilon-caprolactone samples. Surface & Coatings Technology 2013;232:447-455.
130. Kim G, Son J, Park S, Kim W. Hybrid Process for Fabricating 3D Hierarchical Scaffolds Combining Rapid Prototyping and Electrospinning. Macromolecular Rapid Communications 2008;29(19):1577-1581.
131. Mota C, Puppi D, Dinucci D, Errico C, Bartolo P, Chiellini F. Dual-Scale Polymeric Constructs as Scaffolds for Tissue Engineering. Materials 2011;4(3):527-542.
132. Ostrowska B, Jaroszewicz J, Zaczynska E, Tomaszewski W, Swieszkowski W, Kurzydlowski KJ. Evaluation of 3D hybrid microfiber/nanofiber scaffolds for bone tissue engineering. Bulletin of the Polish Academy of Sciences-Technical Sciences 2014;62(3):551-556.
133. Centola M, Rainer A, Spadaccio C, De Porcellinis S, Genovese JA, Trombetta M. Combining electrospinning and fused deposition modeling for the fabrication of a hybrid vascular graft. Biofabrication 2010;2(1).
134. Moroni L, De Wijn JR, Van Blitterswijk CA. Integrating novel technologies to fabricate smart scaffolds. Journal of Biomaterials Science-Polymer Edition 2008;19(5):543-572.
135. Park SH, Kim TG, Kim HC, Yang D-Y, Park TG. Development of dual scale scaffolds via direct polymer melt deposition and electrospinning for applications in tissue regeneration. Acta Biomaterialia 2008;4(5):1198-1207.
136. Pham QP, Sharma U, Mikos AG. Electrospun poly(epsilon-caprolactone) microfiber and multilayer nanofiber/microfiber scaffolds: Characterization of scaffolds and measurement of cellular infiltration. Biomacromolecules 2006;7(10):2796-2805.
137. Sankar D, Shalumon KT, Chennazhi KP, Menon D, Jayakumar R. Surface Plasma Treatment of Poly(caprolactone) Micro, Nano, and Multiscale Fibrous Scaffolds for Enhanced Osteoconductivity. Tissue Engineering Part A 2014;20(11-12):1689-1702.
138. Kim SJ, Jang DH, Park WH, Min B-M. Fabrication and characterization of 3-dimensional PLGA nanofiber/microfiber composite scaffolds. Polymer 2010;51(6):1320-1327.
139. Surmenev RA, Surmeneva MA, Ivanova AA. Significance of calcium phosphate coatings for the enhancement of new bone osteogenesis - A review. Acta Biomaterialia 2014;10(2):557-579.
140. Guarino V, Gloria A, Raucci MG, De Santis R, Ambrosio L. Bio-inspired composite and cell instructive platforms for bone regeneration. International Materials Reviews 2012;57(5):256-275.
141. Kamitakahara M, Ohtsuki C, Miyazaki T. Coating of bone-like apatite for development of bioactive materials for bone reconstruction. Biomedical Materials 2007;2(4):R17-R23.
142. Dorozkhin S. Calcium orthophosphate coatings, films and layers. Progress in Biomaterials 2012;1(1):1-40.

143. Florence B. Biomimetic calcium phosphate coatings: Physicochemistry and biological activity.: University of Twente; 2002.
144. Legeros R. Calcium phosphates in oral biology and medicine. New York: Karger; 1991.
145. Bleek K, Taubert A. New developments in polymer-controlled, bioinspired calcium phosphate mineralization from aqueous solution. Acta Biomaterialia 2013;9(5):6283-6321.
146. Mavis B, Demirtas TT, Gumusderelioglu M, Gunduz G, Colak U. Synthesis, characterization and osteoblastic activity of polycaprolactone nanofibers coated with biomimetic calcium phosphate. Acta Biomaterialia 2009;5(8).
147. Yu H-S, Jang J-H, Kim T-I, Lee H-H, Kim H-W. Apatite-mineralized polycaprolactone nanofibrous web as a bone tissue regeneration substrate. Journal of Biomedical Materials Research Part A 2009;88A(3):747-754.
148. Beskardes IG, Guemuesderelioglu M. Biomimetic Apatite-coated PCL Scaffolds: Effect of Surface Nanotopography on Cellular Functions. Journal of Bioactive and Compatible Polymers 2009;24(6):507-524.
149. Cui W, Li X, Xie C, Zhuang H, Zhou S, Weng J. Hydroxyapatite nucleation and growth mechanism on electrospun fibers functionalized with different chemical groups and their combinations. Biomaterials 2010;31(17):4620-4629.
150. Dorj B, Kim M-K, Won J-E, Kim H-W. Functionalization of poly(caprolactone) scaffolds by the surface mineralization for use in bone regeneration. Materials Letters 2011;65(23-24):3559-3562.
151. Choong C, Yuan S, Thian ES, Oyane A, Triffitt J. Optimization of poly(e-caprolactone) surface properties for apatite formation and improved osteogenic stimulation. Journal of Biomedical Materials Research Part A 2012;100A(2):353-361.
152. Pieters IY, Van den Vreken NMF, Declercq HA, Cornelissen MJ, Verbeeck RMH. Carbonated apatites obtained by the hydrolysis of monetite: Influence of carbonate content on adhesion and proliferation of MC3T3-E1 osteoblastic cells. Acta Biomaterialia 2010;6(4):1561-1568.
153. Geesink RGT, Degroot K, Klein C. Bonding of bone to apatite-coated implants. Journal of Bone and Joint Surgery-British Volume 1988;70(1):17-22.
154. Cunningham BW, Hu N, Zorn CM, McAfee PC. Bioactive titanium calcium phosphate coating for disc arthroplasty: analysis of 58 vertebral end plates after 6-to 12-month implantation. Spine Journal 2009;9(10):836-845.
155. Legeros RZ, Orly I, Gregoire M, Daculsi G, Ducheyne P, Glowacki J, Sauk JJ, Bolander M, Ricci JL. Substrate surface dissolution and interfacial biological mineralization. Bone-Biomaterial Interface 1991:76-88.
156. Doi Y, Iwanaga H, Shibutani T, Moriwaki Y, Iwayama Y. Osteoclastic responses to various calcium phosphates in cell cultures. Journal of Biomedical Materials Research 1999;47(3):424-433.
157. Choong C, Triffitt JT, Cui ZF. Polycaprolactone scaffolds for bone tissue engineering - Effects of a calcium phosphate coating layer on osteogenic cells. Food and Bioproducts Processing 2004;82(C2):117-125.
158. Schiller C, Epple M. Carbonated calcium phosphates are suitable pH-stabilising fillers for biodegradable polyesters. Biomaterials 2003;24(12):2037-2043.
159. Agrawal CM, Athanasiou KA. Technique to control pH in vicinity of biodegrading PLA-PGA implants. Journal of Biomedical Materials Research 1997;38(2):105-114.
160. Dorozhkin SV. Calcium orthophosphates. Journal of Materials Science 2007;42(4):1061-1095.
161. Dorozhkin SV. Calcium Orthophosphates in Nature, Biology and Medicine. Materials 2009;2(2):399-498.
162. Yuan HP, Yang ZJ, Li YB, Zhang XD, De Bruijn JD, De Groot K. Osteoinduction by calcium phosphate biomaterials. Journal of Materials Science-Materials in Medicine 1998;9(12):723-726.

163. Yuan HP, Kurashina K, de Bruijn JD, Li YB, de Groot K, Zhang XD. A preliminary study on osteoinduction of two kinds of calcium phosphate ceramics. Biomaterials 1999;20(19):1799-1806.
164. Wang J, Chen Y, Zhu XD, Yuan T, Tan YF, Fan YJ, Zhang XD. Effect of phase composition on protein adsorption and osteoinduction of porous calcium phosphate ceramics in mice. Journal of Biomedical Materials Research Part A 2014;102(12):4234-4243.
165. Cheng LJ, Shi YJ, Ye F, Bu H. Osteoinduction of calcium phosphate biomaterials in small animals. Materials Science & Engineering C-Materials for Biological Applications 2013;33(3):1254-1260.
166. Barradas AMC, Yuan H, van Blitterswijk CA, Habibovic P. Osteoinductive biomaterials: current knowledge of properties, experimental models and biological mechansims. European Cells & Materials 2011;21:407-429.
167. Kokubo T, Takadama H. How useful is SBF in predicting in vivo bone bioactivity? Biomaterials 2006;27(15):2907-2915.
168. Kokubo T. Formation of biologically active bone-like apatite on metals and polymers by a biomimetic process. Thermochimica Acta 1996;280:479-490.
169. Kokubo T. Apatite formation on surfaces of ceramics, metals and polymers in body environment. Acta Materialia 1998;46(7):2519-2527.
170. Kokubo T, Kushitani H, Sakka S, Kitsugi T, Yamamuro T. Solutions able to reproduce in vivo surface-structure changes in bioactive glass-ceramix A-W3. Journal of Biomedical Materials Research 1990;24(6):721-734.
171. Kokubo T. Apatite formation on surfaces of ceramics, metals and polymers in body environment. Acta Materialia 1998;46(7):2519-2527.
172. Oyane A, Kim HM, Furuya T, Kokubo T, Miyazaki T, Nakamura T. Preparation and assessment of revised simulated body fluids. Journal of Biomedical Materials Research Part A 2003;65A(2):188-195.
173. Lu X, Leng Y. Theoretical analysis of calcium phosphate precipitation in simulated body fluid. Biomaterials 2005;26(10):1097-1108.
174. Tas AC. The use of physiological solutions or media in calcium phosphate synthesis and processing. Acta Biomaterialia 2014;10(5):1771-1792.
175. Barrere F, van Blitterswijk CA, de Groot K, Layrolle P. Nucleation of biomimetic Ca-P coatings on Ti6Al4V from a SBF x 5 solution: influence of magnesium. Biomaterials 2002;23(10):2211-2220.
176. Tas AC, Bhaduri SB. Rapid coating of Ti6A14V at room temperature with a calcium phosphate solution similar to 10x simulated body fluid. Journal of Materials Research 2004;19(9):2742-2749.
177. Yang F, Wolke JGC, Jansen JA. Biomimetic calcium phosphate coating on electrospun poly (epsilon-caprolactone) scaffolds for bone tissue engineering. Chemical Engineering Journal 2008;137(1):154-161.
178. Kretlow JD, Mikos AG. Review: Mineralization of synthetic polymer scaffolds for bone tissue engineering. Tissue Engineering 2007;13(5):927-938.
179. Muller L, Muller FA. Preparation of SBF with different HCO3- content and its influence on the composition of biomimetic apatites. Acta Biomaterialia 2006;2(2):181-189.
180. Tanahashi M, Matsuda T. Surface functional group dependence on apatite formation on self-assembled monolayers in a simulated body fluid. Journal of Biomedical Materials Research 1997;34(3):305-315.
181. Vesel A, Junkar I, Cvelbar U, Kovac J, Mozetic M. Surface modification of polyester by oxygen- and nitrogen-plasma treatment. Surface and Interface Analysis 2008;40(11):1444-1453.
182. Oyane A, Uchida M, Yokoyama Y, Choong C, Triffitt J, Ito A. Simple surface modification of poly(epsilon-caprolactone) to induce its apatite-forming ability. Journal of Biomedical Materials Research Part A 2005;75A(1).

183. Oyane A, Uchida M, Choong C, Triffitt J, Jones J, Ito A. Simple surface modification of poly(epsilon-caprolactone) for apatite deposition from simulated body fluid. Biomaterials 2005;26(15):2407-2413.
184. Arafat MT, Lam CXF, Ekaputra AK, Wong SY, Li X, Gibson I. Biomimetic composite coating on rapid prototyped scaffolds for bone tissue engineering. Acta Biomaterialia 2011;7(2):809-820.
185. Murphy WL, Mooney DJ. Bioinspired growth of crystalline carbonate apatite on biodegradable polymer substrata. Journal of the American Chemical Society 2002;124(9):1910-1917.
186. Barrere F, van Blitterswijk CA, de Groot K, Layrolle P. Influence of ionic strength and carbonate on the Ca-P coating formation from SBFx5 solution. Biomaterials 2002;23(9):1921-1930.
187. Qu HB, Wei M. The effect of temperature and initial pH on biomimetic apatite coating. Journal of Biomedical Materials Research Part B-Applied Biomaterials 2008;87B(1):204-212.
188. Chou YF, Huang WB, Dunn JCY, Miller TA, Wu BM. The effect of biomimetic apatite structure on osteoblast viability, proliferation, and gene expression. Biomaterials 2005;26(3):285-295.
189. Taguchi T, Kishida A, Akashi M. Hydroxyapatite formation on/in poly(vinyl alcohol) hydrogel matrices using a novel alternate soaking process. Chemistry Letters 1998(8):711-712.
190. Ngiam M, Liao S, Patil AJ, Cheng Z, Chan CK, Ramakrishna S. The fabrication of nano-hydroxyapatite on PLGA and PLGA/collagen nanofibrous composite scaffolds and their effects in osteoblastic behavior for bone tissue engineering. Bone 2009;45(1):4-16.
191. Yu H-S, Hong S-J, Kim H-W. Surface-mineralized polymeric nanofiber for the population and osteogenic stimulation of rat bone-marrow stromal cells. Materials Chemistry and Physics 2009;113(2-3).
192. Araujo JV, Martins A, Leonor IB, Pinho ED, Reis RL, Neves NM. Surface controlled biomimetic coating of polycaprolactone nanofiber mesh architectures. Tissue Engineering 2007;13(7).
193. Vaquette C, Ivanovski S, Hamlet SM, Hutmacher DW. Effect of culture conditions and calcium phosphate coating on ectopic bone formation. Biomaterials 2013;34(22):5538-5551.
194. Zou B, Li X, Zhuang H, Cui W, Zou J, Chen J. Degradation behaviors of electrospun fibrous composites of hydroxyapatite and chemically modified poly(DL-lactide). Polymer Degradation and Stability 2011;96(1):114-122.
195. Chen J, Chu B, Hsiao BS. Mineralization of hydroxyapatite in electrospun nanofibrous poly(L-lactic acid) scaffolds. Journal of Biomedical Materials Research Part A 2006;79A(2):307-317.
196. Cai Q, Xu Q, Feng Q, Cao X, Yang X, Deng X. Biomineralization of electrospun poly(L-lactic acid)/gelatin composite fibrous scaffold by using a supersaturated simulated body fluid with continuous CO2 bubbling. Applied Surface Science 2011;257(23):10109-10118.
197. Jaiswal AK, Chandra V, Bhonde RR, Soni VP, Bellare JR. Mineralization of nanohydroxyapatite on electrospun poly(L-lactic acid)/gelatin by an alternate soaking process: A biomimetic scaffold for bone regeneration. Journal of Bioactive and Compatible Polymers 2012;27(4):356-374.
198. Ghasemi-Mobarakeh L, Prabhakaran MP, Morshed M, Nasr-Esfahani M-H, Ramakrishna S. Electrospun poly(epsilon-caprolactone)/gelatin nanofibrous scaffolds for nerve tissue engineering. Biomaterials 2008;29(34):4532-4539.
199. Cui W, Li X, Xie C, Chen J, Zou J, Zhou S, Weng J. Controllable growth of hydroxyapatite on electrospun poly(DL-lactide) fibers grafted with chitosan as potential tissue engineering scaffolds. Polymer 2010;51(11):2320-2328.

200. Mikos AG, Lyman MD, Freed LE, Langer R. Wetting of poly(L-lactic acid) and poly(DL-lactic-co-glycolic acid) foams for tissue-culture. Biomaterials 1994;15(1).
201. Yang J, Wan YQ, Tu CF, Cai Q, Bei JZ, Wang SG. Enhancing the cell affinity of macroporous poly(L-lactide) cell scaffold by a convenient surface modification method. Polymer International 2003;52(12).
202. Oliveira AL, Costa SA, Sousa RA, Reis RL. Nucleation and growth of biomimetic apatite layers on 3D plotted biodegradable polymeric scaffolds: Effect of static and dynamic coating conditions. Acta Biomaterialia 2009;5(5):1626-1638.
203. Kweon DK, Kawasaki N, Nakayama A, Aiba S. Preparation and characterization of starch/polycaprolactone blend. Journal of Applied Polymer Science 2004;92(3):1716-1723.
204. Miyaji F, Kim HM, Handa S, Kokubo T, Nakamura T. Bonelike apatite coating on organic polymers: novel nucleation process using sodium silicate solution. Biomaterials 1999;20(10):913-919.

Chapter 2: Rationale and aims

Rationale and aims

An ideal bone scaffold should exhibit a porous, interconnected and permeable structure to allow for cell infiltration and exchange of nutrients and metabolites and also should exhibit the appropriate surface structure and chemistry for cell adhesion and proliferation. In addition, the scaffold should be biodegradable, biocompatible and ideally bioactive. Evidently, the design of the construct is as crucial as the material it is made of.

The biocompatible and biodegradable polyesters PCL and PDLLA are interesting candidates for the fabrication of BTE scaffolds due to their established safety in clinical use and appropriate biodegradation kinetics. Both PCL and PDLLA are easy to manufacture with advanced processing techniques currently investigated in BTE research, such as electrospinning and 3D plotting.

With the electrospinning technique nanofibrous scaffolds are produced that are characterized by a high surface-to-volume ratio and high porosity with interconnected pores, resembling the ECM. In addition, electrospun fibers provide the favorable surface topography for cell attachment due to their nanoscale features and random fiber orientation. However, many researchers have encountered limitations with regard to cell infiltration and migration into the interior of the nanofiber mats due to the relative small pores associated with electrospun scaffolds. Consequently, this results in 2D cell layers on top of the scaffold instead of the formation of 3D tissues.[1-3]

On the contrary, the filaments of 3D plotted scaffold have a fixed geometry and are in the micrometer range. The resulting pore sizes in 3D plotted scaffolds are relatively large compared to the dimensions of a cell, which enables the cells to infiltrate into the interior of the scaffold, but often leads to a low seeding efficiency and to a non-uniform distribution of cells throughout the scaffold.[4]

Recently, reports have been published on the fabrication of hierarchical structures composed of both nanofibers and microfibers and thus combining both fabrication techniques. Hence, the inverse pore size limitations encountered with the two techniques could cancel each other out, while combining the positive characteristics of the two scaffolds. Such multiscale scaffolds possess innovative property combinations, not otherwise attainable with a single fiber scale and have been found to be favorable in bone regenerative purposes.[5-10]

However, irrespective of the fabrication technique or the fiber scale, PCL and PDLLA scaffolds lack bioactivity due to their hydrophobic nature.[11] In order to enhance the bioactivity of polyester scaffolds, coating with an apatite layer has been applied.[12-15] These coated scaffolds show improved cell response compared to uncoated scaffolds, but the cell viability

is still low in comparison to the positive controls. Ideally, the calcium phosphate layer should be a nanocrystalline carbonated apatite, resembling the mineral present in natural bones.[16] Moreover, Pieters *et al.* reported that apatites with a carbonate content equal to or higher than 11 wt% show an improved cell adhesion and proliferation in comparison to that on carbonate-free apatites.[17]

Although the multiscale scaffolds hold great promise in the field of BTE, to date research on the calcium phosphate coating of these scaffolds is lacking. Such scaffold could come close to the ideal BTE scaffold as it combines the positive effects of electrospinning and 3D plotting on the one hand and PCL/PDLLA and bone-like apatite on the other hand.

Single fiber scale electrospun PCL[14,18-20] and PDLLA[21-23] scaffolds and 3D plotted PCL[24] scaffolds have been coated with a calcium phosphate layer. However, the reproducibility of the coating procedure, the homogeneity of the coating and obtaining an apatite coating with high carbonate content still seems to be challenging. In addition, even for the same scaffold type, there is a great variety in the mineralization parameters reported, so that the composition and morphology of the obtained coating differ from study to study. The challenge upon coating the nano- to micrometer fibers of electrospun scaffolds is not to obstruct the pores of the construct with the deposited apatite. Whereas the latter is no problem for 3D plotted scaffolds due to their larger pores, the coating procedure for these scaffolds is generally more aggressive and longer compared to that for electrospun scaffolds.

In order to successfully coat multiscale scaffolds it is essential to reckon the large difference in fiber diameters throughout the scaffold that range from ~0.5-50 µm for the electrospun fibers to ~100-350 µm for the 3D plotted filaments. Hence, a coating procedure adequate for the coating of 3D plotted filaments, could possibly be too aggressive and too long for the thin electrospun fibers with the risk of damaging the nanofibers and/or compromising the porous structure. Vice versa, the coating procedure applicable for electrospun fibers could be too mild to obtain a homogenous and reproducible coating on 3D plotted filaments. Consequently, in order to coat a multiscale scaffold it will be necessary to compromise between the adequate coating procedures for the constituting fibers.

Based on these considerations, the aims of this study were:

- To optimize the apatite coating on novel electrospun PCL and PDLLA fiber mats and evaluate the osteoblastic cell response on the coatings.
- To explore the possibility of depositing a homogenous apatite coating with a carbonate content of more than 11 wt% on 3D plotted PCL scaffolds and determine to what extent

the presence of carbonate in the apatite lattice has a beneficial effect on osteoblastic cell behavior.

- To obtain a multiscale PCL scaffold, fabricated by a combination of electrospinning and 3D plotting, coated with an apatite containing a high concentration of carbonate and evaluate the osteoblastic cell response on this scaffold.

The polyester scaffolds in the present study were fabricated and investigated following a similar approach;

Figure 14: Process diagram of the stepwise approach followed in the present thesis.

The first aspect of the present study was the fabrication of the polyester scaffolds. A total of four porous polyester scaffolds were developed and investigated (Figure 15).

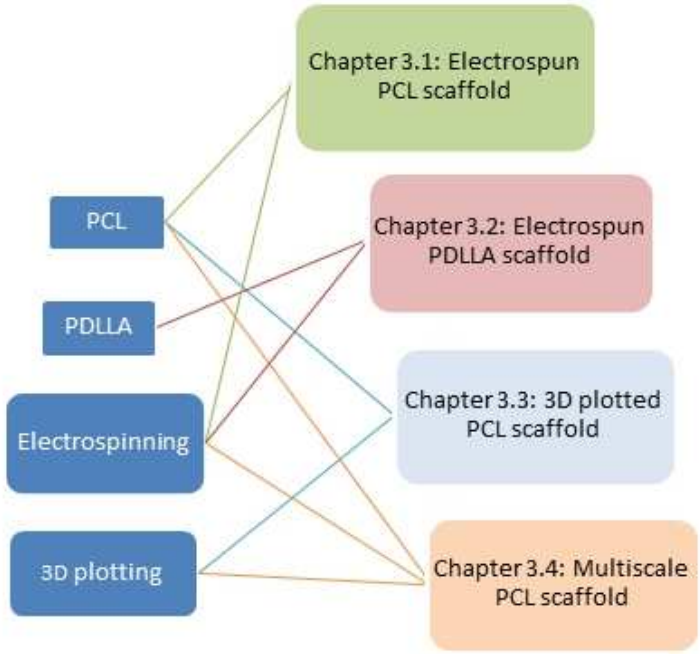

Figure 15: Overview of the four scaffolds developed in the present thesis.

References

1. Sill TJ, von Recum HA. Electro spinning: Applications in drug delivery and tissue engineering. Biomaterials 2008;29(13):1989-2006.
2. Subbiah T, Bhat GS, Tock RW, Pararneswaran S, Ramkumar SS. Electrospinning of nanofibers. Journal of Applied Polymer Science 2005;96(2):557-569.
3. Bhardwaj N, Kundu SC. Electrospinning: A fascinating fiber fabrication technique. Biotechnology Advances 2010;28(3):325-347.
4. Declercq HA, Desmet T, Berneel EEM, Dubruel P, Cornelissen MJ. Synergistic effect of surface modification and scaffold design of bioplotted 3-D poly-epsilon-caprolactone scaffolds in osteogenic tissue engineering. Acta Biomaterialia 2013;9(8):7699-7708.
5. Srinivasan S, Jayakumar R, Chennazhi KP, Levorson EJ, Mikos AG, Nair SV. Multiscale Fibrous Scaffolds in Regenerative Medicine. In: Jayakumar R, Nair SV, editors. Biomedical Applications of Polymeric Nanofibers; 2012. p 1-20.
6. Centola M, Rainer A, Spadaccio C, De Porcellinis S, Genovese JA, Trombetta M. Combining electrospinning and fused deposition modeling for the fabrication of a hybrid vascular graft. Biofabrication 2010;2(1).
7. Moroni L, De Wijn JR, Van Blitterswijk CA. Integrating novel technologies to fabricate smart scaffolds. Journal of Biomaterials Science-Polymer Edition 2008;19(5):543-572.
8. Park SH, Kim TG, Kim HC, Yang D-Y, Park TG. Development of dual scale scaffolds via direct polymer melt deposition and electrospinning for applications in tissue regeneration. Acta Biomaterialia 2008;4(5):1198-1207.
9. Mota C, Puppi D, Dinucci D, Errico C, Bartolo P, Chiellini F. Dual-Scale Polymeric Constructs as Scaffolds for Tissue Engineering. Materials 2011;4(3):527-542.
10. Kim G, Son J, Park S, Kim W. Hybrid Process for Fabricating 3D Hierarchical Scaffolds Combining Rapid Prototyping and Electrospinning. Macromolecular Rapid Communications 2008;29(19):1577-1581.
11. Holzwarth JM, Ma PX. Biomimetic nanofibrous scaffolds for bone tissue engineering. Biomaterials 2011;32(36):9622-9629.
12. Araujo JV, Martins A, Leonor IB, Pinho ED, Reis RL, Neves NM. Surface controlled biomimetic coating of polycaprolactone nanofiber mesh architectures. Tissue Engineering 2007;13(7).
13. Chen J, Chu B, Hsiao BS. Mineralization of hydroxyapatite in electrospun nanofibrous poly(L-lactic acid) scaffolds. Journal of Biomedical Materials Research Part A 2006;79A(2):307-317.
14. Yang F, Wolke JGC, Jansen JA. Biomimetic calcium phosphate coating on electrospun poly (epsilon-caprolactone) scaffolds for bone tissue engineering. Chemical Engineering Journal 2008;137(1):154-161.
15. Ngiam M, Liao S, Patil AJ, Cheng Z, Chan CK, Ramakrishna S. The fabrication of nano-hydroxyapatite on PLGA and PLGA/collagen nanofibrous composite scaffolds and their effects in osteoblastic behavior for bone tissue engineering. Bone 2009;45(1):4-16.
16. Hofmann I, Mueller L, Greil P, Mueller FA. Precipitation of carbonated calcium phosphate powders from a highly supersaturated simulated body fluid solution. Journal of the American Ceramic Society 2007;90(3):821-824.
17. Pieters IY, Van den Vreken NMF, Declercq HA, Cornelissen MJ, Verbeeck RMH. Carbonated apatites obtained by the hydrolysis of monetite: Influence of carbonate content on adhesion and proliferation of MC3T3-E1 osteoblastic cells. Acta Biomaterialia 2010;6(4):1561-1568.
18. Yu H-S, Hong S-J, Kim H-W. Surface-mineralized polymeric nanofiber for the population and osteogenic stimulation of rat bone-marrow stromal cells. Materials Chemistry and Physics 2009;113(2-3).
19. Araujo JV, Martins A, Leonor IB, Pinho ED, Reis RL, Neves NM. Surface controlled biomimetic coating of polycaprolactone nanofiber meshes to be used as bone

extracellular matrix analogues. Journal of Biomaterials Science-Polymer Edition 2008;19(10):1261-1278.
20. Mavis B, Demirtas TT, Gumusderelioglu M, Gunduz G, Colak U. Synthesis, characterization and osteoblastic activity of polycaprolactone nanofibers coated with biomimetic calcium phosphate. Acta Biomaterialia 2009;5(8).
21. Cui W, Li X, Zhou S, Weng J. In situ growth of hydroxyapatite within electrospun poly(DL-lactide) fibers. Journal of Biomedical Materials Research Part A 2007;82A(4):831-841.
22. Cui W, Li X, Xie C, Zhuang H, Zhou S, Weng J. Hydroxyapatite nucleation and growth mechanism on electrospun fibers functionalized with different chemical groups and their combinations. Biomaterials 2010;31(17):4620-4629.
23. Zou B, Li X, Zhuang H, Cui W, Zou J, Chen J. Degradation behaviors of electrospun fibrous composites of hydroxyapatite and chemically modified poly(DL-lactide). Polymer Degradation and Stability 2011;96(1):114-122.
24. Park SA, Lee JB, Kim YE, Kim JE, Lee JH, Shin JW, Kwon IK, Kim W. Fabrication of biomimetic PCL scaffold using rapid prototyping for bone tissue engineering. Macromolecular Research 2014;22(8):882-887.

Chapter 3: Article presentation

1 Calcium phosphate coating of an electrospun PCL scaffold

Part of the research is based on the article:

Optimization of the activation and nucleation steps in the precipitation of a calcium phosphate primer layer on electrospun poly(ε-caprolactone).

Nathalie Luickx, Natasja Van den Vreken, Willem D'Oosterlinck, Lien Van der Schueren, Heidi Declercq, Karen De Clerck, Maria Cornelissen, Ronald Verbeeck.

Journal of Biomedical Materials Research Part A 2015; 103(2): 511-524.

Abstract: Electrospun poly(ε-caprolactone) (PCL) is a potential scaffold for bone tissue engineering. However, due to its hydrophobic nature, the material lacks bioactivity. Coating the PCL fibers with a calcium phosphate (CP) layer is one approach to overcome this problem. In this study the coating of PCL nanofibers with a CP primer layer was optimized in a three-step procedure. First, wetting of the hydrophobic PCL samples was enhanced by ethanol dipping. Reactive hydroxyl– and carboxylgroups were subsequently generated by an ultrasonic assisted hydrolysis of the fiber surface with sodium hydroxide solution. These reactive groups served as nucleation point for CP precipitates in the last step in which the samples were alternately dipped in calcium and phosphate rich solutions. Hence, a reproducible thin layer of CP was deposited onto the fiber surface, with the preservation of the porous structure of the scaffold. Infrared spectroscopy was used to identify the deposited CP and revealed that a calcium-deficient apatite (CDHAp) was formed. MC3T3-E1 cells were seeded on untreated and CDHAp coated PCL scaffolds. Cell viability, adhesion and proliferation were analyzed after 1, 7 and 14 days of culture using fluorescence microscopy and a Presto Blue ™ assay. Cell adhesion and proliferation on the untreated PCL samples was low throughout the experiment. The CDHAp coating enhanced the MC3T3-E1 cell response, as the number of attached cells was augmented and cells showed similar morphologies as the ones found in the positive control.

Electrospun PCL scaffold

1.1 Introduction

Three-dimensional (3D) scaffolds with an interconnected pore system are interesting candidates for reconstructive surgery of bony defects. Due to similarity with the extracellular matrix (ECM) porous scaffolds promote cell adhesion, proliferation and differentiation compared to dense scaffolds.[1,2,3] Interconnectivity of the pores is necessary to allow cell in-growth, vascularization and efficient transport of nutrients, oxygen, growth factors and metabolites.[4] The scaffold material should be biocompatible, bioactive and osteoconductive.[5,6] The mechanical strength of the scaffolds should be similar to that of the surrounding tissue so that the scaffolds can provide a dimensional stability in the body. In an ideal case, the scaffold is biodegradable with a degradation rate comparable with the rate of new bone formation. In this way, while the scaffold is degrading, the surrounding bone cells simultaneously form new bone without affecting the mechanical stability. Finally, when the scaffold is completely degraded, the initial bone defect is filled with newly formed bone tissue.[7,8]

Synthetic biodegradable aliphatic polyesters such as the Food and Drug Administration (FDA) approved polylactic acid (PLA), polyglycolic acid (PGA), polycaprolactone (PCL) and their copolymers are interesting scaffold materials.[6,9] These polymers are easy to manufacture into different shapes and the mechanical properties and degradation kinetics can be tailored by varying the monomer composition and molecular weight. These properties give the materials a worldwide attention for use as resorbable sutures, drug delivery systems and orthopedic fixation devices such as pins and screws.[10,11,12] Another advantage of these polyesters is the ability to process them by means of an electrospinning process into three-dimensional structures with high surface-to-volume ratio, high porosity and with an interconnected pore system similar to the ECM.[13,14] However, the polyesters lack bioactivity and are too elastic for bone regenerative purposes.[15,16] An additional problem is the release of acidic by-products during degradation of the polymer, which can cause inflammation.[6,17]

To address these problems, the electrospun fibers can be coated with an apatitic mineral phase.[8,18,19] The apatite structure is chemically comparable to the mineral phase found in natural bone.[4] Polymer-mineral composites have shown improved bioactivity and mechanical strength as compared to pure polymer scaffolds.[20,21] Moreover, the resorption of the apatite layer could contribute to the neutralization of the acidic polymer degradation by-products. The latter is ascribed to the reaction of calcium ions and the carboxyl end-groups generated during degradation of the polymer, to form calcium carboxylate chain ends. This complexation results in an increased solubility of the calcium phosphate, causing an increase

of the pH. As a result, the acidic autocatalytic degradation of the polymer is slowed down, so that possible inflammation reactions are avoided or at least less severe.[6]

Various attempts have been made to coat electrospun PLA[22,23], PCL[18,21] and the co-polymer poly(lactic-co-glycolic acid) (PLGA)[7,19] with bone-like mineral. Despite a great variety in the described mineralization procedures, generally a three-step procedure is followed: activation, nucleation and maturation. The first step is intended to create hydroxyl groups and negatively charged carboxyl groups on the fiber surface by cleaving polyester bonds. The second step involves the nucleation of calcium phosphate (CP) particles on the fiber surface by an alternate dipping process.[18,19,24,25] In the third step a final CP coating is deposited by immersing the samples in a supersaturated solution with respect to apatite, such as simulated body fluid (SBF). Upon incubation in SBF the CP primer layer acts as a template on which apatite grows spontaneously by consuming Ca^{2+} - and PO_4^{3-} - ions from the solution.[18,21,22,26] Differences in the mineralization procedures described in the literature are probably due to the use of different types of polyesters, solvents, electrospinning parameters, and hence, different fiber diameters of the electrospun scaffolds. Moreover, the scanning electron microscope (SEM) images of the coated PCL samples represented in literature show profuse mineralization of the nanofibers, which compromised the porous structure.[24,26] In addition, the electrospinning solvents used, such as N,N-dimethylformamide[22], dichloromethane[26], chloroform[18] and 2,2,2-trifluoroethanol[21] are toxic. During electrospinning some of the toxic solvent may be retained in the resulting polymer fiber and could negatively affect the biological performance of the scaffold.[27]

Recently, Van der Schueren *et al.* optimized the electrospinning procedure of PCL using a new low-toxic solvent consisting of a mixture of 90% formic acid and 10% acetic acid.[28] PCL is one of the most commonly used biodegradable polymers for bone tissue engineering due to its lack of toxicity, low cost and slow degradation profile.[12,29] The objective of this study is to coat the PCL fiber mats, electrospun with the solvent mixture formic acid/acetic acid, with a thin CP layer. No optimized procedure to reproducibly coat PCL nanofibers is recorded in literature. Hence, the initial activation procedure and the subsequent deposition of a CP primer layer onto the PCL nanofibers are optimized. In search of an optimal procedure the reproducibility of the procedure and preservation of the porous structure upon coating is a prerequisite. The optimized parameters giving the most reproducible and adequate coating were selected for an *in vitro* study, comparing the adhesion and proliferation of pre-osteoblastic cells (MC3T3-E1) on CP coated samples and untreated electrospun PCL samples.

1.2 Materials and Methods

Freshly prepared demineralized water (Milli-Q system, Millipore, Billerica, USA) was used for the preparation of the solutions. PCL pellets were purchased from Sigma-Aldrich (St. Louis, US). Sodium chloride (NaCl), ethanol (EtOH; technical 95 vol. %), sodium hydroxide solution (NaOH; 1 M), 4 % buffered formaldehyde and acetone (analytical) were obtained from VWR BDH Prolabo (Leuven, Belgium). Hydrochloride (HCl; 37 vol. %), sodium phosphate (Na_2HPO_4) and chloroform were purchased from Merck (Darmstadt, Germany) and calcium chloride ($CaCl_2.2H_2O$) from J.T. Baker (Deventer, The Netherlands).

1.2.1 Electrospun mats

The fabrication process of the electrospun PCL mats is described in detail by Van der Schueren *et al*.[28] Briefly, a 14 wt% PCL solution was made by dissolving PCL pellets in the binary solvent system 90 % formic acid/10 % acetic acid (both Sigma-Aldrich). The polymer solution was then loaded into a syringe (Becton Dickinson, Franklin Lakes, US) and a high voltage electric field of 18 kV (Glassman High Voltage Series EH Source, High Bridge, US) was applied to draw the fibers from the spinneret (17 G needle) onto the collector plate. A constant feed rate of 1 ml/h was applied using a syringe pump (KD Scientific, Syringe Pump Series 100, Holliston, US) and a distance of 12 cm was maintained between the tip of the spinneret and the collector plate. The electrospun meshes were soaked for 24 h in 0.9 wt % NaCl in order to remove any residual solvent present. The thickness of the meshes was measured using a digital micrometer (Mitotoyo 293-521-30, Kruibeke, Belgium). The morphology of the electrospun PCL fibers was analyzed using a scanning electron microscope (SEM; FEI Quanta 200 F, Hillsboro, US). Prior to SEM measurements, the samples were coated with gold using a sputter coater (Balzers Union Highland Scientific SCD 030, Bedford, UK). Surface hydrophobicity was characterized by means of static water contact-angle measurements (WCA). WCA measurements were carried out at room temperature using a contact-angle measuring system (DataPhysics OCA20, San Jose, US). Each measurement was repeated three times and the average WCA after 10 seconds was calculated.

1.2.2 Surface activation

Samples of 1 x 1 cm² were immersed at room temperature in 10ml/cm² EtOH, NaOH solution, HCl solution or combinations of these. The composition of the solutions and the immersion times are summarized in Table 1. During immersion the samples were either continuously stirred on an orbital shaker (Fisher Bioblock Scientific, Hampton, US) at 85 rpm or placed in an ultrasonic bath (Elma Transonic 700/H, Ruiselede, Belgium). After each immersion, samples were rinsed for 30 seconds in demineralized water. The effect of different activation methods on the fiber morphology was analyzed by SEM. The effect on

sample hydrophobicity was characterized by WCA measurements. In order to evaluate and compare the efficiency of the different activation methods, the activated samples were treated with calcium and phosphate rich solutions using a standard nucleation procedure. In this procedure the activated samples were first dipped in 20 ml/cm² 75 mM $CaCl_2.2H_2O$ solution for 1 minute, washed with demineralized water for 30 seconds, dipped in 20 ml/cm² 75 mM Na_2HPO_4 solution for 1 minute and washed for 30 seconds with demineralized water. This cycle of four steps was repeated six times. Subsequently, the samples were stained with Alizarin Red S (ARS; Sigma-Aldrich). For ARS staining the samples were rinsed for 30 seconds with demineralized water and fixed in 4 % buffered formaldehyde for 30 minutes. ARS powder was dissolved in demineralized water to a final concentration of 40 mM and pH was adjusted to 4.1 using 1 M NaOH solution. The scaffolds were stained on a glass cover plate with an excess of ARS solution for 10 minutes after which the scaffolds were rinsed repeatedly in demineralized water in order to wash off all unbound dye. At a pH of 4.1 ARS stains the surface of fibers coated with a calcium containing layer red. The color intensity is linearly correlated with the local calcium concentration.[30,31]

The morphology of the samples after treatment with the standard nucleation procedure was analyzed using SEM. All experiments were performed in triplicate. The activation method resulting in a reproducible and overall mineralization after treatment with the standard nucleation procedure was selected for further testing.

Table 1

The composition of the solution and the immersion times applied in the surface activation experiments. During immersion in various solutions samples were either placed on a shaker or in an ultrasonic bath. Resulting WCA of the activated PCL samples measured after 10 seconds (with the corresponding standard deviation (SD)).

Sample ID	Solution(s)	Concentration(s)	Immersion time(s)	WCA (SD) (°)
PCL	-	-	-	131.9 (2.8)
Shaker (85 rpm)				
NaOH-6h	NaOH	1M	6h	119.9 (14.9)
NaOH-24h	NaOH	1M	24h	5.6 (9.7)
NaOH-5M	NaOH	5M	6 h	3.4 (5.9)
HCl	HCl	1M	6 h	130.2 (5.4)
NaOH-HCl	NaOH – HCl	1M – 1M	3 h – 3 h	131.6 (4.3)
EtOH	EtOH	95 vol%	1.5 min	N.A.
EtOH-3h	EtOH – NaOH	95 vol% – 1 M	1.5 min – 3 h	88.4 (24.5)
EtOH-6h	EtOH – NaOH	95 vol% – 1 M	1.5 min – 6 h	0 (0)
Ultrasonic bath				
EtOH-10min	EtOH – NaOH	95 vol% – 1M	1.5 min – 10 min	0 (0)
EtOH-40min	EtOH – NaOH	95 vol% – 1M	1.5 min – 40 min	0(0)

WCA:Water contact angle

1.2.3 Calcium-phosphate nucleation

A CP coating was achieved by an alternate dipping process in $CaCl_2.2H_2O$ and Na_2HPO_4 solutions. Important parameters in this coating procedure were the number of cycles, concentration and immersion time of both the $CaCl_2.2H_2O$ and the Na_2HPO_4 solutions. In order to efficiently optimize these five parameters at the same time, a variable size simplex algorithm was used.[32] An optimized coating was a thin homogeneous primer layer of CP particles. In the maturation phase this primer layer can grow thicker while incorporating impurities, without compromising the porous structure of the matrix.

Samples were immersed in 20 ml of solution/cm² and washed for 30 seconds with demineralized water after every immersion. A minimum of three samples was prepared. The morphology of the CP coating on the nanofibers was analyzed by SEM. The homogeneity of the CP coating and the reproducibility of the procedures were evaluated using ARS calcium staining. Following the removal of most of the polymer by dissolution, the type of calcium phosphate deposited was identified by infrared (IR) spectrometry. Samples were cut in

smaller pieces and immersed in 250 µl/cm² chloroform for 10 minutes. Subsequently 750 µl/cm² acetone was added. After centrifugation (2 minutes; 7000 rpm) the supernatant solution was removed. The remaining pellet was washed with 1ml/cm² aceton followed by centrifugation (2 minutes; 7000 rpm) and removal of the supernatant. This washing-step was repeated twice, the remaining powder was dried overnight in order to remove residual aceton. IR spectra of the CP powder dispersed in KBr tablets were recorded using a Fourier-transform IR (FT-IR) spectrophotometer (Perkin Elmer Instruments, Waltham, US).

In order to select the best and most reproducible procedure, the experiments resulting in adequately coated samples were repeated tenfold.

1.2.4 Cell culture and seeding

Monolayers of MC3T3-E1 pre-osteoblasts (subclone 14, ATCC) were routinely cultivated in α-minimum essential medium (α-MEM) (glutaMAX-1 ^{TM} Gibco, Ghent, Belgium) supplemented with 10% fetal bovine serum (FBS) (heat inactivated, EC approved, Invitrogen) and 1 mM sodium pyruvate (Invitrogen, Ghent, Belgium) at 37 °C and in 95% air/5% CO_2. The medium was changed twice a week.

Samples with the most reproducible CP coating on the nanofibers were selected for a cell viability study. Untreated PCL was used as control. CP coated and untreated samples were transferred into a 24-well suspension tissue culture plate (Greiner bio-one, Frickenhausen, Belgium) and sterilized under UV-light for 30 minutes. Forty thousand MC3T3-E1 cells diluted in 500 µl culture medium were added to each well containing a sample, or to a polystyrene 24-well standard tissue culture plate (Greiner Bio-one; positive control) and were incubated for 14 days.

1.2.5 Cell viability, adhesion and proliferation

The PrestoBlue^{TM} assay (Invitrogen) was applied to quantify the number of viable cells that are attached on the CP coated and untreated samples after 1, 7 and 14 days of culture.

The PrestoBlue™ reagent is a blue resazurin-based non-fluorescent solution. Resazurin enters the cells where it is transformed to the red and fluorescent resorufin by the reducing power of the mitochondria.[33] The samples and the control were rinsed with culture medium after which 450 µl culture medium and 50 µm PrestoBlue™ reagent was added to each well. After 2 h incubation at 37 °C in a dark room, 400 µl medium was transferred to a new plate. In order to measure fluorescence the plate was inserted in a multilabel plate reader (Victor³, Perkin-Elmer). The number of viable and attached cells is linearly correlated with the signal, and viability was calculated as a percentage of the positive control after 14 days.

Cell viability, adhesion and proliferation after 1, 7 and 14 days on the CP coated and untreated samples was visualized using fluorescence microscopy after performing live/dead staining (calcein acetoxymethyl (AM) ester (Tebu-Bio, Boechout, Belgium) /propidium iodide (PI) (Sigma-Aldrich)). PI cannot pass through intact cell membranes, but may freely enter dead cells with compromised cell membranes where PI intercalates into double-stranded DNA and emits red fluorescence (excitation: 535 nm, emmision: 617 nm). Calcein AM is a non-fluorescent, membrane-permeable dye. Under intracellular esterase activity the dye converts to a membrane-impermeable, green fluorescent compound (excitation: 490 nm, emission: 515 nm).[34] After 1, 7 and 14 days the samples and positive controls were rinsed with 500 µl phosphate buffered saline (PBS) after which 500 µl PBS containing 1 µl PI and 1 µl calcein AM was added to each well. After 10 minutes incubation in a dark room, samples were evaluated with a fluorescence microscope (Olympus Type U-RFL-T, Aartselaar, Belgium).

Each material and the controls were tested in triplicate.

1.2.6 Statistical analysis

Significant differences between the mean WCA were calculated using a student's t-test at 0.05 confidence level. Viability was evaluated using 2-factor ANOVA with the substrate and the incubation time as independent variables. Significant differences between means were calculated using a Holm-Sidak multiple-comparison test at the 0.05 confidence level.

1.3 Results

1.3.1 Morphology and hydrophobicity of activated PCL nanofibers mats

The PCL meshes have a thickness of 57.52 µm with a standard deviation (SD) of 18.22 µm. SEM images of the electrospun PCL nanofibers are shown in figure 1A. The average diameter of the nanofibers is 419 nm with a SD of 100 nm. The untreated PCL nanofiber mat is white and the average water contact angle of the untreated PCL is 131.9° with a SD of 2.8° (Table 1).

Electrospun PCL scaffold

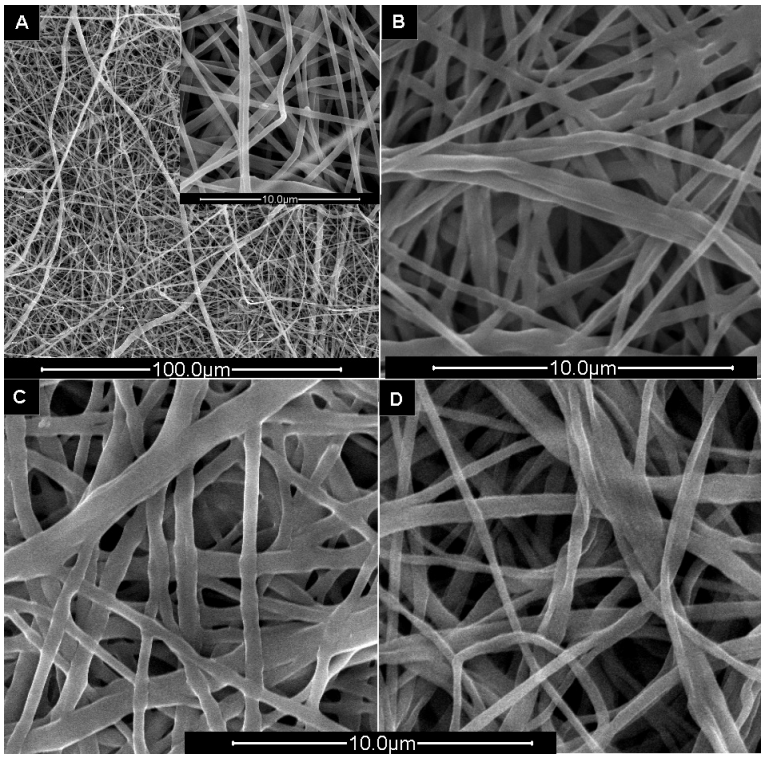

Figure 1. SEM images of A) untreated, B) NaOH-24h treated, C) NaOH-HCl treated and D) EtOH-40min treated PCL nanofiber

SEM images of the PCL nanofibers after activation according to the conditions of experiments NaOH-24h, NaOH-HCl and EtOH-40min are shown in figure 1B-D (table 1). In figure 1D the EtOH-40min treated sample shows no changes in fiber morphology and is representative for all samples except for samples treated with the experimental conditions of NaOH-24h and NaOH-HCl. In the latter, fibers appear molten and are conglutinated at contact points. The change is more distinct in samples treated with the experimental conditions of NaOH-HCl.

The effect of the different activation processes on the wettability of PCL, as reflected by the WCA, is seen from table 1. Immersion of the samples for 6 hours in 1 M NaOH solution, 1 M HCl solution or a combination of both does not affect the WCA ($p > 0.075$). By increasing the immersion time in NaOH solution to 24 h, or the concentration of NaOH solution to 5 M, the WCA angle of the PCL samples decreases to 3.4° and 5.6° respectively. Dipping the samples in EtOH for 1.5 minute results in a visible increase in wettabilitiy, as is shown in figure 2. The PCL sample treated with EtOH absorbs water and appears translucent (grey), while untreated PCL remains white and water repellent. However, when the EtOH treated sample dries, it colors overall white and no significant difference in WCA can be detected between the EtOH dipped and the untreated PCL (130.8° vs. 131.9°, $p = 0.45$). EtOH dipping followed by an immersion for 3 h in 1 M NaOH solution results in a slight decrease in WCA (88.4°). After a 6 h immersion in 1 M NaOH solution the WCA drops to

zero. The WCA is also zero after treating the samples with a combination of EtOH and the immersion in NaOH solution under ultrasonic conditions (EtOH-10min/40min; table 1)

Figure 2. Digital image of sample halfway dipped in ethanol and subsequently dipped in demineralized water. EtOH dipped region is translucent (grey) (A), the untreated PCL remains white after dipping in water (B).

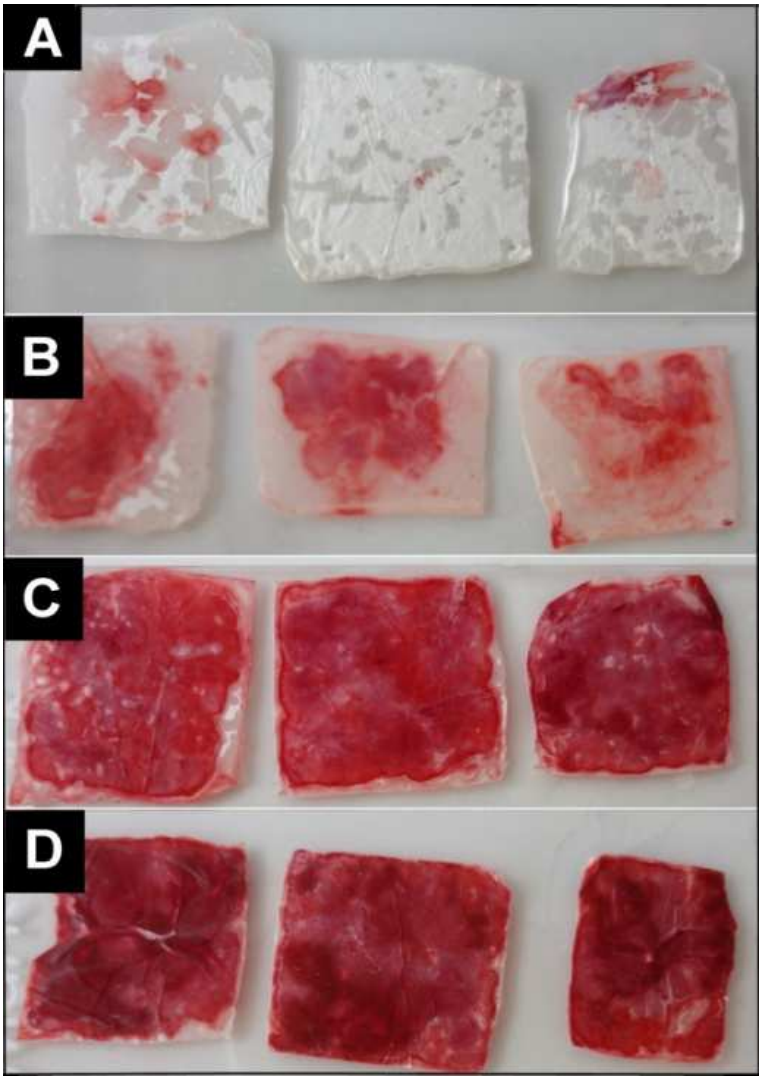

Figure 3. Digital images of Alizarin Red stained samples after activation and treatment with the standard nucleation procedure. A) NaOH-HCl activated samples show no staining B) EtOH treated samples show no uniform staining C) EtOH–10min and D) EtOH-40min activated samples show complete staining with some difference in color intensities.

1.3.2 Comparison of the activation methods

The digital image of the PCL samples activated with the experimental conditions of NaOH-HCl is given in figure 3A and is also representative for the samples activated with HCl solution. The samples activated according to these conditions show, apart from a few colored spots no staining, indicating the absence of CP deposits. The samples show few translucent spots, the majority of the samples remain white and water repellent. The digital image of the PCL samples activated with EtOH in figure 3B is representative for those activated with the experimental conditions of NaOH-6h, NaOH-24h, NaOH-5M, EtOH-3h and EtOH-6h. Some parts of the samples remain white, whereas some parts of the samples stain, indicating the presence of calcium phosphate deposits. The combination of EtOH dipping and ultrasonic NaOH solution immersion for both 10 and 40 minutes (figure 3C and D respectively) results in staining of the entire surface of the samples, with some differences in color intensities across the sample surfaces.

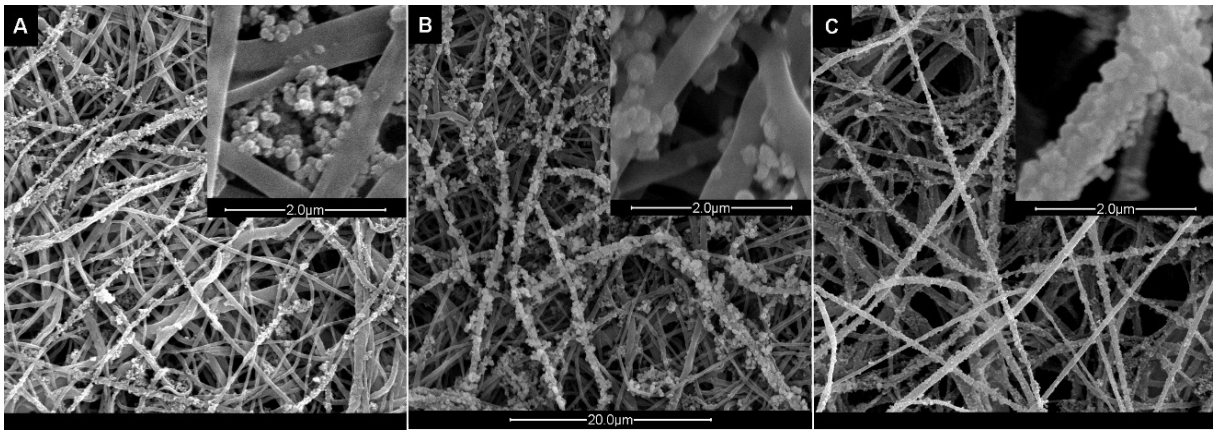

Figure 4. SEM images of PCL nanofiber mats activated according to the experimental conditions of A) EtOH) B) EtOH – 10min and C) EtOH – 40min followed by treatment with the standard nucleation procedure.

SEM images of samples activated according to the experimental conditions of EtOH, EtOH-10min, EtOH-40min and treated with the standard nucleation procedure are shown in figure 4. Considering the partial staining of samples activated according to the experimental conditions of EtOH, only stained regions were analyzed by SEM. The corresponding SEM image in figure 4A is representative for all samples with incomplete staining. The surface shows lumps of CP accumulations, in some cases obstructing the pores. Fiber coverage on the other hand is minimal with some discrete CP deposits on the fiber surface. For the samples activated with the parameters of experiment EtOH-10min, the surface of the fibers is partly coated with lumps of CP, with no accumulations of CP precipitates obstructing the

pores (figure 4B). For the samples treated with the experimental conditions of EtOH-40min, the pore structure is completely preserved and the majority of the fibers are completely covered with a CP layer (figure 4C). EtOH dipping followed by a 40 minutes immersion in NaOH solution under ultrasonic conditions is the best activation method since it results in the most reproducible CP coating with preservation of the porous structure after treatment with the standard nucleation procedure. However, since the deposited CP coating is not completely homogeneous, the nucleation procedure needed optimization.

1.3.3 Optimization of the CP nucleation

The conditions of the standard nucleation procedure are used as starting point for the design of the primary vertex. Five additional experimental conditions are generated by varying one factor while holding all other factors constant. The conditions of the experiments generated by the simplex are given in table 2. Based on the ARS staining and the morphology of the coated fibers, the samples obtained by the different experiments can be divided into two categories.

a Poor, not reproducible or heterogeneous coating

The digital image of samples treated with the parameters of experiment P-5 shown in figure 5A is representative for the samples treated with the experimental conditions of experiments P-1 to P-7 (table 2). The CP deposition on all these samples is poor, indicated by the fact that they remain mainly white after ARS staining. In figure 5B the digital image of samples treated with the conditions of experiment N-9 is shown. The figure is representative for samples treated with the conditions of experiments N-1 to N-10 (table 2). In this group of experiments, treatment of samples using the same experimental conditions results in mutual different color intensities, indicating that the procedure is not reproducible. The digital image of the samples treated with the experimental conditions of experiment H-9 (figure 5C) is representative for samples treated with the experimental conditions of experiments H-1 to H-10 (table 2). The staining of these samples is not homogeneous, as indicated by the differences in color intensities among different regions of the same sample.

b Homogeneous and reproducible coating

The digital and SEM image of samples treated with the experimental conditions of experiment D-1 are given in figure 6. The figure is also representative for the samples treated with the experimental conditions of experiment D-2 (table 2). The digital image shows intense dark coloring of the samples (figure 6(top)). The SEM images show profuse mineralization with almost complete coverage of the surface and disappearance of the pore and fiber structure (figure 6(bottom)). Samples treated with the experimental conditions of experiments A-1 to A-4 stain pale pink. Results of the reproducibility test for these four experiments are summarized in figure 7. Samples treated with the experimental conditions of exp A-1 to A-3

show variations in staining, with locally white spots and lighter and darker staining. Samples treated with the experimental conditions of exp A-4 show a predominantly uniform pale pink ARS staining. Although SEM images show no visible coating of the samples treated with the parameters of exp A-1 (figure 8A), the SEM images of the samples treated with the experimental conditions of exp A-2 to A-4 show an increase in roughness of the fiber surface. The latter indicates the presence of a very thin layer on the fibers (figure 8B - D).

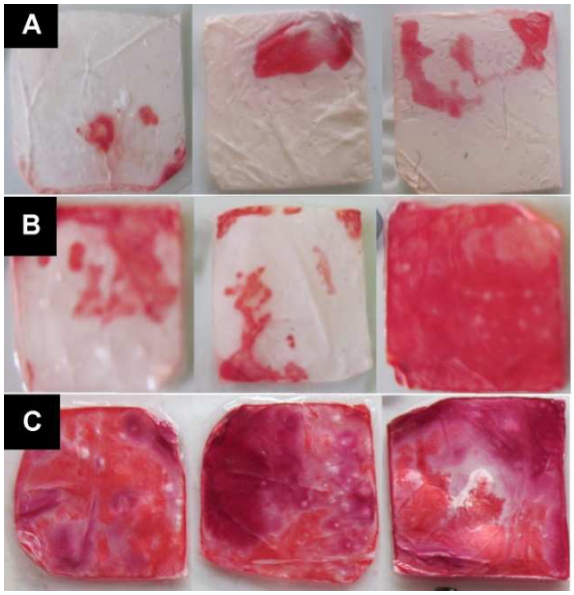

Figure 5. Digital images of samples treated with the conditions of the experiments generated by the simplex. A) poor staining: P-5 B) not-reproducible staining: experiment N-9 C) heterogeneous staining: experiment H-9.

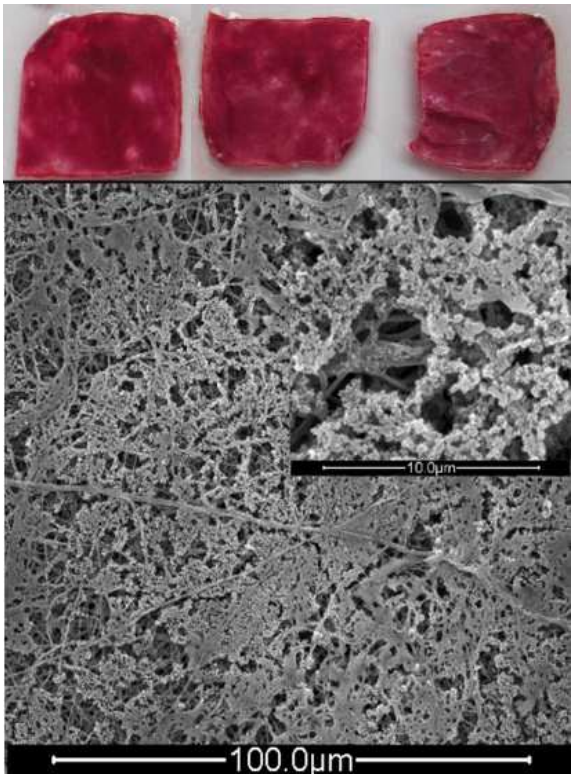

Figure 6. Digital image of ARS stained samples (top) and SEM images (bottom) after treatment with the experimental conditions of experiment D-1.

Electrospun PCL scaffold

Figure 7. Digital images of reproducibility assay, experiments A-1 to A-4 were repeated ten-fold.

Table 2

Conditions of the experiments used for the optimization of the calcium phosphate nucleation step. Based on resulting ARS staining and morphology of coating, experiments are organized as poor (P), not reproducible (N), heterogeneous (H), dark (D) and adequate (A). In bold are the experimental conditions of the start simplex, including the standard nucleation procedure(*).

		$CaCl_2.2H_2O$		Na_2HPO_4	
Exp	# Cycles	Concentration (mM)	Immersion time (s)	Concentration (mM)	Immersion time (s)
P-1	3	34.01	75.60	34.01	80.16
P-2	4	45.68	66.22	45.68	68.82
P-3	4	52.55	54.76	52.55	65.69
P-4	3	45.40	67.61	87.33	48.76
P-5	10	3.92	78.71	27.85	33.91
P-6	8	55.44	64.92	12.33	52.35
P-7	6	87.99	77.29	8.61	35.82
N-1	1	75.00	60.00	75.00	60.00
N-2	4	52.50	48.00	52.50	48.00
N-3	6	69.38	60.00	69.38	60.00
N-4	4	53.83	76.29	53.83	50.99
N-5	5	58.13	62.05	58.13	53.26
N-6	3	89.06	55.92	52.25	64.38
N-7	7	32.81	55.92	52.25	64.38
N-8	5	67.89	72.24	31.07	55.38
N-9	4	56.31	64.69	64.50	52.66
N-10	8	60.96	62.98	20.80	37.00
H-1*	**6**	**75.00**	**60.00**	**75.00**	**60.00**
H-2	**6**	**75.00**	**30.00**	**75.00**	**60.00**
H-3	**6**	**18.75**	**60.00**	**75.00**	**60.00**
H-4	**6**	**75.00**	**60.00**	**75.00**	**30.00**
H-5	**6**	**75.00**	**60.00**	**18.75**	**60.00**
H-6	4	50.25	90.00	50.25	48.00
H-7	4	48.23	72.00	48.23	43.20
H-8	5	64.75	63.90	64.75	42.54
H-9	5	59.07	49.10	59.07	59.61
H-10	8	30.04	52.22	48.14	57.03
D-1	5	64.56	35.16	64.56	59.98
D-2	5	59.98	64.48	59.98	49.11
A-1	**2**	**75.00**	**60.00**	**75.00**	**60.00**
A-2	4	53.51	69.00	53.51	47.40
A-3	6	78.81	59.82	42.00	46.92
A-4	8	32.30	71.11	35.98	44.07

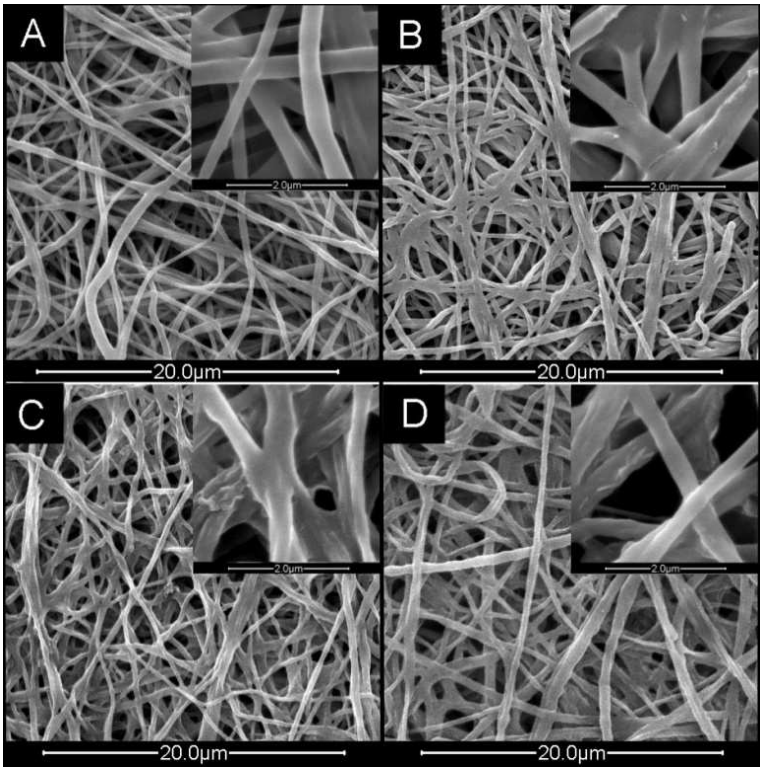

Figure 8. SEM images of samples treated with the experimental conditions of A) A-1 B) A-2 C) A-3 and D) A-4.

1.3.4 FTIR analysis

The FTIR spectrum of the CP precipitated on the samples after calcium phosphate treatment with the experimental procedure of experiment A-4 is shown in figure 9. Peaks due to the v_4-PO_4^{3-} bending at 500 – 700 cm $^{-1}$ and the v_1 and v_3 stretching of PO_4^{3-} groups around 970, 1045 and 1100 cm^{-1} are typical peaks of an apatitic phase. The peak around 878 cm^{-1} , arising from the v_5-P-O(H) deformation of HPO_4^{2-} and the absorbance at 1138 cm^{-1} indicate the presence of HPO_4^{2-} groups. Consequently, the CP coating is not a pure apatite but a calcium-deficient apatite (CDHAp; $Ca_{10-x}(HPO_4)_x(PO_4)_{6-x}(OH)_{2-x}$ (with $0 < x < 1$)). Three weak peaks around 1250, 1300 and 1475 cm^{-1}, and three more intense peaks around 1740, 2830 and 3025 cm^{-1}, can be assigned to PCL since they correspond with intense peaks found in the infrared spectrum of untreated PCL.

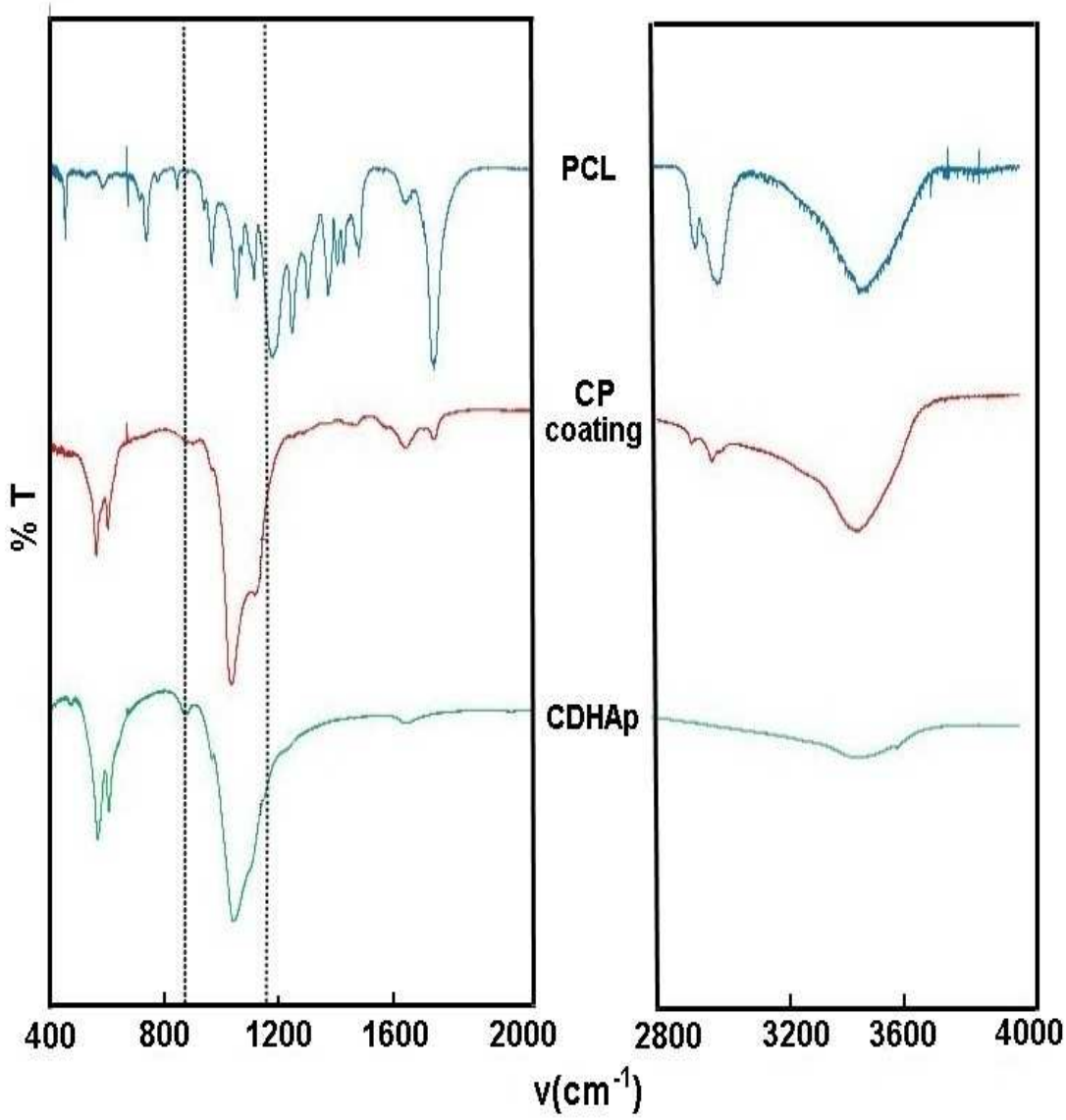

Figure 9. Infrared spectrum of the CP coating on the samples treated with the conditions of experiment A-4. For comparison the IR spectra of PCL and CDHAp are shown. The dotted lines mark HPO_4^{2-} absorptions.

1.3.5 Cell viability, adhesion and proliferation on electrospun PCL fiber mats

After 24h of incubation, the amount of viable cells attached to the CP coated and untreated PCL samples are similar. The cells are round on the untreated PCL samples, and elongated on the CP coated samples (figure 10A and 10D).

After 7 days of incubation, cell attachment or cellular spreading is not changed in untreated PCL. The majority of cells is still small and round, although a limited number of cells form extensions. On the CP coated samples, the amount of viable cells increased. Cells show elongated morphologies and are forming extensions.

Electrospun PCL scaffold

At day 14 the amount of cells attached to the untreated samples slightly increased. Regions of high cell density can be observed as shown in figure 10C. The majority of the cells are large, round. Cell attachment and spreading increased on the CP treated samples. The morphology is similar to the observed morphology of cells in the confluent positive culture. On the untreated sample the number of dead cells increased progressively from 1 to 14 days. An overall low amount of dead cells is present on the CP treated samples.

The quantity of viable and attached MC3T3-E1 cells on the CP coated and untreated samples after 1, 7 and 14 days (as reflected by the Presto Blue^{TM} assay and expressed as % viable cells) is illustrated in figure 11. At day 1 and day 7, the amount of attached cells on the untreated PCL samples is 1.9% of the positive control. After 14 days the amount of attached cells increased significantly ($p = 0.017$) to 6.5%. After 1 day of incubation there is no significant difference between the untreated and treated samples. 13 respectively 32.2 % of attached cells is observed after 7 and 14 days. This amount of attached cells on the CP coated samples are significantly higher than the cell viabilities on the untreated samples ($p = 0$), but still low when compared to the control.

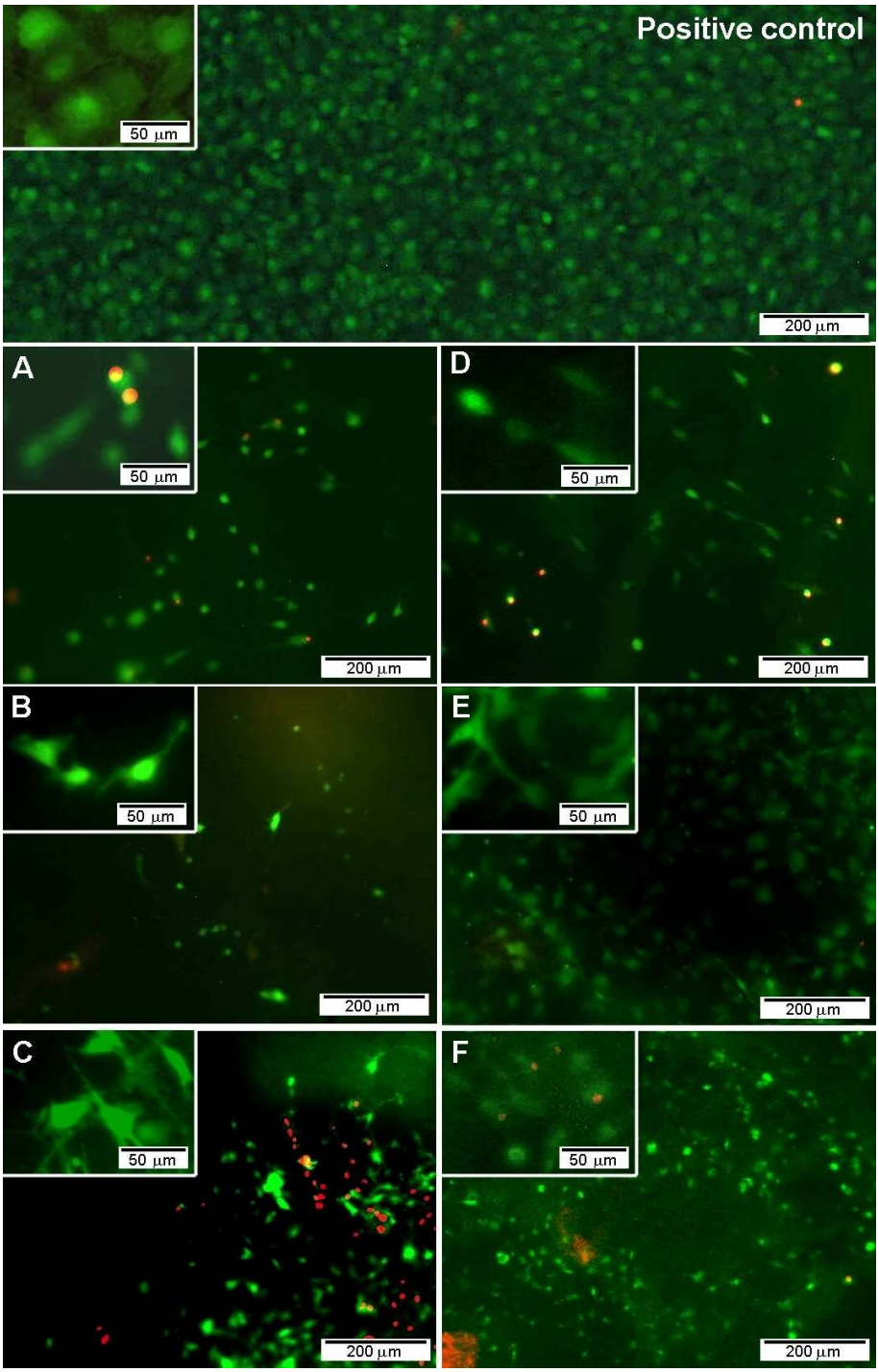

Figure 10. Morphology of MC3T3-E1 pre-osteoblast cells attached to untreated PCL fiber mats (A-C) or CaP treated PCL fiber mats (D-F) after 1 day (A-D), 7 days (B-E) and 14 days (C-F) of culture. The positive control is a tissue culture polystyrene plate.

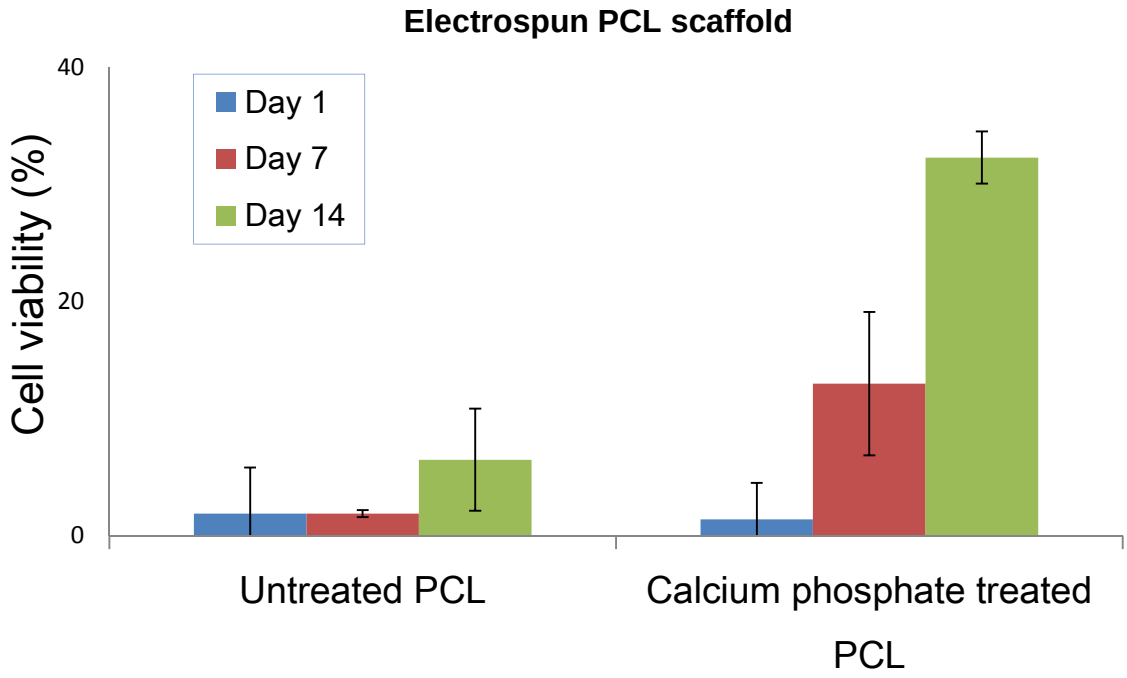

Figure 11. Cell viability on untreated and calcium phosphate treated samples after 1, 7 and 14 days of incubation. The cell viability was calculated as a percentage of the positive control at day 14 of culture. Error bars represent standard deviations.

1.4 Discussion

An electrospun PCL material is interesting as bone tissue engineering scaffold because of its 3D structure, interconnected pore system, biocompatibility and biodegradability. However, as a result of the hydrophobic nature of PCL, the scaffold lacks cell adhesion domains, minimizing the surface bioactivity.[2] In addition, the acidic degradation products have detrimental effects on the cells. Coating the fiber surface with a homogeneous layer of CP creates a composite combining the flexibility, high porosity and surface area of the electrospun polymer, with the biocompatibility, osteoconductivity and bone-bonding ability of the CP. [2,9,18] Ideally the polymer fibers are coated with a thin layer of bone-like apatite, without compromising the porous structure. Two reported techniques for the coating of electrospun polyester fibers are the alternate dipping procedure in calcium and phosphate rich solutions and/or the incubation in SBF.[18,19,21,22,24-26] Experiments reveal that in the case of PCL no CP could be deposited onto the fiber surface using only one of these two techniques.[25,35] This can be explained by the hydrophobic nature of the material, and hence, by the lack of chemical groups on the fiber surface.[18] In order to overcome this obstacle the scaffold needs to be activated. This involves the rapid and local degradation of the fiber surface, creating reactive carboxylated groups on the fiber surface throughout the scaffold.

1.4.1 Activation

Treatment of electrospun PCL samples with an aqueous NaOH solution, is a frequently used method to create reactive carboxylated groups on the fiber surface and to modify the surface wettability.[18,24,25] Partial surface hydrolysis causes random chain cleavage

of the ester linkages on the polymer backbones located at the surface, generating reactive carboxyl and hydroxyl groups.[18,36] The hydrolysis of ester bonds is an acid catalyzed process, which makes HCl solution also a possible activating agent.[37,38] The present study shows that treatment of the electrospun PCL samples with HCl solution alone or in combination with NaOH solution has no effect on the hydrophobicity as reflected by WCA measurements (table 1). This is substantiated by the fact that these samples show no CP deposition after treatment with the standard nucleation procedure.

Activation with 1 M NaOH solution for 6 h results in PCL samples with a slightly decreased WCA (table 1). Increasing the immersion time or the concentration of the NaOH solution enhances this effect. However, treatment with the standard nucleation procedure only results in local spots of CP precipitation as visualized by the ARS staining. Apparently, the surface of the PCL fibers is not homogeneously activated. This can be explained by the surface hydrophobicity of the PCL samples, which hinders the diffusion of the aqueous NaOH solution into the air-filled pores.[39,40] Hence morphology could play a role, as larger pores are expected to have a greater ability to be infiltrated with NaOH solution.

To overcome the problems associated with the hydrophobic nature of PCL, it is necessary to obtain a uniform hydrophilic sample surface prior to immersion in NaOH solution. Since EtOH is a well-known wetting medium for polyesters, it is applied as pre-treatment medium to wet the PCL samples.[40] Upon dipping in EtOH the color of the PCL samples alters from white to grey as they are soaked with the alcohol, indicating that the samples are hydrophilic (figure 3). However, after drying the samples a decrease in WCA is not observed, suggesting that hydrophobicity is restored. PCL samples treated with the standard nucleation procedure immediately after EtOH dipping only show partial CP deposition, indicating EtOH alone is unable to generate a sufficient number of reactive surface groups.

EtOH treatment followed by an immersion in 1 M NaOH solution for 3h does not create a hydrophilic surface, so that samples show no uniform CP deposition after treatment with the standard nucleation procedure (table 1; figure 4). After treatment with EtOH and a 6 h immersion in 1 M NaOH solution, the samples are hydrophilic while samples immersed for 6 h in NaOH solution alone are still hydrophobic, as reflected by the WCA measurements (table 1). Clearly, the EtOH pre-treatment enhances the wettability of the samples. However, after treatment with the standard nucleation procedure, even the EtOH pre-wetted samples show no uniform CP deposition. This could be explained by the diffusion controlled infiltration occurring at the pore sites. When the samples are first pre-wetted with EtOH and then placed in an aqueous solution of NaOH, the NaOH solution diffuses into the pores, mixes with EtOH and finally replaces EtOH.[39] It can be expected that this diffusion controlled infiltration is faster when pores are larger. Differences in the pore size result in differences in the

infiltration so that the amount of generated carboxylated groups depends on the local porosity of the samples resulting in an inhomogeneous activation with the NaOH solution.

To promote an effective influx of NaOH solution into the pores, the samples are pre-wetted with EtOH and immersed in 1 M NaOH solution under ultrasonic conditions. The effects of ultrasound are derived particularly from acoustic cavitation as bubble collapses near the material surface result in jets of liquid impinging at high velocity onto the surface. The micro-jets hitting the samples result in an enhanced contact between the PCL fiber surface and the surrounding NaOH solution, enhancing the mass transport and diffusion of the solution into the pores.[41] An additional physical effect of ultrasound includes the erosive action of the micro-jets hitting the surface of the material. The resulted roughening of the surface creates an ideal surface for subsequent coating.[42] Pre-wetting the samples with EtOH followed by immersion in NaOH solution under ultrasonic conditions appears to be a fast and effective activation method. A hydrophilic surface was obtained after only 10 minutes of immersion in 1M NaOH solution (table 1). However, the PCL fibers were only partially covered with CP. After subjecting the EtOH pre-wetted samples to 40 minutes of ultrasonic immersion in a 1M NaOH solution, the surface is successfully activated as reflected by the complete CP coverage of the PCL fibers after subsequent treatment with the standard nucleation procedure (figures 3D and 4C). Since the deposited CP layer on these samples is not homogeneous, the conditions of the nucleation step need to be optimized.

1.4.2 Nucleation

In the nucleation phase five parameters of the alternate dipping process are optimized simultaneously: the number of cycles, concentration of and immersion time in both the calcium and the phosphate rich solutions. The ARS staining and SEM images show that specific combinations of these five parameters can create ideal conditions for the deposition of a homogeneous and reproducible CP coating. Only six combinations result in such CP coating on the PCL fibers. The experimental conditions of experiments D-1 and D-2 result in a profuse mineralization with almost complete coverage of the surface (figure 7 bottom). Such situation leaves no room for maturation of the CP layer in a next step. The parameters of experiments A-1 to A-4 result in a thin and homogenous coating. The reproducibility assay shows that the parameters of experiment A-4 result in the most reproducible coating.

FTIR spectrophotometry reveals that the deposited CP coating obtained by treating the activated samples with the parameters of experiment A-4 is calcium-deficient hydroxy apatite (CDHAp) (figure 9). SEM images of the corresponding samples show no deposited CP crystals, only a slight roughening of the fiber surface, which could indicate the nanocrystallinitiy of the CDHAp crystals (figure 8D). CDHAp nanocrystals are shown to exhibit physicochemical characteristics similar to those of bone nanocrystals. Due to their

calcium deficiency, CDHAp nanocrystals are more soluble and have an increased bioresorption rate *in vivo* compared to stoichiometric HAp.[43,44] In line with this it can be expected that coating of the PCL nanofibers with nanoscaled CDHAp crystals could improve the cellular response as compared to untreated PCL.

1.4.3 Cell viability, adhesion and proliferation

The amount of cells attached on the untreated PCL samples is low (figure 11). Even after 14 days of culture cells are not able to attach well to the samples.[45] The observed cellular behavior could be expected due to the hydrophobic nature of the untreated PCL samples (table 1). The hydrophobicity hinders the initial biological responses, such as protein adsorption, making it difficult for the cells to adhere to such surfaces.[46] The CDHAp coating on the PCL nanofibers enhances the MC3T3-E1 cell response. CDHAp coated samples show an increase in the amount of attached cells throughout the experiment (figure 11). After 14 days of culture cells are well attached on the CDHAp coated surface and show similar cellular morphologies as the control (figure 10 D-F). Our results corroborate the findings of other authors who also compared the response of MC3T3-E1 pre-osteoblasts cultured on pure electrospun PCL and electrospun PCL samples coated with an apatite phase. Although these studies do not indicate the reproducibility of their coating procedure, nor that the fibers are adequately covered, all reports conclude that the hydrophilic CP coating improved the pre-osteoblasts cellular attachment and growth.[24,26]

Pieters *et al*. reported that apatites with a carbonate content equal to or higher than 11% show an improved cell adhesion and proliferation in comparison to that on carbonate-free apatite.[47] Based on these findings it would be interesting to attempt to incorporate carbonate ions in the apatite lattice. In order to do this, the CDHAp coated PCL samples can be incubated in a SBF-like solution. During this maturation phase the CDHAp primer layer can grow and incorporate carbonate ions, mimicking the apatite phase found in the ECM of bone.

1.5 Conclusion

In the present study, coating of electrospun PCL nanofibrous scaffold with a thin primer layer of CP was optimized. The electrospun PCL scaffold was produced with a new low-toxic solvent mixture of formic acid/acetic acid was used. Adequate coating was achieved in a two step procedure. First, the polymer surface was uniformly activated without any obvious change in the fiber structure. Next, the fibers were coated with a homogeneous, thin and reproducible CDHAp coating, with preservation of the porous structure. Such CDHAp coating on the surface of the PCL nanofibers improved the osteogenic response and

enhanced the cell affinity when compared to the uncoated PCL samples. In order to further enhance the cellular response, the incorporation of carbonate ions in the apatite lattice is recommended. Such carbonated apatite more closely resembles the mineral found in bone.

1.6 References

1. Gupte M, Ma P. Nanofibrous scaffolds for dental and craniofacial applications. Journal of dental research 2012; 9(3): 227 -234.
2. Jang J, Castano O. Electrospun materials as potential platforms for bone tissue engineering. Advanced drug delivery reviews 2009; 61: 1065 -1083.
3. Wei G, Ma P. Nanostructures biomaterials for regeneration. Advanced functional materials 2008; 18: 3568 -3582.
4. Holzwarth J, Ma P. Biomimetic scaffolds for bone tissue engineering. Biomaterials 2011; 32: 9622-9629.
5. Burg K, Porter S, Kellam J. Biomaterial development for bone tissue engineering. Biomaterials 2000; 21: 2347-2359.
6. Hutmacher D. Scaffolds in tissue engineering bone and cartilage. Biomaterials 2000; 21: 2529-2543.
7. Stevens B, Yang Y, Mohandas A, Stucker B, Nguyen K. A review of materials, fabrication methods, and strategies used to enhance bone regeneration in engineered bone tissue. Journal of biomedical materials research B 2008; 85B: 573-582.
8. Liao S, Murugan R, Chan C, Ramakrishna S. Processing nanoengineered scaffolds through electrospinning and mineralization suitable for biomimetic bone tissue engineering. Journal of the mechanical behavior of biomedical materials 2008; I: 252-260.
9. Stevens M. Biomaterials for bone tissue engineering. Materials Today 2008; 11(5): 18-25.
10. Ashammakhi N, Rokkanen P. Absorbable polyglycolide devices in trauma and bone surgery. Biomaterials 1997; 18: 3-9.
11. Gupta A, Kumar V. New emerging trends in synthetic biodegradable polymers – Polylactide: A critique. European polymer journal 2007; 43(10): 4053-4074.
12. Woodruff M, Hutmacher D. The return of a forgotten polymer – Polycaprolactone in the 21ste century. Progress in polymer science 2010; 35: 1217-1256.
13. Doshi J, Reneker D. Electrospinning process and applications of electrospun fibers. Journal of electrostatics 1995; 35: 151-160.
14. Li W, Cooper J. Fabrication and characterization of six electrospun poly(α-hydrocyester)-based fibrous scaffolds for tissue engineering applications. Acta biomaterialia 2006; 2: 377-385.
15. Cui W, Li X, Zhou S, Weng J. In situ growth of hydroxyapatite within electrospun poly(DL-lactide) fibers. Journal of biomedical material research A 2007; 82A: 831- 841.
16. Yang F, Both S, Yang X, Walboomers F, Jansen J. Development of an electrospun nano-apatite/PCL composite membrane for GTR/GBR application. Acta biomaterialia 2009; 5: 3295-3304.
17. Rezwan K, Chen Q, Blaker J, Boccaccini A. Biodegradable and bioactive porous polymer/inorganic composite Scaffolds for bone tissue engineering. Biomaterials 2006; 27: 3413-3431.
18. Araujo J, Martins A, Leonor I, Pinho E, Reis R, Neves N. Surface controlled biomimetic coating of polycaprolactone nanofiber meshes to be used as bone extracellular matrix analogues. Journal of biomaterials science, polymer edition 2008; 19(10): 1261-1278.
19. Ngiam M, Liao S, Patil A, Cheng Z, Chan C, Ramakrishna S. The fabrication of nano-hydroxyapatite on PLGA and PLGA/ collagen nanofibrous composite scaffolds and their effects in osteoblastic behavior for bone tissue engineering. Bone 2009; 45: 4-16.
20. Andric T, Wright L, Taylor B, Freeman J. Fabrication and characterization of three-dimensional electrospun scaffolds for bone tissue engineering. Journal of biomedical material research A 2012; 100A: 2097-2105.
21. Yang F, Wolke J, Jansen J. Biomimetic calcium phosphate coating on electrospun poly(ε-caprolactone) scaffolds for bone tissue engineering. Chemical engineering journal 2008; 137: 154-161.
22. Chen J, Chu B, Hsiao B. Mineralization of hydroxyapatite in electrospun nanofibrous poly(L-lactid acid) scaffolds. Journal of biomedical material research A 2006; 79A: 307-317.

23. Cui W, Li X, Xie C, Chengying X, Zhuang H, Zhou S, Weng J. Hydroxyapatite nucleation and growth mechanism on electrospun fibers functionalized with different chemical groups and their combinations. Biomaterials 2010; 31: 4620-4629.
24. Yu H, Jang J, Kim T, Lee H, Kim H. Apatite-mineralized polycaprolactone nanofibrous web as a bone tissue engineering substrate. Journal of biomedical material research A 2009; 88A: 747-754.
25. Oyane A, Uchida M, Choong C, Triffitt J, Jones J, Ito A. Simple surface modification of poly(ε-caprolactone) for apatite deposition from simulated body fluid. Biomaterials 2005; 26: 2407-2413.
26. Mavis B, Demirtas T, Gumusderelioglu M, Gunduz G, Colak U. Synthesis, characterization and osteoblastic activity of polycaprolactone nanofibers coated with biomimetic calcium phosphate. Acta biomaterialia 2009; 5: 3098-3111.
27. Lanutti J, Reneker D, Ma T, Tomasko D, Farson D. Electrospinning for tissue engineering scaffolds. Materials science and engineering C 2007; 27: 504-509.
28. Van der Schueren, L, De Schoenmaker B, Kalaoglu O, De Clerck K. An alternative solvent system for the steady state electrospinning of polycaprolactone. European polymer journal 2011; 47(6): 1256-1263.
29. Yoshimoto H, Shin Y, Terai H, Vacanti J. A biodegradable nanofiber scaffold by electrospinning and its potential for bone tissue engineering. Biomaterials 2003; 24: 2077-2082.
30. Walter F, Parker L, Morgan S, Deming S. Sequential simplex optimization: a technique for improving quality and productivity in research, development and manufacturing. Boca Raton: CRC Press LLC 1999
31. Gregory C, Gunn W, Peister A, Prockop D. An Alizarin red-based assay of mineralization by adherent cells in culture: comparison with cetylpyridinium chloride extraction. Analytical biochemistry 2004; 329 (1): 77-84.
32. Madurantakam P, Rodriguez I, Cost C, Viswanathan R, Simpson D, Beckman M, Moon P, Bowlin G. Multiple factor interactions in biomimetic mineralization of electrospun scaffolds. Biomaterials 2009; 30: 5456 -5464.
33. http://www.invitrogen.com/site/us/en/home/brands/Molecular-Probes/Key-Molecular-Probes-Products/PrestoBlue-Cell-Viability-Reagent.html
34. http://www.ebioscience.com/media/pdf/best-protocols/viability-staining.pdf
35. Li X, Xie J, Yuan X, Xia Y. Coating of electrospun poly(ε-caprolactone) fibers with gelatin and calcium phosphate and their use as biomimetic scaffolds for bone tissue engineering. Langmuir 2008; 24:14145 -14150.
36. Yoo H, Kim T, Park T. Surface-functionalized electrospun nanofibers for tissue engineering and drug delivery. Advanced drug delivery reviews 2009; 61: 1033-1042.
37. Boland E, Telemeco T, Simpson D, Wnek G, Bowlin G. Utilizing acid pretreatment and electrospinning to improve biocompatibility of poly(glycolic acid) for tissue engineering. Journal of biomedical material research B 2004; 71B: 144-152.
38. Tanahashi M, Yao T, Kokubo T, Minoda M, Miyamoto T, Nakamura T, Yamamuro T. Apatite coated on organic polymers by biomimetic process – Improvement in adhesion to substrate by HCl treatment. Journal of materials science: materials in medicine 1995; 6(6): 319-326.
39. Mikos A, Lyman M, Freed L, Langer R. Wetting of poly(L-lactic acid) and poly(DL-lactic-co-glycolic acid) foams for tissue engineering. Biomaterials 1994; 15: 55-58.
40. Yang J, Wan Y, Tu C, Cai Q, Bei J, Wang S. Enhancing the cell affinity of macroporous poly(L-lactide) cell scaffold by convenient surface modification method. Polymer international 2003; 52: 1892-1899.
41. Suslick K, Price G. Applications of ultrasound to materials chemistry. Annuals reviews of material science 1999; 29: 295-326.
42. Cobley A. Ultrasound sonochemistry – A more sustainable approach to surface modification? Surface engineering 2009; 25(8): 559-563.
43. Dorozhkin S. Calcium orthophosphates. Journal of materials science 2007; 42: 1061-1095.
44. Dorozhkin S. Nanosized and nanocrystalline calcium orthophosphates. Acta biomaterialia 2010; 6: 715-734.
45. Shah A, Sinha R, Hickok N, Tuan R. High-resolution morphometric analysis of human osteoblastic cell adhesion on clinically relevant orthopedic alloys. Bone 1999; 24: 499-506.
46. Ghasemi-Mobarakeh L, Morshed M, Karbalaie K, Fesharaki M, Nasr-Esfahani M, Baharvand H. Electrospun poly(ε-caprolactone) nanofiber mat as extracellular matrix. Yakhteh medical journal 2008; 10(3): 179-184.
47. Pieters I, Van den Vreken N, Declercq H, Cornelissen M, Verbeeck R. Carbontated apatites obtained by the hydrolysis of monetite: Influence of carbonate content on adhesion and proliferation of MC3T3-E1 osteoblastic cells. Acta biomaterialia 2010; 6: 1561-1568.

2 Calcium phosphate coating of an electrospun PDLLA scaffold

Part of the research is based on the article:

Optimization of the time efficient calcium phosphate coating on electrospun poly(D,L-lactide).

Nathalie Luickx, Natasja Van den Vreken, Jonas Segaert, Heidi Declercq, Maria Cornelissen, Ronald Verbeeck

Journal of Biomedical Materials Research Part A 2015; 103(8): 2720-2730.

Abstract: The coating of fibrous polyester constructs with a layer of bioactive calcium phosphate (CP) is efficient to improve the potential use as bone tissue engineering scaffold. In the present study a fast procedure for the coating of electrospun poly(D,L-lactide) (PDLLA) fibers with a CP layer was optimized. The fiber surface was activated by immersion in demineralized water under ultrasonication. The resulting reactive groups served as nucleation points for CP precipitation, induced by alternate dipping of the samples in Ca^{2+} and PO_4^{3-} rich solutions. Variations in the conditions of the alternate dipping procedure, in particular the number of cycles, concentration and immersion time of both solutions, not only affected the degree of surface mineralization but also the type of deposited CP. For the current experimental conditions, in about 30 minutes either a slightly carbonated calcium deficient apatite (CDAp; $Ca_{10-x-y}(PO_4)_{6-x-y}(HPO_4)_y(CO_3)_x(OH)_{2-x-y}$) or a combination of apatite and dicalcium phosphate dihydrate (DCPD; $CaHPO_4.2H_2O$) was formed. The cell viability, adhesion and proliferation of MC3T3-E1 cells on untreated samples were compared to samples coated with either an adequate amount of CDAp, an excess of CDAp or an excess of a combination of apatite and DCDP. After 7 days of culture the number of attached cells was significantly higher on all CP coated samples compared to the untreated PDLLA. In particular the samples coated with an adequate amount of CDAp showed an exceedingly enhanced cell response with similar cell morphologies as the ones found on the positive control.

Electrospun PDLLA scaffold

Electrospun PDLLA scaffold

2.1 Introduction

For the reconstruction of bone defects, three-dimensional (3D) scaffolds with an interconnected pore system are intensively investigated. As such porous scaffold shows structural similarity with the extracellular matrix (ECM) cell adhesion, proliferation and differentiation is enhanced compared to dense scaffolds.[60] In order to allow cell in-growth, vascularization and efficient transport of nutrients, oxygen, growth factors and metabolites, interconnectivity of the pores is necessary.[9] The material used to fabricate the scaffold should be biocompatible, bioactive and osteoconductive. Ideally, the scaffold is biodegradable with a degradation rate equal to the bone repair rate so as to ensure the mechanical stability. Finally, when the scaffold is completely degraded, the initial bone defect is filled with newly formed bone tissue.[21]

The aliphatic polyesters polylactic acid (PLA), polyglycolic acid (PGA), polycaprolactone (PCL) and their copolymers are interesting scaffold materials. These Food and Drug Administration (FDA) approved polymers are biodegradable and easy to manufacture into different shapes. [22,41] The mechanical properties and degradation kinetics of the polyesters can be tailored by using various molecular weights and copolymers.[42] Special interest goes out to PLA, that exists in three morphologically distinct polymers due to the chiral nature of its monomer. PDLA and PLLA, the two stereo-regular polymers are semicrystalline. PDLLA is the racemic polymer obtained from a mixture of PDLA and PLLA in a 1/1 ratio and it is amorphous. The latter results in a degradation time of PDLLA of 12 to 16 months in the human body, which is shorter than that of PDLA and PLLA. This relative short degradation time is the main reason for the use of PDLLA as surgical suture material and as a controlled drug delivery device. PDLLA also has great potential as bone tissue engineering scaffold due to its well established safety in clinical use and suitable biodegradation time. [42,96,103] By processing PDLLA by means of electrospinning a 3D nanofibrous structure with high surface-to-volume ratio, high porosity and an interconnected pore system can be manufactured.[62]

However, due to the hydrophobic nature of polyesters, the bioactivity of PDLLA scaffolds is low.[194,208] In order to enhance the bioactivity without changing the intrinsic properties of the material, coating of the polyester surface with an apatite layer is applied. Such calcium phosphate (CP) layer is chemically comparable to the mineral phase found in natural bone and acts as an excellent cell support to maintain desirable cell-substrate interactions.[145,190,207,209,210] Polymer-mineral composites apparently have improved bioactivity and mechanical strength compared to pure polymer scaffolds.[211,212] Moreover, the resorption of the apatite layer could contribute to the neutralization of the acidic polymer degradation by-products, which could cause inflammation. [22,41,93] The neutralization is ascribed to the

reaction of calcium ions and the carboxyl end-groups generated during degradation of the polymer, to form calcium carboxylate chain ends. This complexation results in an increased solubility of the CP, causing an increase of the pH. As a result, the acidic autocatalytic break down of the polymer is slowed down.

In literature, little is reported on the CP coating of pure PDLLA fiber mats. Chen *et al.* describe a CP coating procedure of electrospun PLLA samples by long-term incubation in a simulated body fluid (SBF). After 7 days of incubation CP deposits are visible and after 14 days the fibers are completely covered with a layer of slightly carbonated apatite.[195] Cui *et al.* showed that a CP coating was not formed on electrospun PDLLA samples after an incubation of 6 days in a SBF solution with a 1.5 times higher ion concentration than regular SBF (1.5xSBF). Due to its hydrophobicity and inability to induce nucleation and growth of CP on the fiber surface, PDLLA lacks bioactivity.[207] On the other hand, when PDLLA samples were subjected to an activation procedure prior to the SBF incubation, a CP coating was formed after 7 days of incubation in 2xSBF.[211] The activation procedure is necessary to create reactive carboxyl groups on the fiber surface by cleaving the polyester bonds. Apparently the presence of carboxyl groups is required to promote the deposition of a CP layer on the fiber surface.[211,213] Despite the fact that incubation in SBF is a relative easy coating procedure, an inherent drawback of the method is the time required to deposit an adequate amount of CP.[214]

In order to accelerate the process of CP formation on porous polymer scaffolds, an alternate soaking procedure is interesting.[189,214] In this process, the polymer samples are alternately dipped in solutions containing high concentrations of calcium and phosphate ions, which accelerates the process of CP coating compared to the conventional incubation in SBF.

As for electrospun PDLLA no rapid and reproducible procedure to coat the fiber surface with a CP layer is available, the objective of this study is to optimize the CP coating of electrospun PDLLA by a two-step procedure. In the first step the surface of the fibers is activated to create the necessary carboxyl groups. In the second step, activated samples are subjected to an alternate dipping process in Ca^{2+} and PO_4^{3-} rich solutions in order to deposit a CP coating. In search of an optimal procedure, not only the time required to deposit an adequate CP layer, but also the reproducibility of the procedure, the homogeneity of the coating and preservation of the porous structure upon coating are a prerequisite. The optimized parameters giving the most reproducible and adequate coating were selected for an *in vitro* study, comparing the adhesion and proliferation of pre-osteoblastic cells (MC3T3-E1) on CP coated samples and untreated electrospun PDLLA samples.

2.2 Materials and Methods

Freshly prepared ultra-pure demineralized water (Milli-Q system, Millipore, Billerica, US) was used for the preparation of the solutions.

2.2.1 PDLLA electrospun mats

PDLLA pellets were purchased from Purac (Purasorb PDL20, inherent viscosity ~ 2.0 dl/g, Gronichem, The Netherlands). A 17 wt% PDLLA solution was prepared by dissolving a measured amount of PDLLA pellets in a mixed solvent of N,N-dimethylformamide (DMF; Merck, Darmstadt, Germany) and acetone (VWR, Leuven, Belgium) with a volume ratio of 2/1 (DMF/acetone), at room temperature. To ensure complete dissolution the polymer/solvent mixture was magnetically stirred at room temperature for 4 h, and then loaded into a 50 ml syringe (Becton Dickinson, Franklin Lakes, US). During the electrospinning process the polymer solution was pumped from the syringe into a 17 G needle. A constant feed rate of 1 ml/h was applied using a syringe pump (Syringe Pump Series 100, KD Scientific, Holliston, US) and a distance of 13 cm was maintained between the tip of the spinneret and the collector plate. A high voltage electric field of 6-7 kV (Series EH Source, Glassman High Voltage, High Bridge, US) was applied to draw the fibers from the spinneret onto the collector plate. The electrospinning was performed in a flow hood, at room temperature (22 ± 2°C) and at an ambient relative humidity of max. 55%.

The thickness of the resulting fiber mats was measured with an electronic micrometer (Digimatic Micrometer Series 293, Mitutoyo, Kruibeke, Belgium). The morphology of the electrospun fibers was evaluated using a scanning electron microscope (SEM; FEI Quanta 200 FEG, Hillsboro, VS). Prior to the SEM-measurements, the samples were coated with gold using a sputter coater (SCD 030, Balzers Union Ltd., Balzers, Liechtenstein). Image analysis software (SigmaScan Pro 5, SPSS Science, Chicago, US) was used to determine the average fiber and pore diameter, fifty diameter measurements were carried out on four samples from different fiber mats.

2.2.2 Activation of the polyester surface

Electrospun fiber mats were cut in pieces of 1 x 1 cm^2. In order to induce a hydrophilic surface samples were either dipped in 10 ml ethanol for 1 second (EtOH; VWR) or placed in an ultrasonic bath (Transsonic T700/H, Elma Ultrasonic, Ruiselede, Belgium). After EtOH dipping the PDLLA samples were washed extensively with demineralized water. For the ultrasonic activation, each sample was transferred in a plastic container filled with 40 ml demineralized water. The containers were subsequently placed in the ultrasonic bath for 3 seconds.

The effect of both procedures on the fiber morphology was analyzed by SEM. In order to evaluate and compare the efficiency of the different activation methods of the fiber surface, the activated samples were alternately immersed in Ca^{2+} and PO_4^{3-} rich solutions using a standard nucleation procedure. In this procedure samples were first dipped in 20 ml/cm² 1000 mM $CaCl_2.2H_2O$ solution (JT Baker, Deventer, The Netherlands) for 1 min, washed with demineralized water for 30 seconds, dipped in 20 ml/cm² 600 mM Na_2HPO_4 solutions (Merck) for 1 min and washed again for 30 seconds with demineralized water. This cycle of four steps was repeated five times. Samples were subsequently stained with Alizarin Red S (ARS; Sigma-Aldrich) solution prepared by dissolving ARS powder in demineralized water to a final concentration of 40 mM and adjusting the pH to 4.1 using 1 M NaOH. Scaffolds were stained on a glass cover plate with an excess of ARS solution for 10 minutes after which the scaffolds were rinsed repeatedly in demineralized water till all unbound dye was washed off. At a pH of 4.1 ARS stains the surface of the CP coated fibers red by binding to the precipitated calcium-ions. The color intensity is linearly correlated with the local calcium concentration.[215] The morphology of the samples after treatment with the standard nucleation procedure was analyzed using SEM. All experiments were carried out at room temperature in triplicate in order to evaluate the reproducibility of the procedure.

2.2.3 Optimization calcium phosphate coating

Coating of the fibers with a thin and homogenous CP layer was achieved by an alternate dipping process in $CaCl_2.2H_2O$ and Na_2HPO_4 solutions. Important parameters of this coating procedure are the concentration of and incubation time in both the Ca^{2+} (C_{Ca} and $T_{Ca)}$ and the PO_4^{3-} rich (C_P and T_P) solutions as well as the number of cylces. In order to efficiently optimize these five parameters at the same time, a variable size simplex algorithm was used.[216] As a base for the generation of the simplex, the parameters of the standard nucleation procedure were used. Experimental conditions generated by the simplex were carried out until a homogenous, thin and reproducible coating of the fibers was obtained.

Activated samples were immersed for a specific time in 20 ml/cm² of $CaCl_2.2H_2O$ and Na_2HPO_4 solutions, each with a given concentration. The samples were washed in 40 ml demineralized water for 30 seconds after each immersion. This procedure was repeated for a specific number of cycles. A minimum of three samples was prepared in order to evaluate the reproducibility of the procedure. The morphology of the CP coating on the fibers was analyzed by SEM. The homogeneity of the CP coating and the reproducibility of the procedures was evaluated by ARS calcium staining. Based on the intensity of the red color after ARS staining, samples were assigned a mineralization score from 0 to 4. The higher the mineralization score, the more intense the red staining color. Samples that remain white after ARS staining were scored 0.

The type of calcium phosphate deposited on the samples was identified by infrared (IR) spectrometry. Samples were immersed in a mixture of 1 ml/cm² acetone and 50 µl/cm² chloroform (Merck) for 10 minutes at room temperature to dissolve the polymer. After centrifugation (2 min; 7000 rpm) the supernatant solution was removed. The remaining pellet was washed with 1ml/cm² acetone followed by centrifugation (2 minutes, 7000 rpm) and removal of the supernatant. This washing-step was repeated twice and the remaining powder was dried overnight at room temperature in order to remove residual acetone. IR spectra of the obtained CP powder dispersed in KBr (Merck) tablets were recorded using a Fourier-transform IR (FT-IR) spectrophotometer (Perkin Elmer Instruments, Waltham, US).

2.2.4 Cell culture and seeding

Monolayers of MC3T3-E1 pre-osteoblasts were routinely cultivated in α-minimum essential medium (α-MEM) (glutaMAX-1 ^{TM} Gibco BRL, Belgium) supplemented with 10% fetal bovine serum (FBS) (heat inactivated, EC approved) and 1 mM sodium pyruvate (Invitrogen, Belgium) at 37°C and in 95% air/5% CO_2 . The medium was changed twice a week.

For the cell viability study samples were selected that were coated with a different type of CP and/or a different degree of surface mineralization of the polymer fibers. Untreated electrospun PDLLA was used as control. CP coated and untreated PDLLA samples were transferred into a 24-well polystyrene standard tissue culture plate (Greiner Bio-one, Frickenhausen, Wemmel, Belgium) and sterilized under UV-light for 30 minutes. Forty thousand MC3T3-E1 cells diluted in 500 µl culture medium were added to each well containing a sample or to a 24-well standard tissue culture plate (positive control). The tissue culture plates were incubated for 7 days.

2.2.5 Cell viability

Cell viability on the CP coated and untreated samples was analyzed after 1 and 7 days of culture with a PrestoBlue^{TM} viability reagent assay (Invitrogen, Carlsbad, US). The samples were rinsed with culture medium after which 450 µl culture medium and 50µl PrestoBlue^{TM} reagent was added to each well. After 2 h incubation at 37°C in a dark room, the medium was transferred to a new plate. The fluorescence was measured with a multilabel plate reader (Victor³, Perkin-Elmer). The quantity of viable cells is linearly correlated with the signal, and the viability was calculated as a percentage of the positive control after 7 days. Each material was tested in triplicate.

The morphology of the attached cells visualized after 1 and 7 days of culture using a calcein acetoxymethyl (AM) ester (Tebu-Bio, Belgium)/propidium iodide (PI) (Sigma-Aldrich)

live/dead staining. PI freely enters dead cells with compromised cell membranes where it intercalates into double-stranded DNA and emits red fluorescence (excitation: 535 nm, emmision: 617 nm). Calcein AM is a non-fluorescent, membrane-permeable dye. Under intracellular esterase activity the dye converts to a membrane-impermeable, green fluorescent compound (excitation: 490 nm, emission: 515 nm). The samples were rinsed with 500 µl phosphate buffered saline (PBS) after which 500 µl PBS, 1 µl PI and 1 µl calcein AM was added to each well. After 10 minutes incubation in a dark room, samples were evaluated with a fluorescence microscope (Type U-RFL-T, Olympus, Belgium).

2.2.6 Statistical analysis

Viability was evaluated using 2-factor ANOVA with the composition of the sample surface and the incubation time as independent variables. Significant differences between means were calculated using a Holm-Sidak multiple-comparison test at the 0.05 confidence level.

2.3 Results

2.3.1 PDLLA electrospun fibers

Electrospinning for 40 minutes results in fiber mats with an average thickness of 0.060 mm with a standard deviation (SD) of 0.009 mm. The fibers have an average diameter of 1.55 µm with a SD of 0.24 µm. The distribution of the fiber diameters (n=200) is shown in figure 1 (right). The SEM image of the electrospun fiber mat in figure 1 (left) shows that the fibers are randomly oriented with irregularly shaped pores. The average pore diameter is 9.97 µm with a SD of 4.90 µm.

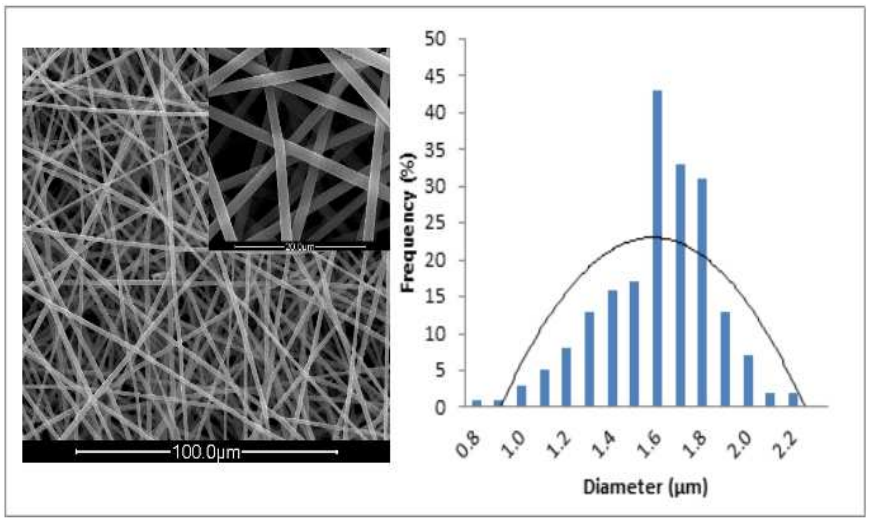

Figure 1. Left: SEM image of an PDLLA fiber mat after 40 minutes of electrospinning. Right: Frequency distribution for fiber diameters measured on the electrospun PDLLA samples (n=200).

2.3.2 Surface activation

Digital images of ARS stained samples treated with EtOH and subsequently treated according to the parameters of the standard nucleation procedure are shown in figure 2A (top). Samples show a heterogeneous staining, as some parts of the samples remain white and some parts color pale pink to dark red. This indicates that calcium was locally present on the fiber surface but in different concentrations. In addition, SEM images of EtOH dipped samples (figure 2A bottom) reveal that the microstructure of the samples is affected as numerous fibers are broken. Therefore no further experiments were carried out with this type of activation.

Samples immersed in an ultrasonic bath for 3 seconds prior to the treatment according to the standard nucleation procedure, are uniform dark red after ARS staining, indicating that the calcium deposits are evenly distributed across the surface. Figure 2B (top) shows that similar results are obtained when repeated, demonstrating the reproducibility of the procedure. The SEM image of these samples in figure 2B (bottom) shows that all fibers are intact. The fiber surfaces are completely covered with a CP layer and even in-between the fibers CP deposits are present. Since ultrasonic immersion in demineralized water for 3 seconds followed by treatment with the standard nucleation procedure results in a reproducible and homogenous CP coating without affecting the fiber integrity, ultrasonication was chosen as the activation method for the next experimental phase in which the nucleation step is optimized.

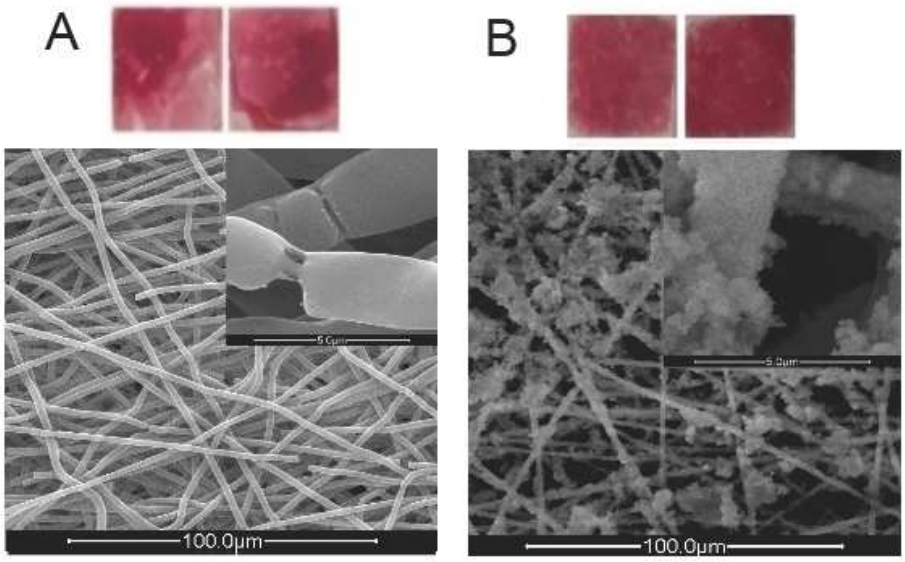

Figure 2. A) top: Digital image of ARS stained sample after EtOH dipping and subsequent treatment with the standard nucleation procedure (SNP), bottom: SEM image of EtOH dipped samples, B) top: digital image of ARS stained samples after ultrasonication and subsequent treatment with the SNP, bottom: SEM image of samples after ultrasonic activation and subsequent treatment with the SNP.

2.3.2 Optimization nucleation step

The conditions of the experiments generated by the simplex are given in table 1 together with the mineralization score of the resulting samples. Based on the mineralization score and the morphology of the coated fibers, the samples obtained from the different experiments can be divided into three categories.

a Samples with poor coating (score 0)

The digital image of the samples treated with the parameters of experiment P-c shown in figure 3A is representative for all samples with a mineralization score of 0 (table 1). These samples remain mostly white after ARS staining. SEM images of the corresponding samples show that the fiber surface is not covered with a CP layer, only some local CP accumulations in-between the fibers are present.

b Samples with adequate mineralization (score 1)

Two experimental conditions result in an adequate coating of the PDLLA fibers (Ad-a and Ad-b; table 1). ARS stained samples prior treated with the experimental conditions of Ad-a and Ad-b are pink (figure 3B and 3C top respectively). Although the intensity of staining is darker and more homogenous for the samples treated with the experimental conditions of Ad-b compared to Ad-a, on SEM images the difference is less pronounced (figure 3C and 3B bottom respectively). Both treatments result in a thin and homogenous CP coating of the fibers, without any excess of CP clogging the pores.

c Samples with an excess of mineralization (scores 2 – 4)

Figure 3 shows the digital images of samples treated with the experimental conditions of experiment Exp-g (figure 3D), Exp-k (figure 3E) and Exp-s (figure 3F). These samples are scored 2, 3 and 4 respectively and are each representative for all samples with the same score. SEM images of samples rated with a mineralization score of 2 in figure 3D show CP accumulations in-between and on the fibers. Although locally some CP deposits obstruct the pores, the fibrous structure is still distinguishable. The latter is more difficult for samples rated with a mineralization score 3, where the pores are mainly obstructed with CP accumulations as the fibers are excessively covered with CP (figure 3E). In samples with a mineralization score of 4, the surface is completely covered with CP, pores and fibers are almost completely indistinguishable. The porous structure is completely compromised by the deposited CP (figure 3F).

Electrospun PDLLA scaffold

Table 1. Conditions of the experiments used for the optimization of the calcium phosphate nucleation step. Based on the ARS staining and morphology of coating, experiments are assigned a mineralization score. The type of calcium phosphate deposited on the samples was identified using infrared (IR) spectrometry.

		$CaCl_2.H_2O$		Na_2HPO_4			
Exp	No. Of Cycles	Concentration (mM)	Immersion Time (s)	Concentration (mM)	Immersion Time (s)	Score	IR
SNP	6	1000	60	600	60	4	CDAp
P-a	8	412	50	632	175	0	-
P-b	6	41	70	148	120	0	-
P-c	2	1000	120	750	120	0	-
Ad-a	6	82	35	295	120	1	CDAp/DCPD
Ad-b	4	750	120	100	60	1	CDAp
Exp-a	9	118	15	574	250	2	CDAp
Exp-b	6	1000	120	250	120	2	CDAp
Exp-c	4	479	60	646	185	2	CDAp
Exp-d	7	439	40	189	90	2	CDAp
Exp-e	4	456	55	677	255	2	CDAp
Exp-f	6	146	60	347	215	2	CDAp
Exp-g	6	164	70	590	240	2	CDAp
Exp-h	6	288	25	642	280	3	CDAp
Exp-i	8	207	60	663	185	3	CDAp
Exp-j	6	82	70	295	240	3	CDAp
Exp-k	6	743	90	639	135	3	CDAp
Exp-l	6	705	50	704	155	3	CDAp
Exp-m	8	575	60	603	160	4	CDAp
Exp-n	6	164	35	590	120	4	CDAp
Exp-o	7	461	20	947	150	4	CDAp
Exp-p	6	250	120	750	120	4	CDAp
Exp-q	6	1000	30	750	120	4	CDAp
Exp-r	10	700	85	690	85	4	CDAp
Exp-s	8	580	70	666	70	4	CDAp
Exp-t	6	375	85	699	160	3	CDAp/DCPD
Exp-u	6	312	30	610	215	3	CDAp/DCPD
Exp-v	6	1000	120	750	30	4	CDAp/DCPD

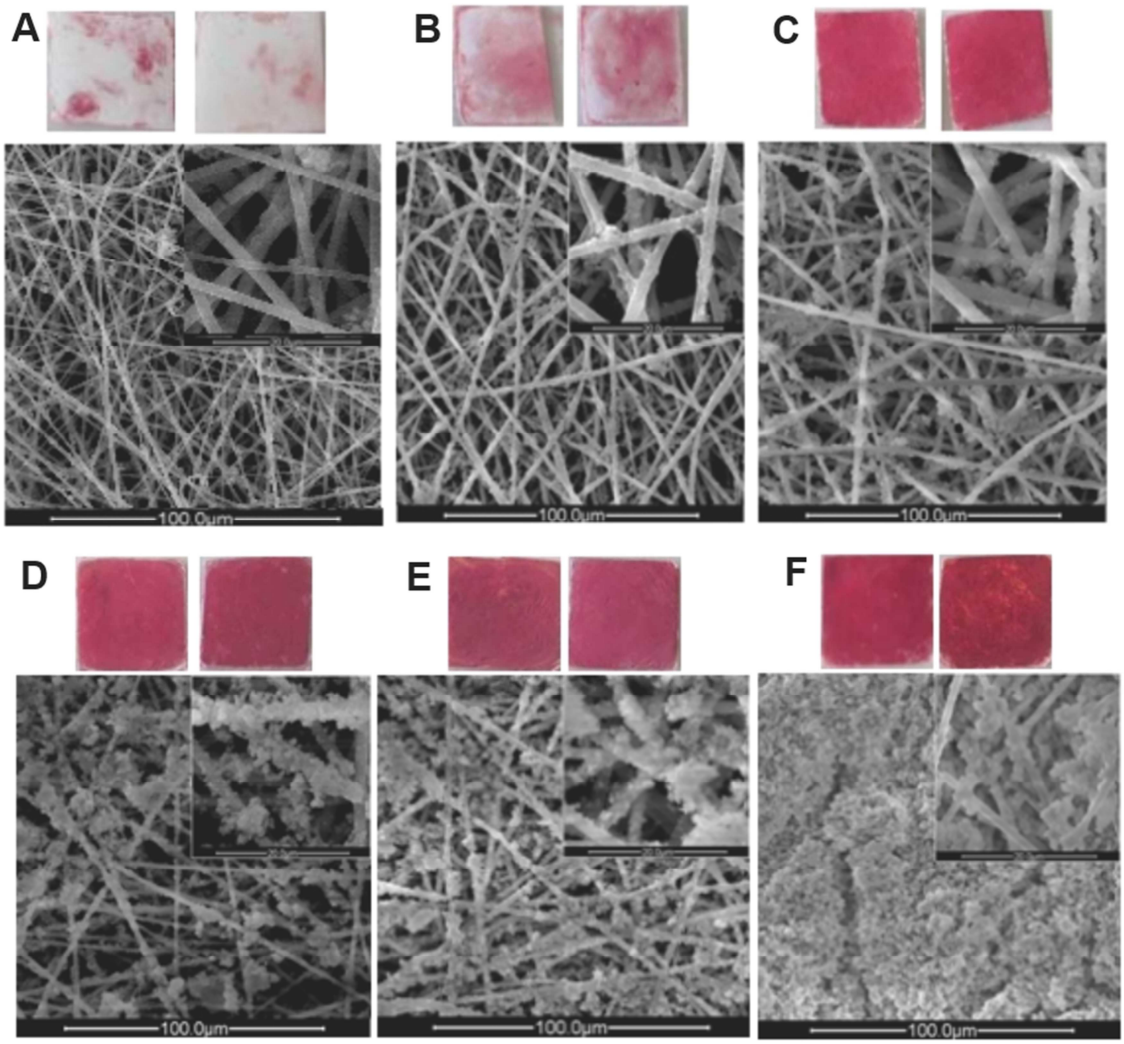

Figure 3. Digital image of ARS stained samples (top) and SEM images (bottom) of samples after treatment with the parameters of experiment A) P-c (mineralization score 0) B) Ad-a and C) Ad-b (mineralization score 1), D) Exp-g (mineralization score 2), E) Exp-k (mineralization score 3) and F) Exp-s (mineralization score 4).

2.3.3 FTIR analysis

The type of CP deposited on all samples with a mineralization score from 1 to 4 is identified by FTIR (table 1 and figure 4). Based on the band profiles of the IR spectra, two types of CP are detected; slightly carbonated calcium-deficient apatite (CDAp; $Ca_{10-x-y}(PO_4)_{6-x-y}(HPO_4)_y(CO_3)_x(OH)_{2-x-y}$) and a combination of CDAp and dicalcium phosphate dihydrate (DCPD; $CaHPO_4.2H_2O$).

The IR spectrum of the CP deposition on the samples after alternate dipping in Ca^{2+} and PO_4^{3-} rich solutions according to the experimental conditions of SNP shows peaks due to the v_4-PO_4^{3-} bending at 500 to 700 cm^{-1} and the v_1 and v_3 stretching of PO_4^{3-} groups around 970, 1045 and 1100 cm^{-1}. These are typical peaks of an apatite phase. In addition, three weak peaks in the IR spectra at 870, 1425 and 1470 cm^{-1} indicate the presence of CO_3^{2-} substituting for PO_4^{3-} in the apatite lattice (so-called B-type CO_3^{2-}) resulting in a slightly carbonated apatite phase. The CO_3^{2-} is probably native from atmospheric CO_2.

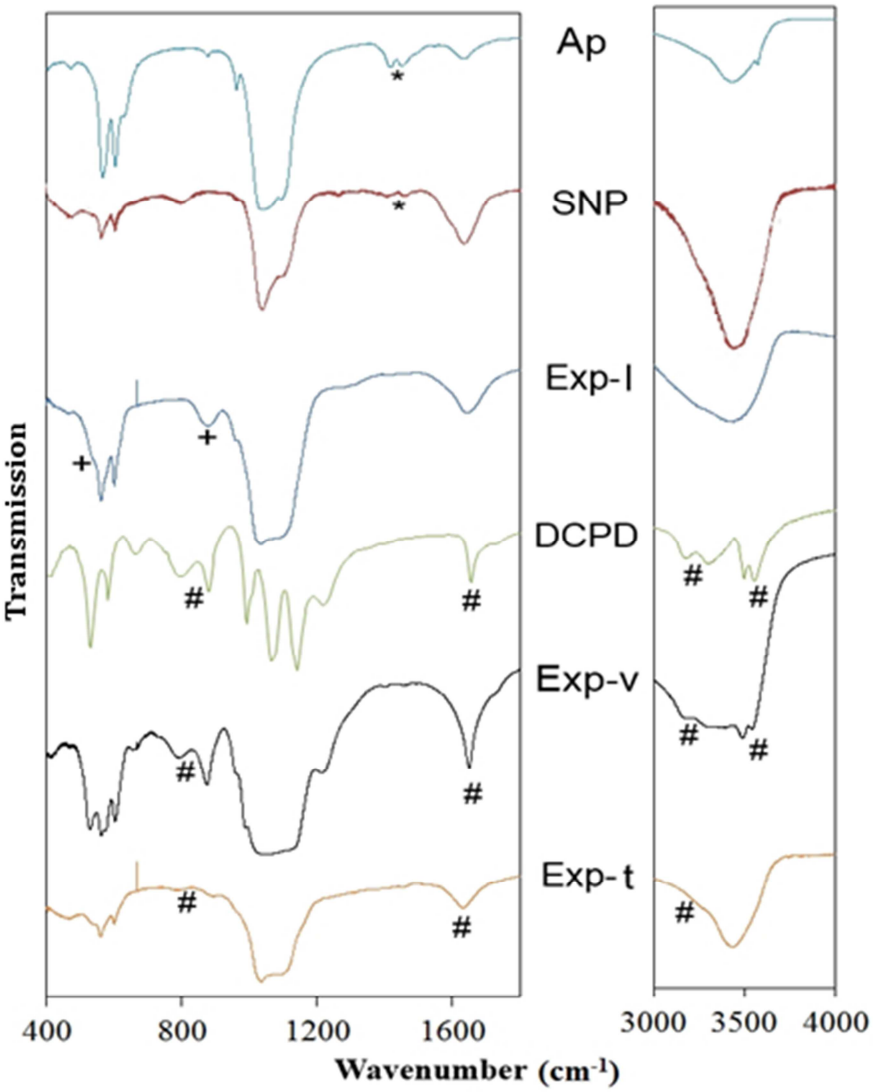

Figure 4. Infrared spectra of the CP coating on the samples treated with the experimental conditions of experiment SNP, Exp-I, Exp-v and Exp-t. For comparison the IR spectra of apatite (Ap) and DCPD are shown. CO_3^{2-} absorptions are marked by *, HPO_4^{2-} absorptions are marked by + and the typical peaks of DCPD are marked by #.

The FTIR spectrum of the CP coating on the sample treated with experimental conditions of Exp-I is representative for the spectra of the CP present on the samples treated with the experimental conditions of Ad-b and Exp-a – Exp-s (figure 4). In these spectra the typical peaks of a slightly carbonated apatite are also found. However, the low intensity of the CO_3^{2-} signal at 1425 and 1470 cm^{-1} compared to that of the signal at 870 cm^{-1} suggests that the peak at 870 cm^{-1} is not caused solely by the v_2 – vibration of CO_3^{2-}. The peak at 870 cm^{-1} can be mainly ascribed to the v_5-P-O(H) deformation in HPO_4^{2-}. The presence of HPO_4^{2-} substituting for PO_4^{3-} in the apatite lattice is supported by the shoulder of the peak around 530 cm^{-1}. Apparently, the deposited CP is a slightly carbonated calcium-deficient apatite with a stoichiometry $Ca_{10-x-y}(PO_4)_{6-x-y}(HPO_4)_y(CO_3)_x(OH)_{2-x-y}$. The competition between HPO_4^{2-} and CO_3^{2-} for the substitution of PO_4^{3-} then results in a CDAp with x>>y for the experimental conditions of SNP and in a CDAp with x<<y for the experiments Exp-I, Ad-b and Exp-a – Exp-s.

Besides the typical peaks of CDAp, bands typical of DCPD are present in the FTIR spectrum of the CP depositions on samples treated with the experimental conditions of Exp-v, (figure 4). The peaks at 530 and 580 cm^{-1} arise from O-P-O bending vibrations and those at 785, 860 and 1215 cm^{-1} indicate P-O(H) deformations of HPO_4^{2} in DCPD. The peaks around 984, 1060 and 1133 cm^{-1} can be assigned to PO_4^{3-} stretching vibrations. At 665 cm^{-1} the water peak arising from γ_{OH} vibrations in H_2O is visible. The peak at 1645 cm^{-1} arises from the H – O – H deformations in water. The series of peaks at 3155, 3280, 3485 and 3540 cm^{-1} arise from OH - stretching modes in H_2O. These results suggest the deposited CP is a combination of CDAp and DCPD.

The combination of peaks typical for CDAp and DCPD can also be found in the spectra recorded for samples treated with the experimental conditions of Ad-a and Exp-t and u. The spectrum associated with Exp-t is shown in figure 4, and is representative for the spectra associated with experiments Ad-a and Exp-u. The intensity of the peaks typical for DCPD are lower than in the spectrum associated with Exp-v. Around 785, 860 and 1215 cm^{-1}, the peaks arising from P-O(H) deformations in HPO_4^{2-} - groups are slightly visible. The shoulders arising from the OH - stretching in H_2O can be seen around 3155 and 3280 cm^{-1}. It is clear that the CP coating on these samples is not a pure apatite but apatite in combination with a small amount of DCPD, the latter however to a lesser extent than on samples treated with the conditions of Exp-v.

2.3.4 Cell viability on electrospun PDLLA fiber mats

For the cell viability study samples are selected that are treated with the experimental conditions of Ad-b, Exp-q and Exp-v. These samples are coated with either an adequate amount of CDAp (Ad-b), an excess of CDAp (Exp-q) or an excess of a combination of Ap and DCPD (Exp-v). The corresponding SEM images are shown in figure 5A, 5B and 5C respectively.

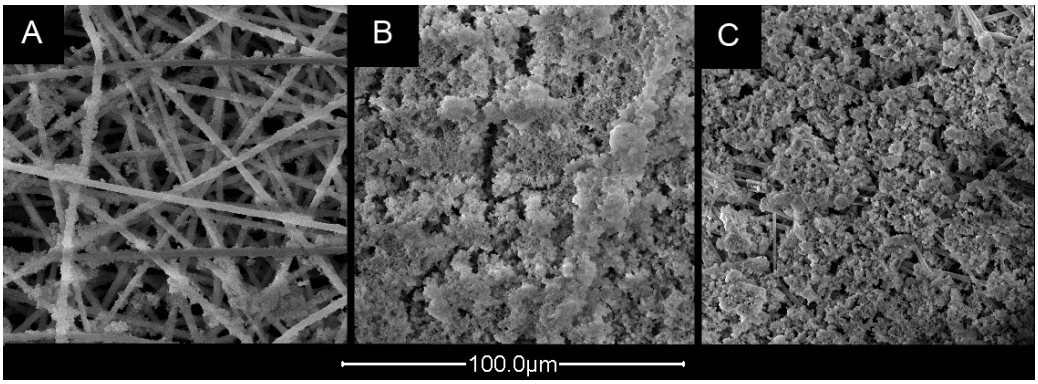

Figure 5. SEM images of the samples coated with A) an adequate amount of CDAp, B) an excess of CDAp and C)an excess of a combination of CDAp and DCPD. These samples were used to assess the MC3T3-E1 cell viability.

Electrospun PDLLA scaffold

The quantity of viable and attached MC3T3-E1 cells on the CP coated and untreated samples after 1 and 7 days, as reflected by the Presto Blue™ assay and expressed as a percentage of the positive control, is illustrated in figure 6. At day 1 and day 7, the amount of attached cells on the untreated PDLLA samples is less than 5% of the positive control. After 1 day of incubation there is no significant difference between the untreated samples and the samples coated with an excess of CP. The number of attached cells on the samples coated with an adequate amount of CDAp, however, is significantly higher than on the untreated samples ($p = 0.037$). At day 7, the number of viable cells on all CP coated samples is significantly higher than on the untreated PDLLA ($p \leq 0.034$). From day 1 to day 7 there is only a significant proliferation on the samples coated with an adequate amount of CDAp ($p < 0.001$). The number of attached cells on these samples reaches 105% of the positive control, which is significantly higher than on the samples treated with an excess of CP ($p < 0.001$). Between the two samples coated with an excess of CP, there is no significant difference in the amount of viable cells ($p = 0.262$).

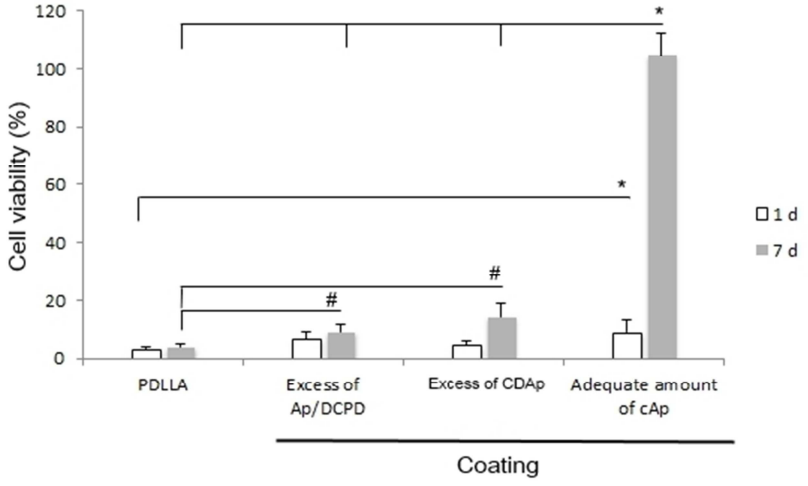

Figure 6. Cell viability on untreated PDLLA and samples coated with an excess of CDAp and DCDP, an excess of CDAp and an adequate amount of CDAp after 1 and 7 days of incubation. The cell viability was calculated as a percentage of the positive control at day 7 of culture.

After 24h of incubation, on the untreated samples (figure 7A) more dead cells are observed than on the CP coated samples (figure 7C-G). The cells are round and small on the untreated PDLLA samples, but show elongated morphologies on all CP coated samples.

After 7 days of incubation, the morphology of viable cells on the untreated samples (figure 7B) and on the samples treated with an excess of CP (figure 7D and 7F) remains more or less the same. On the untreated PDLLA samples, fewer dead cells are observed, but the majority of cells is still small and round (figure 7B). Cell attachment and spreading increases on samples coated with an adequate amount of CP (figure 7H). The morphology of the cells is similar to the morphology observed for cells in the confluent positive culture.

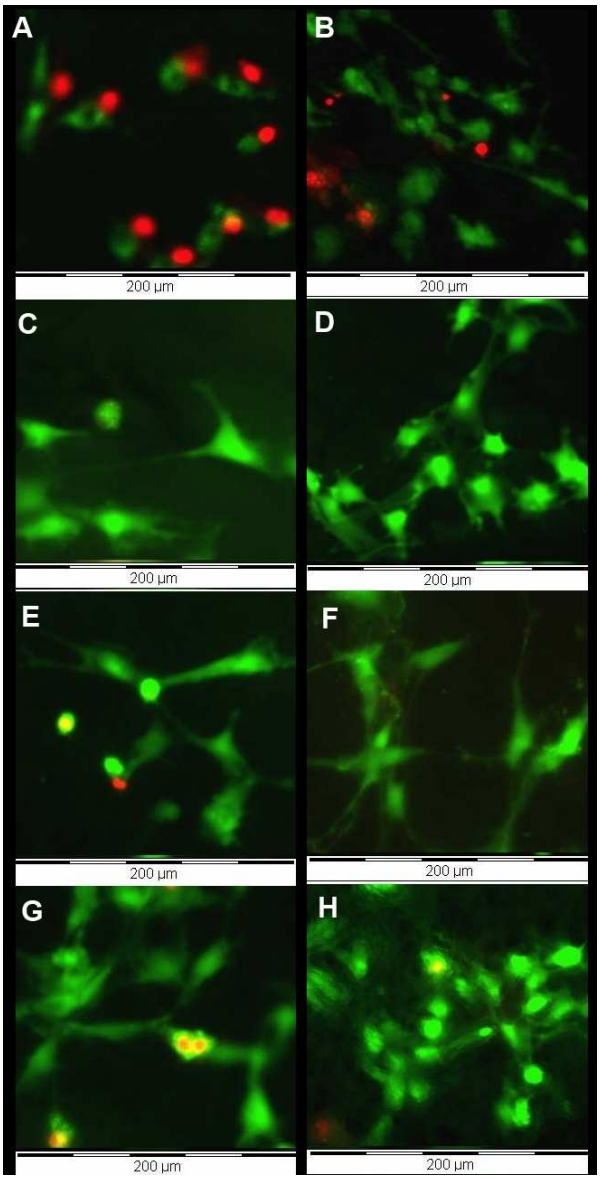

Figure 7. Morphology of MC3T3-E1 pre-osteoblast cells attached to untreated PDLLA fiber mats (A and B), samples coated with an excess of Ap and DCPD (C and D), samples coated with an excess of CDAp (E and F) and samples coated with an adequate amount of CDAp (G and H) after 1 day (A , C, E and G) and 7 days (B, D, F and H) of culture. Live cells are stained green and dead cells are stained red.

2.4 Discussion

In this study a porous 3D electrospun polyester structure coated with a thin and homogenous layer of apatite is made that can be a good substrate for cell adhesion and growth and has great potential as bone tissue engineering scaffold. Amorphous PDLLA is chosen due to its degradation time of 12 to 16 months in the human body which is adequate to ensure support during tissue regeneration without compromising the formation of new bone tissue.[42,96,103]

Using the present electrospinning parameters, beadles and randomly oriented PDLLA microfibers with a narrow fiber diameter distribution were obtained with high reproducibility. The resulting irregular shaped pores had a rather large diameter of about 10 µm which could improve the transport of nutrients and metabolites through the scaffold and enables the infiltration of cells.[124]

In literature, the coating of PLA fibers is generally described as a two-step procedure of surface activation followed by mineralization in SBF. During initial surface activation, the fiber surface undergoes a hydrolysis which is known to result in enhanced hydrophilicity, as the result of an increase in the amount of carboxyl and hydroxyl groups on the surface.[214] Previous studies showed that in particular a high density of carboxyl groups on the fiber surface promotes the formation of a CP coating.[211,214] Upon incubation in SBF, during the initial stages of nucleation, the interaction between calcium ions and carboxyl groups on the activated PDLLA surface might lead to the formation of a $–[COO^-Ca^{2+}]^+$ or $–(COO^-)_2Ca^{2+}$ through ion exchange. During subsequent soaking in sodium phosphate solution, it is expected that phosphate ions will interact with the calcium ions on the fiber surface.[214]

For PDLLA, activation of the fiber surface is required as direct incubation of samples in 1.5xSBF did not result in a CP deposition after 6 days.[207] Pre-immersion of the samples in EtOH resulted in a CP coating of the fibers upon incubation in 2xSBF for 7 days. However, an incubation period of 7 days in order to ensure adequate coating is quite long. Hence, the overall coating procedure needs optimization in order to reduce the time required to deposit an adequate amount of CP. One approach to accelerate the mineralization process is to perform a nucleation step using the alternate dipping technique instead of using SBF solutions. With this technique solutions can be used that contain much higher concentrations of calcium and phosphate ions than is possible in SBF solutions.

2.4.1 Activation

In literature described activation methods are the immersion in EtOH and/or NaOH, with or without ultrasonication. As reported previously for electrospun PDLLA, the immersion in NaOH resulted in severe degradation of the fibrous scaffold.[195] According to Cui *et al*., immersion of PDLLA nanofibers (700 nm – 1 µm) in EtOH till soaked followed by an incubation in SBF for 6 days resulted in intact fibers with a homogenous CP coating.[211] Even though the fibers in the present study are in the micrometer range (1.55 µm with a SD of 0.24 µm), the present results showed that the PDLLA fibers were broken after 1 second dipping in EtOH (figure 2A). Destruction of the fibrous microstructure could affect the mechanical and degradation properties of the material which is not favorable for the bone tissue engineering scaffold potential of the material.[214] Luickx *et al.* activated PCL electrospun samples using a combination of NaOH immersion under ultrasonication.[217] As NaOH is unsuitable for PLA, the procedure was adjusted and samples were immersed in ultrapure water under ultrasonication. Upon treatment of the samples in an ultrasonic bath for 3 seconds followed by treatment with the standard nucleation procedure and ARS staining, samples stained uniform red (figure 2B top). SEM images confirmed that the fibers were completely covered with a layer of CP with accumulations on and in-between the fibers (figure 2B bottom).

Moreover, the fiber structure remained completely intact. The activation effects of ultrasound are mainly due to acoustic cavitation as bubble collapses near the material surface result in jets of liquid impinging at high velocity onto the surface. The acoustic cavitation apparently is able to cleave the ester bonds of the polyester and create carboxyl groups on the fiber surface. The micro-jets hitting the surface of the material also result in roughening of the surface which facilitates the rapid growth of CP compared to smooth surfaces.[214,218,219] Ultrasonic activation was selected for further experiments since this activation method results in a homogenous activation of the fiber surface without affecting the fiber morphology.

2.4.2 Nucleation

The current procedure of activation under ultrasonication followed by a nucleation step using an alternate soaking technique takes about 30 minutes which is a quite faster than the 6 days of incubation in the experiments of Cui *et al*.[211] However, as treatment with the standard nucleation procedure also results in the deposition of CP particles in-between the fibers (figure 2B bottom), the nucleation procedure was further optimized in order to obtain a thin and homogenous layer of CP with preservation of the porous structure.

The nucleation procedure was optimized using a variable simplex algorithm[216] with specific emphasis on the reproducibility of the procedure and the thickness and uniformity of the deposited layer. The present study optimized the five parameters of the alternate dipping process simultaneously: the number of cycles, concentration of and immersion time in both the Ca^{2+} and the PO_4^{3-} rich solutions (table 1).

Based on the high number of experimental conditions resulting in samples with a high degree of mineralization (SNP and Exp-a – Exp-v), it can be assumed that once the samples were successfully activated a CP coating was easily deposited on the fiber surface. The challenge however was to limit the CP deposition in order to obtain a thin and homogenous CP layer on the fibers. ARS staining and SEM images show that only one specific combination of the five parameters result in the ideal conditions for the deposition of a homogenous, thin and reproducible CP coating on the PDLLA fibers (Ad-b). FTIR spectrophotometry reveals that the deposited CP coating obtained by treatment of the activated samples with the parameters of experiment Ad-b is CDAp (figure 4). SEM images of the corresponding samples show that the CP deposit results in a slight roughening of the fiber surface, which could indicate the nanocrystallinitiy of the CDAp crystals (figure 3C). CDAp nanocrystals are known to exhibit physicochemical characteristics similar to those of bone nanocrystals. Coating of PDLLA microfibers with nanoscaled CDAp crystals is thus expected to improve the cellular response as compared to untreated PDLLA. In addition, due

to their calcium deficiency, CDAp nanocrystals are more soluble and have an increased bioresorption rate *in vivo* compared to stoichiometric HAp.[220,221]

The majority of the experimental conditions result in the deposition of CDAp (SNP, Ad-b and Exp-a – Exp-s) with the general formula $Ca_{10-x-y}(PO_4)_{6-x-y}(HPO_4)_y(CO_3)_x(OH)_{2-x-y}$. During the formation of CDAp there is a competition between CO_3^{2-} and HPO_4^{2-} for the substitution of PO_4^{3-} in the apatite lattice. Substitution by HPO_4^{2-} results in a more stable structure, which could explain the observation that only one experimental condition results in the deposition of a CDAp with x>>y (SNP; table 1). Beside CDAp some samples are coated with a combination of apatite and DCPD (Ad-a and Exp-t – Exp-v).

Cui *et al*.[211] found a linear relationship between the surface concentration of carboxyl groups and the amount of CP deposits. However, all samples in the present study were subjected to the same activation treatment so that it can be assumed that they have an equal number of surface carboxyl groups. Variations in mineralization degree and the type of CP can then only be caused by variations in the parameters of the alternate dipping procedure. However, due to the interdependence of the five parameters in each nucleation experiment, no correlation can be found between the individual parameters and the resulting degree of mineralization nor the type of CP coating. Neither was there a correlation between the degree of mineralization and the type of CP deposited. Supposedly small variations in the Ca^{2+} – and PO_4^{3-} concentrations and ratio will affect the pH of the solution surrounding the samples. This is in line with the observation that the precipitated calcium phosphate phase depends on the pH and the Ca/P ratio of the mineralization solution.[7,222]

2.4.3 Cell viability study

The cellular response to an implant is associated with a complex biological system that involves protein adsorption, protein-cell interactions and cell signaling pathways. The surface morphology and chemistry of the material influence the amount of protein adsorption which in turn controls cell attachment. Hence, the pore structure of the surface as well as the morphology and chemical composition of the CP coating will affect the cell viability of the substrate.[156,223,224]

In the present study the influence of a CDAp coating on PDLLA electrospun samples on the cell viability of MC3T3-E1 cells was investigated. Samples with an open interconnected pore system were included in the study as well as samples with their surface completely covered with CDAp. To this end samples were treated with the experimental conditions of Ad-b and Exp-q respectively. In addition, in order to evaluate the influence of different types of CP coatings, samples treated with the experimental conditions of Exp-v resulting in an Ap/DCDP coating were also included in the study.

The amount of cells attached on the untreated PDLLA samples is low throughout the experiment. The cells are not well attached to the surface even after 7 days of culture (figure 6, 7A and 7B). The observed cellular behavior could be expected due to the hydrophobic nature of the untreated PDLLA samples. The hydrophobicity hinders the initial biological responses, such as protein adsorption, impeding cell attachment.[156] The activation and subsequent CP coating of the PDLLA nanofibers significantly enhances the MC3T3-E1 cell response after 7 days of culture (figure 6). After one week of culture, samples coated with an adequate amount of CDAp showed a significant higher number of viable cells compared to the two samples coated with an excess of CP. This could be expected due to the critical role of scaffold porosity in cell seeding and proliferation.[50,104]

DCPD was expected to show a poor cell response as it is known to increase the Ca^{2+} and PO_4^{3-} concentration of the culture medium upon incubation due to its high solubility.[156] However, no significant difference in cell viability could be seen between the samples coated with an excess of CDAp and an excess of CDAp/DCDP. During incubation in the culture medium, the small fraction of DCDP in the coating most probably is converted rapidly to the more stable apatite, which could explain the similar results for both samples coated with an excess of CP.[225]

Based on the excellent results of the osteoblast viability study, CP coating of PDLLA microfibers with CDAp is a promising strategy for the improvement of the bone tissue engineering scaffold potential of electrospun PDLLA. Compared to other reports involving the mineralization of PDLLA by incubation of the samples in SBF for prolonged periods of time, the optimized procedure described in the present study results in a rapid, reproducible and uniform coating of the PDLLA microfibers.

2.5 Conclusion

In the present study, the coating of an electrospun PDLLA microfibrous scaffold with a thin homogenous layer of CP was optimized. In a simple two-step procedure an adequate coating was achieved after 20 minutes. In the first step, the polymer surface was uniformly activated without any obvious change in the fiber structure. In the second step, the fibers were coated with a homogeneous, thin and reproducible CDAp layer, with preservation of the porous structure. Such CDAp coating on the surface of the PDLLA nanofibers drastically improved the osteogenic response and enhanced the cell affinity when compared to the uncoated PDLLA samples.

2.6 Acknowledgements

The authors gratefully acknowledge Prof. Dr. De Clerck and Dr. Van der Schueren of the Department of Textiles (Ghent University) for their support in the fabrication of the electrospun scaffolds.

2.7 References

1. Jang JH, Castano O, Kim HW. Electrospun materials as potential platforms for bone tissue engineering. Advanced Drug Delivery Reviews 2009;61(12):1065-1083.
2. Holzwarth JM, Ma PX. Biomimetic nanofibrous scaffolds for bone tissue engineering. Biomaterials 2011;32(36):9622-9629.
3. Stevens MM. Biomaterials for bone tissue engineering. Materials Today 2008;11(5):18-25.
4. Hutmacher DW. Scaffolds in tissue engineering bone and cartilage. Biomaterials 2000;21(24):2529-2543.
5. Stevens B, Yang YZ, MohandaS A, Stucker B, Nguyen KT. A review of materials, fabrication to enhance bone regeneration in methods, and strategies used engineered bone tissues. Journal of Biomedical Materials Research Part B-Applied Biomaterials 2008;85B(2):573-582.
6. Rezwan K, Chen QZ, Blaker JJ, Boccaccini AR. Biodegradable and bioactive porous polymer/inorganic composite scaffolds for bone tissue engineering. Biomaterials 2006;27(18):3413-3431.
7. Engelberg I, Kohn J. Physicochemical properties of degradable polymers used in medical applications - A comparative-study. Biomaterials 1991;12(3):292-304.
8. Robinson BP, Hollinger JO, Szachowicz EH, Brekke J. Calvarial bone repair with porous D,L-polylactide. Otolaryngology-Head and Neck Surgery 1995;112(6):707-713.
9. Li WJ, Cooper JA, Mauck RL, Tuan RS. Fabrication and characterization of six electrospun poly(alpha-hydroxy ester)-based fibrous scaffolds for tissue engineering applications. Acta Biomaterialia 2006;2(4):377-385.
10. Arima Y, Iwata H. Effect of wettability and surface functional groups on protein adsorption and cell adhesion using well-defined mixed self-assembled monolayers. Biomaterials 2007;28(20):3074-3082.
11. Zou B, Li X, Zhuang H, Cui W, Zou J, Chen J. Degradation behaviors of electrospun fibrous composites of hydroxyapatite and chemically modified poly(DL-lactide). Polymer Degradation and Stability 2011;96(1):114-122.
12. Bleek K, Taubert A. New developments in polymer-controlled, bioinspired calcium phosphate mineralization from aqueous solution. Acta Biomaterialia 2013;9(5):6283-6321.
13. Liao S, Chan CK, Ramakrishna S. Stem cells and biomimetic materials strategies for tissue engineering. Materials Science & Engineering C-Biomimetic and Supramolecular Systems 2008;28(8):1189-1202.
14. Araujo JV, Martins A, Leonor IB, Pinho ED, Reis RL, Neves NM. Surface controlled biomimetic coating of polycaprolactone nanofiber meshes to be used as bone extracellular matrix analogues. Journal of Biomaterials Science-Polymer Edition 2008;19(10).
15. Cui W, Li X, Zhou S, Weng J. In situ growth of hydroxyapatite within electrospun poly(DL-lactide) fibers. Journal of Biomedical Materials Research Part A 2007;82A(4):831-841.
16. Ngiam M, Liao S, Patil AJ, Cheng Z, Chan CK, Ramakrishna S. The fabrication of nano-hydroxyapatite on PLGA and PLGA/collagen nanofibrous composite scaffolds and their effects in osteoblastic behavior for bone tissue engineering. Bone 2009;45(1):4-16.

17. Cui W, Li X, Xie C, Chen J, Zou J, Zhou S, Weng J. Controllable growth of hydroxyapatite on electrospun poly(DL-lactide) fibers grafted with chitosan as potential tissue engineering scaffolds. Polymer 2010;51(11).
18. Andric T, Wright LD, Taylor BL, Freeman JW. Fabrication and characterization of three-dimensional electrospun scaffolds for bone tissue engineering. Journal of Biomedical Materials Research Part A 2012;100A(8):2097-2105.
19. Grizzi I, Garreau H, Li S, Vert M. Hydrolytic degradation of devices based on poly(DL-lactic acid) size-dependence. Biomaterials 1995;16(4):305-311.
20. Chen J, Chu B, Hsiao BS. Mineralization of hydroxyapatite in electrospun nanofibrous poly(L-lactic acid) scaffolds. Journal of Biomedical Materials Research Part A 2006;79A(2):307-317.
21. Yoo HS, Kim TG, Park TG. Surface-functionalized electrospun nanofibers for tissue engineering and drug delivery. Advanced Drug Delivery Reviews 2009;61(12):1033-1042.
22. Kothapalli CR, Shaw MT, Olson JR, Wei M. Fabrication of novel calcium phosphate/poly(lactic acid) fiber composites. Journal of Biomedical Materials Research Part B-Applied Biomaterials 2008;84B(1):89-97.
23. Taguchi T, Kishida A, Akashi M. Hydroxyapatite formation on/in poly(vinyl alcohol) hydrogel matrices using a novel alternate soaking process. Chemistry Letters 1998(8):711-712.
24. Madurantakam PA, Rodriguez IA, Cost CP, Viswanathan R, Simpson DG, Beckman MJ, Moon PC, Bowlin GL. Multiple factor interactions in biomimetic mineralization of electrospun scaffolds. Biomaterials 2009;30(29).
25. Walker F, Parker L, Morgan S, Deming S. Sequential simplex optimization: a technique for improving quality and productivity in research, development and manufacturing: Boca Raton: CRC Press LLC; 1999.
26. Leong MF, Rasheed MZ, Lim TC, Chian KS. In vitro cell infiltration and in vivo cell infiltration and vascularization in a fibrous, highly porous poly(D,L-lactide) scaffold fabricated by cryogenic electrospinning technique. Journal of Biomedical Materials Research Part A 2009;91A(1):231-240.
27. Luickx N, Vreken NVd, D'Oosterlinck W, Schueren LVd, Declercq H, Clerck KD, Cornelissen M, Verbeeck R. Optimization of the activation and nucleation steps in the precipitation of a calcium phosphate primer layer on electrospun poly(ε-caprolactone). Journal of Biomedical Materials Research Part A 2014.
28. Suslick KS, Price GJ. Applications of ultrasound to materials chemistry. Annual Review of Materials Science 1999;29.
29. Cobley A. Ultrasound Sonochemistry - A more sustainable approach to surface modification? Surface Engineering 2009;25(8).
30. Ghasemi-Mobarakeh L, Morshed M, Karbalaie K, Fesharaki M, Nasr-Esfahani MH, Baharvand H. Electrospun poly (epsilon-caprolactone) nanofiber mat as extracellular matrix. Yakhteh 2008;10(3).
31. Shah AK, Sinha RK, Hickok NJ, Tuan RS. High-resolution morphometric analysis of human osteoblastic cell adhesion on clinically relevant orthopedic alloys. Bone 1999;24(5).
32. Driessens F, Verbeeck R. Biominerals: CRC Press; 1990.
33. Ma P, Elisseeff J. Scaffolding in tissue engineering: CRC Press; 2006.
34. Dorozhkin SV. Calcium orthophosphates. Journal of Materials Science 2007;42(4).
35. Doi Y, Iwanaga H, Shibutani T, Moriwaki Y, Iwayama Y. Osteoclastic responses to various calcium phosphates in cell cultures. Journal of Biomedical Materials Research 1999;47(3):424-433.
36. Li J, He F, Ye J. Effect of the surface topographic modification on cytocompatibility of hardened calcium phosphate cement. Applied Surface Science 2013;274:237-240.
37. Ma PX, Zhang RY, Xiao GZ, Franceschi R. Engineering new bone tissue in vitro on highly porous poly(alpha-hydroxyl acids)/hydroxyapatite composite scaffolds. Journal of Biomedical Materials Research 2001;54(2):284-293.

38. Liu XH, Ma PX. Polymeric scaffolds for bone tissue engineering. Annals of Biomedical Engineering 2004;32(3):477-486.
39. Boanini E, Gazzano M, Bigi A. Ionic substitutions in calcium phosphates synthesized at low temperature. Acta Biomaterialia 2010;6(6):1882-1894.

3 Calcium phosphate coating of a 3D plotted PCL scaffold

Part of the research is based on the article:

3D plotted poly(ε-caprolactone) scaffolds coated with hydroxyapatite with high carbonate content for bone tissue engineering applications.

Nathalie Luickx, Natasja Van den Vreken, Felke Steijns, Nicolas Van Damme, Kim Ragaert, Heidi Declercq, Maria Cornelissen, Ronald Verbeeck.

Article submitted to Biomedical Materials

Abstract: There is a strong need for bone scaffolds to serve as temporary constructs to restore the function of critical sized bone defects. In this study, 3D plotting was used for the production of porous poly(ε-caprolactone) (PCL) scaffolds. In order to enhance the bioactivity, the present study aimed to coat the scaffolds with an apatite layer with high carbonate content using experimental simulated body fluid (SBF) solutions. In a preliminary study the pH and the hydrogencarbonate (HCO_3^-) and magnesium (Mg^{2+}) contents of experimental SBF solutions were studied in relation to the type of calcium phosphate and the carbonate content of the precipitates formed in these solutions. SBF solutions in which hydroxyapatite precipitates with a high carbonate content (≤ 10.5 wt%) formed were selected for the coating of the PCL scaffolds. On one hand, the apatite coating was thicker and more homogenous when formed in SBF solutions with a low pH compared to SBF solutions with a higher pH. On the other hand, the carbonate content of the coating increased with increasing HCO_3^- concentration of the SBF solution, and was the highest when the solutions were deprived of Mg^{2+}. Analysis of the cell viability, adhesion and proliferation of MC3T3-E1 cells on 3D plotted PCL scaffolds coated with hydroxyapatite with different carbonate contents showed that a carbonate content of at least 10 wt% carbonate improved the osteogenic cell response when compared to uncoated PCL scaffolds and scaffolds coated with a hydroxyapatite with a low carbonate content.

3D plotted PCL scaffold

3D plotted PCL scaffold

3.1 Introduction

Despite the high regenerative capacity of bone, the body is incapable of self-healing in case of a critical sized bone defect caused by severe trauma or after a bone tumor resection. In such a case a surgical intervention is needed. One approach to restore and maintain tissue function is the insertion of a porous three-dimensional (3D) biodegradable scaffold that serves as a temporary 3D replacement of the extracellular matrix, providing a mechanical platform to support adhesion, proliferation and differentiation of cells. While new bone tissue is generated, the scaffold slowly degrades in non-toxic components and eventually only new, functional and healthy tissue remains.[15,24,41]

Material choice, design and fabrication of tissue scaffolds are still challenging topics in regenerative medicine, particularly for load bearing scaffolds in bone tissue engineering. Multiple biological properties must be met, such as biocompatibility, bioactivity and osteoconductivity.[20,27] The mechanical strength of the scaffolds should be similar to that of the surrounding tissue so that the scaffold can provide a dimensional stability in the body.[41] A non-negligible aspect in the fabrication of a bone scaffold is the internal geometry; interconnecting pores with a size ranging from 100 to 400 µm are necessary to assure cell and tissue infiltration and nutrient and metabolite diffusion.[226,227]

Preferentially the shape of the scaffold should perfectly fit into the tissue defect of the individual patient. The first step to design such a patient-specific scaffold is creating a 3D digital image of the defect by means of computed tomography (CT) scanning. Computer aided design/computer aided manufacturing (CAD/CAM) software converts this obtained virtual object into a sequence of slices and this digital information can then be transferred to a rapid prototyping (RP) machine.[127,228] During the last decade, tissue engineering has benefited from the development of RP techniques, which resulted in the production of free-form porous scaffolds with custom-tailored architectures. A solid model corresponding to the real 3D object is built layer-by-layer.[127,229] Various RP techniques are available. They differ in the materials that can be used and in the way the materials are deposited to form a 3D object.[46,70,230]

The Food and Drug Administration (FDA) approved family of aliphatic poly(α-esters) such as poly-(lactic acid) (PLA), poly-(glycolic acid) (PGA), poly-(ε-caprolactone) (PCL) and their copolymers are widely used as scaffolding material. These polymers are biocompatible as they do not elicit an inflammatory response and their non-toxic degradation products are excreted from the human body along natural pathways. Degradation kinetics, mechanical properties and crystallinity can be tailored by varying the molecular weight and

copolymerization.[89,231] Due to their thermoplasticity, they can be processed by melting and subsequent shaping, after or during which the polymer solidifies.

One way to process thermoplastic polyesters is 3D plotting, a micro-extrusion type RP technique. 3D plotting allows the fabrication of scaffolds with customized shape, filament diameters (typically between 100-500 µm), and controllable porosity, in both geometry and interconnectivity.[66,232,233] For 3D plotting, processing of the polyester starts from the base granulate material which has the advantage of working without a solvent, excluding the use of difficult to remove and/or cytotoxic solvents.[234] Moreover, scaffolds created by 3D plotting commonly show superior control over mechanical properties and structural integrity when compared to the solution-based counterparts of the same polymer.[134]

Several authors have reported the application of the 3D plotting technique in the production of PCL [67,227,235] and PLA [66] scaffolds. However, due to the thermal vulnerability of PLA, the use of this polyester with the 3D plotting technique is limited. When heated for an extended time above the melting temperature, chain scissions may occur, effectively degrading the material.[236] Therefore, in the current study PCL is selected because of its favorable properties for thermoplastic processing due to its high thermal stability.[96] The melting point of 60°C and high decomposition temperature of 350°C of PCL allow a wide range of extrusion temperatures.[237] In addition, PCL has a long degradation time in the human body (> 24 months), which is needed to maintain the desired mechanical properties for larger constructs. However, the large pore sizes and highly symmetrical geometrical designs of 3D plotted scaffolds often lead to a low seeding efficiency. So, Declerq *et al.* [205] showed that the scaffold design, the pore size and geometry in particular, had an impact on the seeding efficiency, colonization and differentiation of MC3T3-E1 pre-osteoblastic cells. In scaffolds with a 0°/90° design, the open channels and relatively large pore sizes resulted in low seeding efficiency due to significant cell loss. More compact scaffold architectures, with a 0°/45°/90°/-45° design and a pore size of 100-150 µm, positively influenced the seeding efficiency and differentiation.

Another disadvantage of especially PCL scaffolds, is their hydrophobic nature, which hinders the initial biological responses, such as protein adsorption, making it difficult for the cells to adhere to the polyester surface.[60,150,238,239] In order to improve the bioactive properties of PCL scaffolds, coating of the PCL surface with a bone-like apatite mineral has been reported.[85,146,147,150,182,183,240] In general, the mineralization of PCL scaffold is achieved in three consecutive steps: activation, nucleation and maturation. During the activation step, reactive hydroxyl and carboxyl groups are created on the polyester surface by cleavage of the ester bonds. This step reduces the hydrophobicity and improves bioactivity of the scaffold.[69,157]

Oyane *et al*.[183] showed that activation of the PCL surface is imperative for subsequent calcium phosphate coating. In the second step, scaffolds are alternately dipped in calcium – and phosphate rich solutions. During this step, calcium phosphate nuclei are deposited onto the PCL surface.[69,157,183] In a final step, the scaffolds are incubated in a simulated body fluid (SBF) solution with a similar inorganic content as human blood plasma (Table 1). SBF, introduced by Kokubo *et al*.[170], is a metastable and slightly oversaturated solution with respect to apatite. Incubation of the pre-treated PCL scaffolds in SBF results in the deposition of a calcium phosphate layer on the scaffold.[167] The coating is initiated by a process of heterogeneous nucleation of calcium phosphate clusters that aggregate, grow and mature at the PCL surface.[167,241] PCL scaffolds fabricated with various techniques including electrospinning [177,210], fused deposition modeling [157,242], film blowing [151] and solvent casting [243] were successfully coated with a surface mineral layer. The coated scaffolds showed improved cell attachment and proliferation when compared to pure PCL scaffolds.[119,151,157] However, a limited number of studies on the calcium phosphate coating of 3D plotted PCL scaffolds have been reported.[85]

Because the mineral phase of bone tissue is a low crystalline carbonate substituted apatite with a carbonate content of 3.2 – 13 wt%, the PCL scaffold should ideally be coated with a bonelike carbonated apatite. In addition, carbonate incorporation in apatites enhances the solubility near physiological pH and hence the bioresorbability. Several studies showed that the cell adhesion, proliferation and metabolic activity of osteoblasts was increased on apatites with a high carbonate content (> 11 wt%), compared to hydroxyapatite.[152,244] However, in standard SBF, the concentration of hydrogencarbonate ions (4.2 mM) is much lower when compared with that of plasma (27 mM). As a result, precipitates and coatings formed in such SBF solutions have a low carbonate content (~ 2.5 wt%) and hence a slow bioresorption rate.[245,246] Hence, increasing the carbonate content of the precipitated calcium phosphate by SBF maturation has become a topic of interest. Experiments with SBF containing higher concentrations of hydrogencarbonate ions were performed and the precipitates obtained from such solutions appeared to be more similar to the calcified tissues.[243,244,246] However, coating of 3D plotted PCL scaffolds with a calcium phosphate coating with high carbonate content has not been studied.

The present paper reports on the surface mineralization of 3D plotted PCL scaffolds with a homogenous calcium phosphate layer with a high carbonate content. In a preliminairy study, various experimental SBF solutions with varying carbonate and magnesium ion concentrations and pH were prepared. The influence of the carbonate and magnesium content and the initial pH of the SBF-like solution on the composition of the precipitates was analyzed. Actual coating was obtained by maturation of the PCL scaffolds in SBF-like

aqueous solutions, in which apatites with a high carbonate content were found to precipitate. The influence of the carbonate and magnesium content and the initial pH of the SBF-like solution on the coating formation and composition was analyzed. In an *in vitro* study, the adhesion and proliferation of pre-osteoblastic cells (MC3T3-E1) on PCL scaffolds coated with calcium phopshate with a low, medium and high carbonate content were compared.

3.2 Materials and Methods

Freshly prepared demineralized water (Milli-Q system, Millipore, Billerica, USA) was used for the preparation of the solutions. PCL pellets were provided by Perstorp (Perstorp, Sweden). Ethanol (technical grade 95 vol.%), sodium hydroxide solution (NaOH; 1 M), sodium chloride (NaCl), tris(hydroxymethyl)aminomethane (TRIS) and acetone were obtained from VWR BDH Prolabo (Leuven, Belgium). Sodium bicarbonate ($NaHCO_3$), disodium phosphate (Na_2HPO_4), potassium phosphate dibasic (K_2HPO_4), magnesium chloride ($MgCl_2.6H_2O$), hydrochloride (HCl; 37 vol.%), sodium sulfate (Na_2SO_4) and chloroform were purchased from Merck (Darmstadt, Germany) and potassium chloride (KCl) and calcium chloride ($CaCl_2.2H_2O$) from J.T. Baker (Deventer, The Netherlands).

3.2.1 Scaffold production

Samples were produced by 3D plotting using the BioScaffolder® device (SysEng, Salzgitter-Bad, Germany). Optimization of the processing parameters was carried out by Ragaert *et al*.[66]. In short, PCL pellets are molten at 100°C after which the melt is transported forward by a rotating extrusion screw (15 rpm) and pressed through a 27 gauge needle (200 µm). Regular filaments are deposited at a constant plotting feed (F) of 115 mm/min on a plotting table at room temperature. For this study, samples of 1 x 1 cm² were plotted in four consecutive layers each with a relative orientation of 45°, resulting in scaffolds with a 0°/45°/90°/-45° overlay pattern. Digital images of the fabricated scaffolds were obtained with a Keyence 3D microscope (VHX-500F; Elmwood Park, US). Image analysis software (SigmaScan Pro 5, SPSS Science, Chicago, US) was used to determine the average filament diameter (FD) and strand distance (SD). For each parameter, measurements of five random locations on the scaffold were averaged.

3.2.2 SBF precipitation study

3.2.2.1 Preparation of the experimental SBF solutions

Based on the composition of 2xSBF, with ion concentrations adjusted to twice those of normal SBF, various SBF solution were prepared by changing the ion concentrations of Mg^{2+} and HCO_3^- ions as summarized in Table 1. The Mg^{2+} and HCO_3^- concentration were varied between 3 mM – 0mM, and 21 mM – 84 mM, respectively. In order to maintain all

other ion concentrations equal to those in 2xSBF, it was necessary to adjust the Cl^- concentration (Table 1).

Table 1: Ion concentration of human blood plasma (HBP), normal SBF, two times concentrated SBF (2xSBF) and the experimental 2xSBF solutions (xCyM) with varying concentrations of carbonate- (xC), magnesium- (yM) and chlorine-ions.

	Ion concentration (mM)							
SBF solution	Na^+	K^+	Mg^{2+}	Ca^{2+}	Cl^-	HCO_3^-	HPO_4^{2-}	SO_4^{2-}
HBP	142.0	5.0	1.5	2.5	103.0	27.0	1.0	0.5
SBF	142.0	5.0	1.5	2.5	147.8	4.2	1.0	0.5
2xSBF	284.0	10.0	3.0	5.0	206.0	8.4	2.0	1.0
21C3M	284.0	10.0	3.0	5.0	283.0	21.0	2.0	1.0
21C2M	284.0	10.0	2.0	5.0	281.0	21.0	2.0	1.0
21C1M	284.0	10.0	1.0	5.0	279.0	21.0	2.0	1.0
21C0M	284.0	10.0	0.0	5.0	277.0	21.0	2.0	1.0
42C3M	284.0	10.0	3.0	5.0	262.0	42.0	2.0	1.0
42C2M	284.0	10.0	2.0	5.0	260.0	42.0	2.0	1.0
42C1M	284.0	10.0	1.0	5.0	258.0	42.0	2.0	1.0
42C0M	284.0	10.0	0.0	5.0	256.0	42.0	2.0	1.0
63C3M	284.0	10.0	3.0	5.0	241.0	63.0	2.0	1.0
63C2M	284.0	10.0	2.0	5.0	239.0	63.0	2.0	1.0
63C1M	284.0	10.0	1.0	5.0	237.0	63.0	2.0	1.0
63C0M	284.0	10.0	0.0	5.0	235.0	63.0	2.0	1.0
84C3M	284.0	10.0	3.0	5.0	220.0	84.0	2.0	1.0
84C2M	284.0	10.0	2.0	5.0	218.0	84.0	2.0	1.0
84C1M	284.0	10.0	1.0	5.0	216.0	84.0	2.0	1.0
84C0M	284.0	10.0	0.0	5.0	214.0	84.0	2.0	1.0

Each experimental 2xSBF solution was prepared by mixing calculated volumes of concentrated solutions of NaCl, KCl, Na_2HPO_4, $MgCl_2.6H_2O$, $CaCl_2.2H_2O$ and Na_2SO_4, in that order. During stirring the pH was adjusted to 5±0.1 for the experimental 2xSBF solutions at low pH and to 7.75±0.05 for the solutions at high pH by adding 1 M HCl and/or 1 M NaOH solution. Next, a calculated amount of $NaHCO_3$ was dissolved in order to obtain a 2xSBF solution with a carbonate concentration of 21 mM, 42mM, 63mM or 84mM (21C, 42C, 63C and 84C respectively).

3.2.2.2 Incubation of the solutions

Twenty ml of each solution was placed in a container thermostated at 37°C under dynamic conditions (50 rpm) for seven days. The precipitates formed during incubation were filtered through a Millipore filter (22 µm), washed three times with demineralized water, dried at 37°C and weighted. All experiments were conducted in duplo.

3.2.2.3 Analysis of the precipitates

The morphology of the precipitates was analyzed using SEM (FEI Quanta 200 F, Hillsboro USA). Prior to the SEM measurements, the samples were coated with gold using a sputter coater (Balzer Union Highland Scientific SCD 030, Bedford, UK). The dimensions of the crystal aggregates were measured using digital imaging software (SigmaScan Pro 5.0, SPSS Science, Chicago, USA).

The phase composition of the precipitates was identified with Fourier transform infra-red spectroscopy (FT-IR, Spectrum One, Perkin Elmer Instruments, Waltham, USA). IR spectra of the precipitates dispersed in KBr tablets were recorded between 400 and 4000 cm^{-1}. The carbonate content of the precipitates was determined by gas chromatography (Model 8500, Perkin Elmer Instruments) based on the method of Godinot *et al*. [247]. As such, a calculated amount of precipitate was dissolved by adding 10% H_3PO_4 (Merck) in a closed vial. The incorporated carbonate in the specimens is released as CO_2 which is injected in the gas chromatograph. Florida Rock with 3.81 wt% carbonate was used as standard to obtain the calibration curve.

3.2.3 Influence of ionic composition of the SBF solution on the calcium phosphate coating

3.2.3.1 Pre-mineralisation treatment

In order to induce a hydrophilic surface, each sample was immersed in 20 ml ethanol for 1 minute after which the PCL samples were washed with 40 ml demineralized water for 5 minutes. Next, each sample was transferred into a plastic container filled with 20 ml 1 M NaOH solution, which was placed in an ultrasonic bath (Transsonic T700/H, Elma Ultrasonic, Ruiselede, Belgium) at 37°C for 15 minutes. After this activation treatment the samples were transferred into a plastic container filled with 40 ml demineralized water and placed in the ultrasonic bath at 37°C for 5 minutes.

To enable the deposition of small calcium phosphate nucleates, the activated samples were alternately immersed in Ca^{2+} and PO_4^{3-} rich solutions using a standard nucleation procedure. During this procedure, each sample was first dipped in 50 ml of 200 mM $CaCl_2.2H_2O$ solution for 1 minute, washed with 50 ml demineralized water for 30 seconds, dipped in 50 ml 200 mM Na_2HPO_4 solution for 1 minute and washed again for 30 seconds with 50 ml demineralized water. The alternate dipping process was conducted at room temperature and automated using a dipcoater (RDC30 Multidip, Bungard, Windeck, Germany). The treatment cycle of four steps was repeated five times and all solutions were stirred regularly at 250 rpm during the procedure.

3.2.3.2 SBF maturation

Experimental 2xSBF solutions in which apatite with a high carbonate content (> 10 wt%) was found to precipitate, were selected for a maturation study. After treatment of the samples with the pre-mineralization procedure, each sample was incubated in 20 ml experimental 2xSBF solution at 37°C under dynamic conditions (50 rpm). The solution was refreshed after 4 days of incubation. After 7 days of incubation, the PCL samples were washed extensively with demineralized water and dried overnight at room temperature. All experiments were conducted in triplicate.

The amount, homogeneity and morphology of the calcium phosphate coating was analyzed by measuring the weight of the samples, Alizarin Red S staining (ARS; Sigma-Aldrich) and SEM imaging, respectively. ARS powder was dissolved in demineralized water to a final concentration of 40 mM and the pH was adjusted to 4.1 using 1 M NaOH solution. The scaffolds were stained an a glass cover plate with an excess of ARS solution for 10 minutes after which the scaffolds were rinsed repeatedly with demineralized water to wash off all unbound dye. At pH 4.1 ARS stains the surface of filaments coated with a calcium containing layer red. The color intensity is linearly correlated with the local calcium concentration.[248]

For the identification of the coating with IR spectroscopy, the polymer scaffold was dissolved. Samples were immersed in 1 ml chloroform for 10 minutes and after centrifugation (2 minutes, 7000 rpm) the supernatant was removed. This step was repeated once. Next, 1 ml acetone was added to the remaining calcium phosphate powder and after centrifugation (2 minutes, 7000 rpm) the supernatant was removed. After repeating this step once, the powder was dried overnight at room temperature and analyzed with IR spectroscopy (see 3.2.2.3).

3.2.4 Cell culture tests

3.2.4.1 Cell culture and seeding

Monolayers of MC3T3-E1 pre-osteoblasts (mouse calvaria pre-osteoblast cells, ATCC) were cultured in α-minimum essential medium (α-MEM) (glutaMAX-1^{TM}, Gibco Invitrogen, Ghent, Belgium) supplemented with 10% fetal bovine serum (FBS) (heat inactivated, EC approved, Gibco Invitrogen) and 1 mM sodium pyruvate (Gibco Invitrogen) at 37°C in 95% air/5% CO_2. The medium was changed twice a week.

Three sets of calcium phosphate coated 3D plotted PCL samples were selected for the cell viability study; samples coated with a homogenous apatite layer with a low, intermediate and high carbonate content. Untreated 3D plotted PCL samples were used as control. Calcium phosphate coated and untreated samples were sterilized under UV-light for 30 minutes. After sterilization the samples were placed in 48-well tissue culture dishes

(suspension culture plates, Greiner Bio-One, Frickenhausen, Wemmel, Belgium). To each sample either 300,000 or 40,000 MC3T3-E1 cells, diluted in 500 µl culture medium, were added, for the live/dead staining and PrestoBlue™-assay (Invitrogen), respectively. For both techniques, either 300,000 or 40,000 MC3T3-E1 cells, diluted in 500µl culture medium, were added to an adhesion plate (Nunc, Life Technologies, Merelbeke, Belgium) as positive control. The cell/scaffold constructs and the positive controls were cultured for 28 days (5%CO_2/95% air, 37°C) with the medium changed twice a week.

3.2.4.2 Cell viability and morphology

The PrestoBlue™-assay was applied to quantify the number of viable cells that attached on the calcium phosphate coated and untreated samples after 1, 7, 15, 21 and 28 days of culture. The PrestoBlue™-reagent is a blue resazurin-based non-fluorescent solution. Resazurin enters the cells where it is transformed to the red and fluorescent resorufin by the reducing power of the mitochondria.

The samples and the control were rinsed with culture medium after which 450 µl culture medium and 50 µL PrestoBlue™-reagent was added to each well. After 2 h incubation at 37 °C in a dark room, 400 µl medium was transferred to 24-well dish (Greiner Bio-One). The fluorescence of the medium was measured in a multilabel plate reader (Victor³, Perkin-Elmer) (excitation: 560 nm, emission: 590 nm). The number of viable and attached cells is linearly correlated with the signal, and viability was calculated as a percentage of the positive control of the respective day.

Cell viability and morphology after 1, 7, 15, 21 and 28 days on the calcium phosphate coated and untreated samples was visualized using fluorescence microscopy after performing live/dead staining with calcein acetoxymethyl (AM) ester (Tebu-Bio, Boechout, Belgium) and propidium iodide (PI) (Sigma-Aldrich). PI cannot pass through intact cell membranes, but may freely enter dead cells with compromised cell membranes where PI intercalates into double-stranded DNA and emits red fluorescence (excitation: 488 nm, emission: 617 nm). Calcein AM is a non-fluorescent, membrane-permeable dye. Under intracellular esterase activity the dye converts to a membrane-impermeable, green fluorescent compound (excitation: 490 nm, emission: 520 nm). After 1, 7, 15, 21 and 28 days the samples and positive controls were rinsed with 500 µl phosphate buffered saline (PBS) after which 500 µl PBS containing 1 µl PI and 1 µl calcein AM was added to each well. After 10 minutes incubation in a dark room at room temperature, samples were evaluated with a fluorescence microscope (Olympus Type U-RFL-T, Aartselaar, Belgium).

Each material and the controls were tested in triplicate.

3.2.5 Statistical analysis

A 1-factor analysis of variance (ANOVA) in conjunction with Bonferonni's post hoc test was used to compare the differences between the mean mass and the carbonate content of the precipitates. Cell viability was evaluated using 2-factor ANOVA with the substrate and the incubation time as independent variables. Significant differences between means were calculated using a Holm-Sidak multiple-comparison test. Differences among groups were considered as statistically significant at $p < 0.05$.

3.3 Results

3.3.1 Scaffold structural characterization

The 0°/45°/90°/-45° overlay pattern of the produced scaffolds is shown in figure 1. The scaffolds of 1x1 cm² have an average weight of 36.04 mg (standard deviation (SD) = 6.78 mg) and an average thickness of 614.23 µm (SD = 27.76 µm). The filament diameter (FD) is 191.67 µm (SD = 6.60 µm) with a strand distance (SD') of 322.18 µm (SD = 35.99 µm) (Figure 2C). The resulting pore diameter is 119.88 µm (SD = 31.25 µm).

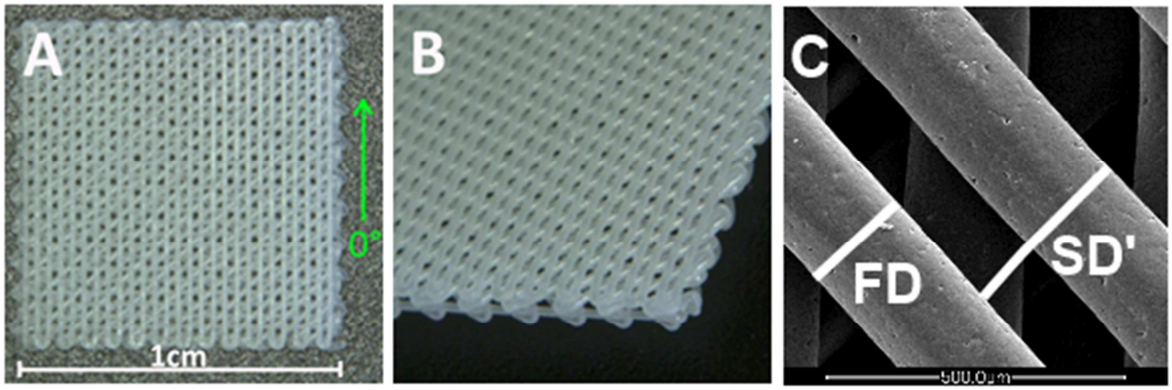

Figure 1: Microscopic (A, B) and SEM (C) images of the 3D plotted PCL scaffold: (A) Microscopic image of top view, (B) Microscopic image of side view, (C) SEM image with an indication of the filament diameter (FD) and the strand distance (SD').

3.3.2 SBF precipitation study

All experimental 2xSBF solutions summarized in table 1 are prepared at low and high pH, indicated by the suffix L and H in the notation, respectively.

3.3.2.1 Influence of Mg^{2+} and HCO_3^- concentration on precipitate formation

The mass of the precipitates formed in the experimental 2xSBF solutions at high and at low pH after 7 days of incubation is shown in figure 2.

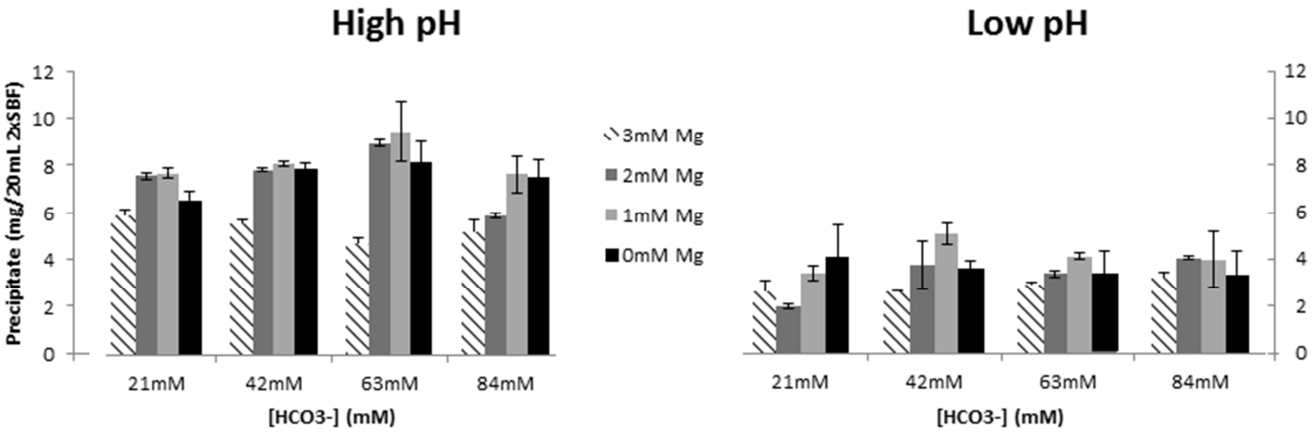

Figure 2: The amount of precipitate (mg/20 mL 2xSBF) formed after 7 days incubation in experimental 2xSBF solutions with varying magnesium – and carbonate concentrations at low and at high pH. Error bars represent standard deviations.

The amount of precipitate formed in the experimental 2xSBF solutions is not significantly influenced by the HCO_3^--concentration or the Mg^{2+}- concentration. Incubation of the solutions at a high pH results in a higher amount of precipitates compared to incubation at low pH.

Moreover, the morphology of the precipitates differs depending on the pH of the solution, as is demonstrated by the SEM images in figure 3, different precipitate structures were formed. Representatively, figure 4 shows the SEM images of the precipitates formed after 7 days in 42C3ML (Figure 4A) and 42C3MH (Figure 4B). The average diameter of the crystal aggregates is 0.48 µm (SD = 0.13 µm) and 48.21 µm (SD = 17.37 µm), respectively. Precipitates formed in experimental 2xSBF solutions at high pH consisted of significantly larger crystal aggregates compared to precipitates formed in the same 2xSBF solution incubated at low pH.

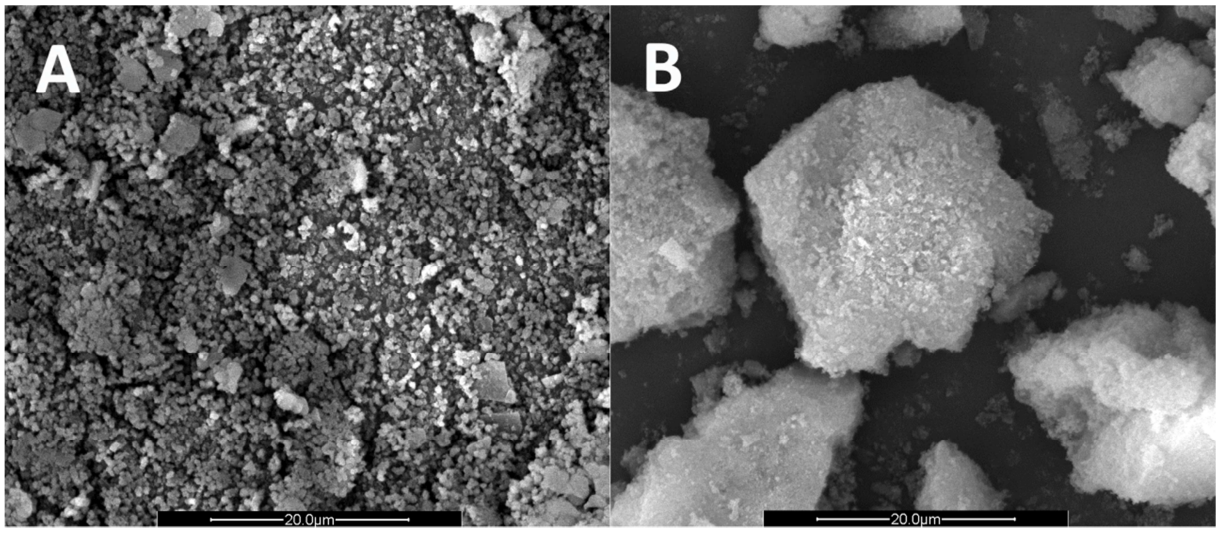

Figure 3: SEM micrographs of the precipitates formed after 7 days in 42C3M solutions at A) low pH and B) high pH.

The carbonate content of the precipitates formed in the experimental 2xSBF solutions is summarized in table 2. The carbonate content tends to increase with increasing HCO_3^--concentration in the solution at a given pH and Mg^{2+}-concentration. This trend is less pronounced in solutions with a low pH and high Mg^{2+}-concentration. The carbonate content decreases with increasing Mg^{2+}-concentration in the solution at a given HCO_3^--concentration and pH. This trend is more pronounced at high pH and at higher HCO_3^--concentration in the solution.

Table 2: Carbonate content of the precipitates formed after 7 days incubation in experimental 2xSBF solutions with varying magnesium and carbonate concentrations at low and at high pH. Standard deviation in brackets.

	21 mM HCO_3^-		**42 mM HCO_3^-**		**63 mM HCO_3^-**		**84 mM HCO_3^-**	
	High pH	Low pH	High pH	Low pH	High pH	Low pH	High pH	Low pH
3 mM Mg^{2+}	7.39 (0.04)	n.d.	8.06 (0.23)	n.d.	8.48 (0.06)	8.22 (0.52)	10.54 (0.11)	11.79 (0.06)
2 mM Mg^{2+}	8.37 (0.35)	n.d.	10.24 (0.24)	7.74 (0.27)	10.55 (0.37)	7.53 (0.18)	10.71 (1.15)	12.04 (0.56)
1 mM Mg^{2+}	7.74 (0.26)	7.56 (n.d.)	10.58 (0.12)	8.97 (0.40)	14.47 (0.03)	11.29 (0.23)	17.82 (1.13)	11.82 (0.06)
0 mM Mg^{2+}	9.04 (0.09)	6.99 (0.337)	10.93 (0.28)	11.03 (0.19)	16.8 (1.91)	12.84 (0.65)	21.6 (0.78)	14.72 (0.62)

3.3.2.2 Identification of the precipitates

Based on the band profiles of the IR spectra of the precipitates formed after seven days of incubation, four types of calcium phosphates are detected; carbonated amorphous calcium phosphate (ACP), B-type carbonated hydroxyapatite (B-type HAp), A-type and B-type carbonated hydroxyapatite (A/B-type HAp) and a mixture of B-type hydroxyapatite and calcite ($CaCO_3$) (B-type HAp/$CaCO_3$). Figure 4 shows some IR-spectra representative for these precipitates. An overview of the experimental 2xSBF solutions and the resulting calcium phosphate phase is given in figure 5.

The IR spectrum in the precipitates formed in the 63COML and 42C2ML solutions are representative for the spectra of B-type HAp (Figure 4). These spectra show peaks due to the v_4-PO_4^{3-} bending around 603 to 569 cm^{-1} and the v_3 stretching of PO_4^{3-} groups around 1045 and 1100 cm^{-1}. These are typical peaks of a HAp phase. The peak around 1620 cm^{-1} arises from the H – O – H deformations in water. Typical peaks in the IR spectra at 880, 1420 and 1460 cm^{-1} indicate the presence of CO_3^{2-} that substitutes for PO_4^{3-} in the apatite lattice (B-type substitution). The intensity of these peaks increases with increasing carbonate content in the precipitates.[152,179] The intensity of the peaks attributed to the presence of CO_3^{2-} are higher in the spectrum of the precipitates formed in the 63C0ML solution compared to the ones found in the spectrum of the precipitates formed in the 42C2ML solution. This is in line with the carbonate content of these precipitates amounting to 12.84 wt% and 7.74 wt%, respectively (table 2).

The spectrum of A/B-type HAp is represented by the spectrum obtained from the precipitates formed in the 21C1ML solution (Figure 4). Besides the typical peaks of B-type HAp, additional bands around 1545 cm^{-1} and 1480 cm^{-1} are present. The latter indicates that some CO_3^{2-} substitutes for OH^- in the apatite lattice (A-type substitution).[152,179]

Besides the typical peaks of B-type HAp, a small but sharp CO_3^{2-} peak at 720 cm^{-1} is present in the IR spectrum of the precipitate formed in the 84C0MH solution (Figure 4). This peak indicates the presence of $CaCO_3$ as a separate phase.[249]

In the IR spectrum of the precipitates formed in the 63C3MH solution, the PO_4^{3-} peak in the region 603 to 569 cm^{-1} are not resolved which is typical for the presence of an amorphous mineral phase. The peaks around 1460 cm^{-1} and 1420 cm^{-1} show the presence of CO_3^{2-}, substituting for PO_4^{3-}, in the amorphous calcium phosphate (Figure 4).

Figure 5 shows that experimental 2xSBF solutions with both a high Mg^{2+} and HCO_3^- concentration result in the precipitation of ACP. On the other hand, low Mg^{2+} and HCO_3^- concentrations result in the precipitation of HAp. A-type carbonate substitution in the HAp

lattice takes place when the HCO_3^- concentration in the SBF solutions is ≤ 42 mM, preferably when the Mg^{2+} concentration is low (≤ 1 mM). At higher HCO_3^- concentrations, only B-type carbonate substitution occurs. Apart from the B-type carbonated HAp, an additional calcite phase precipitates in SBF solutions with a high HCO_3^- concentration in combination with a low Mg^{2+} concentration.

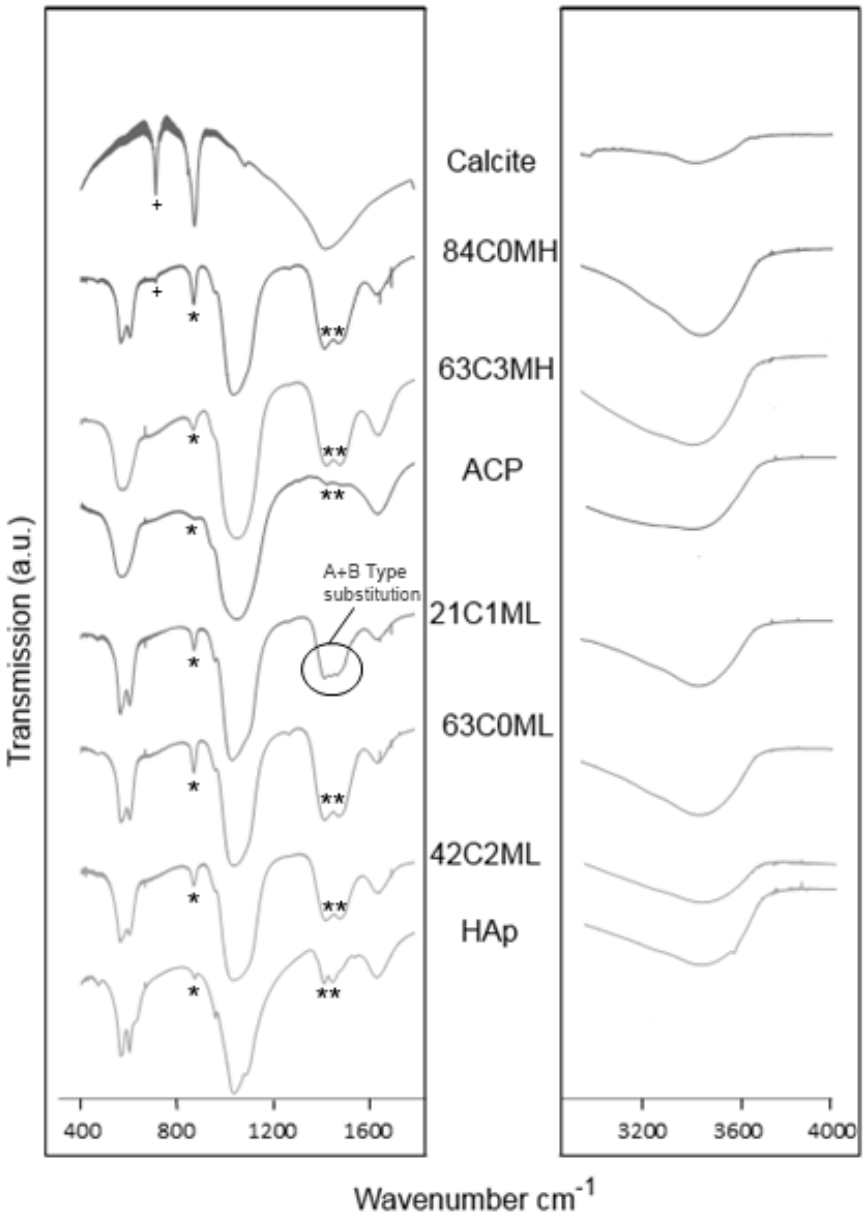

Figure 4: Infrared spectra of the precipitates formed in 42C2ML, 63C0ML, 21C1ML, 63C3MH and 84C0ML experimental 2xSBF solutions after 7 days of incubation. For comparison, the IR spectra of hydroxyapatite (HAp) with a low carbonate content, amorphous calcium phosphate (ACP) and calcite are shown. Typical peaks of B-type substitution (CO_3^{2-} for PO_4^{3-}) and calcite are marked by * and +, respectively.

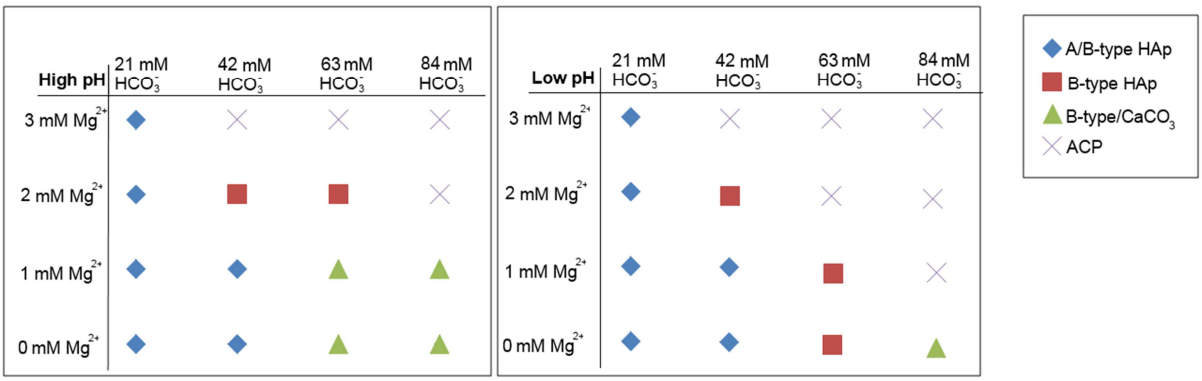

Figure 5: An overview of the calcium phosphate phases precipitates in the experimental 2xSBF solutions after 7 days of incubation. A/B type HAp: A-type and B-type hydroxyapatite; B-type HAp: B-type hydroxyapatite; B-type HAp/$CaCO_3$: a combination of B-type hydroxyapatite and calcite; ACP: carbonated amorphous calcium phosphate.

In general, the ratio R of the intensity of the IR peak of CO_3^{2-} (A_c) at 1460 – 1420 cm^{-1} and that of PO_4^{3-} (A_p) at 1090 – 1050 $cm^{-}1$ increases with increasing carbonate content (wt%) of the precipitate as shown in figure 6. A regression analysis demonstrates that the relationship between the ratio $R=A_c/A_p$ and the carbonate content is represented at the 95% confidence level by the equation (with coefficient of determination $R^2 = 0.924$)

$$wt.\% = (0.44 \pm 1.18) + (27.9 \pm 3.7)\, R \qquad (1)$$

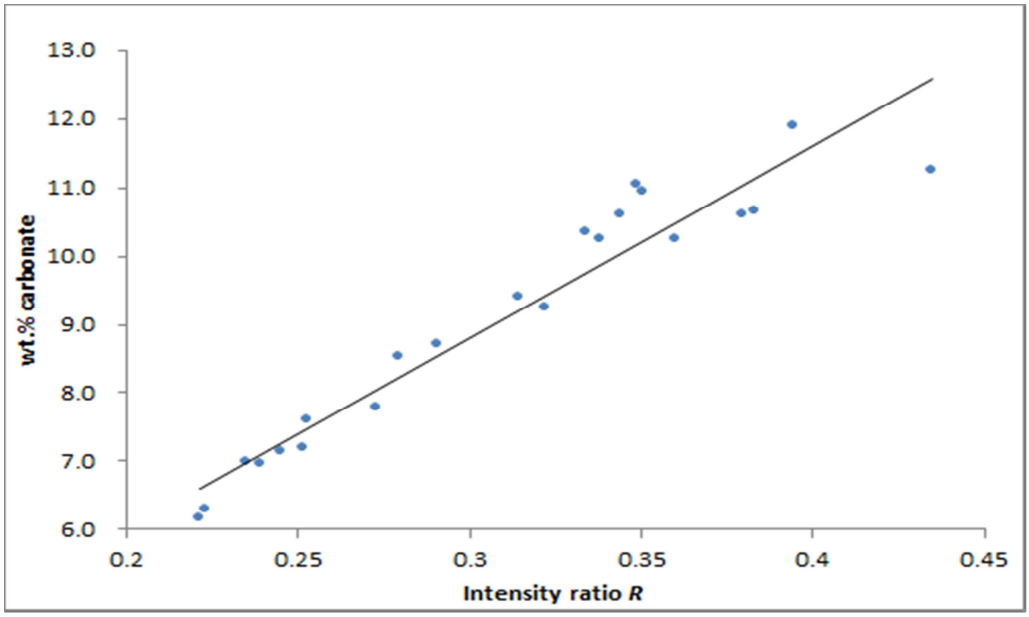

Figure 6: Linear relationship between average carbonate content (wt%) *y* of the precipitates formed in the experimental 2xSBF solutions and the intensity ratio *R* of the CO_3^{2-} and PO_4^{3-} peaks in the associated IR spectra at 1460-1420 cm^{-1} and 1090-1050 cm^{-1}, respectively.

3.3.3 Maturation study

For the actual coating of the PCL scaffolds, only experimental 2xSBF solutions resulting in calcium phosphate precipitates were formed carbonate content of at least 10.5 wt%, were selected. SBF solutions in which calcite co-precipitated were excluded from the maturation study. In order to investigate the effect of the HCO_3^- concentration of the experimental 2xSBF solution on the coating of PCL samples, 21C0ML was included in the maturation study. For comparison, a set of samples were coated by maturation in standard 2xSBF.

The results of the maturation study are summarized in Table 3. Based on the IR spectra used for the identification of the mineral coatings of the scaffolds, the carbonate content of the calcium phosphate deposited on the samples was determined using equation 1. The precipitated calcium phosphate phases and their carbonate content analyzed in the precipitation study are also presented in Table 3 to allow comparison of the precipitate and the coating formed in the same experimental 2xSBF solution.

Table 3 shows that maturation of the samples in SBF solutions with a lower pH result in a higher weight increase and a darker, more homogenous coloring of the samples after ARS staining compared to samples matured in SBF solutions with a high pH.

The type of calcium phosphate deposited on the samples apparently depends on the HCO_3^- and Mg^{2+} concentration of the SBF solution. On the samples incubated in 2xSBF solutions with a high HCO_3^- and Mg^{2+} concentration, predominantly an ACP coating is deposited. However, compared to the results of the precipitation study, ACP is deposited on the samples at lower HCO_3^- and Mg^{2+} concentration . Incubation of the samples in 2xSBF solutions with no Mg^{2+} ions in combination with a low HCO_3^- concentration, results in the deposition of A/B-type or B-type HAp. The CO_3^{2-} content of the coating is higher when incubation is carried out in SBF solutions with high HCO_3^- concentrations. This trend is clearly seen for the experimental SBF solutions without Mg^{2+} and containing 21 mM, 42 mM or 63 mM HCO_3^- (21C0ML, 42C0ML and 63C0ML, respectively) which result in a calcium phosphate coating with respectively 10.76, 12.71 and 15.50 wt% CO_3^{2-}. In general, the incorporation of CO_3^{2-} in the apatite lattice, seems to be easier during the coating process compared to precipitation.

3D plotted PCL scaffold

Table 3: The experimental 2xSBF solutions used for the maturation study, ranked according to increasing weight increase (with standard deviation (SD)) of the samples after 7 days of incubation and digital images of the corresponding samples after ARS staining. For comparison, the type and the carbonate content of the precipitates formed in the SBF solutions are also given.

	Coating				Precipitate	
	Weight increase after 7 days (%) (SD)	**ARS**	**CP phase**	**wt% [a] CO_3^{2-}**	**CP phase**	**wt% CO_3^{2-}**
84C3MH	No weight increase		*n.d.*		ACP	10.54
84C2MH	No weight increase		ACP	16.62	ACP	10.72
63C2MH	No weight increase		ACP	10.20	B-type HAp	10.55
42C1MH	No weight increase	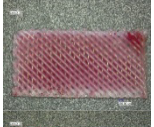	B-type HAp	12.71	A/B-type HAp	10.58
42C0MH	0.6 (0.3)	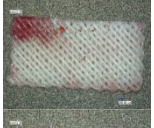	B-type HAp/$CaCO_3$	*n.d.*	A/B-type HAp	10.94
84C2ML	1.5 (0.5)		ACP	13.83	ACP	12.05
84C1ML	1.7 (0.6)	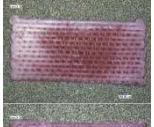	ACP	11.87	ACP	11.83
63C1ML	2.2 (0.6)		ACP	10.48	B-type HAp	11.29
2xSBF	10.2 (2.9)	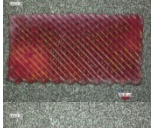	A/B-type HAp	4.62	*n.d.*	*n.d.*
21C0ML	13.1 (1.3)	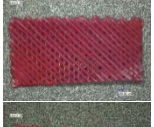	A/B-type HAp	10.76	A/B-type HAp	6.99
63C0ML	15.2 (3.5)		B-type HAp	15.50	B-type HAp	12.84
42C0ML	16.9 (1.1)		B-type HAp	12.71	A/B-type HAp	11.03

n.d.: not determined
a: determined by IR spectroscopy using equation 1

3.3.4 Cell culture tests

For the cell viability study, samples were selected that are coated upon maturation in 2xSBF, 21C0ML and 63C0ML. These samples are coated with HAp with a carbonate content of respectively 4.62, 10.76 and 15.50 wt%. The corresponding SEM images are shown in figure 7. The selected coatings represent an adequate weight increase (Table 3) and cover the filaments of the scaffolds homogenously, without compromising the porous structure.

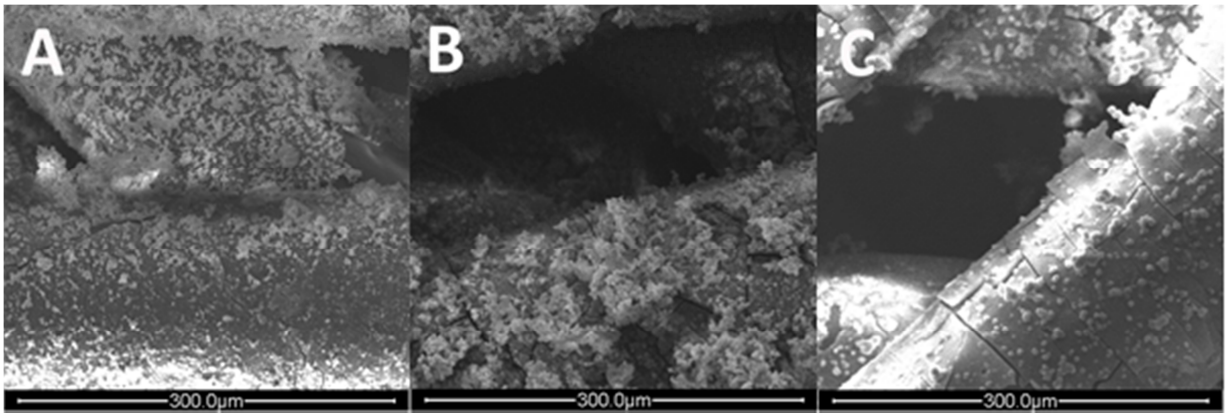

Figure 7: SEM images of the samples coated with HAp with (A) a high carbonate content of 15.50 wt%, (B) a medium carbonate content of 10.76 wt% and (C) a low carbonate content of 4.62 wt%.

The quantity of viable and attached MC3T3-E1 cells on the calcium phosphate coated and untreated PCL samples after 1, 7, 15, 21 and 28 days of culture, as reflected by the Presto Blue^{TM}-assay, is illustrated in figure 8.

After 1 day of incubation, the number of viable cells on all calcium phosphate coated samples is significantly higher than on the untreated PCL samples ($p < 0.001$). For the calcium phosphate coated samples, the cell viability is significantly higher on the samples coated with HAp with a medium carbonate content ($p \leq 0.05$). At day 7 the cell viability is still the highest on the samples coated with a calcium phosphate with a medium carbonate content, but it differs only significantly from the cell viability on the samples coated with HAp with a low carbonate content ($p < 0.001$). After 15, 21 and 28 days of culture, there is no significant difference in cell viability between the samples ($p \geq 0.115$). At day 28, however, the cell viability on all calcium phosphate coated samples is clearly higher compared to the untreated PCL samples, but the difference is not significant.

3D plotted PCL scaffold

From day 1 to 15, there is a significant increase in the number of cells on the untreated PCL samples ($p \leq 0.001$). The cell viability on the coated samples significantly starts to increase after 7 days of incubation for the samples coated with HAp with a low and medium carbonate content ($p \leq 0.004$), and after 15 days of incubation for the samples coated with HAp with a high carbonate content ($p < 0.001$). The cell viability stagnates after 21 days of culture, as there is no more significant increase in cell viability from day 21 to 28 on any sample ($p = 1$).

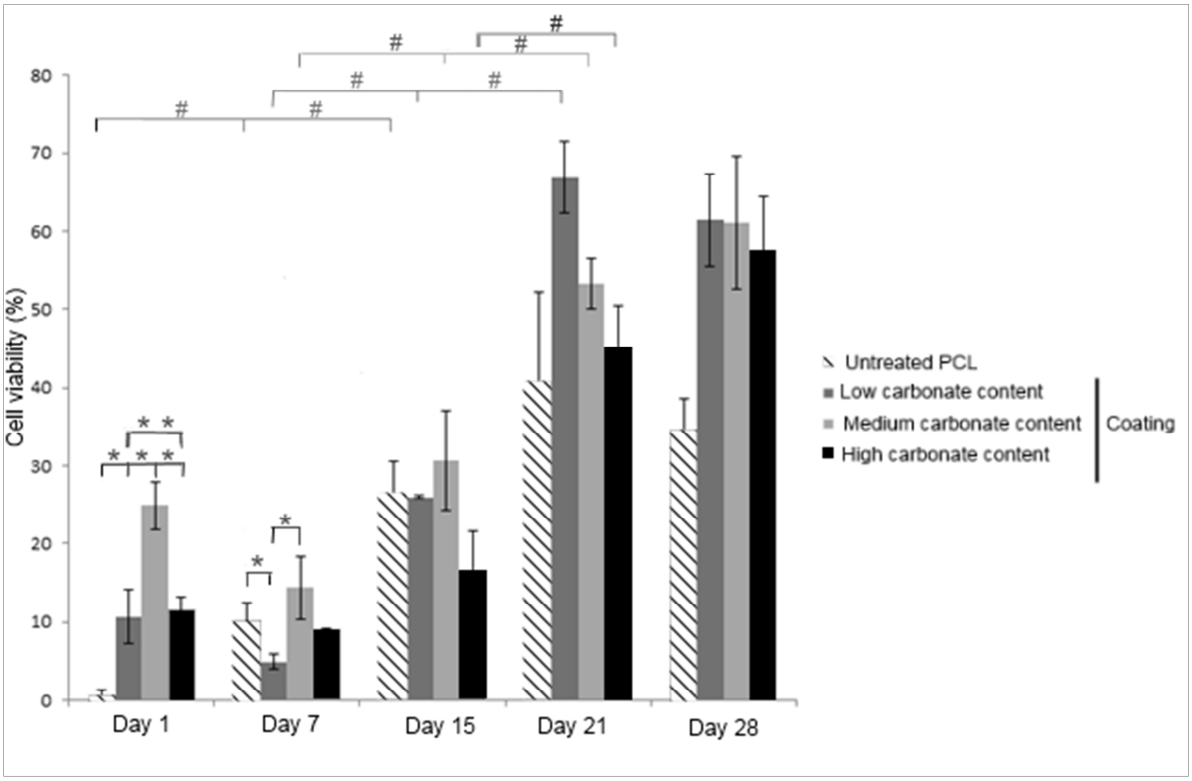

Figure 8: Cell viability of MC3T3-E1 cells on untreated PCL and samples coated with HAp with a low, medium and high carbonate content after 1, 7, 15, 21 and 28 days of incubation. The cell viability was calculated as a percentage of the positive control of the respective day. Statistical differences ($p<0.05$) in the cell viability are annotated with lines and as follows: *, statistically difference between samples at the same day of incubation; #, statistically difference between samples on consecutive incubation days. Error bars represent standard deviations.

Figure 10 shows the morphology of the MC3T3-E1 pre-osteoblast cells after 15 days of culture on the positive control. Although the amount of viable cells differs only significantly after 1 day of culture among the calcium phosphate coatings, large differences in cell morphology can be observed when evaluating the PCL samples by fluorescence microscopy after live/dead staining (Figure 10).

The number of cells on the untreated PCL samples is low throughout the experiment, with predominantly round and dead cells (Figure 10A-10E).

3D plotted PCL scaffold

After 1 and 7 days of incubation, a rather small number of cells are visible on the calcium phosphate coated samples (Figure 10F, G, K, L, P and Q). The cells on these samples are small and round, with some cells forming cellular extensions. After 7 days the largest number of viable cells is present on the samples coated with HAp with a high carbonate content (Figure 10Q).

At day 15, the cells present on the samples coated with a calcium phosphate with medium carbonate content are large with a star shaped morphology and form cellular extensions (Figure 10M). The samples coated with a low and high carbonate content show a similar image; the filaments in the top layer of the scaffolds are homogenously covered with viable cells, whereas on the filaments below, mostly dead cells are visible (Figure 10H and R, respectively). The cell number and cell morphology on the samples coated with a low carbonate content remains more of less the same after 21 days and 28 days of culture compared to 15 days of culture (Figure 10I and J, respectively). There is however a small increase in the live/dead cell ratio.

For the samples coated with HAp with a medium and high carbonate content, the number of viable cells increases after 21 days of culture (Figure 10N and S, respectively). The filaments are fully covered with viable cells, and some pores are even bridged by them. The morphology of the viable cells is similar to the morphology observed for the cells in the confluent positive culture (Figure 9), which indicates a good adhesion of the cells.

After 28 days of culture, the filaments of the samples coated with HAp with a medium carbonate content are fully covered with well-attached cells (Figure 10O). On the samples coated with a HAp with a high carbonate content, the number of viable cells is stable compared to 21 days of culture. A large number of dead cells are however visible on the underlying layer (Figure 10T).

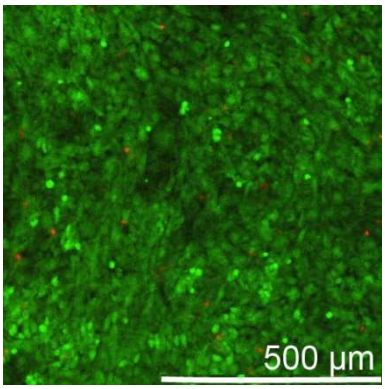

Figure 9: Fluorescence micrographs after live/dead staining of MC3T3-E1 cell on the positive control after 15 days of culture.

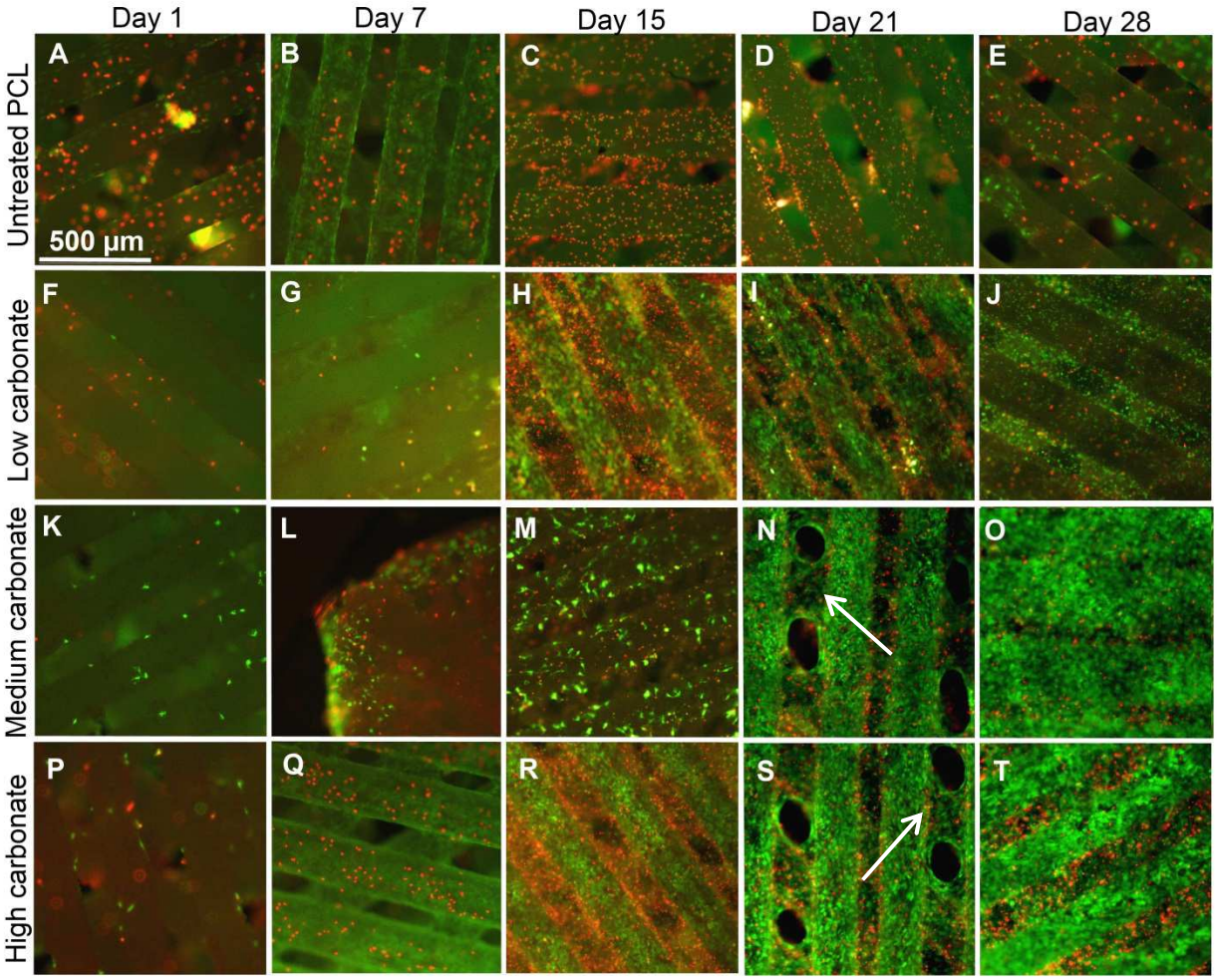

Figure 10: Fluorescence micrographs after live/dead staining of MC3T3-E1 cells cultured on untreated 3D plotted PCL scaffolds (A-E) and samples coated with HAp with a low carbonate content (F-J), a medium carbonate content (K-O) and a high carbonate content (P-T) for 1 day (A, F, K and P), 7 days (B, G, L and Q), 15 days (C, H, M and R), 21 days (D, I, N and S) and 28 days (E, J, O and T). Annotations: bridging of pores.

3.4 Discussion

A 3D plotted PCL scaffold with a 0°/45°/90°/-45° architecture and a pore diameter of 120 µm is interesting as BTE scaffold to support cell adhesion and in-growth due to its adequate 3D and interconnected pore structure.[205,226] Moreover, PCL is a biodegradable and biocompatible material that has been extensively studied as material for the fabrication of BTE scaffolds.[239] However, due to its hydrophobic nature, PCL lacks bioactivity.[250,251] In order to enhance the bioactivity and osteoconductivity of PCL scaffolds, coating of the surface with a homogenous layer of calcium phosphate is recommended.[69,151,183]

To enable the deposition of a calcium phosphate layer, the PCL surface first needs to be activated. The activation procedure used in the present study was adopted from Luickx *et al.* [69] and included pre-wetting with ethanol and ultrasonic activation with a NaOH solution. During this two-step activation, the hydrophobicity of the scaffold is sufficiently reduced and functional groups are created onto the PCL surface, respectively. Following activation the

scaffolds are alternately dipped in calcium – and phosphate-ion rich solutions in order to deposit calcium phosphate nuclei on the surface. Finally, the scaffolds are incubated in an experimental SBF solution during which the calcium phosphate nuclei grow further *in situ* (maturation) to form a continuous layer on the PCL surface without compromising the porous structure of the scaffold. Ideally, the composition and structure of the calcium phosphate coating should be identical to bone apatite, which is a HAp with a high carbonate content.

As it is well known that the composition of the calcium phosphate deposited in an aqueous solution is largely dependent on the solution composition, the effect of varying the magnesium and carbonate concentration, two inhibitors of apatite crystal growth, and the initial pH, on the coating formation and carbonate incorporation was investigated.

3.4.1 Precipitation study

In analogy with Barrere *et al.*[186], a preliminary study was conducted to analyze the precipitates formed in the experimental SBF solutions, prior to the actual coating of the PCL samples. In this study, the composition of the experimental SBF solutions was based on the 2xSBF solution of Kokubo *et al.* [167], in which the Mg^{2+}-, HCO_3^-- and the Cl^-- concentrations were adjusted. A double concentrated SBF solution (2xSBF) was preferred as in normal SBF nucleation and precipitation of calcium phosphates are rather slow [146,167,183,252], whereas in condensed SBF solutions (e.g. 5xSBF or 10xSBF) the chemical composition of the precipitates was found to be less similar to that of bone with increasing ion concentration [252,253]. Compared to the recipe of Kokubo *et al*.[167], TRIS buffer was not used in the experimental 2xSBF solutions. TRIS is not present in the human body and it has the tendency to affect the extent of mineralization significantly by forming complexes with various cations, including Ca^{2+} and Mg^{2+}.[174,253] In addition, $NaHCO_3$ was added in powder form as a final step in the preparation of the experimental 2xSBF solutions. In this way, the loss of carbonate in the form of CO_2 release, otherwise occurring upon the pH reducing step during preparation, was avoided.[249,253]

The present study clearly shows that the initial pH of the solution strongly affects the calcium phosphate precipitate formation and structure. During preparation of the experimental 2xSBF solutions at high pH, precipitation occurred in the solution when the pH was augmented to the final pH of 7.75±0.05. A higher pH is associated with a significant decrease of the solubility of the calcium phosphate thus resulting in an advanced and accelerated nucleation and crystal growth in the solution.[179,254,255] Accordingly, after 7 days of incubation, compared to the low pH, the high initial pH conditions resulted in more pronounced precipitation (Figure 2 and 3).

In some studies the HCO_3^- concentration of SBF solutions was increased in order to increase the carbonate content of the precipitated calcium phosphate.[179,244] The highest HCO_3^- concentration used in literature, however, is 27 mM, as found in human blood plasma. The resulting calcium phosphate precipitates had a higher carbonate content compared to the precipitates formed in standard SBF, but with a maximum of 9 wt%. In the present study, 2xSBF solutions with HCO_3^- concentrations ranging from 21 mM up to 84 mM were used (Table 1), resulting in the formation of precipitates with a carbonate content of 7.39 wt% to 21.6 wt% (Table 2). As might be expected, the carbonate content of the precipitates increased with increasing HCO_3^- concentration of the SBF solutions, corroborating with previous experiments.[256-258]

In literature, little information is found on the combined effect of Mg^{2+} and HCO_3^- on the formation of calcium phosphate precipitates in SBF, neither on the effect of Mg^{2+} on the incorporation of CO_3^{2-} in the lattice of the calcium phosphates.

The Mg^{2+} and HCO_3^- concentration in the SBF solution also affected the type of the precipitated calcium phosphate (Figure 5). A high HCO_3^- concentration (≥ 42 mM) and the presence of Mg^{2+} (≥ 1 mM) resulted in the formation of ACP. The formation of ACP precursor clusters is always present during the precipitation of calcium phosphates from supersaturated solutions. Such clusters are the transient solution precursors for the formation of apatitic calcium phosphates.[253] It has been reported that Mg^{2+} and HCO_3^- have a strong inhibitory effect on crystal growth and phase transition to apatite in favor of the amorphous phase.[254] The inhibitory effect of Mg^{2+} has been attributed to its adsorption at active growth sites in competition with the chemically similar but larger Ca^{2+}. Carbonate ions are known to inhibit apatite crystal growth as they enter the apatite lattice, substituting the anionic phosphate (B-type substitution) or hydroxyl groups (A-type substitution).[7,249,259,260]

The order in which Mg^{2+} and HCO_3^-, individually or in combination inhibit crystal growth and hence decrease crystallinity and promote the formation of ACP is

$$(Mg^{2+} + CO_3^{2-}) \gg Mg^{2+} \gg CO_3^{2-} \quad [7,249]$$

The synergistic effect of Mg^{2+} and CO_3^{2-} on the formation of ACP probably results from the incorporation of both ions into the calcium phosphate structure.

Low concentrations of the crystal growth inhibitors facilitate the phase transformation of the ACP precursor into the more stable and crystalline HAp (Figure 5). The present study showed that a decrease of the Mg^{2+} concentration in the SBF solution results in the formation of a calcium phosphate with a higher carbonate content (Table 2). This can be explained by the synergistic effect of Mg^{2+} and HCO_3^- on the crystallinity of the precipitated calcium

phosphate; higher Mg^{2+} - and HCO_3^- concentrations are known to inhibit the crystal growth of the formed calcium phosphate phase thus decreasing also the incorporation of CO_3^{2-}. Hence, calcium phosphate precipitates with a high carbonate content are obtained by increasing the HCO_3^- concentration and decreasing the Mg^{2+} concentration of the SBF solution.

The dominant form of carbonate incorporation in the apatite lattice is B-type substitution. A-type carbonated apatite in combination with B-type carbonated apatite precipitated in SBF solutions with 21 mM HCO_3^- and 42 mM HCO_3^- if the Mg^{2+} concentration is low (≤ 1 mM). These results corroborate the findings of Barralet *et al.*[258] that carbonate was substituted into A and B-sites of the HAp lattice if the carbonate contents were low. At higher carbonate contents, the carbonate was located predominantly in the B-site.

In the 2xSBF solution with high carbonate and low magnesium concentration, the pH of the solution clearly affects the phase composition of the precipitates. So, in 63C2M at low pH, ACP precipitates formed, whereas B-type carbonated HAp is formed at high pH. This is caused by the higher rate of phase transformation of ACP to HAp, as HAp is more stable at a higher pH.[249,254]

Apart from B-type carbonated HAp, calcite co-precipitated as separate phase in the 63C1M, 63C0M and 84C1M solutions, at high pH and the 84C0M at low and high pH. At higher carbonate concentration and higher pH, more CO_3^{2-} species are available, which easily bind with Ca^{2+} to form calcite.[7,175,249] In addition, augmentation of the carbonate concentration results in an increase of the pH of the solution due to the buffering effect of HCO_3^-/CO_3^{2-}, which could explain why calcite is also formed in 84C0ML at low initial pH.[175,186] Calcite also only formed at low magnesium concentrations (≤ 1 mM), which could be attributed to the ability of Mg^{2+} to inhibit calcite precipitation by associating with CO_3^{2-} to form a stable aqueous $MgCO_3$.[249] The presence of $MgCO_3$ could however not be demonstrated with IR spectroscopy. Evidently, the carbonate content as determined by gas chromatography of these precipitates is high (from 14.47 to 21.6 wt%) (Figure 4). However, these results give no information about the amount of carbonate substitution in the HAp lattice.

3.4.2 Maturation study

Maturation of the PCL samples in the selected 2xSBF solutions showed that more coating formed on the samples upon incubation at a low initial pH compared to high initial pH (Table 3). Additionally, within the SBF solutions with a low initial pH, the degree of coating increased with decreasing magnesium concentration. The observed enhanced coating in solutions with low pH and magnesium concentration could be explained by the delayed precipitation at these conditions. Indeed, magnesium is known to disturb calcium phosphate

surfaces by hindering crystal growth, and a lower pH results in a lower degree of oversaturation and increased calcium phosphate solubility, which is in favor of the deposition of calcium phosphate on the substrate surface. A higher pH is associated with a higher degree of oversaturation and decreased solubility of calcium phosphates which result in a fast precipitation of calcium phosphate in the SBF solution.[179] Thus less ionic species are available in the solution for the deposition of calcium phosphate on the PCL samples. Furthermore, there is a competition between early formed calcium phosphate salts acting as seeds, and the heterogeneous nucleation on the PCL surface. When calcium phosphate globules form too fast in the solutions, the competition is detrimental to the coating formation.[175,186] In addition, the precipitates formed in the SBF solutions with high pH were significantly larger than the ones formed in the solutions at low pH. When calcium phosphate globules are small, they remain well adhered onto the substrate, whereas larger globules easily detached from the substrate.[186,254,255]

Table 3 shows that the type of calcium phosphate deposited onto the samples was not always the same as the precipitates formed in the same SBF solution. Barrere *et al*.[186] previously also combined a preliminary precipitation study prior to the actual coating of samples, but unfortunately only identified the precipitates formed in the experimental SBF solutions (5xSBF) and not the concurrent coating formed on the substrates (Ti6Al4V plates). Probably they assumed that the precipitates and the coating deposited from the same SBF solution were identical. No other studies were found in literature that identified both the precipitates and the coating formed in SBF solutions. The difference between the precipitates and the coating formed in the same SBF solutions could be due to an interaction between the functional groups on the PCL samples and the ions in the solution. There is evidence that the character of the deposited mineral phase is not only dependent on the composition of the mineralization solution but also on the inducing charged groups.[178]

The ratio of the peaks at 1460-1420 cm^{-1} (A_c) and 1090-1050 cm^{-1} (A_p) can be used to calculate the carbonate content of the calcium phosphate layer (Equation (1)). The carbonate content in the deposited coating calculated from A_c/ A_p was systematically higher in the deposited coating compared to the precipitates formed in the same experimental 2xSBF solution. This could possibly also be explained by the interaction between the functional groups on the PCL surface and the ions in the solution. The risk of a systematic overestimation of the carbonate content using Equation (1) should however also be taken into consideration.

3.4.3 Cell viability and morphology

Osteoblast behavior is sensitive to biochemical and topographical features of their substrate. In the present study the effect of a calcium phosphate coating with low, medium and high carbonate content on 3D plotted PCL samples on the cell viabilitity of MC3T3-E1 cells was examined. Although the PrestoBlue^{TM}-assay only showed a significant higher amount of viable, adherent cells on the calcium phosphate coated samples after 1 day of culture (Figure 9), large differences were observed when evaluating the PCL samples by fluorescent microscopy after live/dead staining (Figure 11). Throughout the 28 days of the experiment, low cell viability was observed on the untreated PCL samples and cells show a round morphology (Figure 11A – E). The observed cellular behavior could be expected due to the hydrophobic nature of PCL, which is known to hinder the initial biological responses and cell attachment. PCL however is biocompatible, and cells are indeed able to adhere to PCL scaffolds. The latter could explain the observed increase in cell viability with increasing incubation time (Figure 9). After 15 days of culture, all of the struts of the calcium phosphate coating scaffold were covered with cells, independent of the carbonate content of the coating. Nevertheless, bridging of the pores was only achieved for the samples coated with a calcium phosphate with a carbonate content of at least 10.76 wt% (Figure 11N and S). On these samples the cells have a spread morphology and form a confluent layer. A decrease in charge density and crystallinity at the HAp surface, as well as changes in the crystal morphology of the apatite coating, might attribute to changes in composition and 3D structure of the protein adsorption layer and hence to the observed cell behavior. It was indeed recently reported that apatites with high carbonate content and consequently low crystallinity were the most performant in terms of cell adhesion and proliferation.[152]

The present study clearly demonstrates that the coating of 3D plotted PCL with a HAp layer with a carbonate content of 10 wt% or more is a promising strategy for the improvement of its bone tissue engineering scaffold potential.

3.5 Conclusion

In this paper, a 3D plotted PCL porous scaffold was coated with a calcium phosphate layer in three consecutive steps; activation, nucleation and maturation. During the activation step, functional groups are created on the PCL surface. Subsequent treatment of the samples with a standard nucleation procedure enables the nucleation of calcium phosphate particles on the surface. In a final step, the samples are incubated in an SBF solution which enables the maturation of the calcium phosphate layer. By varying the pH and the composition of the SBF solution, the type and the composition of the calcium phosphate layer can be varied. The present study showed that incubation of the samples in SBF solutions with a low pH resulted in a thicker and more homogenous coating, whereas higher

carbonate contents were obtained when the carbonate concentration was augmented and the magnesium concentration of the mineralization solution reduced. Such calcium phosphate coating, with at least 10 wt% carbonate improved the osteogenic response and enhanced the cell affinity when compared with the uncoated PCL samples and samples coated with a calcium phosphate with a low carbonate content.

3.6 References

1. Wu SL, Liu XM, Yeung KWK, Liu CS, Yang XJ. Biomimetic porous scaffolds for bone tissue engineering. Materials Science & Engineering R-Reports 2014;80:1-36.
2. Shrivats AR, McDermott MC, Hollinger JO. Bone tissue engineering: state of the union. Drug Discovery Today 2014;19(6):781-786.
3. Hutmacher DW. Scaffolds in tissue engineering bone and cartilage. Biomaterials 2000;21(24):2529-2543.
4. Lichte P, Pape HC, Pufe T, Kobbe P, Fischer H. Scaffolds for bone healing: Concepts, materials and evidence. Injury-International Journal of the Care of the Injured 2011;42(6):569-573.
5. Burg KJL, Porter S, Kellam JF. Biomaterial developments for bone tissue engineering. Biomaterials 2000;21(23):2347-2359.
6. Karageorgiou V, Kaplan D. Porosity of 3D biomaterial scaffolds and osteogenesis. Biomaterials 2005;26(27):5474-5491.
7. Jeon H, Kim GH. Effect of the internal microstructure in rapid-prototyped polycaprolactone scaffolds on physical and cellular properties for bone tissue regeneration. Applied Physics a-Materials Science & Processing 2012;108(4):901-909.
8. Sun W, Darling A, Starly B, Nam J. Computer-aided tissue engineering: overview, scope and challenges. Biotechnology and Applied Biochemistry 2004;39:29-47.
9. Giannitelli SM, Accoto D, Trombetta M, Rainer A. Current trends in the design of scaffolds for computer-aided tissue engineering. Acta Biomaterialia 2014;10(2):580-594.
10. Hollister SJ, Levy RA, Chu TM, Halloran JW, Feinberg SE. An image-based approach for designing and manufacturing craniofacial scaffolds. International Journal of Oral and Maxillofacial Surgery 2000;29(1):67-71.
11. Peltola SM, Melchels FPW, Grijpma DW, Kellomaki M. A review of rapid prototyping techniques for tissue engineering purposes. Annals of Medicine 2008;40(4):268-280.
12. Melchels FPW, Domingos MAN, Klein TJ, Malda J, Bartolo PJ, Hutmacher DW. Additive manufacturing of tissues and organs. Progress in Polymer Science 2012;37(8):1079-1104.
13. Arafat MT, Gibson I, Li X. State of the art and future direction of additive manufactured scaffolds-based bone tissue engineering. Rapid Prototyping Journal 2014;20(1):13-26.
14. Seal BL, Otero TC, Panitch A. Polymeric biomaterials for tissue and organ regeneration. Materials Science & Engineering R-Reports 2001;34(4-5):147-230.
15. Nair LS, Laurencin CT. Biodegradable polymers as biomaterials. Progress in Polymer Science 2007;32(8-9):762-798.
16. Li MG, Tian XY, Chen XB. A brief review of dispensing-based rapid prototyping techniques in tissue scaffold fabrication: role of modeling on scaffold properties prediction. Biofabrication 2009;1(3).
17. Ragaert K, Cardon L, Dekeyser A, Degrieck J. Machine design and processing considerations for the 3D plotting of thermoplastic scaffolds. Biofabrication 2010;2(1).
18. Callister W, Rethwish D. Materials Science & Engineering; 2010.

19. Park S, Kim G, Jeon YC, Koh Y, Kim W. 3D polycaprolactone scaffolds with controlled pore structure using a rapid prototyping system. Journal of Materials Science-Materials in Medicine 2009;20(1):229-234.
20. Moroni L, De Wijn JR, Van Blitterswijk CA. Integrating novel technologies to fabricate smart scaffolds. Journal of Biomaterials Science-Polymer Edition 2008;19(5):543-572.
21. Wang F, Shor L, Darling A, Khalil S, Sun W, Guceri S, Lau A. Precision extruding deposition and characterization of cellular poly-epsilon-caprolactone tissue scaffolds. Rapid Prototyping Journal 2004;10(1):42-49.
22. Zein I, Hutmacher DW, Tan KC, Teoh SH. Fused deposition modeling of novel scaffold architectures for tissue engineering applications. Biomaterials 2002;23(4):1169-1185.
23. Ragaert K, Dekeyser A, Cardon L, Degrieck J. Quantification of Thermal Material Degradation During the Processing of Biomedical Thermoplastics. Journal of Applied Polymer Science 2011;120(5):2872-2880.
24. Engelberg I, Kohn J. Physicochemical properties of degradable polymers used in medical applications - A comparative-study. Biomaterials 1991;12(3):292-304.
25. Ragaert K, De Somer F, De Baere I, Cardon L, Degrieck J. Production and evalution of PCL scaffolds for tissue engineering heart valves. Advanced in Production Engineering & Management 2011;6(3):163-172.
26. Declercq H, Desmet T, Berneel E, Dubruel P, Cornelissen MJ. Synergistic effect of surface modification and scaffold design of bioplotted 3-D poly-epsilon-caprolactone scaffolds in osteogenic tissue engineering. Acta Biomaterialia 2013;9(8):7699-7708.
27. Jang JH, Castano O, Kim HW. Electrospun materials as potential platforms for bone tissue engineering. Advanced Drug Delivery Reviews 2009;61(12):1065-1083.
28. Choi W-Y, Kim H-E, Koh Y-H. Production, mechanical properties and in vitro biocompatibility of highly aligned porous poly(epsilon-caprolactone) (PCL)/hydroxyapatite (HA) scaffolds. Journal of Porous Materials 2013;20(4):701-708.
29. Dorj B, Kim M-K, Won J-E, Kim H-W. Functionalization of poly(caprolactone) scaffolds by the surface mineralization for use in bone regeneration. Materials Letters 2011;65(23-24):3559-3562.
30. Woodruff MA, Hutmacher DW. The return of a forgotten polymer-Polycaprolactone in the 21st century. Progress in Polymer Science 2010;35(10):1217-1256.
31. Yu H-S, Jang J-H, Kim T-I, Lee H-H, Kim H-W. Apatite-mineralized polycaprolactone nanofibrous web as a bone tissue regeneration substrate. Journal of Biomedical Materials Research Part A 2009;88A(3):747-754.
32. Mavis B, Demirtas TT, Gumusderelioglu M, Gunduz G, Colak U. Synthesis, characterization and osteoblastic activity of polycaprolactone nanofibers coated with biomimetic calcium phosphate. Acta Biomaterialia 2009;5(8).
33. Xie J, Zhong S, Ma B, Shuler FD, Lim CT. Controlled biomineralization of electrospun poly(epsilon-caprolactone) fibers to enhance their mechanical properties. Acta Biomaterialia 2013;9(3):5698-5707.
34. Oyane A, Uchida M, Yokoyama Y, Choong C, Triffitt J, Ito A. Simple surface modification of poly(epsilon-caprolactone) to induce its apatite-forming ability. Journal of Biomedical Materials Research Part A 2005;75A(1).
35. Oyane A, Uchida M, Choong C, Triffitt J, Jones J, Ito A. Simple surface modification of poly(epsilon-caprolactone) for apatite deposition from simulated body fluid. Biomaterials 2005;26(15):2407-2413.
36. Park SA, Lee JB, Kim YE, Kim JE, Lee JH, Shin JW, Kwon IK, Kim W. Fabrication of biomimetic PCL scaffold using rapid prototyping for bone tissue engineering. Macromolecular Research 2014;22(8):882-887.
37. Choong C, Triffitt JT, Cui ZF. Polycaprolactone scaffolds for bone tissue engineering - Effects of a calcium phosphate coating layer on osteogenic cells. Food and Bioproducts Processing 2004;82(C2):117-125.

38. Luickx N, Van den Vreken N, D'Oosterlinck W, Van der Schueren L, Declercq H, De Clerck K, Cornelissen M, Verbeeck R. Optimization of the activation and nucleation steps in the precipitation of a calcium phosphate primer layer on electrospun poly(ε-caprolactone). Journal of Biomedical Materials Research Part A 2015;103:511-524.
39. Kokubo T, Kushitani H, Sakka S, Kitsugi T, Yamamuro T. Solutions able to reproduce in vivo surface-structure changes in bioactive glass-ceramic A-W3.. Journal of Biomedical Materials Research 1990;24(6):721-734.
40. Kokubo T, Takadama H. How useful is SBF in predicting in vivo bone bioactivity? Biomaterials 2006;27(15):2907-2915.
41. Dey A, Bomans PHH, Mueller FA, Will J, Frederik PM, de With G, Sommerdijk NAJM. The role of prenucleation clusters in surface-induced calcium phosphate crystallization. Nature Materials 2010;9(12):1010-1014.
42. Araujo JV, Martins A, Leonor IB, Pinho ED, Reis RL, Neves NM. Surface controlled biomimetic coating of polycaprolactone nanofiber meshes to be used as bone extracellular matrix analogues. Journal of Biomaterials Science-Polymer Edition 2008;19(10).
43. Yang F, Wolke JGC, Jansen JA. Biomimetic calcium phosphate coating on electrospun poly (epsilon-caprolactone) scaffolds for bone tissue engineering. Chemical Engineering Journal 2008;137(1):154-161.
44. Oyane A, Uchida M, Choong C, Triffitt J, Jones J, Ito A. Simple surface modification of poly(epsilon-caprolactone) for apatite deposition from simulated body fluid. Biomaterials 2005;26(15).
45. Choong C, Yuan S, Thian ES, Oyane A, Triffitt J. Optimization of poly(e-caprolactone) surface properties for apatite formation and improved osteogenic stimulation. Journal of Biomedical Materials Research Part A 2012;100A(2):353-361.
46. Lebourg M, Suay Anton J, Gomez Ribelles JL. Characterization of calcium phosphate layers grown on polycaprolactone for tissue engineering purposes. Composites Science and Technology 2010;70(13):1796-1804.
47. Araujo JV, Cunha-Reis C, Rada T, da Silva MA, Gomes ME, Yang Y, Ashammakhi N, Reis RL, El-Haj AJ, Neves NM. Dynamic Culture of Osteogenic Cells in Biomimetically Coated Poly(Caprolactone) Nanofibre Mesh Constructs. Tissue Engineering Part A 2010;16(2):557-563.
48. Pieters IY, Van den Vreken NMF, Declercq HA, Cornelissen MJ, Verbeeck RMH. Carbonated apatites obtained by the hydrolysis of monetite: Influence of carbonate content on adhesion and proliferation of MC3T3-E1 osteoblastic cells. Acta Biomaterialia 2010;6(4):1561-1568.
49. Landi E, Tampieri A, Celotti G, Langenati R, Sandri M, Sprio S. Nucleation of biomimetic apatite in synthetic body fluids: dense and porous scaffold development. Biomaterials 2005;26(16):2835-2845.
50. Stoch A, Jastrzebski W, Brozek A, Trybalska B, Cichocinska M, Szarawara E. FTIR monitoring of the growth of the carbonate containing apatite layers from simulated and natural body fluids. Journal of Molecular Structure 1999;511:287-294.
51. Muller L, Conforto E, Caillard D, Muller FA. Biomimetic apatite coatings - Carbonate substitution and preferred growth orientation. Biomolecular Engineering 2007;24(5):462-466.
52. Godinot C, Bonel G, Torres L, Mathieu J. Chromatographic assay of carbonate in the submilligram range - application to carbonate assy of calcified tissue.Microchemical Journal 1984;29(1):92-105.
53. Gregory CA, Gunn WG, Peister A, Prockop DJ. An Alizarin red-based assay of mineralization by adherent cells in culture: comparison with cetylpyridinium chloride extraction. Analytical Biochemistry 2004;329(1).
54. Muller L, Muller FA. Preparation of SBF with different HCO3- content and its influence on the composition of biomimetic apatites. Acta Biomaterialia 2006;2(2):181-189.
55. Cao X, Harris W. Carbonate and magnesium interactive effect on calcium phosphate precipitation. Environmental Science & Technology 2008;42(2):436-442.

56. Shor L, Guceri S, Wen X, Gandhi M, Sun W. Fabrication of three-dimensional polycaprolactone/hydroxyapatite tissue scaffolds and osteoblast-scaffold interactions in vitro. Biomaterials 2007;28(35):5291-5297.
57. Kinoshita Y, Maeda H. Recent Developments of Functional Scaffolds for Craniomaxillofacial Bone Tissue Engineering Applications. Scientific World Journal 2013.
58. Barrere F, van Blitterswijk CA, de Groot K, Layrolle P. Influence of ionic strength and carbonate on the Ca-P coating formation from SBFx5 solution. Biomaterials 2002;23(9):1921-1930.
59. Dorozhkina EI, Dorozhkin SV. Structure and properties of the precipitates formed from condensed solutions of the revised simulated body fluid. Journal of Biomedical Materials Research Part A 2003;67A(2):578-581.
60. Jalota S, Bhaduri SB, Tas AC. Effect of carbonate content and buffer type on calcium phosphate formation in SBF solutions. Journal of Materials Science-Materials in Medicine 2006;17(8):697-707.
61. Tas AC. The use of physiological solutions or media in calcium phosphate synthesis and processing. Acta Biomaterialia 2014;10(5):1771-1792.
62. Chou YF, Chiou WA, Xu YH, Dunn JCY, Wu BM. The effect of pH on the structural evolution of accelerated biomimetic apatite. Biomaterials 2004;25(22):5323-5331.
63. Gopi D, Nithiya S, Shinyjoy E, Kavitha L. Spectroscopic investigation on formation and growth of mineralized nanohydroxyapatite for bone tissue engineering applications. Spectrochimica Acta Part a-Molecular and Biomolecular Spectroscopy 2012;92:194-200.
64. Kim HM, Kishimoto K, Miyaji F, Kokubo T, Yao T, Suetsugu Y, Tanaka J, Nakamura T. Composition and structure of the apatite formed on PET substrates in SBF modified with various ionic activity products. Journal of Biomedical Materials Research 1999;46(2):228-235.
65. Dorozhkina EI, Dorozhkin SV. Surface mineralisation of hydroxyapatite in modified simulated body fluid (mSBF) with higher amounts of hydrogencarbonate ions. Colloids and Surfaces a-Physicochemical and Engineering Aspects 2002;210(1):41-48.
66. Barralet J, Best S, Bonfield W. Carbonate substitution in precipitated hydroxyapatite: An investigation into the effects of reaction temperature and bicarbonate ion concentration. Journal of Biomedical Materials Research 1998;41(1):79-86.
67. Martin RI, Brown PW. The effects of magnesium on hydroxyapatite formation in vitro from CaHPO4 and Ca-4(PO4)(2)O at 37.4 degrees C. Calcified Tissue International 1997;60(6):538-546.
68. Apfelbaum F, Mayer I, Rey C, Lebugle A. Magnesium in maturing synthetic apatite - a Fourier-transform infrared analysis. Journal of Crystal Growth 1994;144(3-4):304-310.
69. Driessens F, Verbeeck R. Biominerals: CRC Press; 1990.
70. Barrere F, van Blitterswijk CA, de Groot K, Layrolle P. Nucleation of biomimetic Ca-P coatings on Ti6Al4V from a SBF x 5 solution: influence of magnesium. Biomaterials 2002;23(10):2211-2220.
71. Kretlow JD, Mikos AG. Review: Mineralization of synthetic polymer scaffolds for bone tissue engineering. Tissue Engineering 2007;13(5):927-938.

4 Calcium phosphate coating of a multiscale PCL scaffold

Part of the research is based on the article:

Calcium phosphate coating of a microfibrous/nanofibrous multiscale scaffold.

Nathalie Luickx, Natasja Van den Vreken, Nicolas Van Damme, Kim Ragaert, Maria Cornelissen, Heidi Declercq

Article in preparation

Abstract: In recent year, the fabrication of multiscale fibrous scaffolds containing both micro- and nanofibers has attracted a lot of attention in tissue engineering. The combination of nanofibers and microfibers is a promising approach in which the microfibrous structure provides the porous 3D structural environment with mechanical integrity while the nanofibers provide the favorable surface topography with nanoscale features for cell attachment. In this study, 3D plotting was used for the production of microfibrous poly(ε-caprolactone) (PCL) scaffolds. The 3D plotted scaffolds were coated with a thin layer of PCL nanofibers by means of electrospinning. In order to enhance the bioactivity, the present study aimed to coat the multiscale PCL scaffolds with an apatite layer with high carbonate content using a mineralization solution with ions concentrations based on simulated body fluid (SBF). Analysis of the cell viability, adhesion and proliferation of MC3T3-E1 cells showed that the cells attached well to the multiscale scaffold. An enhanced cell response was obtained when the multiscale scaffolds were coated with a carbonated hydroxyapatite layer. The developed structures are believed to have great potential for the 3D organization and guidance of cells that are important for engineering 3D bone tissue.

4.1 Introduction

Scaffold-based bone tissue engineering is popular due to the potential of current scaffold fabrication technologies to mimic the architecture of the natural extracellular matrix (ECM). The ideal scaffold is biocompatible, biodegradable, bioactive and osteoconductive. In addition, the scaffold should exhibit a high and interconnected porosity as well as a high surface to volume ratio and possess mechanical properties comparable with the tissue being engineered.[21,41] The diameter of the interconnected pores must be between 100-300 µm. These pores are necessary to allow the infiltration of cells, vascularization and efficient transport of oxygen, nutrients and metabolites.[9,261] Such a scaffold promotes cell adhesion, proliferation and differentiation.[60]

Various polymers and fabrication techniques have been investigated to produce such an ideal bone tissue engineering scaffold.[21,41,50,261] Synthetic biodegradable aliphatic polyesters such as the Food and Drug Administration (FDA) approved polylactic acid (PLA), polyglycolic acid (PGA), polycaprolactone (PCL) and their copolymers are interesting scaffold materials.[21,41,89] These polyesters are biocompatible and the mechanical properties and degradation kinetics can be tailored by varying the monomer composition and molecular weight. Due to their thermoplasticity these polymers are processable by 3D plotting[46,66,84]. This technique is widely studied for the fabrication of bone tissue engineering scaffolds thanks to its ability to produce polymeric matrices with reproducible interconnected pore systems.[60]

3D plotting is a layer-by-layer additive manufacturing technique, based on computer aided design (CAD) and manufacturing (CAM). A single layer of the scaffold is obtained by depositing an extruded filament of a thermoplastic polymer melt according to the pattern described by the positioning system. This is repeated for all subsequent layers of the scaffold until the 3D geometry is completed. Because 3D plotting can produce scaffolds with complex structures, this system is particularly interesting for bone tissue engineering as the scaffold can be fabricated to perfectly fit the bone defect.[67]

3D scaffolds are composed of filaments of which the diameter can be between 100-500 µm and possess a porous structure large enough for the migration of cells through the construct, enabling *in vitro* cell adhesion and proliferation throughout the whole scaffold. However, it is reported that cells attached to different filaments are hardly able to interact due to the large interfilament distance of a couple of hundred micrometers, causing limited bridging between cells.[68]

Bridge forming between the filaments may be improved by laying down a fine network of randomly orientated nanofibers on the filaments, creating a hybrid scaffold. Such a fine

nanofiber network can be fabricated by means of the electrospinning process where electrostatic forces are used to produce fine fibers from polymer solutions or melts. Electrospun fibers have a diameter ranging from less than 100 nm to 10 µm and resulting fiber meshes have a high and interconnected porosity with a large surface-to-volume ratio. Due to their large surface area electrospun nanofiber meshes contain a high amount of binding sites for proteins that modulate cell adhesion. Hence, the nanofeatures of the scaffold enhance cell adhesion, viability, proliferation and differentiation.[15] Their pore dimensions from nanometers up to a few micrometers, allows a cell to adhere on multiple fibers simultaneously. However, *in vitro* studies on nanofiber meshes demonstrated the formation of only a monolayer of cells and cell infiltration in the meshes was limited due to the small pore size. In order to enable cell infiltration, only a very thin network consisting of a few layers of nanofibers should be spun over the 3D scaffolds. Several studies demonstrated that such hybrid polyester scaffolds improved adhesion, proliferation and spreading of chondrocytes[130,135,262], MSCs[262] and pre-osteoblastic cells[131] compared to scaffolds built up by either nanofibers or microfibers individually. The interaction between the cells and the hybrid scaffold were improved as the cells were able to colonize the interfilament gap due to the presence of a nanofibrous layer between the microfibers. The hybrid scaffolds also showed a higher amount of cells distributed throughout the scaffold. Hence, the combination of nanofibers and microfibers is a promising approach in which the microfibrous structure provides the porous 3D structural environment with mechanical integrity while the nanofibers provide the favorable surface topography with nanoscale features for cell attachment.[90,130,131,133,135,262]

PCL is one of the most commonly used polyesters for the fabrication of bone tissue engineering scaffolds due to its lack of toxicity, low cost and slow degradation profile.[239] Due to its melting point of 60°C and high decomposition temperature of 350°C, PCL is most suitable for thermoplastic processing.[237] In addition, because of the excellent solubility in a number of organic solvents, PCL is easily processable by electrospinning.[108] Consequently, the bone tissue engineering scaffold potential of nanofibrous[263], microfibrous[68] and nano-/microfibrous PCL scaffolds[135], fabricated by respectively electrospinning, 3D plotting and a combination of both, has been investigated.

A disadvantage in the use of polyesters scaffolds is their poor mechanical strength and hydrophobic nature.[178,240] The latter hinders the initial biological responses, such as protein adsorption, making it difficult for the cells to adhere to their surfaces.[238] In order to improve surface properties of PCL scaffolds, some authors report the surface coating with a bone-like apatitic mineral. PCL scaffolds fabricated through electrospinning[69,120] and 3D plotting[85] were successfully coated with a surface calcium phosphate (CP) layer. The mineralized scaffolds

showed improved cell attachment and proliferation and augmented mechanical strength compared to pure PCL scaffolds.[69,120,145,151,178] In this paper, a microfibrous/nanofibrous hybrid PCL scaffold is fabricated using 3D plotting and electrospinning. In order to improve the scaffold's potential use in bone tissue engineering a mineralization procedure is applied. Because the mineral phase of bone tissue is a low crystalline carbonate substituted apatite with a carbonate content of 3.2 – 13 wt%, the PCL scaffold should ideally be coated with a bonelike carbonated apatite. Such a 3D scaffold with nanofibrous features and bioactive apatite coating provides a 3D environment to support cell ingrowth as well as functionality related to the surface affinity for enhanced cell attachment and growth. The pure microfiber 3D plotted PCL scaffold, the hybrid PCL scaffold and the CP coated scaffolds were compared in terms of surface morphology, cell-attachment and cell in-growth.

4.2 Materials and Methods

4.2.1 Materials

Freshly prepared demineralized water (Milli-Q system, Millipore, Billerica, US) was used for the preparation of the solutions. PCL pellets for the electrospinning scaffold were purchased from Sigma-Aldrich (St. Louis, US) and for the 3D plotting PCL was purchased from Perstorp (Malmö, Sweden). Sodium chloride (NaCl), ethanol (technical grade, 95 vol.%), sodium hydroxide solution (NaOH; 1 M), tris-(hydroxymethyl) aminomethane (TRIS) and acetone were obtained from VWR BDH Prolabo (Leuven, Belgium). Sodium bicarbonate ($NaHCO_3$), disodium phosphate (Na_2HPO_4), potassium phosphate dibasic (K_2HPO_4), magnesium chloride ($MgCl_2.6H_2O$), hydrochloride (HCl; 37 vol.%), sodium sulfate (Na_2SO_4) and chloroform were purchased from Merck (Darmstadt, Germany) and potassium chloride (KCl) and calcium chloride ($CaCl_2.2H_2O$) from J.T. Baker (Deventer, The Netherlands).

4.2.2 Fabrication of a hybrid nano-/microscale scaffold

4.2.2.1 Production of 3D microfibrous scaffolds by 3D plotting

The 3D PCL scaffolds were manufactured by 3D plotting on a BioScaffolder machine (SysEng, Singapore) as described by Ragaert *et al.*.[237] The BioScaffolder is composed of a screw extrusion head equipped with a micronozzle (gauge 27, inner diameter 200 µm) to produce a polymer melt filament. The polymer was molten at 100°C and deposited on a plotting table at room temperature. Spindle speed of the extrusion screw was constant at 15 rpm. The consecutive layers were deposited with a relative layer orientation of 45°. For the present study four layered scaffolds of 1x1cm^2 were produced, thus with an overall pattern of 0°/45°/90°/-45°.

4.2.2.2 Deposition of electrospun fibers onto 3D plotted scaffolds

The electrospinning of PCL is described in detail by Van der Schueren *et al*..[21] Briefly, a 14 wt% PCL solution was made by dissolving PCL pellets in the binary solvent system 90 % formic acid/10 % acetic acid (both Sigma-Aldrich). The polymer solution was then loaded into a syringe (Becton Dickinson, Franklin Lakes, US) and a high voltage electric field of 18 kV (Glassman High Voltage Series EH Source, High Bridge, US) was applied to draw the fibers from the spinneret (gauge 17 needle) onto the collector plate. A constant feed rate of 1 ml/h was applied using a syringe pump (KD Scientific, Syringe Pump Series 100, Holliston, US) and a distance of 12 cm was maintained between the tip of the spinneret and the collector plate. The 3D plotted PCL scaffolds were placed on the collector plate. Fibers were deposited for 1 second on each site of the scaffold in order to coat the complete scaffold surface with a thin layer of electrospun fibers.

4.2.3 Coating of the scaffolds

4.2.3.1 Activation step

For the activation of the hybrid scaffolds the optimized activation procedure of Luickx *et al*.[69] was slightly adjusted. Samples were immersed at room temperature in 10 mL/cm² ethanol for 1 minute and washed for 5 minutes in demineralized water. Next, samples are immersed in a 1 M NaOH solution for 40 minutes under ultrasonic conditions and washed for 5 minutes in demineralized water.

4.2.3.2 Nucleation step

Deposition of a thin primer layer of CP nucleates was achieved by an alternate dipping process in $CaCl_2.2H_2O$ and Na_2HPO_4 solutions in which the parameters of the previously optimized nucleation procedure were used.[69] Samples were first immersed in 100 mL of 32.30 mM $CaCl_2.2H_2O$ for 70 seconds, washed for 30 seconds with demineralized water, next the samples were immersed in 100 ml of 35.98 mM Na_2HPO_4 solution for 45 seconds and washed for 30 seconds in demineralized water. During sample immersion the solutions were stirred at 250 rpm. This cycle of four steps was repeated seven times.

4.2.3.3 Maturation step

In order to coat the samples with an apatite layer with varying carbonate content, the samples were further subjected to an incubation in 20 ml of two different SBF-based solutions for up to 24h at 37°C under dynamic conditions (50 rpm). For coating with an apatite with low carbonate content the samples were incubated for 24h in a two times concentrated SBF solution (2xSBF). For coating with an apatite layer with higher carbonate content the samples were incubated for 15h in an experimental SBF solution with a high carbonate ion concentration and without magnesium ions (63C0Mg). The ion concentrations

of the 2xSBF solution and the experimental SBF solution are shown in table 1. The 2xSBF and the 63C0Mg solution were prepared by mixing concentrated ion solutions. The recipes for preparation are shown in table 2. After incubation in the SBF solutions, the samples were dried at room temperature.

Table 1. Ion concentrations and pH of human blood plasma (HBP), original SBF, 2xSBF and 63C0Mg.

	Ion concentration (mM)								
	Na^+	**K^+**	**Mg^{2+}**	**Ca^{2+}**	**Cl^-**	**HCO_3^-**	**HPO_4^{2-}**	**SO_4^{2-}**	**pH**
HBP	142	5	1.5	2.5	103	27	1	0.5	7.4
Original SBF	142	5	1.5	2.5	147.8	4.2	1	0.5	7.4
2xSBF	282	10	3	5	295	8.3	2	1	7.75
63C0Mg	284	10	0	5	235	63	2	1	7.65

Table 2. Concentrations, order and volume of concentrated ion solutions for preparing 1000 ml of 2xSBF.

Ion solution	Concentration (mM)	Order	Volume (ml) 2xSBF	Volume (ml) 63C0Mg
NaCl	1000	1	274	215
KCl	100	2	100	100
Na_2HPO_4	20	3	100	100
$MgCl_2.6H_2O$	30	4	100	-
$NaHCO_3$	84	5	100	-
HCl	1000	6	40	*Adjust to pH 5±0.1*
$CaCl_2.2H_2O$	50	7	100	100
Na_2SO_4	10	8	100	100
TRIS-buffer	500	9	100	-
HCl	1000	10	*Adjust to pH 7.75 ± 0.05*	-
				Add 5.275 g $NaHCO_3$ powder

4.2.4 Characterization of the scaffolds

The morphology of the scaffolds, before and after mineralization, was characterized using a Keyence 3D microscope (VHX-500F; Elmwood Park, US) and a scanning electron microscope (SEM; FEI Quanta 200 F, Hillsboro, US). Prior to SEM measurements, the samples were coated with gold using a sputter coater (Balzers Union Highland Scientific SCD 030, Bedford, UK). Image analysis software (SigmaScan Pro 5, SPSS Science, Chicago, US) was used to determine the average filament diameter (FD) and strand distance (SD). For each parameter, measurements of five random locations on the scaffold were averaged.

The homogeneity of the CP coating and the reproducibility of the procedure was evaluated using ARS calcium staining. Following the removal of most of the polymer by dissolution, the type of calcium phosphate deposited was identified by infrared (IR)

spectrometry. Samples were immersed in 1 ml chloroform for 10 minutes. After centrifugation (2 minutes; 7000 rpm) the supernatant solution was removed. This step was repeated once. The remaining pellet was washed with 1ml acetone followed by centrifugation (2 minutes; 7000 rpm) and removal of the supernatant. This washing-step was repeated once, the remaining powder was dried overnight. IR spectra of the CP powder dispersed in KBr tablets were recorded using a Fourier-transform IR (FT-IR) spectrophotometer (Perkin Elmer Instruments, Waltham, US). The carbonate content of the precipitates was determined by gas chromatography (Model 8500, Perkin Elmer Instruments) based on the method of Godinot *et al*..[247] As such, a calculated amount of precipitate was dissolved by adding 10% H_3PO_4 (Merck) in a closed vial. The incorporated carbonate in the specimens is released as CO_2 which is injected in the gas chromatograph. Florida Rock with 3.81 wt% carbonate was used as standard to obtain the calibration curve.

4.2.5 Cell culture and seeding

Monolayers of MC3T3-E1 pre-osteoblasts (mouse calvaria pre-osteoblast cells, ATCC) were cultured in α-minimum essential medium (α-MEM) (glutaMAX-1™, Gibco Invitrogen, Ghent, Belgium) supplemented with 10% fetal bovine serum (FBS) (heat inactivated, EC approved, Gibco Invitrogen) and 1 mM sodium pyruvate (Gibco Invitrogen) at 37°C in 95% air/5% CO_2. The medium was changed twice a week.

Untreated 3D plotted PCL samples and hybrid PCL samples were used as control. Calcium phosphate coated and untreated samples were sterilized under UV-light for 30 minutes. After sterilization the samples were placed in 48-well tissue culture dishes (suspension culture plates, Greiner Bio-One, Frickenhausen, Wemmel, Belgium). To each sample 40,000 MC3T3-E1 cells, in droplet, were added, for the PrestoBlue™-assay (Invitrogen). For the live/dead staining and the histology, 300,000 cells, diluted in 500 µl culture medium, were added to each sample. For the PrestoBlue™-assay and the live/dead staining, either 40,000 or 300,000 MC3T3-E1 cells, in droplet or diluted in 500 µl culture medium, respectively, were added to an adhesion plate (Nunc, Life Technologies, Merelbeke, Belgium) as positive control. The cell/scaffold constructs and the positive controls were cultured for 14 days (5%CO_2/95% air, 37°C) with the medium changed twice a week.

4.2.6 Characterization of cell/scaffold constructs

4.2.6.1 Cell viability and morphology

The PrestoBlue™-assay was applied to quantify the number of viable cells that attached on the calcium phosphate coated and untreated samples after 1, 7 and 14 days of culture. The PrestoBlue™-reagent is a blue resazurin-based non-fluorescent solution.

Resazurin enters the cells where it is transformed to the red and fluorescent resorufin by the reducing power of the mitochondria.

The samples and the control were rinsed with culture medium after which 450 µl culture medium and 50 µl PrestoBlue™-reagent was added to each well. After 2 h incubation at 37 °C in a dark room, 400 µl medium was transferred to a 24-well dish (Greiner Bio-One). The fluorescence of the medium was measured in a multilabel plate reader (Victor³, Perkin-Elmer) (excitation: 560 nm, emission: 590 nm). The number of viable and attached cells is linearly correlated with the signal, and viability was calculated as a percentage of the positive control of the respective day.

Cell viability and morphology after 1, 7 and 14 days on the calcium phosphate coated and untreated samples was visualized using fluorescence microscopy after performing live/dead staining with calcein acetoxymethyl (AM) ester (Tebu-Bio, Boechout, Belgium) and propidium iodide (PI) (Sigma-Aldrich). PI cannot pass through intact cell membranes, but may freely enter dead cells with compromised cell membranes where PI intercalates into double-stranded DNA and emits red fluorescence (excitation: 488 nm, emission: 617 nm). Calcein AM is a non-fluorescent, membrane-permeable dye. Under intracellular esterase activity the dye converts to a membrane-impermeable, green fluorescent compound (excitation: 490 nm, emission: 520 nm). After 1, 7 and 14 days the samples and positive controls were rinsed with 500 µl phosphate buffered saline (PBS) after which 500 µl PBS containing 1 µl PI and 1 µl calcein AM was added to each well. After 10 minutes incubation in a dark room at room temperature, samples were evaluated with a fluorescence microscope (Olympus Type U-RFL-T, Aartselaar, Belgium).

Each material and the controls were tested in triplicate.

4.2.6.2 Histology

Cell/scaffold constructs were rinsed with Ringer solution, fixed with 4% phosphate-buffered (10 mM) formaldehyde (pH 6.9; 4°C; 24h), dehydrated in a graded alcohol series and embedded in paraffin. 5-7 µm sections were cut and stained with hematoxylin and eosin (H&E).

4.3 Results

4.3.1 Fabrication of the scaffolds

The 1x1cm² 3D plotted PCL scaffolds had a thickness of 626 µm with a standard deviation (SD) of 11 µm. Digital and SEM images of the samples are shown in figure 1A and 1B, respectively. The average filament diameter was 191.67 µm with a SD of 6.60 µm, the average strand distance was 322.18 µm with a SD of 35.99 µm. The resulting pore diameter was 119.88 µm with a SD of 31.25 µm.

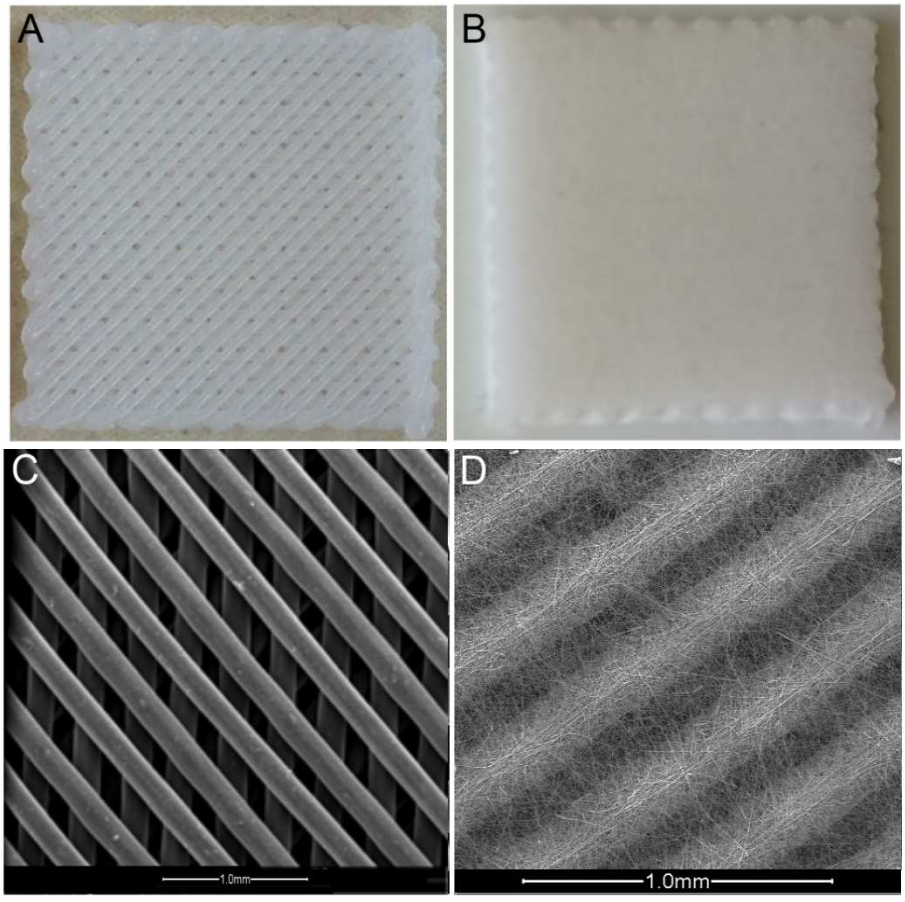

Figure 1: Digital and SEM images of the (A, B) 3D plotted and (C, D) hybrid PCL scaffolds.

Figure 1C and 1D shows the digital image and the SEM image of the hybrid scaffold with the PCL nanofibers collected onto the 3D plotted PCL scaffold. The scaffolds with dimensions of 1x1 cm² had an average thickness is 627 µm with a SD of 8 µm. The deposited PCL nanofibers had an average fiber diameter of 331.37 nm with a SD of 76.39 nm.

4.3.2 Coating of the hybrid scaffolds

4.3.2.1 Pre-mineralization treatment

SEM images of the hybrid PCL scaffold after treatment with the activation and nucleation procedure are shown in figure 2A and 2B, respectively. The samples showed no changes in the micro- and nanostructure, nor in the overall scaffold morphology after immersion in ethanol and NaOH solutions. After subsequent alternate dipping in Ca^{2+} and PO_4^{3-}- rich solutions, mineral crystals could be observed on the fiber surface of the nanofibers situated on top of the microfiber strands. No deposits were visible on the nanofibers bridging over neighboring microfibers in the hybrid scaffold, nor on the microfibers in the 3D PCL scaffold (figure 2A). The presence of CP deposits on the hybrid scaffolds was confirmed by the red color of the samples after ARS staining (figure 2D).

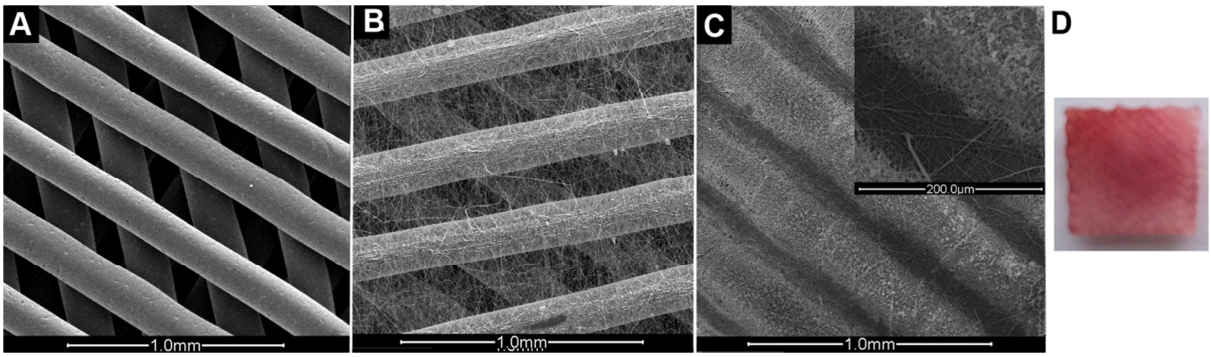

Figure 2: SEM images of (A) 3D plotted PCL samples after treatment with the activation and nucleation procedure, (B) hybrid PCL samples after treatment with the activation procedure and (C) after subsequent treatment with the nucleation procedure. (D) Digital image of ARS stained samples after treatment with the activation and nucleation procedure.

4.3.2.2 Maturation

SEM images of the hybrid scaffolds after subsequent incubation for 24h in 2xSBF and for 15h in the 63C0Mg solution at 37°C are shown in figure 3A-B and 3C-D, respectively. The SEM images showed that a calcium phosphate coating covered the surface of the electrospun fibers. After 24h of incubation in 2xSBF the calcium phosphate deposition was more massive, but still the porous structure of the scaffold was more or less preserved.

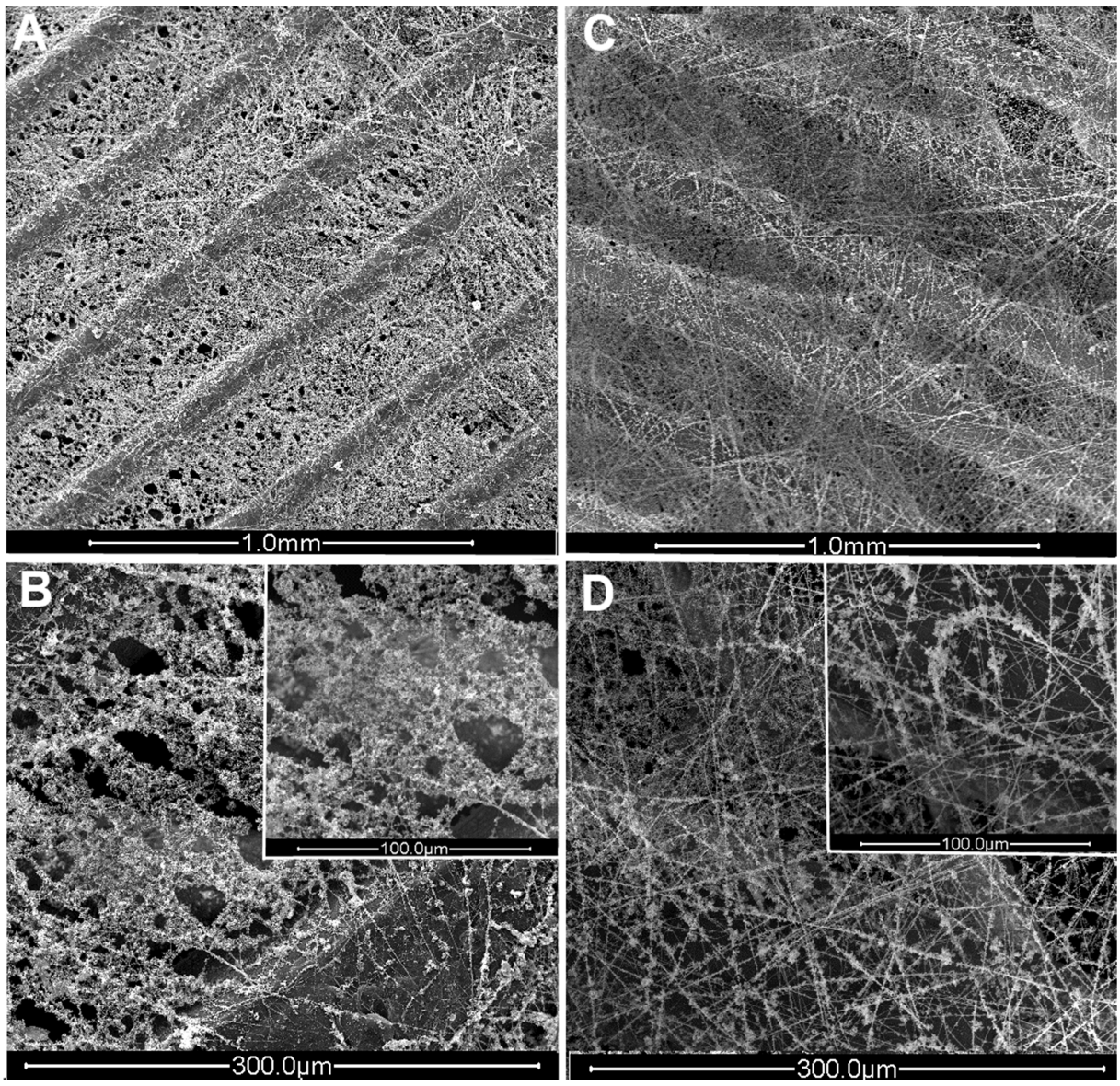

Figure 3: SEM images of hybrid scaffolds after (A,B) 24h incubation in 2xSBF and (C,D) 15h incubation in 63C0Mg, at 37°C.

4.3.2.3 Analysis of the coating

The FTIR spectrum of the calcium phosphate coating deposited on the samples after 24h incubation in 2xSBF and 15h in 63C0Mg is shown in Figure 4.

Incubation of the samples in these solutions resulted in the deposition of a carbonated apatite. The spectrum of the coating formed during incubation in 63C0Mg shows peaks due to the v_4-PO_4^{3-} bending around 603 to 569 cm^{-1} and the v_3 stretching of PO_4^{3-} groups around 1045 and 1100 cm^{-1}. These are typical peaks of a hydroxyapatite phase. The peak around 1620 cm^{-1} arises from the H – O – H deformations in water. Typical peaks in the IR spectra at 880, 1420 and 1460 cm^{-1} indicate the presence of CO_3^{2-} that substitutes for PO_4^{3-} in the apatite lattice (B-type substitution). The spectrum of the sample after incubation in 2xSBF

shows, besides the typical peaks of B-type hydroxyapatite, additional bands around 1545 cm^{-1} and 1480 cm^{-1}. The latter indicates that some CO_3^{2-} substitutes for OH^- in the apatite lattice (A-type substitution).

Evidently, the intensity of the peaks arising from CO_3^{2-} increase with increasing carbonate content in the calcium phosphates. The intensity of the peaks attributed to the presence of CO_3^{2-} are higher in the spectrum of the precipitates formed in the 63C0Mg solution compared to the ones found in the spectrum of the precipitates formed in the 2xSBF solution. This is in line with the carbonate content of these precipitates that amounts to 8.2 wt% and 4.6 wt%, respectively.

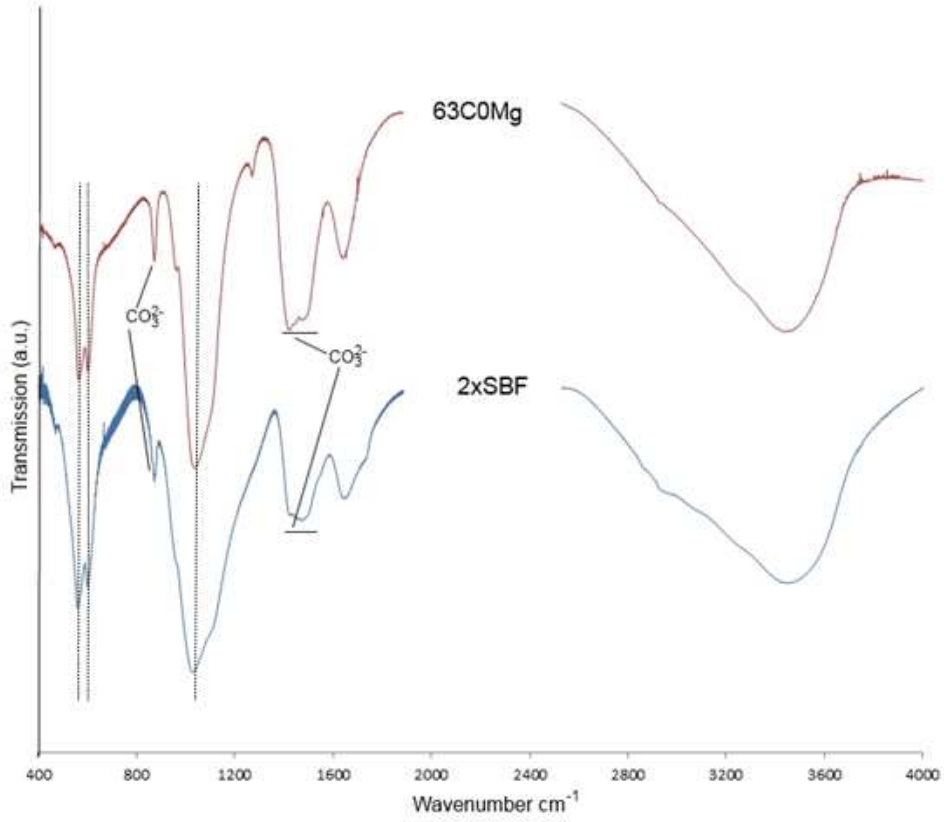

Figure 4: Infrared spectra of the calcium coating formed on the samples after 24h incubation in 2xSBF and 15h in 63C0Mg. Annotations mark CO_3^{2-} absorptions. The dotted lines mark some typical peaks of hydroxyapatite.

4.3.3 Cell culture tests

The quantity of viable and attached MC3T3-E1 cells on the untreated and the calcium phosphate coated PCL samples was determined after 1, 7 and 14 days of incubation, as presented in figure 5.

In comparison to that of the positive control, the attachment of the cells on the scaffolds was low. Although no statistical significant difference could be found, the amount of cells was lower on the untreated 3D plotted scaffolds than on the multiscale scaffolds at any given time

point. The amount of viable cells was also systematically higher on the calcium phosphate coated scaffolds compared to the untreated samples. The best results in terms of cell viability and proliferation were obtained for the hybrid scaffolds coated with a high carbonate content. Only for these scaffolds the amount of viable cells significantly increased after 14 days, compared to 1 and 7 days ($p \leq 0.037$).

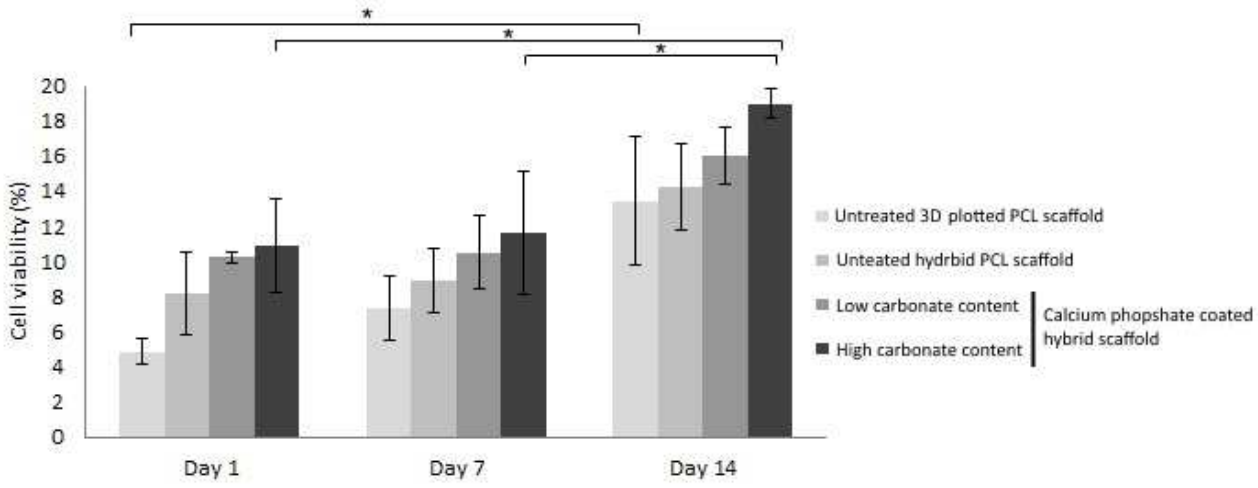

Figure 5: Cell viability of MC3T3-E1 cells on untreated 3D plotted PCL scaffolds, untreated hybrid PCL scaffolds and hybrid PCL scaffolds coated with HAp with a low and high carbonate content after 1, 7 and 14 days of incubation. The amount of attached cells was quantified by a PrestoBlue assay. The cell viability was calculated as percentage of the positive control after 14 days. Statistical differences ($p \leq 0.05$) in the cell viability are annotated with *. Error bars represent standard deviations.

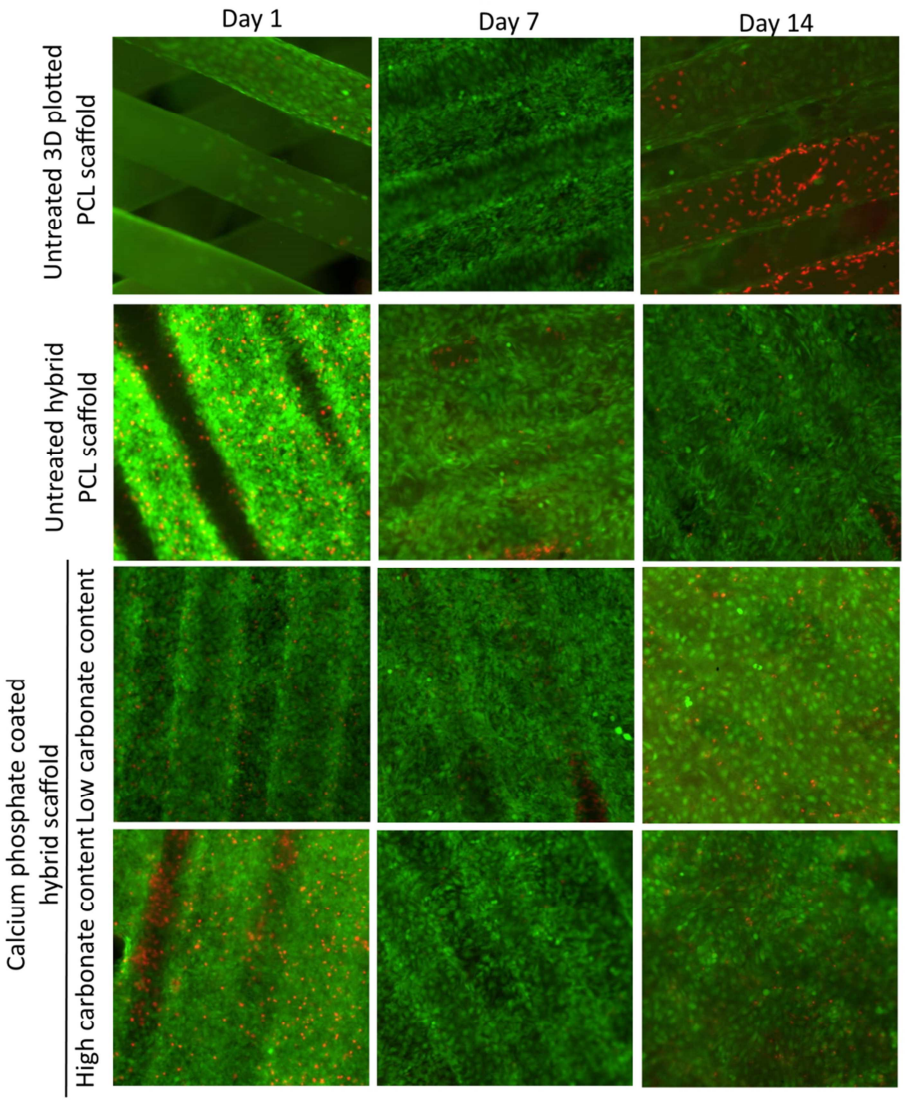

Figure 6: Fluorescence micrographs after live/dead staining of MC3T3-E1 cells cultured on untreated 3D plotted PCL scaffolds, untreated hybrid PCL scaffolds, hybrid PCL scaffolds coated with a calcium phosphate with low carbonate content and hybrid PCL scaffolds coated with a calcium phosphate with high carbonate content after 1, 7 and 14 days of culture.

The MC3T3 cell viability and morphology on the four scaffolds after 1, 7 and 14 days is shown in figure 6. For the untreated 3D plotted scaffolds, only some of the filaments were covered with cells after 1 day of culture, whereas after 7 days of culture all filaments were fully covered with cells. After 14 days of culture, a lot of dead cells were visible on the filaments. For the untreated multiscale scaffold the cells preferred to colonize the surface covering the microfilaments. After 7 days of culture the cells formed a monolayer covering the complete surface of the scaffold. Whereas on the calcium phosphate coated scaffolds, a monolayer of cells formed as of 1 day of culture. The majority of the cells continued to remain viable after 2 weeks.

Multiscale PCL scaffold

Cross-sections of the cell/scaffold constructs after H&E staining showed a similar cell infiltration into the scaffolds after an incubation period of 14 days (Figure 7). All scaffolds showed colonization in the center of the scaffold. This indicates that even for the calcium phosphate coated multiscale scaffolds, the cells were able to infiltrate the electrospun mesh that covered the 3D plotted scaffolds. On these calcium phosphate coated scaffolds a high concentration of cells was also present on both sides of the electrospun mesh.

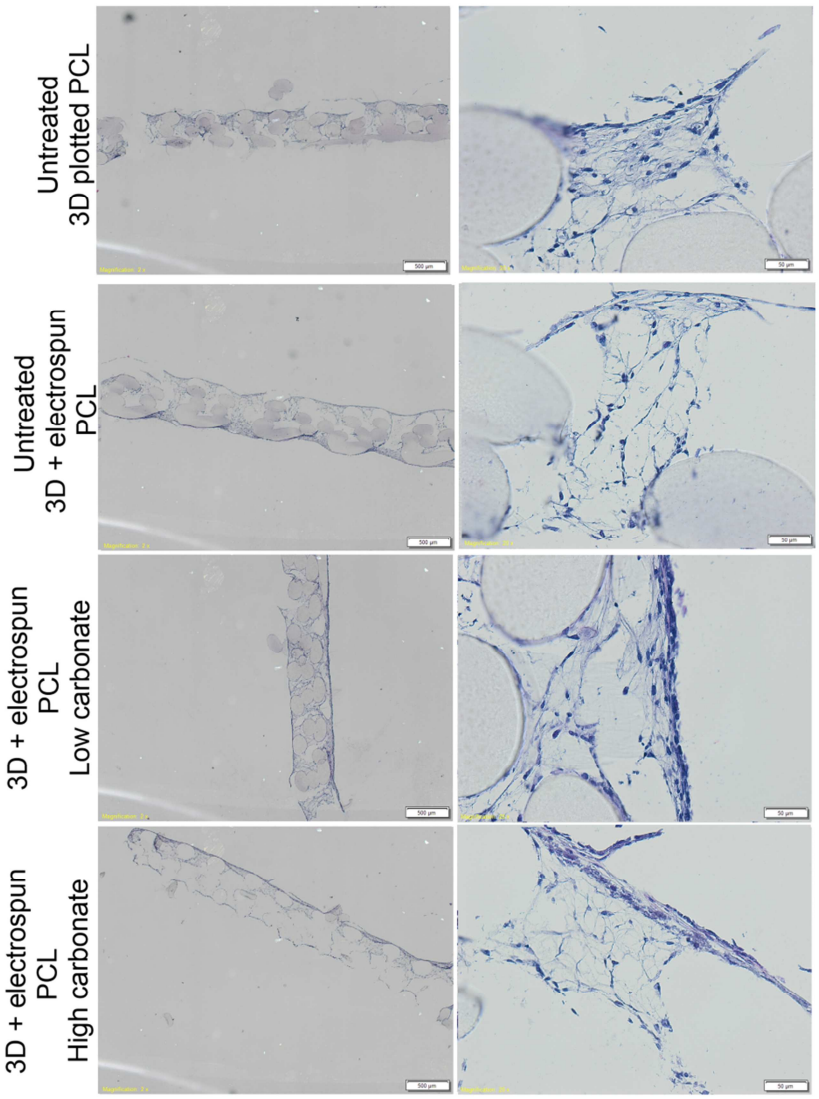

Figure 7: Colonization of the scaffolds after 14 days of incubation. Cross-sections were stained with hematoxylin and eosin (H&E).

4.4 Discussion

4.4.1 Fabrication of a hybrid nano-/microscale scaffold

Multiscale PCL scaffolds were successfully fabricated by combining 3D plotting and electrospinning. The fabrication of the constituting single scale micro – and nanofibrous PCL scaffolds was previously optimized by Ragaert *et al*.[237] and Van der Schueren *et al.*[114], respectively. For the present research, 3D plotted scaffolds with a 0°/45°/90°/-45° architecture, a pore diameter of 120 µm and a filament diameter of approximately 190 µm were fabricated. Scaffolds with such compact architectures showed an enhanced cell seeding efficiency and subsequent differentiation of pre-osteoblastic cells compared to scaffolds with larger pores.[205] During 1 second, an electrospun nanofibrous mesh with fiber diameters of approximately 330 nm was deposited on top of the 3D plotted scaffolds, on both sides. Thickness and coverage of the nanofibrous layer could be controlled by modulating the electrospinnning time. Hence, in the present study the electrospinning time was kept as short as possible in order to deposit a thin nanofibrous mesh without closing off the pores of the 3D plotted scaffolds too much.

The limitation of the current fabrication procedure is that the electrospinning apparatus and the BioScaffolder are two individual devices. An interesting possibility is the integration of the two techniques in a single device. With such a device it would be possible to fabricate scaffold with alternating layers of nanofibers and microfibers. Moreover, the architecture of the scaffold could be more easily tuned during fabrication to obtain a construct of desired morphology and characteristics.

4.4.2 Coating of the scaffolds

For the activation of the multiscale scaffolds the optimized protocol for the activation of electrospun PCL samples was slightly adopted; in order to ensure sufficient wetting the samples were immersed for 1 minute in ethanol. This longer treatment did not affect the morphology of the electrospun fibers (figure 1B). Upon subsequent treatment with the optimized nucleation procedure for electrospun PCL, calcium phosphate nucleates were successfully deposited on the multiscale scaffold. SEM imaging revealed that the calcium phosphate deposited was only present on the nanofibers situated on top of the microfibers.

Incubation of the samples for 24h in 2xSBF and for 15h in 63C0Mg enabled the deposition of hydroxyapatite with a carbonate content of 4.6 and 8.2 wt% respectively. Although the porous structure of the scaffolds was still visible, the coating clearly caused a decrease of the pore diameters.

The carbonate content of the coating obtained by incubation in 63C0Mg was not as high as was expected based on the high carbonate concentration of the SBF-based solution and previous experiments with 3D plotted PCL scaffolds. It can be expected that during prolonged incubation in 63C0Mg, more carbonate would incorporate in the hydroxyapatite lattice. As during longer incubation the calcium phosphate layer also grows further, the incubation period of the current multiscale scaffolds was limited and could not be extended without causing obstruction of the pores.

4.4.3 Cell response

It is well known that micro-or nanotopographical features on the surface of biomaterials can control cellular behaviors such as adhesion, spreading, migration, proliferation and differentiation to a large extent.[135]

As shown in figure 6, for the single scale untreated 3D plotted scaffold the initial cell adhesion was low, which could be expected due to hydrophobic nature of PCL that hinders the adsorption of proteins. After 7 days of culture a higher amount of cells were adhered to the filaments. The cells are however confined to a single filament due to the absence of bridging across microfibers that are too far apart (Figure 6).

Compared to the untreated single scale scaffold, more cells were able to adhere to the untreated multiscale scaffold after 1 day of culture. It was indeed expected that the presence of randomly oriented fibers with nanoscale features would enhance initial cell adhesion and response.[90] After 7 days of culture the cells were directed to bridge between the microfibers which resulted in the formation of a confluent monolayer of cells after 14 days of culture. So even without a calcium phosphate coating, multiscale scaffolds showed an enhanced cell response compared to single scale 3D plotted PCL scaffolds. The positive effect of the addition of nanofibers was confirmed in other studies.[90,136,264]

For the multiscale PCL scaffolds coated with a hydroxyapatite layer with low and high carbonate a further enhancement of cell response was observed, with the highest amount of cell adhesion on the scaffolds coated with the high amount of carbonate. (Figure 5 and 6).

Although a monolayer of cells was formed on the exterior electrospun mesh, figure 7 shows that the cells were able to infiltrate into the interior of the scaffolds. This suggests that as the electrospun mesh was very thin, the attached cells have the ability to push against the nanofibers and migrate into the matrix.

4.5 Conclusion

In order to combine the properties of both microfibers (pores large enough for cell migration) and nanofibers (physical mimicry of native ECM), multiscale scaffolds were fabricated. MCT3T3-E1 cells attached well on the multiscale scaffold, and an enhanced cell response was obtained when the multiscale scaffolds were coated with a carbonated hydroxyapatite layer. The developed structures are believed to have great potential for the 3D organization and guidance of cells that are important for engineering 3D bone tissue. The multiscale scaffolds promote cellular adhesion and growth.

4.6 References

1. Hutmacher DW. Scaffolds in tissue engineering bone and cartilage. Biomaterials 2000;21(24):2529-2543.
2. Stevens MM. Biomaterials for bone tissue engineering. Materials Today 2008;11(5):18-25.
3. Holzwarth JM, Ma PX. Biomimetic nanofibrous scaffolds for bone tissue engineering. Biomaterials 2011;32(36):9622-9629.
4. Loh QL, Choong C. Three-Dimensional Scaffolds for Tissue Engineering Applications: Role of Porosity and Pore Size. Tissue Engineering Part B-Reviews 2013;19(6):485-502.
5. Jang JH, Castano O, Kim HW. Electrospun materials as potential platforms for bone tissue engineering. Advanced Drug Delivery Reviews 2009;61(12):1065-1083.
6. Liu XH, Ma PX. Polymeric scaffolds for bone tissue engineering. Annals of Biomedical Engineering 2004;32(3):477-486.
7. Nair LS, Laurencin CT. Biodegradable polymers as biomaterials. Progress in Polymer Science 2007;32(8-9):762-798.
8. Yilgor P, Sousa RA, Reis RL, Hasirci N, Hasirci V. 3D plotted PCL scaffolds for stem cell based bone tissue engineering. Macromolecular Symposia 2008;269:92-99.
9. Arafat MT, Gibson I, Li X. State of the art and future direction of additive manufactured scaffolds-based bone tissue engineering. Rapid Prototyping Journal 2014;20(1):13-26.
10. Ragaert K, Cardon L, Dekeyser A, Degrieck J. Machine design and processing considerations for the 3D plotting of thermoplastic scaffolds. Biofabrication 2010;2(1).
11. Zein I, Hutmacher DW, Tan KC, Teoh SH. Fused deposition modeling of novel scaffold architectures for tissue engineering applications. Biomaterials 2002;23(4):1169-1185.
12. Hutmacher DW, Schantz T, Zein I, Ng KW, Teoh SH, Tan KC. Mechanical properties and cell cultural response of polycaprolactone scaffolds designed and fabricated via fused deposition modeling. Journal of Biomedical Materials Research 2001;55(2):203-216.
13. Kim G, Son J, Park S, Kim W. Hybrid Process for Fabricating 3D Hierarchical Scaffolds Combining Rapid Prototyping and Electrospinning. Macromolecular Rapid Communications 2008;29(19):1577-1581.
14. Moroni L, Schotel R, Hamann D, de Wijn JR, van Blitterswijk CA. 3D fiber-deposited electrospun integrated scaffolds enhance cartilage tissue formation. Advanced Functional Materials 2008;18(1):53-60.
15. Park SH, Kim TG, Kim HC, Yang D-Y, Park TG. Development of dual scale scaffolds via direct polymer melt deposition and electrospinning for applications in tissue regeneration. Acta Biomaterialia 2008;4(5):1198-1207.
16. Mota C, Puppi D, Dinucci D, Errico C, Bartolo P, Chiellini F. Dual-Scale Polymeric Constructs as Scaffolds for Tissue Engineering. Materials 2011;4(3):527-542.

17. Centola M, Rainer A, Spadaccio C, De Porcellinis S, Genovese JA, Trombetta M. Combining electrospinning and fused deposition modeling for the fabrication of a hybrid vascular graft. Biofabrication 2010;2(1).
18. Srinivasan S, Jayakumar R, Chennazhi KP, Levorson EJ, Mikos AG, Nair SV. Multiscale Fibrous Scaffolds in Regenerative Medicine. In: Jayakumar R, Nair SV, editors. Biomedical Applications of Polymeric Nanofibers; 2012. p 1-20.
19. Woodruff MA, Hutmacher DW. The return of a forgotten polymer-Polycaprolactone in the 21st century. Progress in Polymer Science 2010;35(10):1217-1256.
20. Ragaert K, De Somer F, De Baere I, Cardon L, Degrieck L. Production and evalution of PCL scaffolds for tissue engineering heart valves. Advanced in Production Engineering & Management 2011;6(3):163-172.
21. Cipitria A, Skelton A, Dargaville TR, Dalton PD, Hutmacher DW. Design, fabrication and characterization of PCL electrospun scaffolds-a review. Journal of Materials Chemistry 2011;21(26):9419-9453.
22. Yoshimoto H, Shin YM, Terai H, Vacanti JP. A biodegradable nanofiber scaffold by electrospinning and its potential for bone tissue engineering. Biomaterials 2003;24(12):2077-2082.
23. Kretlow JD, Mikos AG. Review: Mineralization of synthetic polymer scaffolds for bone tissue engineering. Tissue Engineering 2007;13(5):927-938.
24. Xie J, Zhong S, Ma B, Shuler FD, Lim CT. Controlled biomineralization of electrospun poly(epsilon-caprolactone) fibers to enhance their mechanical properties. Acta Biomaterialia 2013;9(3):5698-5707.
25. Choi W-Y, Kim H-E, Koh Y-H. Production, mechanical properties and in vitro biocompatibility of highly aligned porous poly(epsilon-caprolactone) (PCL)/hydroxyapatite (HA) scaffolds. Journal of Porous Materials 2013;20(4):701-708.
26. Araujo JV, Martins A, Leonor IB, Pinho ED, Reis RL, Neves NM. Surface controlled biomimetic coating of polycaprolactone nanofiber meshes to be used as bone extracellular matrix analogues. Journal of Biomaterials Science-Polymer Edition 2008;19(10):1261-1278.
27. Luickx N, Van den Vreken N, D'Oosterlinck, Van den Schueren L, Declercq H, De Clerck K, Cornelissen R, Verbeeck R. Optimization of the activation and nucleation steps in the precipitation of a calcium phosphate primer layer on electrospun poly(ε-caprolactone). Journal of Biomedical Materials Research Part A 2015;103:511-524.
28. Park SA, Lee JB, Kim YE, Kim JE, Lee JH, Shin JW, Kwon IK, Kim W. Fabrication of biomimetic PCL scaffold using rapid prototyping for bone tissue engineering. Macromolecular Research 2014;22(8):882-887.
29. Choong C, Yuan S, Thian ES, Oyane A, Triffitt J. Optimization of poly(e-caprolactone) surface properties for apatite formation and improved osteogenic stimulation. Journal of Biomedical Materials Research Part A 2012;100A(2):353-361.
30. Bleek K, Taubert A. New developments in polymer-controlled, bioinspired calcium phosphate mineralization from aqueous solution. Acta Biomaterialia 2013;9(5):6283-6321.
31. Godinot C, Bonel G, Torres L, Mathieu J. Chromatographic assay of carbonates in the submilligram range - application to carbonate assy of calcified tissue.Microchemical Journal 1984;29(1):92-105.
32. Van der Schueren L, De Schoenmaker B, Kalaoglu OI, De Clerck K. An alternative solvent system for the steady state electrospinning of polycaprolactone. European Polymer Journal 2011;47(6):1256-1263.
33. Declercq HA, Desmet T, Berneel EEM, Dubruel P, Cornelissen MJ. Synergistic effect of surface modification and scaffold design of bioplotted 3-D poly-epsilon-caprolactone scaffolds in osteogenic tissue engineering. Acta Biomaterialia 2013;9(8):7699-7708.

34. Tuzlakoglu K, Bolgen N, Salgado AJ, Gomes ME, Piskin E, Reis RL. Nano- and micro-fiber combined scaffolds: A new architecture for bone tissue engineering. Journal of Materials Science-Materials in Medicine 2005;16(12):1099-1104.
35. Pham QP, Sharma U, Mikos AG. Electrospun poly(epsilon-caprolactone) microfiber and multilayer nanofiber/microfiber scaffolds: Characterization of scaffolds and measurement of cellular infiltration. Biomacromolecules 2006;7(10):2796-2805.

Chapter 4: General discussion and conclusion

Bone tissue has a high regenerative capacity and the normal physiologic reaction to fracture is the spontaneous sequence of events briefly summarized as initial inflammation, followed by soft callus formation, hard callus formation and ultimately bone remodeling. When this natural process does not occur, as in the case of large-scale bone injury caused by trauma, disease or surgical resection, surgical intervention is warranted. Different surgical strategies have been developed, of which BTE represents one promising strategy.

Scaffold-based BTE is a rapidly emerging field that focuses on developing biologically-based substitutes that integrate with and are eventually replaced by host bone. It involves the implantation of ECM analogues that can support cell function and provide structural support. The scaffold must exhibit a porous, interconnected, and permeable structure to permit infiltration of cells and nutrients and should exhibit the appropriate surface structure and chemistry for cell colonization, migration, proliferation and differentiation. Ideally, the scaffold should be made of a biodegradable material, whose degradation rate is coupled to the tissue formation dynamics. In this way the mechanical support of the scaffold would be progressively overtaken by the newly formed tissue. To date, no suitable scaffold has been developed for the repair and regeneration of bone tissue due to its complex composition, structure, mechanical and biological properties.

This thesis aimed to fabricate a biomimetic scaffold for BTE purposes. In order to mimic the natural composite structure of bone, the fabrication of biodegradable polyester coated with a thin layer of bone-like apatite was investigated.

1 Scaffold development

Material selection and processing method selection are two major and primary considerations in the development of an ideal BTE scaffold. The biocompatibility and the surface chemistry of the scaffold is determined by the scaffold material, whereas the (interconnected) porosity and the pore and overall scaffold architecture depend on the fabrication method. Both the scaffold architecture and scaffold chemistry can influence cellular response by means of osteoconductivity and osteoinductivity. The mechanical properties of the scaffold are determined by the type of biomaterial, but also by its structural properties (e.g. porosity, interconnectivity) when processed to create a scaffold.

General discussion and conclusion

1.1 Material selection

Among the multitude of choices of biomaterials, in this thesis, two biocompatible and biodegradable materials were selected due to their tailorable properties; PCL and PDLLA. Both polyester have an established use in clinical practice and differ in their degradation rate and mechanical properties. The semi-crystalline PCL has a long degradation time in the human body (> 24 months), whereas the amorphous PDLLA has a medium long degradation time (12-16 months). Both polyesters are already FDA approved for some specific applications in the human body such as for drug-delivery devices and sutures, which could ensure a smooth introduction to the market.[239] Other advantages of these polyesters are their good solubility, low economic cost, ease of shaping and processing to porous structures as those used in TE.

It should however be noted that some concerns exist about the use of PCL and PDLLA as materials for the fabrication of bone scaffolds. First, the slow degradation of PCL scaffolds. It has been found that a PCL system with a high molecular weight (Mn of 50,000) requires 3 years for complete removal from the host body. In addition, PCL has a significantly low mechanical strength due to the fact that PCL is in the rubbery state at body temperature (high elasticity).[96] As for PDLLA, the physical and some mechanical properties are often not good enough for end-use applications. Since polymers from lactic acids have glass transition temperature (T_g) above body temperature, these scaffolds are stiff with little elasticity in the body and are somewhat brittle at room temperature.[96] The brittleness of PDLLA is an important limitation in its applications in BTE. Both PCL and PDLLA have a good blend-compatibility and blending techniques are an extremely promising approach which can improve the original properties of both polymers.[265-267] Moreover, combining PDLLA and PCL in a certain ratio can result in composite scaffolds with appropriate degradation time.[266] Additionally, mineralization of both polyester scaffolds was also shown to improve the mechanical strength of the scaffolds.[106,157,240,268]

1.2 Processing method selection

In recent years, multiscale fibrous scaffolds containing a combination of micro-and nanoscale fibers have attracted a lot of attention in the TE field. Such scaffolds can be manufactured by combining 3D plotting and electrospinning. However, to date research on the fabrication of such multiscale polyester scaffolds is limited.

In order to investigate the mineralization of such multiscale scaffolds, it was first necessary to fabricate and optimize the mineralization procedure of the constituting elements, namely electrospun nanofibers and 3D plotted microfilaments.

General discussion and conclusion

Electrospinning is one of the most commonly employed techniques in TE for the generation of nanoscaled fibrous structures. The electrospun fibers are in the same scale as the ECM fibril network surrounding the cells in their natural environment, and, therefore, are considered to mimic the physical cues to which the cells are normally exposed. For the electrospun PCL and PDLLA scaffolds used in the present study, the electrospinning process was optimized in order to obtain beadles and randomly oriented nanofibers with small diameter distributions and high reproducibility (Chapter 3.1 Figure 1; Chapter 3.2 Figure 1). The average fiber diameter of the electrospun PCL scaffolds was 419 nm, whereas it was 1.55 µm for the electrospun PDLLA scaffolds. The difference in fiber diameter can be attributed to a difference in conductivity of the solutions used for electrospinning. As a higher voltage is required for steady state electrospinning of the PCL solution than the PDLLA solution, it can be assumed a solution of 14 wt% PCL dissolved in a 90% formic acid/10% acetic acid solvent system has a higher conductivity than a solution of 17 wt% PDLLA dissolved in a DMF/acetone (2/1) solvent system. The application of a higher voltage encourages the reduction of the fibers diameter due to increased stretching of the solution jet as a result of higher levels of charges carried by the solution.[64]

The microporous 3D scaffolds were produced with the 3D plotting technology, which provides an accurate control over internal scaffold micro-architecture and external shape. A serious limitation in the use of 3D plotting for the processing of biodegradable polyesters is the thermal vulnerability of some of the polyesters. When heated for an extended time above their melting temperature, chain scissions may occur, effectively degrading the material. Upon degradation the material flow changes, the scaffolds become more brittle and the geometrical characteristics differ for each scaffold. Thermal degradation of the scaffold material during the production process is also devastating to scaffold reproducibility with respect to mechanical properties. Polymers from lactic acid, such as PDLLA, are highly sensitive to this phenomena and in addition to their inherent brittleness, difficult to process by means of 3D plotting.[236] Even though Ragaert *et al*.[88,236] were able to fabricate 3D plotted PDLLA scaffolds, the structures were too brittle and difficult to handle as they broke easily into pieces. Consequently 3D plotted PDLLA scaffold could not be used for further experiments. Semi-crystalline polymers are more resilient against high temperatures than amorphous polymers, which explains the high thermal stability of PCL. In the present thesis 3D plotted PCL scaffolds with compact architectures, a 0°/45°/90°/-45° design and a pore size of 120 µm were successfully fabricated (Chapter 3.3). Declercq *et al*.[205] previously showed that scaffolds with such compact architecture showed higher seeding efficiency and differentiation compared to scaffolds with larger pores and open channel architectures.

The final objective of this study was set forth by completing an introductory study on the development of a multiscale scaffold. In chapter 3.4 the 3D plotting and electrospinning technique were integrated to create a PCL multiscale system in which the 3D plotted scaffold would give the stable support structure and pore organization for tissue development and the electrospun network would provide topological and physical cues for the cells.

2 Mineralization

As both PCL and PDLLA lack intrinsic bioactivity, much attention has been paid to the *in vitro* mineralization of these materials. For the coating of fibrous polyester scaffolds, in the present thesis a three-step mineralization procedure was applied (Figure 16). The first step involved the activation of the polyester surface, in the second step or nucleation step the samples were alternately dipped in calcium and phosphate rich solutions and finally the samples were incubated in a mineralization solution based on SBF (maturation step).

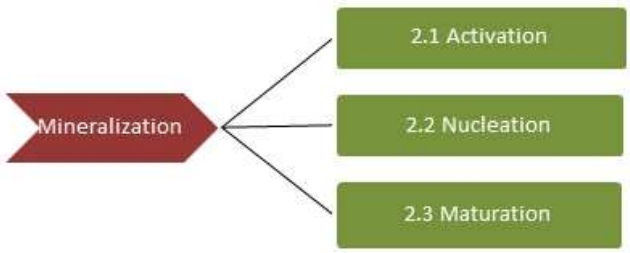

Figure 16: Schematic overview of the three-step mineralization procedure used in the present thesis.

2.1 Optimization surface activation

Due to the hydrophobic nature of PCL and PDLLA it is necessary to create negatively charged functional groups on the scaffold surface in order to enable the deposition of a calcium phosphate layer.[106] The activation method chosen in the present study was partial surface hydrolysis by the wet chemical method (Chapter 1 Figure 12). This was preferred above plasma treatment as the currently available plasma techniques cannot efficiently modify deeply located surfaces due to the limited penetration depth of plasma in the pores of the scaffold.[213] Wet chemical methods can offer the flexibility for surface modification throughout fibrous scaffolds.

However, when biodegradable polymeric fibrous scaffolds are surface-modified using partial hydrolysis, special care must be taken. The type and concentration of the hydrolyzing agent, but also the duration of the hydrolysis are important parameters to consider in order to produce surface functional groups without changing the bulk properties of the material. Furthermore, the activation of the scaffold surface should be homogenous.

Various studies report on the use of an alkaline NaOH solution for the generation of a functionalized and hydrophilic polymer surface.[120,150,157,183,184,195,201,213,269] However, for brittle polyesters such as PDLLA, treatment with NaOH severely degrades the polyester structure.[195] Due to the absence of crystallinity and a higher amount of accessible ester groups in PDLLA, it is more vulnerable to degradation by ester hydrolysis compared to PCL.[270,271] In order to reduce the risk of damaging the PDLLA fibers, the activation method should be as mild as possible. The current research showed that immersion of electrospun PDLLA samples for 3 seconds in ultrapure water under ultrasonication successfully homogenously activated the fiber surface without affecting the fibers. These results show that, from a solution as mild as water, the introduction of ultrasound has some physical and chemical effects that are useful in surface modification:

- Physical: the erosive action of micro-jets hitting the material can roughen the surface, providing an ideal surface for subsequent coating
- Chemical: acoustic cavitations generate localized high pressures that can break bonds on the surface.[272,273]

Even though for the more stable PCL, a more aggressive activation treatment could be expected, the long incubation times[120,147,157,183,184] in or high concentrations[157,184] of the NaOH solutions suggested in literature should be avoided to reduce the risk of loss of mechanical properties or structural integrity of the scaffold. In order to reduce the incubation time and concentration of the NaOH solution, two innovative approaches were investigated in the present research: pre-wetting with ethanol and activation under ultrasonication. Ethanol, a well-known wetting medium of polyester,[274,275] was applied by Yang *et al*.[201] as co-treating medium to make PLLA macroporous scaffolds more hydrophilic and assist the nucleophilic attack by a NaOH solution on the ester bond. Their results showed that upon co-treatment with ethanol lower concentrations of NaOH and shorter treatment times could be applied to reduce the surface hydrophobicity, which resulted in an enhanced cell affinity for the PLLA scaffolds. However, the appliance of ethanol as pre-wetting medium of polyesters during activation-step in a mineralization procedure was a rather new approach, although its ability to reduce the pre-treatment time during calcium phosphate film formation was already investigated by Choi *et al.*[276] for poly(methyl methacrylate) (PMMA) substrates. Based on these findings better results in terms of degree of NaOH solution infiltration were expected by the ethanol pre-treatment procedure because of the reduced hydrophobicity of the polyesters. The present study showed that electrospun PCL scaffolds were indeed successfully activated by ethanol dipping followed by a 40 minutes immersion in NaOH under ultrasonication.

So, with the implementation of ethanol pre-wetting and/or ultrasonication a reproducible, milder and less time-consuming protocol than others reported in literature was achieved for the activation of electrospun PCL and PDLLA scaffolds.

In analogy with the electrospun PCL scaffolds, the activation procedure of the 3D plotted samples was optimized. With the parameters of the optimized two-step activation procedure of electrospun PCL as base, the immersion time in NaOH was reduced from 40 minutes to 15 minutes. A reduction of the activation time could be expected as the pores of the 3D plotted samples are larger, which results in a more sufficient infiltration of the aqueous NaOH solution into the pores of the scaffold.

For the multiscale scaffolds, the activation protocols for electrospun and 3D plotted PCL were combined to a new protocol. Successful activation was demonstrated upon immersion of the samples for 1 minute in ethanol to allow for complete soaking of the scaffold and subsequent immersion in NaOH under ultrasonication for 40 minutes to assure sufficient infiltration of the alkaline solution into the pores of the exterior electrospun PCL layer.

2.2 Nucleation

During activation, carboxylate moieties are created on the polyester surface; those are known to be involved in the deposition of calcium phosphate in SBF. Nevertheless, activation alone is not decisive, and only slightly accelerates calcium phosphate deposition on the polyester surface.[243] Alternate dipping in calcium and phosphate rich solutions after activation of the surface, as proposed first by Taguchi *et al*.[189] and later by Oyane *et al*.[182], has been shown to be effective in inducing apatite deposition. The mechanism of calcium phosphate deposition upon being alternately dipped in calcium and phosphate rich solutions can be explained as follows; when the activated samples are first dipped in the calcium rich solution, the carboxylate groups on the surface attract Ca^{2+} ions from the solution by a chelating ion-exchange reaction. When the samples are subsequently dipped in phosphate rich solution, the Ca^{2+} ions attract the negatively charged PO_4^{3-} ions from the solution. As a result, calcium phosphate nuclei are deposited on the polyester surface with an anchoring effect of the carboxylate groups.[243]

For electrospun scaffolds, due to their nanofibrous structure and narrow pores, the major challenge when depositing a calcium phosphate layer on the fibers, is the preservation of the porous structure and the coating of fibers located in the inner layers of the scaffold. In order to control the deposition of a thin and homogenous calcium phosphate layer, the nucleation procedure for electrospun PCL and PDLLA scaffolds was optimized using a variable simplex algorithm. The use of a simplex facilitates the optimization of multi-parametric procedures.[277-279] In chapter 3.1 and 3.2, the five parameters of the alternate dipping process were

simultaneously optimized: the number of cycles, concentration of and immersion time in both the calcium and phosphate rich solutions, for the electrospun PCL and PDLLA scaffold respectively. The obtained coating on both scaffolds was a slightly carbonated nanocrystalline calcium deficient apatite. As the alternate dipping process is mainly used as an intermediate step in the mineralization procedure, the calcium phosphate phase deposited after this step was rarely identified. Our results are however consistent with Furunzo *et al.*[280], which demonstrated the deposition of a deficient apatite containing carbonate and HPO_4^{2-} ions on silk fabric.

Because of the difficulty of coating electrospun scaffolds without obstructing the pores, further maturation experiments, in which the calcium phosphate primer layer further grows, were not performed with the electrospun scaffolds.

For the 3D plotted PCL scaffolds, the thickness of the calcium phosphate layer deposited during the nucleation process is less of a limiting factor as the pores are much larger compared to the electrospun scaffold. Therefore, a standard nucleation procedure, adopted from literature could be used.[183,184] At this point we were able to automate the otherwise labor intensive method by introducing the use of a dip coater machine, the RDC30 Multidip from Bungard. The robotic arm of the machine was capable of raising and lowering up to six samples simultaneously and placing them into four separate beakers filled with (1) $CaCl_2.2H_2O$-solution, (2) demineralized water, (3) Na_2HPO_4-solution and (4) demineralized water. Although the deposited calcium phosphate seeds could not be visualized by SEM, nor identified by IR, the necessity of the nucleation step was demonstrated as its implementation was shown to accelerate the deposition of a more homogenous calcium phosphate layer upon subsequent incubation in SBF.[281]

Because the exterior layer of the multiscale scaffold consists of electrospun fibers, the parameters of the nucleation procedure optimized for the electrospun PCL scaffolds were used for the nucleation of the multiscale scaffolds. Although not identified, it can be assumed that the deposited coating is also a nanocrystalline calcium deficient apatite, in analogy with the coating deposited on the electrospun samples after treatment with the same nucleation procedure.

2.3 Maturation

Following the activation and nucleation step, the 3D plotted PCL scaffolds and multiscale PCL scaffolds were further subjected to a maturation step in SBF-based solutions in order to deposit a carbonate rich apatite layer on the scaffold surface.

General discussion and conclusion

Bioactive materials form apatite nuclei on their surfaces prior to the spontaneous growth of apatite upon immersion in an SBF solution. In analogy, the surface of the activated and alternately dipped samples can at this stage be considered to be similar to that bioactive materials, having calcium phosphate nuclei on their surface. The nuclei are proposed to activate the growth of an apatite-like coating when immersed in a SBF solution by providing sites for heterogeneous nucleation. Consequently, the formation of a solid calcium phosphate phase, by consuming calcium and phosphate ions from the surrounding solution, is much easier.[243,281]

In the 1990s developed mineralizing solution based on physiological fluids, SBF, can be used to deposit apatitic layers on various substrates at near-physiological temperature and pH.[282,283] This biomimetic coating method offers several advantages, such as coating of temperature-sensitive polymers, formation of phases other than hydroxyapatite, such as carbonated apatite and deposition on porous and complex geometric shapes. In order to enable the formation of highly carbonated apatite it is necessary to change the ionic composition of the original SBF solution. It is well known that the composition of the calcium phosphate layer deposited in aqueous solutions largely depends on the composition of the mineralization solution.[186,257,259]

For the preparation of the experimental SBF solution, concentrated stock solutions were used. SBF preparation from stock solutions was previously proven to be more efficient, user-friendly and repetitive than direct preparation form salt weighing.[243,284] After the synthesis of experimental SBF solutions with the ability to form carbonate rich deposits was established, 3D plotted and multiscale PCL scaffolds were coated with a carbonate rich apatite layer (up to 16 wt% carbonate). Our results showed that in order to deposit an apatite with high carbonate content, the mineralization solution should preferentially be deprived of Mg^{2+} ions, and rich in CO_3^{2-} ions (≥ 42 mM). As a matter of fact, CO_3^{2-} as well as Mg^{2+} have been shown to act as crystal growth inhibitors, by slowing down apatite nucleation in favor of the formation of an amorphous state. Compared to CO_3^{2-}, Mg^{2+} has a stronger inhibitory effect on crystal growth by adsorption onto the surface of the apatite.[175,285] Moreover, there is a synergistic effect of Mg^{2+} and CO_3^{2-} ions on the decrease of crystallinity.[7,249] This may be due to the inactivation of crystal growth sites by adsorption of CO_3^{2-} to the divalent Mg^{2+} cations instead of Ca^{2+}.[243] Although the reduction of the crystal size has been shown to allow for a better physical attachment of the coating on the substrate [175,186], the presence of Mg^{2+} ions in combination with a high concentration of CO_3^{2-} ions clearly hindered the crystal growth too much so that no coating was deposited during incubation in these solutions.

The deposited apatite coating is predominantly a low crystalline B-type carbonated apatite, in which CO_3^{2-} is substituted for PO_4^{3-} in the apatite lattice. These results contradict the hypothesis of Müller *et al.*[246], that assumed that at HCO_3^- concentrations higher than 20 mM both A and B-type carbonated apatite forms. The highest HCO_3^- concentration used in their experimental SBF is 27 mM, from which a carbonated apatite layer with a carbonate content of 9 wt% precipitated. To our opinion, there is no evidence that CO_3^{2-} substituted for OH^- as the characteristic bands associated with A-type substitution could not be observed in the associated IR spectrum, which is in fact in contradiction with their own hypothesis.

Because of its great simplicity, the present surface mineralization protocol has advantages in cost and processing time over other methods. Furthermore, upon optimization of the parameters, the protocol has potential to be applicable to not only 3D plotted and multiscale PCL but also to scaffolds produced with other fabrication techniques and/or materials as well.

To summarize, an overview of the optimized coating procedure of all four scaffold is shown in figure 17.

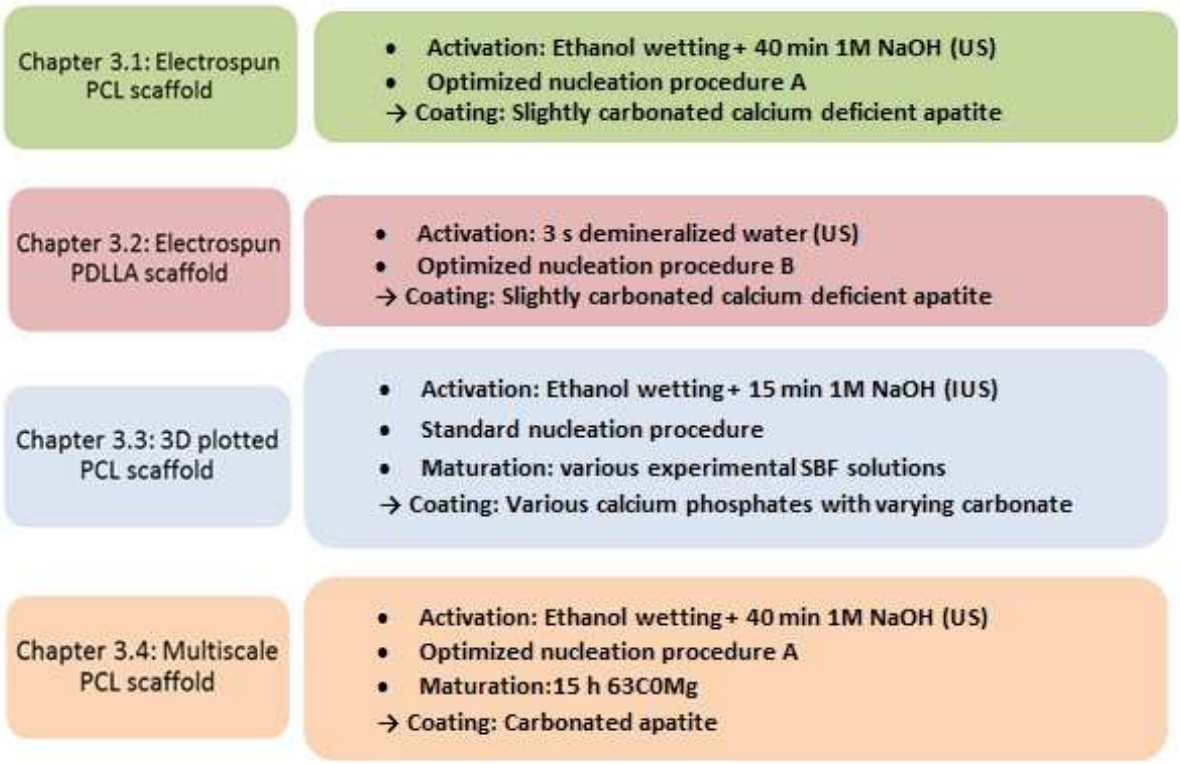

Figure 17: Overview of the optimized step-wise mineralization procedures of the scaffolds investigated in the present thesis.

3 Cell response

When cells approach an implant material, they do not make direct contact with its surface, but with a layer of adsorbed proteins from the culture medium, blood or serum. Hence, it is to these adsorbed proteins, rather than to the surface itself, cells initially respond. Diverse studies using a range of materials have demonstrated the pivotal role of extracellular adhesion proteins – fibronectin and vitronectin in partical – in cell adhesion, morphology and migration.[286] Thus, the ability of materials to adsorb such proteins (in an active state) will determine their ability to support cell adhesion and spreading.[287]

For the electrospun scaffolds the influence of a calcium deficient apatite coating on the cell viability and proliferation was evaluated. For the 3D plotted and multiscale PCL scaffolds, cell response was evaluated for the samples coated with apatite with different carbonate contents. Mouse calvaria-derived pre-osteoblastic cells, MC3T3-E1, were used for the evaluation of biological performance on all scaffolds. These cells are commonly used in similar approaches because of the cell culture reproducibility.[288]

In general, the amount of cells attached to the untreated scaffolds was low throughout all experiments. In addition, the majority of cells showed a rounded morphology. The observed limited cell-biomaterial interactions could be expected due to the hydrophobic nature of the untreated polyesters. Moderately hydrophilic surfaces are known to induce more favorable cell responses than hydrophobic surfaces, by favoring adsorption of vitronectin and/or fibronectin and better preserving the bioactivity of adsorbed proteins.[123,287] The observation that some cellular proliferation occurs during prolonged incubation illustrates a limited or unfavorable protein adsorption. Also, fluorescence micrographs of the untreated samples after calcium/propidium iodide staining generally shows the presence of predominantly green cells. The latter supports the non-toxicity of untreated PCL samples. Comparison of the observed cell viability on untreated electrospun and 3D plotted PCL samples (Chapter 3.1 figure 11 and Chapter 3.2 figure 8, respectively) showed a very low number of attached cells after one day of culture on both scaffolds. After 7 and 14 days of culture, however still rather low, a larger number of cells was able to attach to the 3D plotted samples compared to the electrospun samples. Based on previous reports in literature[118-120,220] the lower cell response on electrospun samples could be expected and can be ascribed to their smaller pore diameter. This results in a limited cell infiltration and cells are only able to adhere to surface of the electrospun samples. The larger pores of the 3D plotted scaffold enable the migration of cells through the samples. As a result, the cells can adhere to the surface of the filaments throughout the samples. The latter represents a larger surface compared to the surface of

the electrospun samples which is reflected in the higher number of attached cells on the untreated 3D plotted PCL samples compared to the untreated electrospun samples.

Our results demonstrated generally higher amounts of viable cells and higher proliferation rates on the mineralized scaffolds compared to the untreated scaffolds. The increase in cell attachment can probably be accounted to an enhancement of proteins adsorption such as fibronectin and vitronectin on the mineralized scaffolds. Moreover, the carbonate content of the apatite layer clearly had an impact on cell attachment and proliferation. Bridging of the pores in the 3D plotted PCL scaffolds was only achieved for the samples coated with a calcium phosphate with a high carbonate content (≥10 wt%). It was indeed previously shown that carbonated apatite powders promote cell attachment and proliferation compared to carbonate-free apatites.[152,289,290] The incorporation of CO_3^{2-} in the apatite lattice results in a decrease of the charge density at the apatite surface and a change in available Ca^{2+} and PO_4^{3-} surface groups which will probably influence the adsorption of proteins.[291] Also, CO_3^{2-} incorporation results in a change of the surface structure as it favors the formation of smaller crystals, with larger surface area. Moreover, the incorporation of carbonate increases the solubility of the apatite in physiological fluids, which may promote the bioresorption of these materials and could also have been a reason for the more pronounced osteoblast proliferation in coating with higher carbonate content.[292]

4 Conclusion

In the present study, electrospun PCL and PDLLA nanofibrous scaffolds were coated with a thin, homogenous primer layer of slightly carbonated calcium deficient hydroxyapatite, with preservation of the porous structure. The optimized protocol enabled a faster deposition of such a calcium phosphate coating at milder conditions than the coating procedures described in literature.

Microfibrous PCL scaffolds, fabricated by the rapid prototyping technique 3D plotting, were successfully coated with highly carbonated hydroxyapatite. By adjustment of the carbonate and magnesium content of the mineralization solution, higher amounts of carbonate incorporation were obtained than previously reported in literature.

Finally, a novel technique for fabricating multiscale polymer scaffolds was presented. 3D plotting was combined with electrospinning to fabricate scaffolds with both nano – and microfibrous structures. Accordingly, the previously optimized coating procedure for the constituting single scale scaffolds were combined for the coating of the multiscale scaffolds with a highly carbonated hydroxyapatite.

Analysis of the cell viability, adhesion and proliferation of MC3T3-E1 cells showed improved osteogenic response and enhanced cell affinity on all calcium phosphate coated scaffolds compared to untreated samples. Moreover, the best results in term of cell adhesion and proliferation were obtained upon coating of the samples with a hydroxyapatite layer with high carbonate content.

5 References

1. Woodruff MA, Hutmacher DW. The return of a forgotten polymer-Polycaprolactone in the 21st century. Progress in Polymer Science 2010;35(10):1217-1256.
2. Engelberg I, Kohn J. Physicochemical properties of degradable polymers used in medical applications - A comparative-study. Biomaterials 1991;12(3):292-304.
3. Chen CC, Chueh JY, Tseng H, Huang HM, Lee SY. Preparation and characterization of biodegradable PLA polymeric blends. Biomaterials 2003;24(7):1167-1173.
4. Xu H, Cui W, Chang J. Fabrication of patterned PDLLA/PCL composite scaffold by electrospinning. Journal of Applied Polymer Science 2013;127(3):1550-1554.
5. Pitt CG, Gratzl MM, Kimmel GL, Surles J, Schindler A. Aliphatic polyesters .2. The degradation of PDLLA, PCL and their copolymers in vivo. Biomaterials 1981;2(4):215-220.
6. Choong C, Triffitt JT, Cui ZF. Polycaprolactone scaffolds for bone tissue engineering - Effects of a calcium phosphate coating layer on osteogenic cells. Food and Bioproducts Processing 2004;82(C2):117-125.
7. Katsanevakis E, Wen X, Zhang N. Creating Electrospun Nanofiber-Based Biomimetic Scaffolds for Bone Regeneration. Biomedical Applications of Polymeric Nanofibers 2012;246:63-100.
8. Jaiswal AK, Chhabra H, Soni VP, Bellare JR. Enhanced mechanical strength and biocompatibility of electrospun polycaprolactone-gelatin scaffold with surface deposited nano-hydroxyapatite. Materials Science & Engineering C-Materials for Biological Applications 2013;33(4):2376-2385.
9. Xie J, Zhong S, Ma B, Shuler FD, Lim CT. Controlled biomineralization of electrospun poly(epsilon-caprolactone) fibers to enhance their mechanical properties. Acta Biomaterialia 2013;9(3):5698-5707.
10. Bhardwaj N, Kundu SC. Electrospinning: A fascinating fiber fabrication technique. Biotechnology Advances 2010;28(3):325-347.
11. Ragaert K, Dekeyser A, Cardon L, Degrieck J. Quantification of Thermal Material Degradation During the Processing of Biomedical Thermoplastics. Journal of Applied Polymer Science 2011;120(5):2872-2880.
12. Ragaert K. Micro-extrusion of thermoplastics for 3D plotting of scaffolds for tissue engineering. Ghent: Ghent University; 2011.
13. Declercq HA, Desmet T, Berneel EEM, Dubruel P, Cornelissen MJ. Synergistic effect of surface modification and scaffold design of bioplotted 3-D poly-epsilon-caprolactone scaffolds in osteogenic tissue engineering. Acta Biomaterialia 2013;9(8):7699-7708.
14. Yoo HS, Kim TG, Park TG. Surface-functionalized electrospun nanofibers for tissue engineering and drug delivery. Advanced Drug Delivery Reviews 2009;61(12):1033-1042.
15. Yang J, Wan YQ, Tu CF, Cai Q, Bei JZ, Wang SG. Enhancing the cell affinity of macroporous poly(L-lactide) cell scaffold by a convenient surface modification method. Polymer International 2003;52(12).
16. Oyane A, Uchida M, Choong C, Triffitt J, Jones J, Ito A. Simple surface modification of poly(epsilon-caprolactone) for apatite deposition from simulated body fluid. Biomaterials 2005;26(15):2407-2413.

17. Chen J, Chu B, Hsiao BS. Mineralization of hydroxyapatite in electrospun nanofibrous poly(L-lactic acid) scaffolds. Journal of Biomedical Materials Research Part A 2006;79A(2):307-317.
18. Arafat MT, Lam CXF, Ekaputra AK, Wong SY, Li X, Gibson I. Biomimetic composite coating on rapid prototyped scaffolds for bone tissue engineering. Acta Biomaterialia 2011;7(2):809-820.
19. Dorj B, Kim M-K, Won J-E, Kim H-W. Functionalization of poly(caprolactone) scaffolds by the surface mineralization for use in bone regeneration. Materials Letters 2011;65(23-24):3559-3562.
20. Araujo JV, Martins A, Leonor IB, Pinho ED, Reis RL, Neves NM. Surface controlled biomimetic coating of polycaprolactone nanofiber meshes to be used as bone extracellular matrix analogues. Journal of Biomaterials Science-Polymer Edition 2008;19(10):1261-1278.
21. Croll TI, O'Connor AJ, Stevens GW, Cooper-White JJ. Controllable surface modification of poly(lactic-co-glycolic acid) (PLGA) by hydrolysis or aminolysis I: Physical, chemical, and theoretical aspects. Biomacromolecules 2004;5(2):463-473.
22. Ulery BD, Nair LS, Laurencin CT. Biomedical Applications of Biodegradable Polymers. Journal of Polymer Science Part B-Polymer Physics 2011;49(12):832-864.
23. Vroman I, Tighzert L. Biodegradable Polymers. Materials 2009;2(2):307-344.
24. Cobley A. Ultrasound Sonochemistry - A more sustainable approach to surface modification? Surface Engineering 2009;25(8):559-564.
25. Suslick KS, Price GJ. Applications of ultrasound to materials chemistry. Annual Review of Materials Science 1999;29:295-326.
26. Yu H-S, Jang J-H, Kim T-I, Lee H-H, Kim H-W. Apatite-mineralized polycaprolactone nanofibrous web as a bone tissue regeneration substrate. Journal of Biomedical Materials Research Part A 2009;88A(3):747-754.
27. Hansson PM, Hormozan Y, Brandner BD, Linnros J, Claesson PM, Swerin A, Schoelkopf J, Gane PAC, Thormann E. Hydrophobic pore array surfaces: Wetting and interaction forces in water/ethanol mixtures. Journal of Colloid and Interface Science 2013;396:278-286.
28. Mikos AG, Lyman MD, Freed LE, Langer R. Wetting of poly(L-lactic acid) and poly (DL-lactic-co-glycolic acid) foams for tissue-culture. Biomaterials 1994;15(1).
29. Choi S-M, Yang W-K, Yoo Y-W, Lee W-K. Effect of surface modification on the in vitro calcium phosphate growth on the surface of poly(methyl methacrylate) and bioactivity. Colloids and Surfaces B-Biointerfaces 2010;76(1).
30. Lebourg M, Suay Anton J, Gomez Ribelles JL. Characterization of calcium phosphate layers grown on polycaprolactone for tissue engineering purposes. Composites Science and Technology 2010;70(13):1796-1804.
31. Taguchi T, Kishida A, Akashi M. Hydroxyapatite formation on/in poly(vinyl alcohol) hydrogel matrices using a novel alternate soaking process. Chemistry Letters 1998(8):711-712.
32. Oyane A, Uchida M, Yokoyama Y, Choong C, Triffitt J, Ito A. Simple surface modification of poly(epsilon-caprolactone) to induce its apatite-forming ability. Journal of Biomedical Materials Research Part A 2005;75A(1).
33. Krause RD, Lott JA. Use of simplex method to optimize analytical conditions in clinical-chemistry. Clinical Chemistry 1974;20(7):775-782.
34. Lundstedt T, Seifert E, Abramo L, Thelin B, Nystrom A, Pettersen J, Bergman R. Experimental design and optimization. Chemometrics and Intelligent Laboratory Systems 1998;42(1-2):3-40.
35. Walter F, Parker L, Morgan S, Deming S. Sequential simplex optimization: a technique for improving quality and productivity in research, development and manufacturing. Boca Rota: CRC Press LLC; 1991.
36. Furuzono T, Taguchi T, Kishida A, Akashi M, Tamada Y. Preparation and characterization of apatite deposited on silk fabric using an alternate soaking process. Journal of Biomedical Materials Research 2000;50(3):344-352.

37. Steijns F. Mineralisatie van 3D-geprinte polymere structuren voor bot regeneratieve doeleinden. Ghent: Ghent University; 2015.
38. Abe Y, Kokubo T, Yamamuro T. Apatite coating on ceramics, metals and polymers using a biological process. Journal of Materials Science-Materials in Medicine 1990;1(4):233-238.
39. Kokubo T, Kushitani H, Sakka S, Kitsugi T, Yamamuro T. Solutions able to reproduce in vivo surface-structure changes in bioactive glass-ceramic A-W3. Journal of Biomedical Materials Research 1990;24(6):721-734.
40. Dorozhkina EI, Dorozhkin SV. Surface mineralisation of hydroxyapatite in modified simulated body fluid (mSBF) with higher amounts of hydrogencarbonate ions. Colloids and Surfaces a-Physicochemical and Engineering Aspects 2002;210(1):41-48.
41. Barrere F, van Blitterswijk CA, de Groot K, Layrolle P. Influence of ionic strength and carbonate on the Ca-P coating formation from SBFx5 solution. Biomaterials 2002;23(9):1921-1930.
42. Martin RI, Brown PW. The effects of magnesium on hydroxyapatite formation in vitro from CaHPO4 and Ca-4(PO4)(2)O at 37.4 degrees C. Calcified Tissue International 1997;60(6):538-546.
43. Bohner M, Lemaitre J. Can bioactivity be tested in vitro with SBF solution? Biomaterials 2009;30(12):2175-2179.
44. Barrere F, van Blitterswijk CA, de Groot K, Layrolle P. Nucleation of biomimetic Ca-P coatings on Ti6Al4V from a SBF x 5 solution: influence of magnesium. Biomaterials 2002;23(10):2211-2220.
45. Kim HM, Kishimoto K, Miyaji F, Kokubo T, Yao T, Suetsugu Y, Tanaka J, Nakamura T. Composition and structure of apatite formed on organic polymer in simulated body fluid with a high content of carbonate ion. Journal of Materials Science-Materials in Medicine 2000;11(7):421-426.
46. Cao X, Harris W. Carbonate and magnesium interactive effect on calcium phosphate precipitation. Environmental Science & Technology 2008;42(2):436-442.
47. Driessens F, Verbeeck R. Biominerals: CRC Press; 1990.
48. Muller L, Conforto E, Caillard D, Muller FA. Biomimetic apatite coatings - Carbonate substitution and preferred growth orientation. Biomolecular Engineering 2007;24(5):462-466.
49. Horbett TA. The role of adsorbed proteins in animal-cell adhesion. Colloids and Surfaces B-Biointerfaces 1994;2(1-3):225-240.
50. Wilson CJ, Clegg RE, Leavesley DI, Pearcy MJ. Mediation of biomaterial-cell interactions by adsorbed proteins: A review. Tissue Engineering 2005;11(1-2):1-18.
51. Wang D, Christensen K, Chawla K, Xiao GZ, Krebsbach PH, Franceschi RT. Isolation and characterization of MC3T3-E1 preosteoblast subclones with distinct in vitro and in vivo differentiation mineralization potential. Journal of Bone and Mineral Research 1999;14(6):893-903.
52. Ghasemi-Mobarakeh L, Morshed M, Karbalaie K, Fesharaki M, Nasr-Esfahani MH, Baharvand H. Electrospun poly (epsilon-caprolactone) nanofiber mat as extracellular matrix. Yakhteh 2008;10(3):179-184.
53. Ko YM, Choi DY, Jung SC, Kim BH. Characteristics of Plasma Treated Electrospun Polycaprolactone (PCL) Nanofiber Scaffold for Bone Tissue Engineering. Journal of Nanoscience and Nanotechnology 2015;15(1):192-195.
54. Araujo JV, Cunha-Reis C, Rada T, da Silva MA, Gomes ME, Yang Y, Ashammakhi N, Reis RL, El-Haj AJ, Neves NM. Dynamic Culture of Osteogenic Cells in Biomimetically Coated Poly(Caprolactone) Nanofibre Mesh Constructs. Tissue Engineering Part A 2010;16(2):557-563.
55. Ghasemi-Mobarakeh L, Morshed M, Karbalaie K, Fesharaki M, Nasr-Esfahani MH, Baharvand H. Electrospun poly (epsilon-caprolactone) nanofiber mat as extracellular matrix. Yakhteh 2008;10(3).

56. Pieters IY, Van den Vreken NMF, Declercq HA, Cornelissen MJ, Verbeeck RMH. Carbonated apatites obtained by the hydrolysis of monetite: Influence of carbonate content on adhesion and proliferation of MC3T3-E1 osteoblastic cells. Acta Biomaterialia 2010;6(4):1561-1568.
57. Landi E, Tampieri A, Mattioli-Belmonte M, Celotti G, Sandri M, Gigante A, Fava P, Biagini G. Biomimetic Mg- and Mg,CO3-substituted hydroxyapatites: synthesis characterization and in vitro behaviour. Journal of the European Ceramic Society 2006;26(13):2593-2601.
58. Melville AJ, Harrison J, Gross KA, Forsythe JS, Trounson AO, Mollard R. Mouse embryonic stem cell colonisation of carbonated apatite surfaces. Biomaterials 2006;27(4):615-622.
59. Feng B, Chen JY, Zhang XD. Interaction of calcium and phosphate in apatite coating on titanium with serum albumin. Biomaterials 2002;23(12):2499-2507.
60. Ellies LG, Carter JM, Natiella JR, Featherstone JDB, Nelson DGA. Quantitative-analysis of early in vivo tissue-response to synthetic apatite implants. Journal of Biomedical Materials Research 1988;22(2):137-148.

Chapter 5: Future perspectives

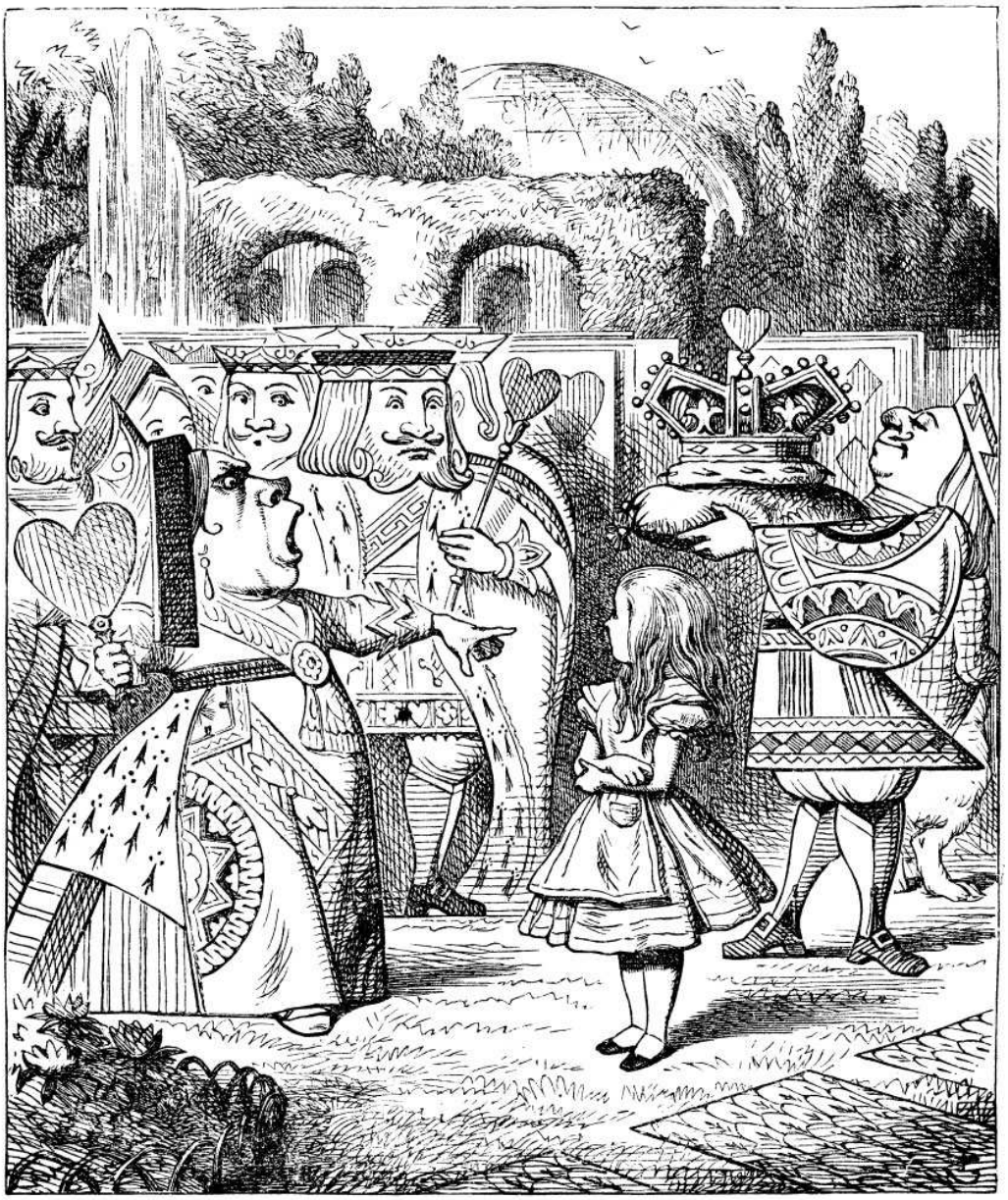

Calcium phosphate coated electrospun scaffolds

Although the final aim of the present study was the coating of electrospun fiber as part of a multiscale scaffold, mineralized electrospun fibers as such have also great potential in BTE and can either be used alone as 2D or 3D matrices or in combination with larger tissue engineered constructs. The following section summarizes some potential applications.

- Electrospinning can also be used to produce and deposit polymeric nanofibers on metallic substrates. Surface coating with polymers provides better corrosion resistance, enhances biocompatibility and cell response and reduces the degradation in physiological environment.[293] Soujanya *et al*.[294] showed that the corrosion rate of electrospun PCL coated AZ31 magnesium alloys was five times lower compared to chemically treated samples. The addition of an apatite coating could increase the bioactivity of the composite structure.
- In order to reduce implant-related infections following invasive orthopedic surgery, an implant can also be coated with antibiotic-loaded electrospun mats. In this way, the release of antibiotic is localized and targeted to the desired site and released at high concentrations over a prolonged period of time. For instance, Zhang et al.[295] coated titanium implants with vancomycin loaded electrospun PLGA. The coated titanium implants exerted antibacterial properties *in vitro* and *in vivo*. Also in this application, coating of the electrospun fibers with an apatite layer could improve the bioactivity of the complete implant. As the coating will shield the antibiotic-loaded electrospun fibers from the surrounding body fluids, the release-profile of the antibiotic will likely be altered.
- In 2011, Kolambkar *et al*.[296] developed a scaffold that consisted of an electrospun PCL nanofiber tube. This scaffold was tested to repair critical sized, femoral segmental defects in rats. Nanofiber tubes were placed around the adjacent bone ends, such that the tube lumen contained the defect. The tube lumen was filled with alginate gel with recombinant bone morphogenetic protein-2 (rhBMP-2). The results indicated that this novel scaffold resulted in consistent bony bridging of the challenging bone defects within 12 weeks. Apatite coating of such nanofiber tubes could eliminate the disadvantageous hydrophobicity of the PCL material, enhance the bioactivity of the tube and possibly even slightly improve the mechanical properties of the construct.

Optimization fabrication technique multiscale scaffolds

The limitation of the current fabrication procedure is that the electrospinning apparatus and the BioScaffolder are two individual devices. An interesting possibility is the integration of the two techniques in a single device. With such a device it would be possible to fabricate scaffolds with alternating layers of nanofibers and microfibers.

Mechanical testing

Analysis of the mechanical properties of the scaffold is an essential element that should still be investigated *in vitro* as well as at load bearing sites *in vivo*. Important in the latter is the degradation behavior of the scaffold; even if the scaffold has sufficient mechanical properties at the time of implantation, the way its mechanical properties change during degradation could also affect function within the tissue defect.

In vitro tests

In order to assess applicability of scaffolds technologies in tissue repair and regeneration, experiments with human cells are of importance prior to in vivo testing

In vivo tests

In vivo studies should be performed to determine the effect of the calcium phosphate coating on bone formation. The resorption of these coatings should also be evaluated. *In vivo*, optimal conditions can be different than *in vitro*, given the fact that *in vivo*, the degradation behavior of both polymer structures and the calcium phosphate coating will be different. Additional needs of nutrient supply, blood vessel ingrowth etc. need to be met as well. In a first approach the scaffolds can be implanted into the subcutaneous dorsal pockets of nude mice, a standard technique used for the evaluation of *in vivo* osteogenic potential of scaffolds. In a next phase osteogenesis can be further evaluated by implantation of the bone scaffolds into a bone defect (in a weight-bearing position) in an animal model.

Eventually, the developed constructs should be investigated in clinical relevant orthopedic defects to test the hypothesis that the coating of biodegradable fibrous polyester scaffolds with a layer of bioactive carbonated apatite leads to improved synthetic graft substitutes.

Clinical translation

While progress has been made to deliver bench to bedside solutions, the rate at which tissue engineering has seen innovations translated to the clinic is slow. The major challenge represents the translation of laboratory-based scaffold preparation processes into “clinically appropriate larger scale production techniques” that are “reproducible, safe, clinically effective and economically acceptable”.[297] In this respect, for the present scaffold, the scaffold fabrication process should be automated and up-scaled. This includes the combined use of 3D plotting and electrospinning, as well as the complete mineralization procedure. An additional concern is obtaining regulary approval.

Finally, upon commercialization, a custom-made patient specific scaffold can be fabricated on demand and on short notice in a GMP/GLP (good manufacturing/laboratory practice) facility and transported to the clinic where the bone reconstructive surgery is perfomed.

References

1. Zomorodian A, Garcia MP, Silva TME, Fernandes JCS, Fernandes MH, Montemor MF. Corrosion resistance of a composite polymeric coating applied on biodegradable AZ31 magnesium alloy. Acta Biomaterialia 2013;9(10):8660-8670.
2. Soujanya G, Hanas T, Chakrapani V, Sunil B, Kumar T. Electrospun nanofibrous polymer coated magnesium alloys for biodegradable implant applications. International conference on advances in manufacturing and materials engineering, ICAMME 2014. Volume 5; 2014. p 817-823.
3. Zhang L, Yan J, Yin Z, Tang C, Guo Y, Li D, Wei B, Xu Y, Gu Q, Wang L. Electrospun vancomycin-loaded coating on titanium implants for the prevention of implant-associated infections. International Journal of Nanomedicine 2014;9:3027-3036.
4. Kolambkar YM, Dupont KM, Boerckel JD, Huebsch N, Mooney DJ, Hutmacher DW, Guldberg RE. An alginate-based hybrid system for growth factor delivery in the functional repair of large bone defects. Biomaterials 2011;32(1):65-74.
5. Archer R, Williams DJ. Why tissue engineering needs process engineering. Nature Biotechnology 2005;23(11):1353-1355.

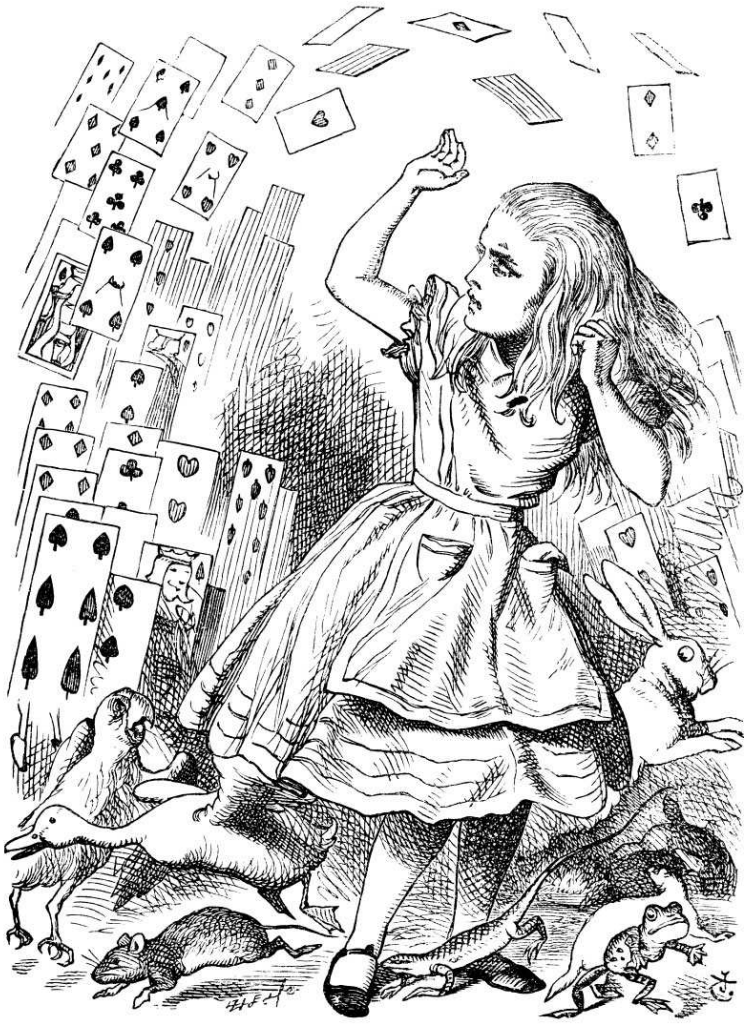

The End